

NO<sub>x</sub> EMISSION CONTROL BY PARTICLE QUENCHING  
IN AN ADVANCED GLASS MAKING PROCESS

K.M. Jeong, R. Tiwary, A. Chatwani, L. Westra, J. Woodroffe,  
F. Hals, and D. Stickler

Avco Research Laboratory, Inc.  
A Subsidiary of Textron, Inc.  
2385 Revere Beach Parkway  
Everett, MA 02149

and

L. Donaldson

Gas Research Institute  
8600 West Bryn Avenue  
Chicago, IL 60631

ABSTRACT

The formation of NO<sub>x</sub> in an advanced glass melting (AGM) process has been studied. In this system, methane is combusted with preheated air at near stoichiometric conditions resulting in a potential for production of a high NO<sub>x</sub> concentration in the exhaust. The minerals required for glass synthesis are entrained as a high loading concentration of fine particles in the preheated air supply. The particles are heated up in suspension by the combustion products. The thermal time scale for gas-particle heat transfer is chosen to be comparable to or less than NO<sub>x</sub> formation kinetic time. This was projected to prevent formation of NO<sub>x</sub> at a concentration corresponding to the adiabatic gas phase combustion temperature. The measured NO<sub>x</sub> concentration in the glass melter exhaust is found to be significantly below anticipated NSPS requirements. A model is proposed for the processes in the AGM based on a kinetics/transport code. The decreased amount of NO<sub>x</sub> formation is attributed to gas/particle thermal quenching effects and, possibly heterogeneous catalytic reduction.

INTRODUCTION

The development of an advanced gas-fired glass melting process (AGM) is being investigated as an alternative to the conventional glass melting furnace which is of the open-hearth type. The advanced glass melter is a technical derivative of a slagging coal combustor developed for magnetohydrodynamic power generation applications [1-3]. A primary goal is to transfer heat very efficiently at high temperatures to entrained glass batch particles. The high particulate loading required for this application presents a unique mechanism for limiting the formation of NO<sub>x</sub>.

High temperature reaction of air feed nitrogen and oxygen to primarily form nitric oxide, NO, is a source of potentially high NO<sub>x</sub> concentrations in the melt furnace exhaust. NO<sub>x</sub> control is achieved in the AGM by using the entrained particulate material as a dispersed heat sink with a very short thermal transient time. Thus, the combustion products are rapidly quenched from the adiabatic temperature at which high NO<sub>x</sub> concentrations would normally result to a much lower temperature. For the size particles considered, the thermal quenching is accomplished on a time scale much shorter than the NO<sub>x</sub> chemical kinetic formation time.

#### AGM CONCEPT AND EXPERIMENTAL SYSTEM

In the glass melter design concept, premixed batch materials are injected as fine particles into a high temperature combustion air line and transported in suspension to a high intensity gas burner. The materials are heated very rapidly in suspension in the turbulent flow field in the burner. A converging nozzle at the exit of the burner accelerates the flow and directs it into a melt separation and homogenizing chamber. The hot materials are separated inertially from the combustion gas and deposited on a collecting surface where initial homogenization occurs. The thin liquid layer flows from the collecting surface to a melt reservoir at the bottom of the chamber where additional homogenization can occur. The combustion products exit the melt separation chamber and are ducted to downstream heat recovery equipment for heating the incoming combustion air.

The experimental system used for development testing of the burner configuration and the separation centerbody is schematically shown in Figure 1. The unit consists of a pre-burner, a main combustor, and a glass receiver. The purpose of the gas-fired pre-burner is to simulate the high temperature preheat since there was no source of high temperature preheated air with which the system would normally operate. The fine glass feed particles are introduced downstream of the pre-burner through three injectors to promote thorough mixing with the gas. Initial tests used cullet as the feed material.

Gaseous oxygen is added to the combustion products of the pre-burner for combustion of the fuel added in the main or glass melting burner. Natural gas is introduced through eight radial injectors just upstream of the main burner. A sudden enlargement at the burner entrance creates a strong vortex flow region to promote mixing of the fuel and oxidizer. Combustion takes place with the particles still entrained in the gas. Rapid quenching of the combusted gas by these particles acts to keep the peak temperature down, thus reducing the NO<sub>x</sub> formation. A convergent nozzle at the exit of the burner accelerates the flow to the velocity required to accomplish the inertial separation of the particulate material from the combustion products, leading to homogenization and glass formation.

## NO<sub>x</sub> TEST RESULTS

The NO<sub>x</sub> concentration in the burner exhaust gas is strongly influenced by the temperature-time history and the oxygen concentration of the gas. The latter is determined by the gas stoichiometry or the air-fuel equivalence ratio used. The process constraint is to maintain a low oxygen concentration as well as a minimal residence time at the peak temperature, yet provide for rapid heat transfer to the entrained batch material. For these conditions, NO<sub>x</sub> concentrations significantly below the equilibrium flame adiabatic stoichiometric level are predicted.

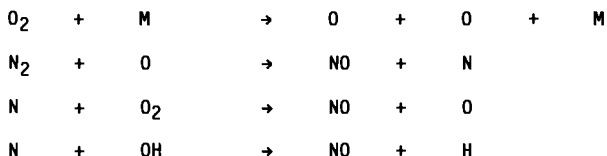
Figure 2 shows the equilibrium concentrations of NO which would be expected in the absence of particle quenching effects. For stoichiometric and fuel rich combustion, the NO equilibrium concentration for various calculated adiabatic flame temperatures reached by combustion with preheated air are indicated. If an emission limit of 4 lbs NO<sub>x</sub>/ton glass produced is assumed, then the maximum allowed NO concentration in the exhaust gas is 970 ppm for stoichiometric conditions.

Tests were conducted over a wide range of gas mass flows and feed loadings to determine system performance. While tests without batch material demonstrated that fuel-rich combustion offers the lowest NO<sub>x</sub> emission due to lower peak flame temperatures, it leads to a lower thermal efficiency because a portion of the combustion energy of the fuel is not released and made available for melting of the glass in the furnace. As a result, the main furnace is typically operated with excess oxygen,  $\phi \sim 1.4$ . The temperature of the melt chamber is approximately 2500F. For these conditions, NO<sub>x</sub> formation is approximately 1200 ppm prior to particle injection. Since the residence time at peak temperature is short, several milliseconds, the NO<sub>x</sub> concentration is less than the equilibrium level shown in Figure 2.

Tests with a four component batch comprising 52% silica, 20% soda ash, 13% calcium carbonate, and 15% cullet demonstrated the AGM's ability to capture, homogenize and fine the molten batch material on the centerbody, producing a fully reacted glass product. As predicted, the NO<sub>x</sub> production of the melter is considerably reduced by the quenching of the combustion gas by the batch particles. Batch injection is found to reduce the exhaust gas NO<sub>x</sub> level to approximately 250 ppm, corresponding to an NO<sub>x</sub> loading of 1 lb/ton glass without flue gas treatment.

### KINETICS/TRANSPORT MODEL

The chemical kinetic reaction mechanism used to model AGM combustion consists of 31 chemical species and 146 elementary chemical reactions. The principal reactions for formation and decomposition of thermal NO are:



The first three reactions, where M is a third body (usually N<sub>2</sub>), represent the important and well known Zeldovich mechanism of atomic exchange reactions. The code utilizes experimentally measured reaction rate parameters or the results of thermodynamic calculations if experimental data are not available. The numerical technique used in these calculations is described by Reference 4.

A thermodynamic equilibrium code is initially used to determine the composition of vitiated air from the combustion of air/CH<sub>4</sub> at T ~ 2500K in the pre-burner. These species account for approximately 40% of the total concentration of initial molecular constituents in the main combustor. Given these values and the concentration of added O<sub>2</sub> and CH<sub>4</sub> necessary to obtain the desired air/fuel ratio, the kinetic model is used to obtain the temporal dependence of key reaction species as a function of initial temperature. Figure 3 shows calculated temporal profiles for T = 1500K and a stoichiometric air/fuel ratio. Following an ignition delay of about 1.6 ms, a peak flame temperature of approximately 2350K is attained. The e-fold NO formation time is ~ 3.0 ms. The corresponding NO mass fraction, 0.003, is in good agreement with thermodynamic equilibrium calculations shown in Figure 4. This value is somewhat higher than the AGM test results, but this is attributed to a lower gas temperature in the glass melter.

The kinetic code is modified to include the effects of solid particles and the calculations are repeated. As Figure 3 indicates, the addition of solid particles reduces the NO<sub>x</sub> concentration from approximately 2000 ppm to 750 ppm, a factor of ~2.5. The AGM test results show still lower NO<sub>x</sub> concentrations in the furnace exhaust, but the general conclusion remains that NO<sub>x</sub> control is achieved by using entrained particulates as a dispersed heat sink with a short thermal transient time. Some errors are introduced in the kinetic calculations due to the difficulty of simulating the process which causes ignition, namely, the expansion of gases into a dump combustor, as well as the use of a flameholder, creating recirculation zones which result in bulk flow and mixing of combusted and uncombusted gases. This is analogous to the experimental situation where ignition would also not take place if methane was to be injected into the gas stream without provisions for flameholding.

A numerical simulation model treating transport processes in the AGM is used to describe  $\text{NO}_x$  formation and decomposition during rapid gas cool down by suspended batch material. The code is 1-D and calculates the temperatures and velocities of gas and particles along the length of the combustor. It assumes that all the particles are entrained in the gas and do not come into contact with each other in the combustor. Gas properties are calculated based on its chemical composition. The batch composition and the gas flow rates were selected to simulate the performance of the AGM. The program starts calculations at the location where particles are injected into the gas and it follows the temperature and velocity of gas and particles as they move along the combustor till the particles separate on the target.

Figure 5 shows the temperature profiles in the combustor section. Cold batch particles (sand, cullet, soda, and lime; batch flow rate=0.12 kg/s) were injected into hot gas coming from the vitiation burner (0.11 kg/s). The particle temperature rises at a rate dependent on the particle size. The flow rates of oxygen and natural gas were 0.037 and 0.0083 kg/s, respectively. The hot combustion gas is initially quenched very rapidly due to the high heat transfer rate from the gas to small particles. The gas temperature exhibits two subsequent sharp drops when oxygen and secondary methane are added to the gas stream. The calculation indicates that the gas cools from its peak temperature to 800-900K in about 12 ms.

At a distance of 1.2 meters from the particle injection location combustion takes place and the gas temperature sharply increases. The particle temperature also rises, but the rate is slower due to particle inertia. By the time the gas exits the combustor, 40 ms after particle injection, the temperature of the gas and the majority of the particles is almost equal, about 1800K. The only exception are the soda particles which due to their large size (150 micron diameter) and, thus, their large thermal inertia, are unable to follow the gas temperature as closely.

A question not presently addressed by the model is the suggestion of  $\text{NO}_x$  control by heterogeneous catalytic reduction. Evidence for such processes is provided by studies of the reduction of  $\text{NO}$  by  $\text{H}_2$  over a  $\text{Rh/SiO}_2$  catalyst [5] and of the decomposition of nitrous oxide on magnesium oxide and cupric oxide [6]. In addition, specific gas-surface interactions have been reported for  $\text{NO}$  and  $\text{SO}_2$  with constituents typically found in entrained fly ash from coal combustion [7]. The effect of batch particle surface absorption sites for catalytic reduction and enhanced  $\text{NO}_x$  control in the AGM process requires additional analysis.

#### SUMMARY

The measured  $\text{NO}_x$  concentration in the advanced glass melter exhaust gas is significantly below anticipated NSPS requirements. This is attributed to gas/particle thermal quenching effects.  $\text{NO}_x$  formation in the high temperature post-flame gases is chosen to occur over a time scale of several milliseconds, whereas heat transfer takes place on a shorter time scale resulting in significantly lower  $\text{NO}_x$  emissions than the equilibrium level for adiabatic gas combustion.

#### ACKNOWLEDGEMENTS

The authors gratefully acknowledge the support of this work by the Gas Research Institute under contract GRI 5086-232-1274.

#### REFERENCES

1. "Coal-Fired Combustor Development Project," Final Technical Report, Prepared by the Avco Everett Research Laboratory for the U.S. Department of Energy, Report No. ET-10787-3, October 1980.
2. D. B. Stickler and R. DeSaro, "Controlled Utilization of Coal Slag in the MHD Topping Cycle," presented at the Engineering Foundation Conference on Ash Deposits and Corrosion Due to Impurities in Combustion Gases, held at New England College, Henniker, NH, June 26-July 1, 1977.
3. J. G. Hnat, "A Direct Glass Melting System with Integrated Heat Recovery - Pressurized System Design," U. S. Patent, Disclosure Document No. 106632, March 8, 1982.
4. A. K. Varma, A. U. Chatwani, and F. V. Bracco, "Studies of Premixed Laminar Hydrogen - Air Flames Using Elementary and Global Kinetics Models," *Combust. Flame* 64: 233-236 (1986).
5. B. J. Savatsky and A. T. Bell, "Nitric Oxide Reduction by Hydrogen Over Rhodium Using Transient Response Techniques," in *Catalysis Under Transient Conditions*, Eds. A. T. Bell and L. L. Hegedus, ACS Symposium Series 178, American Chemical Society, Washington, D. C., 1982, p. 105.
6. H. Kobayashi and K. Hara, "Decomposition of Nitrous Oxide on Magnesium Oxide Compared to that on Cupric Oxide," in *Catalysis Under Transient Conditions*, Eds. A. T. Bell and L. L. Hegedus, ACS Symposium Series 178, American Chemical Society, Washington, D. C., 1982, p. 103.
7. R. V. Siriwardane and J. M. Cook, *J. Coll. Int. Sci.* 104, 250 (1985); 110, 504 (1986).

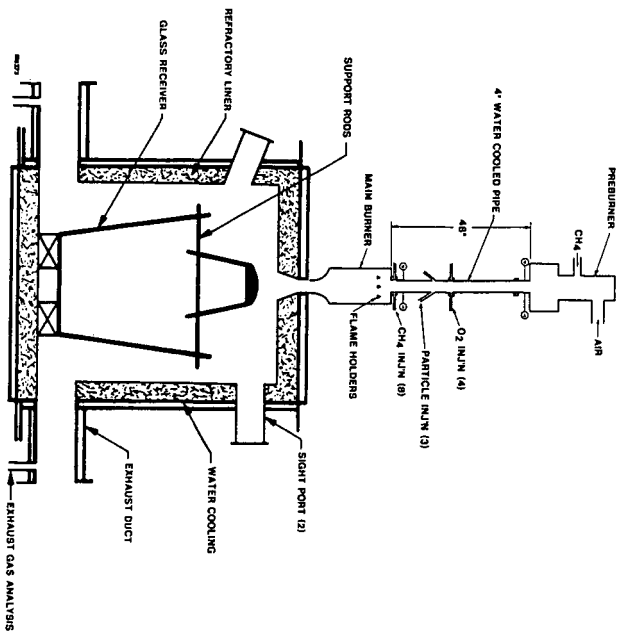


Figure 1 Schematic of AGM Experimental Set-up

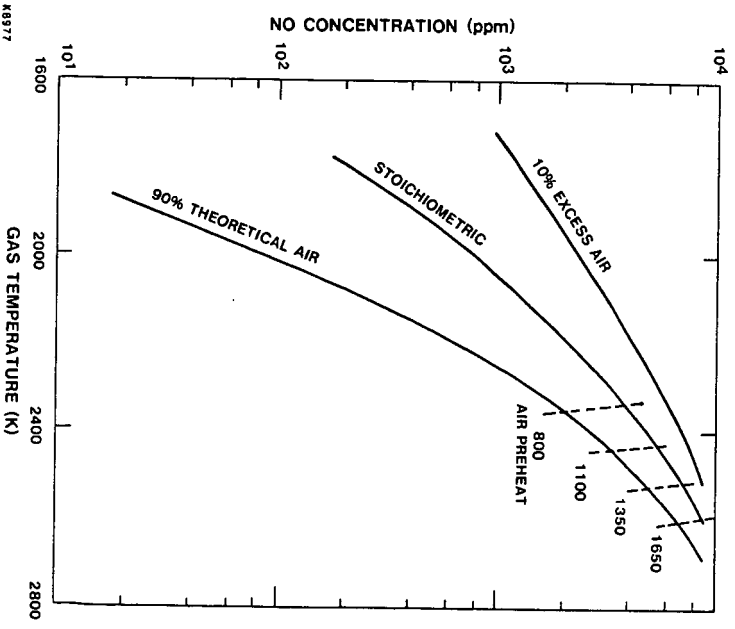


Figure 2 Calculated Equilibrium NO Concentrations for Various Stoichiometries and Gas Temperatures

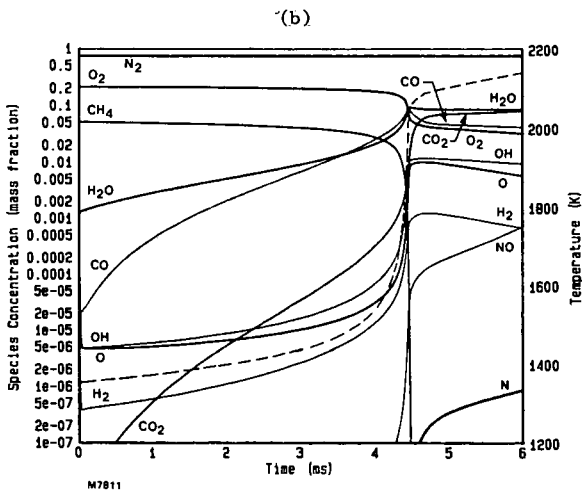
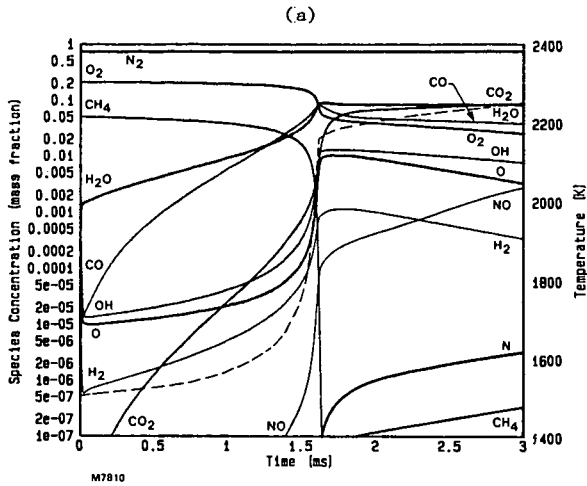


Figure 3 Combustion Species Temporal Profiles  
 (Dashed Line Shows Temperature Profile)  
 (a) Without Solid Particles  
 (b) With Solid Particles

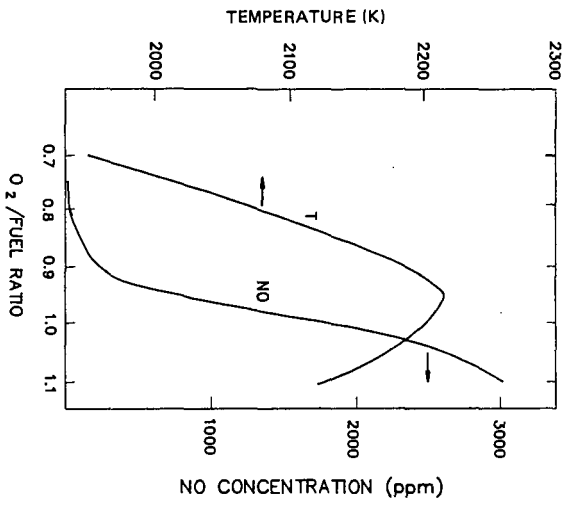


Figure 4 Equilibrium Calculation of Temperature and [NO] as a Function of the Oxygen/Fuel Ratio

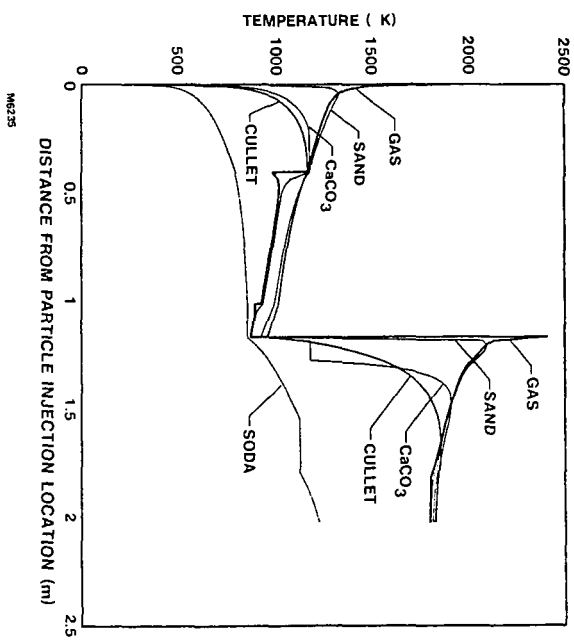


Figure 5 Temperature Profiles in Glass Melter

SO<sub>x</sub>-NO<sub>x</sub> CONTROL IN A STAGED CYCLONE  
COAL COMBUSTOR WITH LIMESTONE INJECTION

B. Zauderer,<sup>1</sup> E. Fleming<sup>1</sup> and W. M. Swift<sup>2</sup>

Coal Tech Corporation  
P. O. Box 154  
Merion Station, PA 19006<sup>1</sup>

Argonne National Laboratory  
9700 South Cass Avenue  
Argonne, Illinois 60439<sup>2</sup>

ABSTRACT

The results of a preliminary experimental study of SO<sub>x</sub>-NO<sub>x</sub> control in a two-stage cyclone coal combustor (2 MW<sub>e</sub>) with limestone injection are presented. The tests were carried out using a finely pulverized West Virginia low-sulfur bituminous coal (0.8% S), an Illinois No. 6 medium-sulfur coal (1.6% S), and an Illinois No. 6 high-sulfur coal (2.7% S). With limestone injection in either the first or second stage of the combustor, SO<sub>2</sub> reductions in excess of 80% were obtained. The sorbent injection tests indicated that the first-stage combustion temperature as influenced by the air/fuel ratio was a major factor in sulfur capture. NO<sub>x</sub> emissions measured at the exit of the second-stage combustor were reduced by up to 55 % over those from single-stage combustion. In addition, the benefits of a staged cyclone combustor for NO<sub>x</sub> control were enhanced when the second-stage gas temperature was minimized, either through increasing second-stage air dilution or by maximizing first-stage carbon conversion.

BACKGROUND AND OBJECTIVES

Recent developments in coal cleaning technology and in the preparation of coal-water slurries have prompted renewed interest in the direct firing of gas turbines with coal-derived fuels, such as partially cleaned fuel gas and coal-water mixtures. Several recent studies have identified the potential economic advantages of these systems over conventional coal-fired power generation (1-3).

An alternative approach to the concept of a coal-fired gas turbine is the direct combustion of the coal in a staged slagging combustor. The slag rejecting combustor has been developed primarily in support of magnetohydrodynamics (MHD) technology. More recently, however, development of the slagging combustor for the control of SO<sub>x</sub> and NO<sub>x</sub> emissions has been considered for application to both the coal-fired gas turbine option and to the retrofit of existing gas and oil-fired boilers.

The concept of the staged slagging combustor for SO<sub>x</sub>/NO<sub>x</sub> control is similar to the LIMB (limestone injection into multi-stage burners) concept being developed for conventional boilers by the U. S. Environmental Protection Agency and the Electric Power Research Institute: namely, staged combustion (fuel-rich first stage) for the control of NO<sub>x</sub> emissions and limestone injection for the control of SO<sub>x</sub> emissions. The added advantage of slag rejection during combustion makes the slagging combustor ideally suited to a wide range of utility and industrial applications, including the coal-fired gas turbine system and gas/oil-to-coal conversions.

Although the amount of data available in the literature is fairly limited, the application of advanced slagging combustors to the control of SO<sub>x</sub>/NO<sub>x</sub> emissions has shown promising results (4,5). In pilot-scale testing of a low NO<sub>x</sub>/SO<sub>x</sub> burner developed by Rockwell International, better than 70% SO<sub>2</sub> reduction, NO<sub>x</sub> emissions below 100 ppm (at 3% O<sub>2</sub>), slag/fly ash removal over 70%, and carbon burnout greater than 99% have been demonstrated in tests with low-sulfur western coals (4). In a few cases, better than 95% SO<sub>x</sub> reduction and zero NO<sub>x</sub> emissions were reported, even when the only calcium used was the calcium inherent in the coal ash.

Equally encouraging results have been reported for the TRW slagging combustor developed in part for MHD applications (5).  $\text{SO}_2$  removals of between 50 and 90% are claimed in limestone injection tests at a Ca/S ratio of 3 for coals with sulfur contents ranging from 0.6 to 2.1%.  $\text{NO}_x$  emissions have ranged from 330 to 450 ppm (at 3%  $\text{O}_2$ ) and carbon conversions were in excess of 99%.

Because of the proprietary aspects of the staged slagging combustor tests just described, details concerning them and the operational parameters that influence the control of  $\text{SO}_2$  and  $\text{NO}_x$  emissions have not been reported. Hence, a series of combustion tests with limestone injection was undertaken in a nominal 2 MW staged slagging combustor at Argonne National Laboratory (ANL). The objective of the tests was to investigate the control of  $\text{SO}_x$  and  $\text{NO}_x$  emissions at conditions simulating direct coal firing into a gas turbine.

## EXPERIMENTAL

### Facility

The test program was conducted in the ANL Fossil Energy Users Laboratory (FEUL), which is a DOE-owned facility constructed to accommodate a wide range of experiments related to coal and oil combustion. The facility has two test legs: one with a combustor capable of burning a variety of liquid fuels (including slurry mixtures) and the other equipped with the two-stage slagging coal combustor used in performing the present work. Each test leg has the necessary independent fuel-feed, support, and control systems. The air compressors, combustion air preheater, effluent control equipment, coolant system, and data acquisition system are shared.

The coal combustor, designed and fabricated by ANL, is illustrated in Fig. 1. The combustor consists of three flanged sections with a fourth section (not shown) downstream of the combustor for instrumentation and gas sampling. The primary combustor consists of two sections: the first section accommodates the combustion air inlet header, coal feed injection nozzle, and a limestone feed port; the second section accommodates a slag tap. Constructed from 24-in. (0.64-m) schedule 20 carbon steel pipe, the primary combustor is refractory lined to a nominal inside diameter of 0.55 m. The overall length is 1.37 m.

As illustrated in Fig. 1, part of the primary combustion air enters axially along the combustor centerline and the remainder enters either tangentially (louvers installed) or radially (louvers removed). The coal to the first stage also enters along the combustor centerline axis. A pintle with an angle of  $45^\circ$  is located at the end of the coal injection line to radially disperse the incoming coal. First-stage limestone injection was accomplished through a port on the front face of the combustor and at an angle that intersected the centerline of the combustor at a point approximately 0.4 m downstream of the coal injector nozzle.

The second stage of the combustor is constructed from 18-in. (0.46-m) schedule standard pipe and is refractory lined to a nominal inside diameter of 0.38 m. The secondary combustion air enters radially through three ports located around the combustor wall. During certain tests, the limestone sorbent was injected through a port just upstream of the secondary air inlet nozzles. The second stage of the combustor is separated from the first stage by a slag baffle with a centerline opening of 0.25 m.

The coal combustor has a nominal thermal input rating of 2 MW, including the sensible heat of the combustion air, which can be preheated up to 1090 K. For the tests that form the subject of this paper, the thermal input to the combustor was in the range 1.1 to 2.4 MW, with most of the tests in the lower end of this range. The split between the primary and secondary combustion air and the ratio of primary axial to swirl air can be independently controlled. For all but one of the tests described herein, the louvers in the primary combustor were not installed; hence, the nonaxial primary combustion air was injected with little or no swirl component.

### Test Coals and Limestone

Three different coals were used in the test program: a West Virginia Alma C seam coal and two Illinois No. 6 seam coals. The results from nominal analyses of the three coals are given in Table 1. The West Virginia coal was primarily selected because nearly 70% of the total sulfur in the coal (0.85 wt %) is organic. It was speculated that this might ensure rapid release of the sulfur from the coal during fuel-rich combustion in the first stage, possibly enhancing the capture of the sulfur by the limestone sorbent. The two Illinois coals were selected because of their higher total sulfur (1.6 and 2.7 wt %) and ash content. A limitation on the limestone hopper capacity and injection rate made testing with a very high sulfur coal (>3 wt %) impractical.

All three coals were delivered to a commercial grinding service where the coals were pulverized and loaded into metal bins with a nominal capacity of 900 kg. The first two coals were pulverized to approximately 98% -200 mesh. The third coal was slightly coarser at 92% -200 mesh. The bins of coal were delivered to ANL and, as needed, automatically loaded into a coal feed storage hopper capable of holding approximately 11,400 kg, a quantity sufficient for combustion tests of 6 to 8 hours.

The limestone used in this work was obtained from Grove Lime Co. in Stephens City, Virginia. This limestone, which contains 95.3 wt %  $\text{CaCO}_3$  and 1.3 wt %  $\text{MgCO}_3$ , was used extensively in the early development of fluidized-bed combustion technology. For this study, the limestone was pulverized to 80% -200 mesh.

### Test Procedure and Conditions

The general procedure adopted for each test was to bring the combustor to the desired initial set of operating conditions over a period of one to two hours. Baseline gas analysis data were then recorded without limestone injection. Limestone would then be injected into the first and/or second stage of the combustor and the composition of the gas exiting the second stage of the combustor would be monitored for changing  $\text{SO}_2$  concentration until a new "steady-state" value of  $\text{SO}_2$  was achieved. The limestone feed would then be discontinued and the  $\text{SO}_2$  level in the combustion gas allowed to return to the baseline value. A change in operating

Table 1. Nominal Analyses of Test Coals (Dry Basis)

Analysis	Coal		
	West Virginia Alma C Seam	Illinois No. 6 (Orient #4 Mine)	Illinois No. 6 (Fidelity #11 Mine)
Test Coal Designation	1	2	3
Moisture, As Received	1.2	4.7	7.0
Proximate Analysis, wt %			
Ash	6.0	9.2	12.3
Volatile Matter	33.8	39.5	35.4
Fixed Carbon	60.2	51.3	52.2
Sulfur	0.85	1.6	2.7
Ultimate Analysis, wt %			
Carbon	81.5	73.9	70.7
Hydrogen	5.2	5.7	4.9
Nitrogen	1.4	1.5	1.4
Sulfur	0.85	1.6	2.7
Ash	6.0	9.2	12.3
Oxygen	5.1	8.2	8.0

parameters would then be made and the above procedure repeated at the new set of conditions. This procedure would generally be repeated three or four times during each combustor test period to obtain data over a range of conditions.

Gas analysis probes were located in the first and second stages of the combustor and also downstream of the second stage. The gas samples were cooled as they were withdrawn from the sampling ports and passed through a gas conditioning system where the sample was filtered free of particulates and dried using a membrane-type dryer. The samples then passed to on-line gas analyzers for CO, O<sub>2</sub>, SO<sub>2</sub>, CO<sub>2</sub>, and NO/NO<sub>x</sub> analysis. The analyzers were calibrated using standard calibration gases at the beginning of each test and at frequent intervals during each test period.

The nominal test conditions and the measured reductions in SO<sub>2</sub> leaving the second stage of the combustion system are listed in Table 2. The parameters varied in the course of this study were the primary and overall air/fuel ratios (stoichiometry), first- and/or second-stage limestone injection, Ca/S molar ratio, and sulfur content of the coal.

## RESULTS

### Combustor Operation

Although the ANL combustor performed very well during the limestone injection tests, the combustor did have a number of performance characteristics that influenced the test program. The ANL combustor, for example, is limited to atmospheric pressure operation, whereas gas turbine applications would require

Table 2. Nominal Test Conditions and Experimental Results

Test Condition	Coal <sup>a</sup>	Coal Feed Rate (kg/h)	Stoichiometry		Limestone Injection		Sulfur Retention (%)
			Primary	Overall	Ca/S	Stage	
2.3-2	1	225	0.5	1.2	3.2	1	23
3.1-2	1	145	0.6	1.7	2.3	1	36
3.1-3	1	145	0.6	1.7	4.4	2	97
4.1-2	1	150	0.7	1.7	2.5	1	49
4.1-3	1	150	0.7	1.7	2.5	2	26
4.2-2	1	150	0.6	1.7	1.0	1	33
5.1-2	2	165	0.9	1.5	3.1	2	49
5.2-2	2	200	0.4	1.2	2.5	1	24
5.3-2	2	140	0.6	1.7	3.6	2	55
5.4-2	2	110	0.9	2.2	4.9	2	31
6.1-2	2	145	1.1	1.7	3.5	2	62
6.2-2	2	135	1.2	1.8	3.6	2	51
6.4-2	2	155	0.6	1.6	2.6	2	72
6.5-2	2	145	0.6	1.7	3.1	2	84
7.1-2	3	170	1.2	1.6	2.6	1	50
7.2-2	3	155	1.2	1.7	2.7	1	44
7.4-2	3	155	0.8	1.7	2.8	2	58
7.5-2	3	155	0.8	1.8	2.9	1	48
8.1-2	3	185	0.6	1.6	2.3	1	55
8.2-2	3	155	0.6	1.7	2.6	1	46

<sup>a</sup> Refer to Table 1 for coal designations

operation at elevated pressure. This was not considered a serious limitation, however, because the identification of parameters affecting  $SO_x/NO_x$  control at atmospheric pressure would generally be useful in any application of the concept.

Also, the available supply of combustion air was insufficient to operate the combustor at high thermal inputs and maintain the high excess air conditions of 180 to 200% required to simulate gas turbine applications. As a result, heat losses to the combustor walls were as high as 15 to 20% of the thermal input. This, together with occasional flameouts of the combustor, resulted in slag solidifying and blocking the slag drain in the first stage of the combustor. As a result, the slag rejection capabilities of the ANL combustor could not be evaluated. Further, it was not possible to determine the quantity of slag and limestone that accumulated in the combustor over the duration of a test. Hence, accurate carbon and sulfur material balances at the individual test conditions could not be determined.

A third factor in the tests, which was not a limitation of the equipment, was the decision to operate the combustor without the swirl louvers in the primary combustor. As a result, the combustor performed essentially as a plug flow unit with respect to both gases and particles. In this respect, the ANL combustor more nearly resembled the Rockwell low  $NO_x/SO_x$  burner cited above.

The high particle loadings and slagging conditions in the primary combustor also made sampling of the first-stage combustion gases very unreliable. Sampling ports would quickly slag over and/or sampling lines plug, making further sampling impossible. While gas sampling lines at the exit of the second stage of the combustor were also prone to plugging, the availability of multiple sampling ports and the ability to periodically clean lines not in use made second-stage gas sampling highly reliable. Hence, the evaluation of combustor performance was largely based on the results of the second-stage gas analysis.

#### Evaluation of Limestone Injection for Sulfur Control

As shown in Table 2, measured reductions in  $SO_2$  emissions ranged from a low of 23% to a high of 97% over the full range of test conditions investigated, including both first- and second-stage sorbent injection. The test results indicate that sulfur capture via limestone injection is a complex phenomenon. Since, however, the air/fuel ratio in the primary combustor has a significant influence on both (1) the rate of sulfur release from the coal and the ratio of  $H_2S$  to  $SO_2$  formed during fuel-rich combustion, and (2) the resulting first- and second-stage gas temperatures, it was found that the  $SO_2$  reduction during sorbent injection exhibited a noticeable dependency on the first-stage air/fuel ratio.

Figure 2 is a plot of the effect of first-stage combustion stoichiometry on reducing  $SO_2$  during first-stage limestone injection. In producing the plot, the sulfur reduction data in Table 2 were normalized to a Ca/S ratio of 3.0 assuming a linear dependency. Figure 2 also includes some data from injection tests with a hydrated limestone in a related series of tests. The results indicate the optimum reduction in  $SO_2$  occurred at an air/fuel stoichiometric ratio in the range 0.5 to 0.7. This is considered to be largely a thermal effect in that higher first-stage air/fuel ratios resulted in excessively high first-stage gas temperatures ( $>1900$  K, calculated). The apparent low reduction in  $SO_2$  during first-stage injection at an air/fuel ratio of 0.4 is not fully understood.

Figure 3 is a similar plot of  $SO_2$  reduction as a function of first-stage air/fuel stoichiometry for second-stage sorbent injection. The observed dependency is generally the same as for first-stage sorbent injection. This may have resulted from the selection of the second-stage sorbent injection location, which was slightly upstream of the secondary air injection. Hence, the first-stage gas temperatures may also have influenced sorbent performance during second-stage injection.

Although the data are fairly limited and exhibit a high degree of scatter, the general results are encouraging in that the overall measured sulfur reductions in excess of 80% at Ca/S ratios on the order of three are consistent with the results reported for the Rockwell and TRW combustors. Considerably more data are needed, however, to fully understand the complex effects of operating parameters on combustor performance.

#### NO<sub>x</sub> Control

Independent of coal type, the staged combustion for NO<sub>x</sub> control exhibited two different dependencies on the first-stage air/fuel ratio, as shown in Fig. 4. The upper curve, which corresponds to less reduction in NO<sub>x</sub> emissions, is representative of tests where the second-stage bulk gas temperature was too high (>1750 K) and/or where carbon conversion in the first stage was relatively low (<70%), leading to excess carryover of fuel-bound nitrogen in the char to the oxidizing second stage of the combustor. Greater NO<sub>x</sub> reductions occurred when either the second-stage temperatures were lower than 1650 K and where carbon conversion in the fuel-rich first stage was high enough (>70%) to allow release and conversion of the fuel bound nitrogen to N<sub>2</sub>.

In both cases, however, measured second-stage NO<sub>x</sub> was reducible to less than 100 ppmv at 15% O<sub>2</sub> by controlling the first-stage stoichiometry. This corresponds to 300 ppmv at 3% O<sub>2</sub>, a value that is again consistent with the results reported by TRW and Rockwell for their combustors.

#### CONCLUSIONS

The results of the preliminary investigation of limestone injection in a staged slagging combustor for the control of SO<sub>x</sub> and NO<sub>x</sub> emissions are very encouraging. Sulfur retentions were in excess of 80% and NO<sub>x</sub> emissions were as low as 100 ppmv (at 15% O<sub>2</sub>). Considerably more testing is required, however, to fully understand the complex mechanisms controlling the sulfur retention process. The results are consistent with those reported for the TRW and Rockwell slagging combustors.

#### ACKNOWLEDGMENTS

We gratefully acknowledge the funding of this work by the U. S. Department of Energy Morgantown Energy Technology Center. We would also like to acknowledge F. G. Teats, H. A. Myers, L. N. Ruppert, and R. A. Molson of Argonne National Laboratory who participated in the operation of the slagging combustor.

#### REFERENCES

1. C. A. Cincotta, "Gas Turbine Systems Research and Development Program," U. S. Department of Energy Report No. DOE/MC/20315-1767 (Sept. 1984).
2. D. A. Horazak et al., "Gas Turbine Systems, Research and Development Program, Final Report," U. S. Department of Energy Report DOE/MC/20324-2033 (Feb. 1986).
3. A. J. Giramonti, "Gas Turbine Systems for Operation on Coal-Derived Fuels, Final Technical Report," U. S. Department of Energy Report No. DOE/MC/20241-T12 (July 1985).
4. O. W. Dykema, "Development of a Low NO<sub>x</sub>/SO<sub>x</sub> Burner," paper presented at the 35th Canadian Chemical Engineering Conference, Calgary, Canada (Oct. 1985).
5. TRW, "Design and Application of TRW's Entrained Coal Combustor," TRW promotional literature, TRW Inc., Redondo Beach, CA (May 1986).

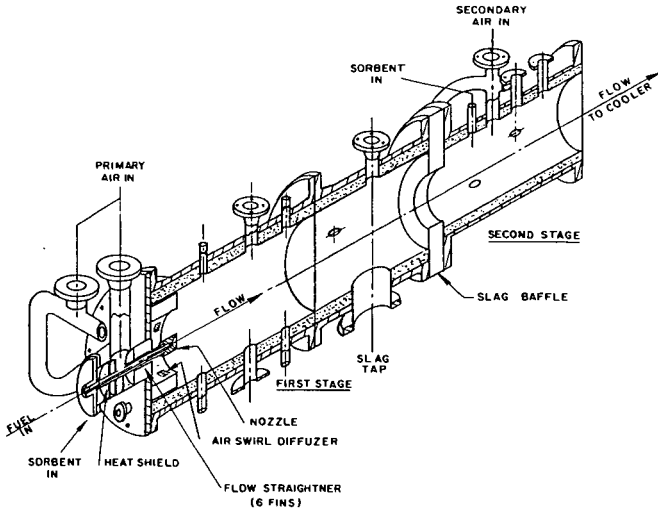


Fig. 1. Schematic of the ANL 2-Stage Slagging Combustor

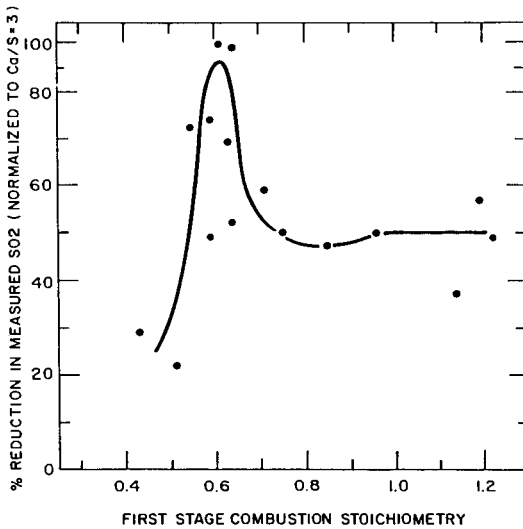


Fig. 2. Measured Reduction in SO<sub>2</sub> with First Stage Limestone Injection

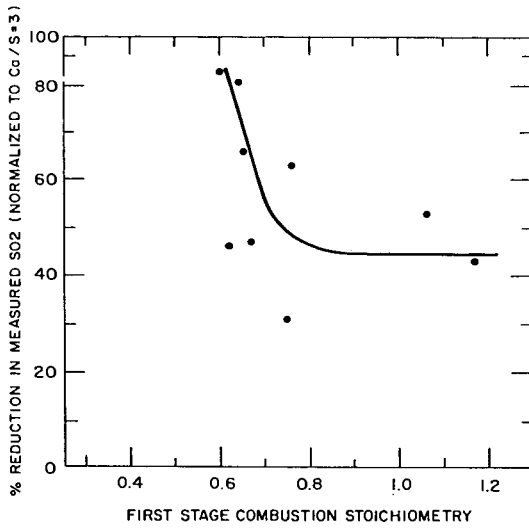


Fig. 3. Measured Reduction in SO<sub>2</sub> with Second Stage Limestone Injection

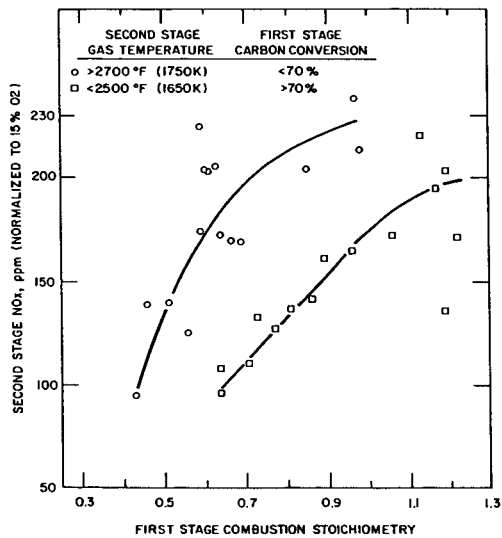


Fig. 4. Measured NO<sub>x</sub> Emissions during Limestone Injection Tests

## SULFUR IMPACT ON COAL-FIRED GAS TURBINES

C. S. Wen and L. H. Cowell

Solar Turbines Incorporated  
P.O. Box 85376  
San Diego, CA 92138-5376

### ABSTRACT

Solar Turbines Incorporated is conducting a DOE-sponsored program to develop coal-fired cogeneration gas turbines. Solar's approach emphasizes the direct combustion of coal in both dry pulverized form, as well as a coal-water slurry, using a rich-lean, two-stage slagging combustor (TSSC). Under TSSC conditions,  $H_2S$  is formed in the atmosphere surrounding burning particles, and may persist in the rich zone, but the dominant sulfur species in the exhaust gas of the lean secondary zone is  $SO_2$ . A sulfur distribution based on TSSC combustion of eastern Kentucky bituminous coal showed that up to 90% of the sulfur was converted to oxides while the remainder combined largely with the ash. The studies made to date have also indicated that over 50% of the alkalis introduced with this coal have been retained with the slag in the primary combustion zone.

### INTRODUCTION

Sulfur is one of the key elements in coal fuel specifications which requires particular attention. Emissions of sulfur oxides as well as the condensation and/or deposition of corrosive sulfates on blades are major problems in the development of coal-fired gas turbines. Substantial sulfur removal will be needed in order to meet environmental standards and to reduce the interaction between sulfur and alkali compounds. Several processes exist so that clean-up of sulfur is feasible, but they are expensive. Economic considerations will continue to force greater usage of minimally cleaned coal (i.e., coal with high ash and/or sulfur content). An understanding of the role of sulfur during coal combustion and its impact on gas turbines will benefit control of sulfur emissions and corrosion. This paper reviews the role of sulfur in two-stage slagging coal combustion and discusses its impact on coal-fired gas turbines.

### EXPERIMENTAL

Combustion tests were performed using a two-stage slagging combustor shown in Figure 1. The following test procedure has been used for all combustor tests conducted in this study. The combustor was started using #2 diesel to light off and establish the desired test conditions. When the wall temperatures were stabilized, a gentle transition to the coal-water mixture was accomplished by turning on the coal fuel and turning off the diesel until the combustor was operating on coal-water mixture only.

In Solar's two-stage slagging combustor, the coal fuel is injected via a series of angled injectors with air into the primary zone where the fuel-rich coal combustion takes place rapidly. The reacting jet flow impinges on the primary centerline and is then constrained by the impact dome and the refractory-lined walls to reverse and exit between the incoming flows. A strong toroidal vortex is formed surrounding the main jet and this acts primarily

as a particle retaining system. Particles smaller than some critical size follow the flow streamlines and escape. Other particles, which are larger than some upper limit, are deposited and form slag on the dome and walls. The molten slag is then collected in a slag pit.

The exhaust raw gases from the primary zone which are relatively free of particles pass into the secondary zone where remaining, unburned chars are then mixed with secondary air where combustion is completed to form desirable combustion products. The hot gas leaving the combustor enters a separator to separate particulate fly ash. Reaction temperature at the primary zone is above 2700°F with estimated temperature in secondary zone of 1600 to 1800°F.

Two coal-water fuels were formulated with high volatile bituminous, eastern Kentucky coals (Kentucky #5 and Elkhorn #2 mines) from AMAX Extractive R & D. Fuels were obtained in the form of aqueous slurries and prepared by physical beneficiation. Coals were cleaned in a static-bath dense-medium separator for refusing sinks and collecting clean coal floats. The float coals typically contained less than 3.9% ash and had calorific heating-values above 14,400 Btu/lb on a dry basis. Stable, pumpable slurries of coal and water were prepared by grinding the dense-medium float coal further in a ball mill to achieve a desired particle size. The finish-ground slurry was blended to with 1.2 to 1.4% of dispersant. A list of fuel properties appears in Table 1.

TABLE 1

Coal-Water Slurry Fuel Characteristics

<u>CWM Batch</u>	<u>A</u>	<u>C</u>
Coal Content of Fuel (wt%)	59.98	54.1
Ash Content of Fuel (st%)	1.85	2.1
Coal Particle Top Size (micron)	44	100
Gross Heating Value (But/lb)	14,518	14,397
Viscosity of Fuel @ 100 sec <sup>-1</sup> (Cp)	400	300
Mean Size, micrometers	----	14.1
Dispersant (wt%)	1.2	1.4
<u>Prominate Analysis of Coal (wt%)</u>		
Ash	3.08	3.88
Volatiles	38.49	36.10
Fixed Carbon	58.43	60.02
<u>Ultimate Analysis of Coal (wt%)</u>		
Carbon	84.00	77.14
Oxygen (by difference)	7.81	14.34
Hydrogen	5.63	5.80
Nitrogen	1.64	1.82
Sulfur	0.92	0.90
<u>Forms of Sulfur (Dry Coal Basis)</u>		
Total Sulfur (wt%)	0.92	0.90
Sulfate	0.05	0.04
Pyritic	0.06	0.01
Organic	0.81	0.85

Sulfur content in all three CWM Fuels are approximately 1 wt% on a dry coal, ash free basis. Physical cleaning removed most of the inorganic sulfur, but left behind organic sulfur. A detailed analysis of sulfur forms (Table 1) further indicated that only trace amounts of sulfate (0.05 wt%) and pyritic sulfur (0.01-0.06%) remained in the sample, the majority was organic sulfur (0.80%). The ash contents in the samples range from 1.9 to 2.1 wt% on a fuel basis. The ash composition analysis (Table 2) indicates the acidic mineral properties in the coal fuels. The base-to-acid ratio is 0.28 for A and 0.18 for C, respectively. The relative amount of the basic and acidic constituents in the ash can be used as a means of predicting the ash fusion temperatures and the slag properties.

TABLE 2  
Ash Slagging Properties

<u>CWM Batch</u>	<u>A</u>	<u>C</u>
<b>Ash Composition</b>		
SiO <sub>2</sub>	43.40	53.0
Al <sub>2</sub> O <sub>3</sub>	27.80	28.1
Fe <sub>2</sub> O <sub>3</sub>	14.10	11.6
CaO	3.33	1.86
MgO	0.816	0.61
Na <sub>2</sub> O	1.37	0.91
K <sub>2</sub> O	0.723	1.03
TiO <sub>2</sub>	2.10	2.07
MnO <sub>2</sub>	0.066	0.065
P <sub>2</sub> O <sub>5</sub>	0.406	0.314
V <sub>2</sub> O <sub>5</sub>	0.078	0.06
PbO	0.072	0.04
<b>Ash Fusion Temperatures (°F)</b>		
<b>Oxidizing/Reducing</b>		
Initial Deformation	2375/2308	2670/2460
Softening	2700/2543	+2700/2605
Hemispherical	+2700/2565	+2740/2650
Fluid	+2700/2698	+2700/2700
Base/Acid Ratio	0.28	0.18
Silica Ratio	79.6	70.4
Viscosity From Equivalent Silica @ 2600°F (poise)	169	575
T <sub>250</sub> Temperature (°F)	2527	2790
Fouling Index	0.38	0.18
Slagging Index	0.26	0.17

## RESULTS AND DISCUSSION

### The Fate of Sulfur in Slagging Coal Combustion

Upon injecting a coal-water slurry into the primary zone, the coal slurries are atomized and undergo a rapid devolatilization followed by a burnout of the char (Refs. 1,2). Figure 2 illustrates a simplified scheme involved in the combustion of a coal particle. The volatile organic and inorganic sulfur species are vaporized from the burning coal particles and are transported to the surface by molecular diffusion. The reducing atmosphere surrounding a burning particle allows the reduction to take place on volatile species, but as soon as the vapors diffuse away from the burning particle, the oxidizing nature of the bulk gas stream would oxidize sulfur species to their highest oxidation state. The rate of sulfur release from coal is very fast from both sulfur bound in the organic matrix and sulfur in discrete minerals even under the local reducing conditions. Recent thermal analysis (Ref. 3) indicated that catalysis or acceleration of coal combustion occurs by its pyrite impurities due to the fact that FeS<sub>2</sub> promotes self-heating and spontaneous combustion of coal.

Under rich zone reducing conditions, pyritic sulfur (pyrite or marcasite, FeS<sub>2</sub>) decomposes to sulfur (S<sub>2</sub>), hydrogen sulfide (H<sub>2</sub>S), and carbonyl sulfide (COS) (Ref. 4). Elemental sulfur is given off at 475°C (887°F) from iron disulfide (pyritic sulfur) with accompanying reduction to FeS (Ref. 5):



The rate of this reaction becomes large above 1000°F. In addition, the decomposition of carbon-hydrogen bonds in coal will occur at relatively low temperatures and yield hydrogen for reduction of FeS<sub>2</sub>. Mineral matter such as silicates or basic minerals in coal may catalyze the reduction of FeS<sub>2</sub> (Ref. 6).



and



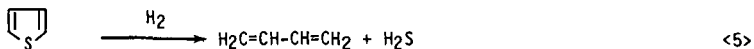
Reaction <2> becomes important above 930°F but reaction <3> is slow even at 1470°F (Ref. 7). The combustion product such as CO can also react with FeS<sub>2</sub> according to:



but the reaction is slow below 1470°F (Ref. 7).

The rich zone devolatilization of organic sulfur is not well documented, however, it is believed that hydrogen sulfide (H<sub>2</sub>S) is the principal product, accounting for typically 90% of the evolved sulfur, with contributions of COS, CS<sub>2</sub>, and S<sub>2</sub> (Ref. 4). However, these species will turn to higher oxidized states, SO<sub>x</sub>, as they are exposed to the primary air stream. Thiophenes represent the dominant organic-sulfur in the coal. Thiophene itself is stable

up to 840°F and dibenzothiophene is stable to at least 1020°F (Ref. 7).  
Reduction of thiophene proceeds according to:



and dibenzothiophene reacts according to:



Sulfur release during coal devolatilization can be inhibited by inherent capture by coal-bound mineral matter, particularly calcium oxides and sodium oxides (Refs. 4,8):



In fuel lean flames and oxidizing atmospheres, over 90% of the sulfur is converted to SO<sub>2</sub> while the remaining several percent exist as SO<sub>3</sub> (Ref. 4). Hydrogen sulfide (H<sub>2</sub>S) which is originally released from pyritic and organic sulfur in the primary zone is rapidly converted to SO<sub>2</sub> in the lean secondary via the sequence (Ref. 9):



The capture of sulfur dioxide with the calcium-based coal minerals could also occur as



but, calcium sulfate is stable only at temperatures below 2200°F (Ref. 10).

Total sulfur conversion to the oxide is generally high in pulverized coal combustion, the remainder largely combining with the ash. Table 3 compares major compositions between a piece of slag retained in the slag pit of primary zone and ash particulates collected from the exhaust gas. A significant amount of sulfur associated with ash particulates was observed, compared to a trace retained in the slag. A sulfur distribution in coal combustion based on TSSC combustion tests of eastern Kentucky bituminous coal is shown, in Table 4 which up to 91% of sulfur was converted to oxides.

TABLE 3  
Composition Analysis (a)

Composition, wt. %	Slag (Primary Zone)	Ash (b) Particulates
SiO <sub>2</sub>	43.7	44.4
Al <sub>2</sub> O <sub>3</sub>	32.6	22.6
TiO <sub>2</sub>	2.04	2.16
Fe <sub>2</sub> O <sub>3</sub>	11.6	9.34
CaO	1.72	1.25
MgO	0.70	0.56
SrO	0.22	0.12
K <sub>2</sub> O	1.07	1.04
Na <sub>2</sub> O	0.75	1.18
P <sub>2</sub> O <sub>5</sub>	0.12	0.39
Cr <sub>2</sub> O <sub>3</sub>	0.08	0.39
CuO	0.02	0.08
MnO <sub>2</sub>	0.10	0.09
NiO	0.09	0.45
PbO	0.03	2.90
V <sub>2</sub> O <sub>5</sub>	0.05	0.06
SO <sub>3</sub>	0.07	11.3

(a) Using batch 'C' CWM as feed  
(b) Carbon-free basis

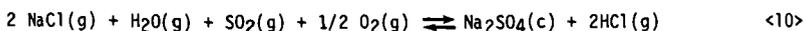
TABLE 4  
Sulfur Distribution in Coal Combustion (a)

Total Sulfur in Fuel	Sulfur Out		
	S Adsorbed as Sulfates in Ash Particulates	(b) S Retained in Slag	S Exhausted as SO <sub>x</sub>
0.63 lb S/10 <sup>6</sup> Btu	0.06 - 0.23	0.001	0.40 - 0.57
100%	9.2 - 36.8%	0.2%	63.0 - 90.6%

(a) Based on an Eastern Kentucky coal having 0.92% wt. S dry coal basis and 8708 Btu/lb CWM where CWM has 60% wt. coal loading (Batch A feed)  
(b) Slag based on an average 70% wt. of slag retention.

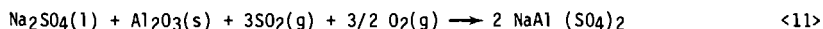
The Effect of Sulfur on Corrosion and Deposition

In combustion, sodium and potassium are likely to be released from coal as the most volatile species, i.e. chloride or hydroxide. However, in a combustion environment at temperatures below about 1800°F, a significant proportion of the vapor alkali will be converted to condensed phase sulfate (Ref. 11).



The estimated residence time required for evaporation of sodium chloride and its conversion to sulfate is about 2 sec. (Ref. 12). Depending on conditions of temperature, pressure, and gas composition, the sulfate could condense onto entrained particulates or nucleate to form an aerosol.

Corrosion could be initiated when the alkali sulfates condense on the metal due to the temperature drop through the turbine and due to the contact with the cooled turbine blades resulting in an increase in alkali sulfate flux to attack the protective oxide (Ref. 13).



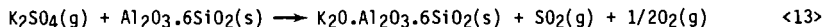
The protective oxide scale (e.g.  $\text{Al}_2\text{O}_3$ ) is destroyed and the subsequent reformation is inhibited.

Corrosion may also occur through an increase in the acidic component ( $\text{SO}_3$ ) to react with protective  $\text{Al}_2\text{O}_3$  scale on steel without the presence of alkali (Ref. 13).



Increased transport of S through the oxide scale will occur and sulfate phase will be formed below the  $\text{Al}_2\text{O}_3$  scale.

The actual mechanism of corrosion in coal-fired gas turbines is not completely understood. Alkali sulfate vapor released during combustion could partially be adsorbed by the aluminosilicates, inherent coal minerals, which are efficient "getters" for alkali metal sulfates (Refs. 11, 14).



The slag removal feature of a slagging combustor can also greatly reduce the impact of coal corrosive materials. Over 50% of the alkali introduced in coal feed can be expected to be removed as slag in the primary combustion zone (Table 5). The short residence times in gas turbine combustor, and particularly in the hot end zone could further reduce alkali metal vaporization. Thus, a precombustion cleaning of coal in conjunction with unique operating features of the slagging combustor may greatly reduce the corrosion severity potential of coal.

The formation mechanism of deposited matter on turbine blades or vanes is believed to start with molten ash or fly slag sticking to the metal surface. Chemical analyses of the exhaust deposit and the slag (Table 6) indicated that the deposited matter has almost identical chemical compositions as the slag collected in the slag pit. Neither contained any significant amount of sulfur or water-soluble alkali sulfate salts. Petrographically, the two materials were similar except that the exhaust deposit contained gas bubbles. X-ray diffraction and electron microprobe studies showed that the two samples consisted basically of a glass phase containing bladed mullite. A spinel-like phase was seen in the deposit material. The mullite and spinel both probably crystallized during solidification of the melt. It has been speculated recently that alkalis may never escape from the coal aluminosilicate coordination environment (Ref. 4). Based on the decomposition mechanisms of coal alkali minerals (illite) as illustrated in Figure 3, surface moisture and mineral water are desorbed at approximately 300°F (150°C), dehydration

takes place between 890-1100°F at which temperature two water molecules are split off from the four hydroxide units, and somewhere between 1560-1832°F decomposition of the anhydride take place to form spinel ( $Al_2FeMg_{1.5}O_6$ ) and glass ( $K_{1.5}Si_{16.5}Al_{1.5}O_6$ ). However, at higher temperatures ( $\approx 3000^\circ F$ ), such as slagging conditions, the spinel can redissolve into the melt, and glass phases (e.g. mullite and cristobalite) may be reformed while gaseous alkali species can be released.

### CONCLUSIONS

The sulfur content of the coal introduced into the gas turbine combustion system dictates the degree to which sulfur capture compounds or hot-gas cleanup must be utilized. The coal desulfurization to a level acceptable for emissions and corrosion control is a key issue in the development of direct coal-fired gas turbines. Uncontrolled sulfur emissions is a direct function of the sulfur level in the coal and will exceed current NSPS levels. Sulfur compounds in the combustor exhaust also have the potential to cause deposition and corrosion on turbine blades. The availability of naturally occurring low-sulfur coal is limited as is the applicability of coal beneficiation. Physical cleaning will remove most of the inorganic sulfur, but will leave behind organic sulfur. Hot aqueous caustic leaching and molten alkali desulfurization can remove part of the organic sulfur, but appear to be expensive. There is also a potential risk of losing volatile and increasing alkali levels in the feed.

Therefore, in the near-term, sulfur control via sulfur retained in rejected slag and sorbent capture during coal combustion represent important routes for development. Coal beneficiation and post combustion gas clean-up upstream of the turbine are alternatives to in-situ sulfur control in the combustor, although the cost effectiveness of these options is questionable. Introduction of lime or dolomite sorbent for sulfur capture will also impact on ash fusion and deposition as well as on inherent coal mineral "getters" for alkali.

TABLE 5  
Slag Retention Properties

Ash or Slag Composition	CWM Batch					
	A			C		
	CWM Feed	Slag	% Removal <sup>(a)</sup> in Slag	CWM Feed	Slag	% Removal <sup>(b)</sup> in Slag
SiO <sub>2</sub>	43.40	46.52	75	53.0	48.7	60
Al <sub>2</sub> O <sub>3</sub>	27.80	28.38	71	28.1	32.6	75
TiO <sub>2</sub>	2.10	1.39	45	2.07	2.04	64
Fe <sub>2</sub> O <sub>3</sub>	14.10	13.71	68	11.6	11.6	65
CaO	3.33	3.54	76	1.86	1.72	60
MgO	0.82	0.47	41	0.61	0.70	74
Na <sub>2</sub> O	1.37	1.09	54	0.91	0.75	53
K <sub>2</sub> O	0.72	0.54	56	1.03	1.07	67
P <sub>2</sub> O <sub>5</sub>	0.41	0.27	50	0.31	0.12	25
	94.05	95.91		99.49	99.30	

(a) Based on 70% slag retention from Batch 'A' CWM

(b) Based on 65% slag retention from Batch 'C' CWM

TABLE 6

Comparison of Compositions between Deposited Material and Slag (a)

Composition, wt.%	Deposited Material	Slag
SiO <sub>2</sub>	51.4	52.3
Al <sub>2</sub> O <sub>3</sub>	29.5	29.2
TiO <sub>2</sub>	1.61	1.53
Fe <sub>2</sub> O <sub>3</sub>	12.0	11.7
CaO	1.95	1.79
MgO	0.66	0.62
SrO	0.23	0.22
K <sub>2</sub> O	0.98	0.99
Na <sub>2</sub> O	0.98	0.96
P <sub>2</sub> O <sub>5</sub>	0.31	0.13
Cr <sub>2</sub> O <sub>3</sub>	0.06	0.07
CuO	0.04	0.01
MnO <sub>2</sub>	0.07	0.07
NiO	0.13	0.09
PbO	0.01	0.01
V <sub>2</sub> O <sub>5</sub>	0.05	0.05
SO <sub>3</sub>	0.07	0.19
Soluble Salts, wt%		
Na <sub>2</sub> O	0.014	0.010
K <sub>2</sub> O	0.004	0.003
SO <sub>3</sub>	0.012	0.012

(a) Deposition run using Batch 'C' CWM feed

ACKNOWLEDGEMENTS

The work described in this paper was performed by Solar Turbines Incorporated under a program sponsored by DOE-Morgantown Energy Technology Center with Mr. Nelson F. Rekos, Jr. as Project Manager.

REFERENCES

1. L.K. Carpenter, F.W. Crouse, Jr., and J.S. Halow, "Coal-Fueled Turbines: Deposition Research", ASME Paper No. 85-GT-213, 1985.
2. R.W. Bryers, "The Impact of Segregated Mineral Matter on Fireside Deposits", Proceedings of 2nd Annual Pittsburgh Coal Conference, Sept. 16-20, 1985, p. 695.
3. E.J. Badin, "Coal Combustion Chemistry - Correlation Aspects", Elsevier, New York, 1984, p. 184.
4. A.R. Garman, G.A. Simons, and A.A. Boni, "Surrogate Fuel Exploratory Tests", DOE/MC/20486-1711, 1984.
5. P.C. Malte, "Mechanisms and Kinetics of Pollutant Formation During Combustion", Washington State University, Thermal Energy Laboratory, Report No. 77-24, 1983.

6. L. Robinson, "Doal Minerals Affect Sulfur in Processing", Hydrocatbon Processing, Nov. 1978, p. 213.
7. A. Attar, "Chemistry, Thermodynamics, and Kinetics of Reactions of Sulfur in Coal-Gas Reactions: A Review", Fuel, 57, 201, 1978.
8. H.S. Muralidhara and J.T. Sears, "Effect of Calcium on Gasification", Coal Processing Technology, Vol. 2, 1976, p. 22.
9. J.C. Kramlich, P.C. Malte, and W.L. Grosshandler, "The Reaction of Fuel-Sulfur in Hydrocarbon Combustion", 18th International Symposium on Combustion, Comb. Institute, 151, 1981.
10. J. Bettelheim and B.H.M. Billenge, "Industrial Air Pollution Handbook," (A.A. Parker, ed.), McGraw-Hill, London, 1978.
11. L.A. Scandrett and R. Clift, "The Thermodynamics of Alkali Removal from Coal-Derived Gases", J Inst. of Energ, 57, 391, 1984.
12. E. Raask, "Mineral Impurities in Coal Combustion", Hemisphere Pub. Corp., New York, 1986, p. 202.
13. E.J. Badin, "Coal Combustion Chemistry - Correlation Aspects", Elsevier, NY, 1984, p. 46 and p. 112.
14. S.G. Kimura, "Alkali Species Characterization for Coal-Fueled Gas Turbine", Final Report, DE-AC21-85MC22164, 1986.

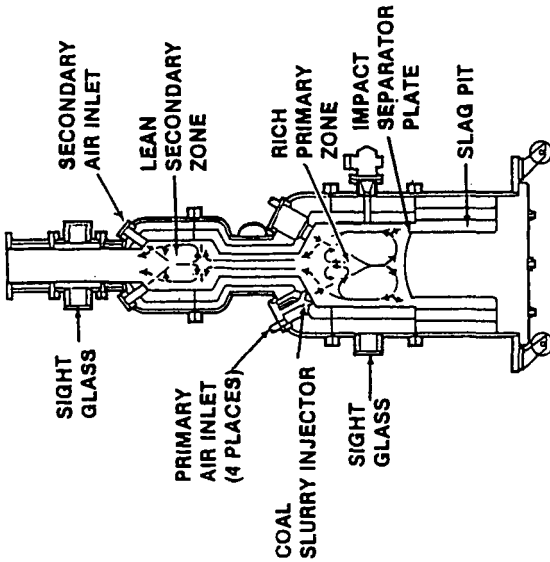


Figure 1. Solar's Two Stage Slagging Combustor

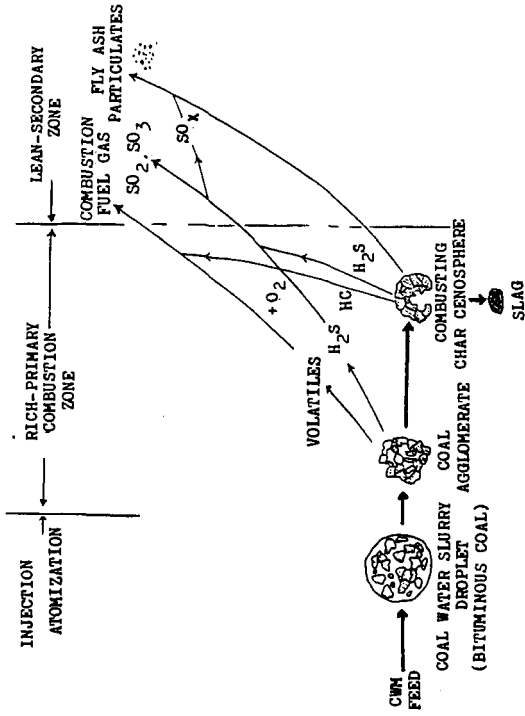


Figure 2. CWM Burnout and Sulfur Routes in Combustion

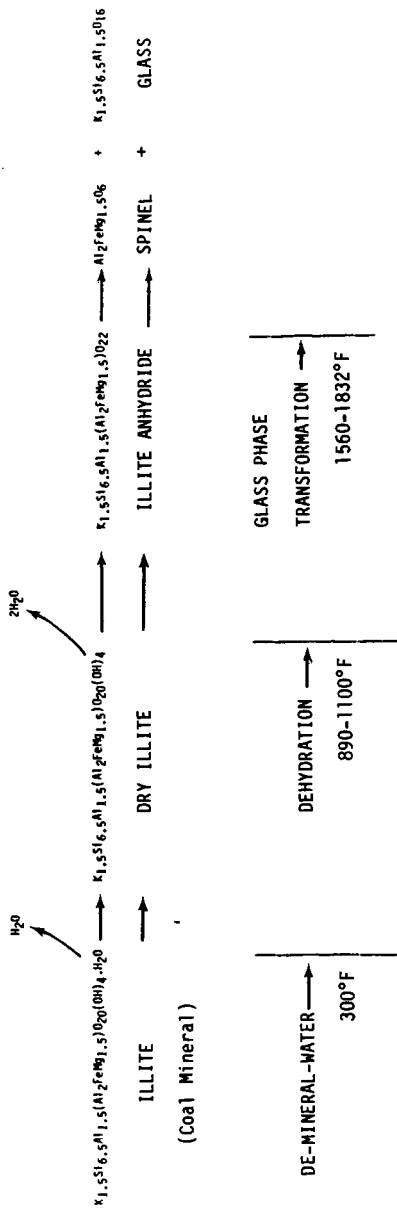


Figure 3. Decomposition Mechanisms of Coal Alkali Mineral

## SOX Control In Fluid Catalytic Cracking

Z. C. Mester, E. J. Aitken and P. G. Ritz

Unocal, Division of Science and Technology, Brea, CA 92621

### Introduction

Refineries today face a growing challenge to stay in compliance with the increasingly stringent environmental regulations. In fluid catalytic cracking (FCC), which is the largest volume gasoline producing process, the main air pollutants are carbon monoxide, sulfur oxides (SOX), nitrogen oxides (NOX), hydrocarbons and particulates.

At high regenerator temperature operation SOX emissions represent the greatest problem, therefore SOX emission control is of primary importance. As an example, in California the current standard is 60kg SO<sub>2</sub> per 1000bbl feed which is less than half of the previous 130kg SO<sub>2</sub> per 1000bbl feed limit. The EPA also proposed a 90% SOX reduction for FCC operations, but this regulation is still pending (1). The following options are available to the refinery to control SOX emissions: selection of low sulfur feed, flue gas scrubbing, feed hydrotreating and catalytic SOX reduction. The first method is of limited use because low sulfur feeds are not easily available. Flue gas scrubbing is effective but also capital intensive and may pose liquid or solid waste disposal problems. Hydrotreating has the advantage of not only reducing SOX but improving liquid yields too. In the long run this process offers economic advantages, however the high initial investment is a major drawback for many refineries. During the last few years catalytic SOX control emerged as an effective and economically attractive alternative to the above methods (2, 3, 4, 5).

SOX catalysts convert sulfur oxides, formed during coke burn-off in the regenerator, to solid sulfur containing species and release them as hydrogen sulfide in the reactor. This step rejuvenates the catalyst which is then recirculated to the regenerator and the cycle is repeated. In the following we present results of our investigation on the effectiveness of some SOX catalysts using TGA, fluidized bed reactor and in-situ infrared spectroscopy.

### Results

The following materials were investigated for SOX performance: alumina, rare earth oxide/alumina, and rare earth oxide/alumina/cobalt oxide. The materials were first evaluated by TGA analysis. The samples were exposed to a gas mixture containing 2000 ppm SO<sub>2</sub>, 4% O<sub>2</sub> and nitrogen. The weight gain of the samples were monitored as a function of the temperature with a 10°C/min ramp between 25 - 750°C. The materials were then cooled down to 25°C under nitrogen; hydrogen was introduced and the temperature was ramped as above. This adsorption-reduction cycle was repeated several times to assure good reproducibility. Each sample started to adsorb SOX appreciably around 300°C. Percent weight gains at 750°C were as follows: 2% for alumina, and 5% for the other two samples. The adsorption curves for the rare earth containing samples passed over a maximum around 650-700°C indicating decomposition beyond this temperature range. In the reduction step the cobalt containing sample started to reduce at the lowest temperature (500°C), followed by rare earth oxide/alumina and alumina (540°C).

The next stage in evaluating SOX materials involved the use of a bench scale fluid bed reactor. In a typical experiment the sample (< 5g) was fluidized by a mixture of SO<sub>2</sub> (2000 ppm) / O<sub>2</sub> (3%) / N<sub>2</sub> (balance) at a temperature which corresponded to FCC regenerator temperatures (650-750°C). After a fixed length of reaction time

(2 hrs), the samples were analyzed for sulfur. The unit can be used to simulate the entire catalytic cycle where the gettinger step is followed by hydrogen reduction and steam injection at temperatures corresponding to those of typical FCC operations. The SOX gettinger experiments at 730°C showed that alumina was the weakest adsorber. The rare earth/alumina and the cobalt impregnated samples had about the same gettinger capacity, each adsorbed 2.5 times more sulfur than alumina alone. When the SOX loaded materials were reduced in a flow of hydrogen at 540°C for 0.5 hrs, the cobalt containing sample regained 62% of its original gettinger capacity, followed by alumina (55%) and rare earth/alumina (40%).

In order to assess the relative rates of SOX uptake and H<sub>2</sub> reduction, in-situ infrared experiments were conducted. In these experiments the formation of surface sulfates - by exposure of the material to an SO<sub>2</sub> (1500 ppm) / O<sub>2</sub> (3%) / N<sub>2</sub> (balance) gas mixture - and the elimination of the surface sulfates - by exposure to H<sub>2</sub> - were followed by monitoring the appropriate band as a function of time. The SOX adsorption step took place at 600°C and the H<sub>2</sub> reduction was carried out at 525°C. The surface sulfur oxide species formed on the materials were predominantly sulfates. For the rare earth containing samples rare earth sulfates were detected as indicated by the appearance of two broad bands centered at 1125 cm<sup>-1</sup> and 1050 cm<sup>-1</sup>. However, a sulfite species also formed on alumina, as evidenced by a band at 1040 cm<sup>-1</sup>, in addition to a sulfate like species (1370 cm<sup>-1</sup>). The SOX gettinger rate, measured by the increase in intensity of the surface S-O stretching vibrational bands, was dependent upon the composition of the materials. For alumina the adsorption rate decreased drastically after approximately 8 min of SO<sub>2</sub> exposure indicating that maximum gettinger capacity was being reached. The gettinger rates (normalized adsorption intensity per minute) in the first 8 min of exposure were: 0.0035 for the sulfate band and 0.0045 for the sulfite band of alumina; 0.016 for the rare earth oxide/alumina and rare earth oxide/alumina/cobalt oxide samples. During the hydrogen reduction step the time required to reduce the band intensity to 50% of the intensity prior to hydrogen exposure decreased in the order: 12 min (sulfate band for alumina), 9 min (sulfite band for alumina), 9 min (sulfate band for rare earth oxide/alumina) and 2 min (sulfate band for rare earth oxide/alumina/cobalt oxide).

## Conclusions

TGA proved to be a useful method to reveal the SOX gettinger potential and regenerability of the materials in a wide temperature range. The fluid bed experiments were useful in evaluating the materials under more realistic conditions related to FCC operations. The infrared study helped to establish the relative rates of SOX gettinger and reductions by hydrogen. The results showed that the rare earth containing materials were superior to alumina in SOX gettinger. It was also shown that cobalt had an accelerating effect in restoring catalyst activity.

## References

- (1) Federal Register, Vol 49, No. 11, January 17, 1984, pp 2058 - 2074.
- (2) Wall, J. D., Hydrocarbon Processing, October 1984, p 45.
- (3) Magnabosco, L. M., Powell, J. W., Katalistiks Fourth Annual Symposium, 1983 Amsterdam.
- (4) Habib, E. T., Oil and Gas Journal, Augustus 8, 1983, p 111.
- (5) Aitken, E. J., Baron, K., McArthur, D. P., Mester, Z. C., Katalistiks Sixth Annual Symposium, 1985 Munich.

## CATALYTIC SOX ABATEMENT OF FCC FLUE GASES

Alak A. Bhattacharyya, Gerald M. Woltermann, Jin S. Yoo(1),  
John A. Karch, and William E. Cormier

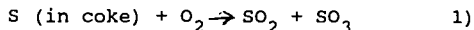
Katalistiks International Inc., 4810 Seton Drive,  
Baltimore, Maryland 21215

### ABSTRACT

A cerium containing magnesium aluminate spinel catalyst is used as a SOx emission reducing catalyst in the hydrocarbon cracking catalyst regeneration zone. In the regeneration zone this catalyst oxidizes the SO<sub>2</sub> to SO<sub>3</sub> and chemisorbs it as sulfate and releases it as H<sub>2</sub>S when it enters the reactor zone. All FCC units are equipped to handle the H<sub>2</sub>S that comes out of the reactor. This paper will discuss some of the materials, such as the cerium containing spinels, that were examined as potential SOx catalysts for FCC units and how they were tested for their ability to remove SOx under conditions prevalent in modern FCC units.

### INTRODUCTION

Sulfur oxide emissions (SOx = SO<sub>2</sub> + SO<sub>3</sub>) from fluid catalytic cracking units (FCCU) are increasingly becoming the target of EPA and local regulations (2). The removal of such pollutants from FCC units has been the subject of a considerable amount of attention over the past few years. The amount of SOx emitted from a FCC unit regenerator is a function of the quantity of sulfur in the feed, coke yield, and conversion. Generally, 45% to 55% of feed sulfur is converted to H<sub>2</sub>S in the FCC reactor, 35% to 45% remains in the liquid products, and about 5 - 10% is deposited on the catalyst in the coke (3). It is this sulfur in the coke which is oxidized to SO<sub>2</sub> (90%) and SO<sub>3</sub> (10%) in the FCC regenerator.



Flue gas scrubbing and feedstock hydrodesulfurization are effective means of SOx control but are laborious and cost intensive. The least costly alternative is the use of a SOx reduction catalyst as an additive to the FCCU catalyst inventory. Designing a catalyst for removal of SOx in a fluid catalyst cracking unit is a challenging problem. One must come up with a particle that will: 1) oxidize SO<sub>2</sub> to SO<sub>3</sub>, 2) chemisorb the SO<sub>3</sub>, and 3) be able to release it as H<sub>2</sub>S as it enters the reactor side of the unit. Another obstacle is the fact that most metals that are in the chemists' repertoire for oxidation or reduction reactions are poisons in the catalytic cracking regime. This paper will discuss some

of the materials that were examined as potential SOx catalysts to remove SOx under conditions prevalent in FCC units.

#### EXPERIMENTAL

Pseudo boehmite alumina (Condea Chemie), high surface area magnesium oxide (C.E. Basic) and  $\text{Ce}(\text{NO}_3)_3 \cdot 6\text{H}_2\text{O}$  (Molycorp) were used as received.

Preparation of  $\text{CeO}_2/\text{Al}_2\text{O}_3$ : A pseudo boehmite alumina (87.7 g) was impregnated with a solution containing 42.9 g of 70%  $\text{Ce}(\text{NO}_3)_3 \cdot 6\text{H}_2\text{O}$  ( $\text{CeO}_2$  content 28.7%) and 40 g water. This material was dried at  $120^\circ\text{C}$  for 3h and calcined at  $700^\circ\text{C}$  for 1h. Surface area of the catalyst was measured to be  $180 \text{ m}^2/\text{g}$ .

Preparation of  $\text{CeO}_2/\text{MgO}$ : A high surface area Magnesium oxide (87.7 g) was impregnated with a solution containing 42.9 g of 70%  $\text{Ce}(\text{NO}_3)_3 \cdot 6\text{H}_2\text{O}$  ( $\text{CeO}_2$  content 28.7%) and 35 g water. This material was dried at  $120^\circ\text{F}$  for 3h and calcined at  $700^\circ\text{C}$  for 1h. Surface area of the catalyst was measured to be  $75 \text{ m}^2/\text{g}$ .

Preparation of  $\text{CeO}_2/\text{Mg}_2\text{Al}_2\text{O}_5$ : A solid solution spinel  $\text{Mg}_2\text{Al}_2\text{O}_5$  was prepared by using required amounts of  $\text{Mg}(\text{NO}_3)_2$  and  $\text{NaAlO}_2$  as per literature procedure (4-6). A portion (87.7 g) of this material was impregnated with a solution containing 42.9 g of 70%  $\text{Ce}(\text{NO}_3)_3 \cdot 6\text{H}_2\text{O}$  ( $\text{CeO}_2$  content 28.7%) and 40 g water. This material was dried at  $120^\circ\text{C}$  for 3h and calcined at  $700^\circ\text{C}$  for 1h. The surface area of the catalyst was measured to be  $140 \text{ m}^2/\text{g}$ .

Thermal studies: Thermogravimetric studies were used for the testing of the materials. This was accomplished by placing a small amount (5 - 25 mg) of virgin sample on a quartz pan and passing a desired gas. The experiment was divided into four zones:

Zone A: Under  $\text{N}_2$ , the sample was slowly ( $20^\circ\text{C}/\text{min.}$ ) heated to  $700^\circ\text{C}$ . This takes about 35 min.

Zone B: Nitrogen was replaced by a gas containing 0.32%  $\text{SO}_2$ , 2.0%  $\text{O}_2$ , and balance  $\text{N}_2$ . The flow rate was 200 mL/min. The temperature was kept constant at  $700^\circ\text{C}$ . This condition was maintained for 30 min.

Zone C: Passage of  $\text{SO}_2$  containing gas was ceased and replaced by  $\text{N}_2$ . Temperature was reduced to  $650^\circ\text{C}$ . This is a 15 min. time zone.

Zone D. Nitrogen was replaced by pure  $\text{H}_2$ . This condition was maintained for 20 min.

Fluidized bed test: A one inch diameter quartz reactor heated by a tube furnace was connected to a gas manifold. Reactor temperature was controlled by a temperature controller with a thermocouple in the middle of the fluidized catalyst bed. A schematic diagram is shown in Figure 5. A blend of DeSOx catalyst in equilibrium FCC catalyst was made such that the concentration of DeSOx catalyst was 1.5 weight per cent.

15 grams of this blend was charged into a quartz reactor. The blend was cycled as described below.

#### SOx Pickup Side of Cycle

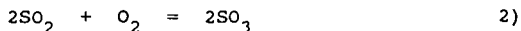
- a. The blend was heated to 732°C in flowing N<sub>2</sub>.
- b. At 732°C N<sub>2</sub> was discontinued, and 5.9% O<sub>2</sub> was allowed to pass through the bed for 4 minutes.
- c. Then 1.5% SO<sub>2</sub> was introduced along with the air for a 15 minute period at 732°C. Approximately 105-115 mg SO<sub>2</sub> was delivered during the test. The reactor effluent was trapped in a peroxide trap.
- d. After 15 minutes of test with SO<sub>2</sub>, the SO<sub>2</sub> flow was stopped, but the oxygen remains on for an additional 4 minutes.
- e. Oxygen was replaced with nitrogen for ten minutes at 732°C.
- f. The catalyst bed was cooled under flowing nitrogen for about 30 minutes.
- g. The peroxide trap was disconnected and worked up as per EPA test no. 6.

#### H<sub>2</sub> Reduction Side of Cycle

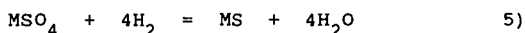
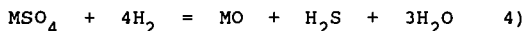
- a. The blend was flushed with N<sub>2</sub> and brought to a temperature of 732°C.
- b. At 732°C the N<sub>2</sub> was shut off, and the catalyst subjected to 100% H<sub>2</sub> for 5 minutes. The reactor effluent was captured in a 1M NaOH trap.
- c. The system was flushed with N<sub>2</sub> at 732°C for 10 minutes, then cooled under flowing N<sub>2</sub>.
- d. Sulfur analysis of the trap determined the amount of sulfur removed with each H<sub>2</sub> treatment.

#### RESULTS AND DISCUSSION:

The sulfur in the coke is mainly oxidized (7) to SO<sub>2</sub> (equation 1). Sulfur dioxide should be further oxidized to SO<sub>3</sub> (equation 2) so that it can be reactive (8) towards metal oxides to form sulfate (equation 3).



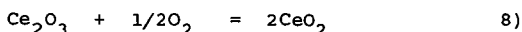
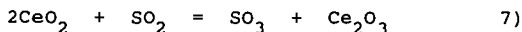
As the operational temperature of the regenerator is increased the formation of  $\text{SO}_3$  is less favored (7). The free energy of formation of  $\text{SO}_3$  (equation 2) is  $-9.5$  KJ/g-mole at  $675$  C and  $-4.4$  KJ/g-mole at  $730^\circ\text{C}$ . The regenerator temperature of an FCC unit is between  $650$  to  $775^\circ\text{C}$ . Catalyzing reaction 2 is one of the major functions of a  $\text{SO}_x$  catalyst. Equation 3 represents the capture of  $\text{SO}_3$  in the regenerator by the catalyst. The catalyst then moves to the FCCU reactor where the sulfate is reduced by hydrogen and other reducing gases to metal oxide and  $\text{H}_2\text{S}$  (equation 4) or metal sulfide (equation 5).



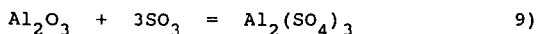
Metal sulfide can be hydrolyzed in the stripper to form the original metal oxide (equation 6).



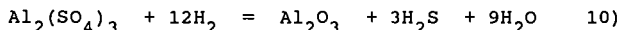
This generally accepted mechanism (3,9-12) and a schematic diagram of an FCCU is shown in Figure 1. A  $\text{SO}_x$  reduction catalyst, thus, has three functions: oxidation, chemisorption, and reductive decomposition. Vanadium pentoxide (13) is an excellent oxidation catalyst and is specially useful for the oxidation of  $\text{SO}_2$  to  $\text{SO}_3$ . However,  $\text{V}_2\text{O}_5$  cannot be used in an FCC unit because it reacts with zeolites present in an FCC catalyst. Our laboratory experiments indicate that platinum can be used for this purpose (4), but it is expensive and is not very effective under actual FCC regenerator conditions (14). Iron oxides are also very effective oxidation catalysts but iron enhances the formation of coke and unfavorably changes the product distribution. Our tests with iron containing catalysts clearly indicate that more coke is formed causing more than normal  $\text{SO}_2$  generation in the regenerator. Cerium dioxide can be used for the oxidation of  $\text{SO}_2$ . We have found that under FCC conditions  $\text{CeO}_2$  is an excellent oxidation catalyst (equation 7) and it regenerates quickly under oxygen (equation 8). An FCC regenerator contains 1 to 3% oxygen.



Once the  $\text{SO}_3$  is formed, it has to be chemisorbed by the catalyst. Alumina can be used for this purpose to form  $\text{Al}_2(\text{SO}_4)_3$  (equation 9).



One of the catalysts that was tested by us and others (15) is CeO<sub>2</sub> on gamma alumina. This can be conveniently prepared by impregnating gamma alumina with Ce(NO<sub>3</sub>)<sub>3</sub>·6H<sub>2</sub>O solution followed by drying and calcining at 730°C for 3h. The amount of CeO<sub>2</sub> was 12.3%. Aluminum sulfate starts to decompose at 580°C (16). Hence one disadvantage of using this catalyst is the fact that any FCC regenerator operating at a temperature higher than 600°C should have some decomposition of Al<sub>2</sub>(SO<sub>4</sub>)<sub>3</sub> (backward reaction of equation 9). A thermogravimetric analysis (TGA) of this catalyst is reported in Figure 2. The catalyst was first preheated to 700°C under N<sub>2</sub> (zone A). Then it was exposed to a gas containing 0.32% of SO<sub>2</sub>, 2.0 % O<sub>2</sub> and balance N<sub>2</sub> at a flow rate of 200 mL/min. (zone B). The weight gain of 5.5% indicated in figure 2 is the amount of SO<sub>3</sub> formed (reaction 7) and absorbed (reaction 9) to form the Al<sub>2</sub>(SO<sub>4</sub>)<sub>3</sub>. The TGA indicates that only 2.5% of all the available Al<sub>2</sub>O<sub>3</sub> is involved in picking up SO<sub>3</sub> during the first 15 min. period. This number is called SO<sub>2</sub> oxidation and absorption index (SOAI) (17). The SOAI of 2.5 for this catalyst is very low when compared to other catalysts described in this paper. The activity decreases considerably during the second 15 min. period. Zone C is when the passage of SO<sub>2</sub> containing gas was ceased and replaced by pure N<sub>2</sub>. At this point the temperature was dropped to 650°C to mimic the FCC conditions. TGA clearly shows that at this temperature the Al<sub>2</sub>(SO<sub>4</sub>)<sub>3</sub> is thermally unstable and releases some of the SO<sub>3</sub> it absorbed in zone 2. However, once the sulfate is formed alumina is regenerated under H<sub>2</sub> fairly easily because aluminum sulfate reduces at 400 to 700°C, which is in the FCC reactor temperature range (equation 10). Figure 2, zone D, is indicative of an efficient reduction of Al<sub>2</sub>(SO<sub>4</sub>)<sub>3</sub> to Al<sub>2</sub>O<sub>3</sub> (equation 10). Alumina is regenerated in about 2 min.



The low SOAI and the thermal instability of the sulfate under FCC conditions clearly indicate that CeO<sub>2</sub> in gamma alumina is not a very effective DeSOx catalyst.

A catalyst was prepared by impregnating MgO with cerium nitrate solution. The composition of the final calcined catalyst was 12.3% CeO<sub>2</sub> on MgO. Since MgO is much more basic than Al<sub>2</sub>O<sub>3</sub> it was hoped that it would be more reactive towards SO<sub>3</sub>. A TGA analysis is shown in Figure 3. The catalyst gains 28.5% weight in 30 min. due to SO<sub>3</sub> absorption (zone B). This is 5.2 times more than the CeO<sub>2</sub>/Al<sub>2</sub>O<sub>3</sub> catalyst. The SOAI of this catalyst is 8.7 which indicates that the SO<sub>3</sub> absorptivity of CeO<sub>2</sub>/MgO catalyst is 3.5 times higher than the corresponding alumina catalyst during the first 15 min. Linearity of the absorption plot (zone B) indicates that the absorption during the second 15 min. is as efficient as the first 15 min. When the passage of the SO<sub>2</sub> containing

gas was ceased and replaced by dry  $N_2$  (zone C), unlike  $CeO_2/Al_2O_3$  catalyst, this material did not lose any weight indicating the thermal stability of the  $MgSO_4$ . Magnesium sulfate is not expected to decompose below  $780^\circ C$  (16). Under  $H_2$ , the sulfate formed reduces at  $650^\circ C$  (zone D), however, the  $MgO$  can not be regenerated as efficiently as the alumina catalyst. About 7.7% of the absorbed material still remains with the catalyst even after 20 min. of  $H_2$  reduction, possibly as  $MgS$  or unreduced  $MgSO_4$ . Fast deactivation of this catalyst is one of the major reasons why  $CeO_2/MgO$  was not considered as a potential  $DeSO_x$  catalyst for FCC units.

The higher reactivity of  $MgO$  prompted us to look for a compound that was more thermally stable. Magnesium aluminate spinels such as  $MgAl_2O_4$  or  $Mg_2Al_2O_5$  were the ones we selected. The latter is a solid solution of pure spinel ( $MgAl_2O_4$ ) and  $MgO$ . Such a solid solution does not destroy the spinel framework. These spinels can be prepared by the calcination of  $Mg, Al$  double hydroxides, formed by the reaction of  $Mg(NO_3)_2$  and  $NaAlO_2$  at pH 8.5 to 9.5. (4-6). The spinel structure is based on a cubic close packed array of oxide ions. Typically, the crystallographic unit cell contains 32 oxygen atoms; one eighth of the tetrahedral holes (of which there are two per anion) are occupied by the divalent metal ion ( $Mg^{2+}$ ), and one-half of the octahedral holes (of which there is one per anion) are occupied by the trivalent metal ion ( $Al^{3+}$ ).

A catalyst prepared by the impregnation of  $Mg_2Al_2O_5$  with  $Ce(NO_3)_3$  was tested for  $SO_x$  removal activity. The final composition was 12.3%  $CeO_2$  on  $Mg_2Al_2O_5$ . A TGA analysis of this material is reported in Figure 4. During preheating (zone A) the material desorbed 7.6% moisture. This material gains 23.3% weight by the absorption of  $SO_3$  which is about the same as the  $CeO_2/MgO$  catalyst. The SOAI of this material is 17 indicating that this catalyst is 6.8 times more active than the  $CeO_2/Al_2O_3$  catalyst. We have previously seen that  $SO_3$  absorption by alumina is negligible and  $MgO$  is an extremely efficient  $SO_3$  absorbing agent. This indicates that in a spinel it is the  $MgO$  structural fragment that is reacting with the  $SO_3$  and our SOAI calculations for spinel catalysts are based on this concept. The SOAI of the spinel containing catalyst is about twice that of the  $CeO_2/MgO$  catalyst. This indicates that the absorption activity of  $MgO$  in spinel is much higher than that of pure  $MgO$ , possibly due to the dispersion of  $MgO$  in the spinel. Linearity of the absorption plot (zone B) indicates that the absorption in the second 15 min. period is as efficient as the first 15 min. period. When the passage of  $SO_2$  containing gas was ceased and replaced by pure  $N_2$  (zone C) no weight loss was observed. This indicates that in zone B only  $MgSO_4$  is formed although this catalyst has nearly 50% alumina. Unlike the  $CeO_2/MgO$  catalyst this catalyst regenerates efficiently under  $H_2$  (zone D). The catalyst completely regenerates

in twenty minutes of  $H_2$  reduction. Although this reduction time is much longer than that experienced in an actual FCC unit, it can be used to compare potential catalysts. It is clear, if we compare Figures 3 and 4, that  $MgSO_4$  reduces much more efficiently in a spinel catalyst compared to pure  $MgO$ . This may be due to the fact that  $MgO$  in a spinel matrix is more sterically hindered than in a magnesia unit cell. Therefore, any sulfate formed whose decomposition would relieve the steric strain is favored, i.e. the decomposition of a sulfated spinel is thermodynamically more favorable than the decomposition of a sulfated magnesia sample.

Since we realized that a cerium containing magnesium aluminate spinel is the most efficient  $DeSO_x$  catalyst that we have tested, a laboratory scale fixed fluidized bed reactor system was set-up (figure 5). Absorption and reduction half-cycles are repeated as described in figure 6 to mimic FCC units. Our system used a one inch diameter quartz reactor that was connected to a gas manifold so that the catalyst could be subjected to different gas mixtures. Reactor temperature was controlled by a controller with a thermocouple in the middle of the fluidized catalyst bed. In most cases a blend of  $DeSO_x$  catalyst in equilibrium catalyst was made, then subjected to a  $760^\circ C$ , 6 hour steaming treatment, and finally tested for  $SO_x$  pickup. The gas stream was analyzed by absorbing the exit gas in a  $H_2O_2$  trap over a period of time, and then using the EPA 6 method for determining  $SO_2$ . The gas stream could also be analyzed instantaneously by an IR analyzer as long as care was taken to remove any  $SO_3$  from the gas stream. In most cases, the sulfated sample was subjected to a reduction with either hydrogen or propane and followed by another  $SO_x$  pickup. This cycle could be repeated several times to see the effect of adding and removing sulfur to a potential  $DeSO_x$  catalyst. By adding solenoid controls to the gas lines and a microprocessor the whole system was eventually computerized so that constant monitoring by an individual was not necessary and runs could be made overnight.

Results obtained from fluidized bed tests are reported in Tables 1 and 2. Tables 1 and 2 represent the results obtained from virgin catalyst and a steam deactivated ( $760^\circ C$ , 6h, 100% steam) catalyst, respectively. The amount of sulfur picked up was calculated by difference between the amount delivered and the amount found in the trap. The amount of sulfur removed was determined by gravimetric analysis of the contents of the  $NaOH$  traps. The concentration of  $DeSO_x$  catalyst was 1.5 wt% in FCC catalyst. The Tables 1 and 2 indicate that steaming only causes a very minor deactivation. Nearly 90% of the fresh activity is retained even after steaming. Moreover, this catalyst picks up sulfur nearly half of its theoretical maximum in 15 min. indicating very high

activity. A mechanism of SOx reduction showing the catalytic cycle is illustrated in Figure 7. This cycle is given to describe the catalytic nature of the DeSOx components. In the figure, the catalyst  $\text{CeO}_2/\text{Mg}_2\text{Al}_2\text{O}_5$  is represented by its active sites, namely  $\text{CeO}_2$  and  $\text{MgO}$ .

#### CONCLUSION

A cerium containing magnesium aluminate spinel material was found to be the most effective DeSOx catalyst that we have studied. This spinel based catalyst was commercialized and is recognized as the leading DeSOx catalyst for FCC units.

#### ACKNOWLEDGEMENTS

The authors would like to thank Emmett Burk, John Magee and Joseph Powell for valuable suggestions.

REFERENCES AND NOTES

1. Present address: Amoco Chemicals Co., Amoco Research Center, Naperville, Illinois 60566.
2. Federal Register, Vol. 49, p.2058, 1984
3. Byrne, J. W.; Spornello, B. K.; Leuenberger, E. L. Oil and Gas J. 1984, 101, Oct. 15.
4. Yoo, J.S.; Jaecker, J.A.; U.S. Patent 4,469,589, Sept. 4, 1984
5. Bhattacharyya, H.; Samaddar, B. N. J. Am. Ceram. Soc. 1978, 61, 279
6. Mukherjee, S. G.; Samaddar, B. N. Trans Indian Ceram. Soc. 1966, 25, 33
7. Baron, K.; Wu, A.H.; Krenzke, L.D. Proc. Symp. on Advances in Cat. Cracking, A.C.S. Washington D.C. 1983, Aug. 28.
8. Magee, J.S.; Ritter, R.E.; Rheaume, L. Hydrocarbon Processing 1979, 58, 123
9. Thiel, P.G.; Blazek, J.J.; Rheaume, L.; Ritter, R.E.; Additive R by Davison Chemical, private publication.
10. McArthur, D.P.; Simpson, H.D.; Baron K. Oil and Gas J. 1981, p. 55, Feb. 23
11. Bertolacini, R.; Lehman, G.; Wollaston, E. U.S. Patent 3,835,031, Sept. 10, 1974
12. Habib, E.T. Oil and Gas J. 1983, p. 111, Aug. 8
13. Mars, P. Masessen, J.G.H. J. Catal. 1968, 10, 1
14. Powell, J.W. Personal communications.
15. Lowell, P.S.; Schwitzgebel, K.; Parsons, T.B.; Sladek, K.J. Ind. Eng. Chem. Process Des. Dev. 1971, 10, 384
16. Mu, Jacob; Perlmutter, D.D.. Ind. Eng. Chem. Process Des. Dev. 1981, 20, 640
17. SOAI = SO<sub>2</sub> Oxidation and Absorption Index; defined as the percentage of absorbent that is involved in picking up SO<sub>2</sub> which is produced by the oxidation of SO<sub>2</sub> in presence of the catalyst in 15 min. at a standard TGA condition

Table 1

Sulfur Picked Up And Removed at 732°C  
On Virgin 12.3% CeO<sub>2</sub> On Mg<sub>2</sub>Al<sub>2</sub>O<sub>5</sub>

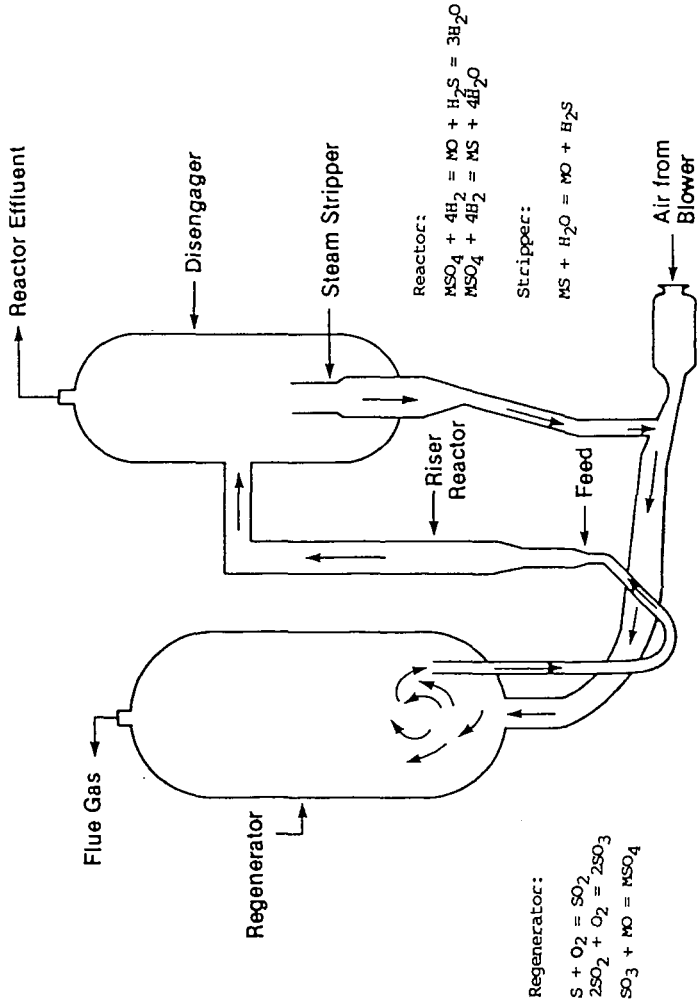
SOx Pickup-H <sub>2</sub> -Reduction	Mg Sulfur Theoretical Maximum	Mg Sulfur Picked Up	Mg Sulfur Removed
First Cycle	79	44	45
Second Cycle		42	44
Third Cycle		39	39
Fourth Cycle		37	37
Fifth Cycle		38	40
Sixth Cycle		37	-

Table 2

Sulfur Picked Up And Removed At 732°C  
On Steamed 12.3% CeO<sub>2</sub> On Mg<sub>2</sub>Al<sub>2</sub>O<sub>5</sub>

SOx Pickup-H <sub>2</sub> -Reduction	Mg Sulfur Theoretical Maximum	Mg Sulfur Picked Up	Mg Sulfur Removed
First Cycle	79	39	38
Second Cycle		36	36
Third Cycle		34	35
Fourth Cycle		31	35
Fifth Cycle		28	-

FIGURE 1  
SCHEMATIC DIAGRAM OF A TYPICAL FCC UNIT



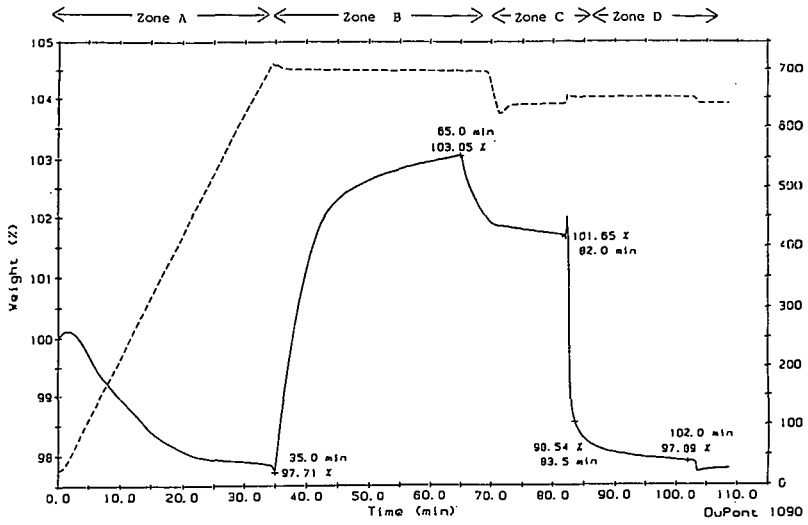


Figure 2. TGA Test of a CeO<sub>2</sub>/Al<sub>2</sub>O<sub>3</sub> Catalyst

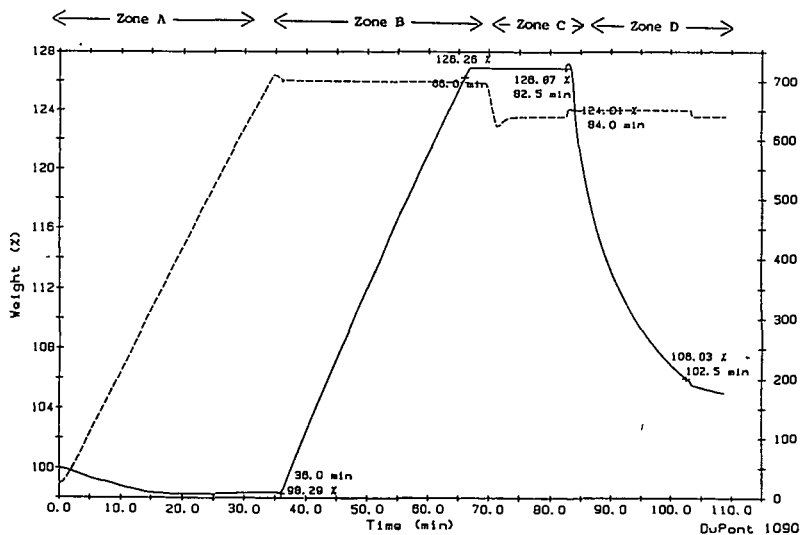


Figure 3. TGA Test of a CeO<sub>2</sub>/MgO Catalyst

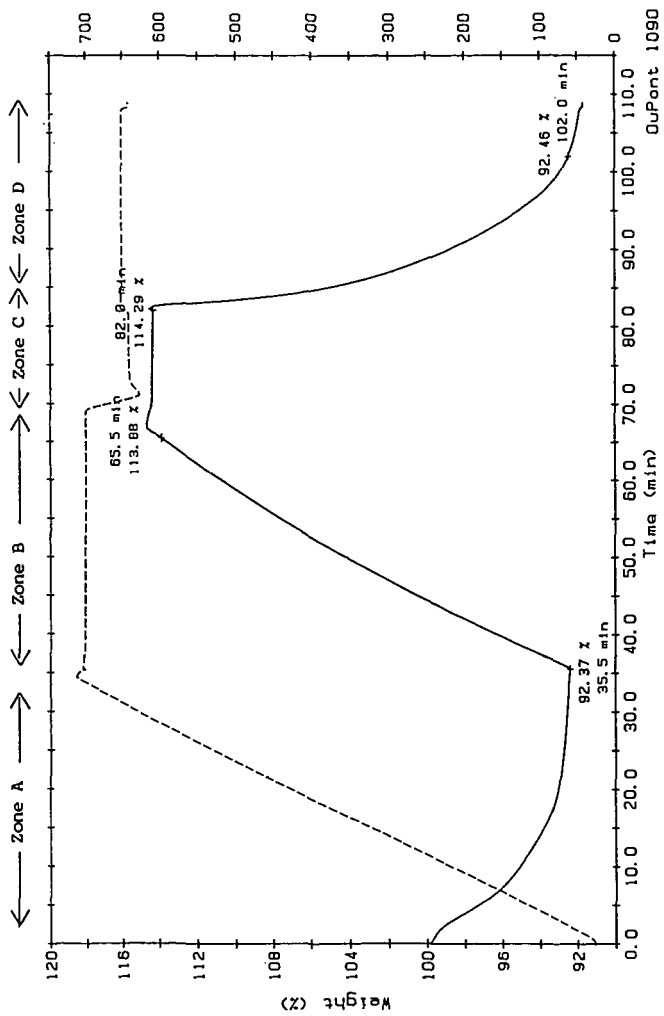


Figure 4. TGA Test of a  $\text{CeO}_2/\text{Mg}_2\text{Al}_2\text{O}_5$  Catalyst

Figure 5

A Laboratory Scale Fixed Fluidized Bed Reactor System

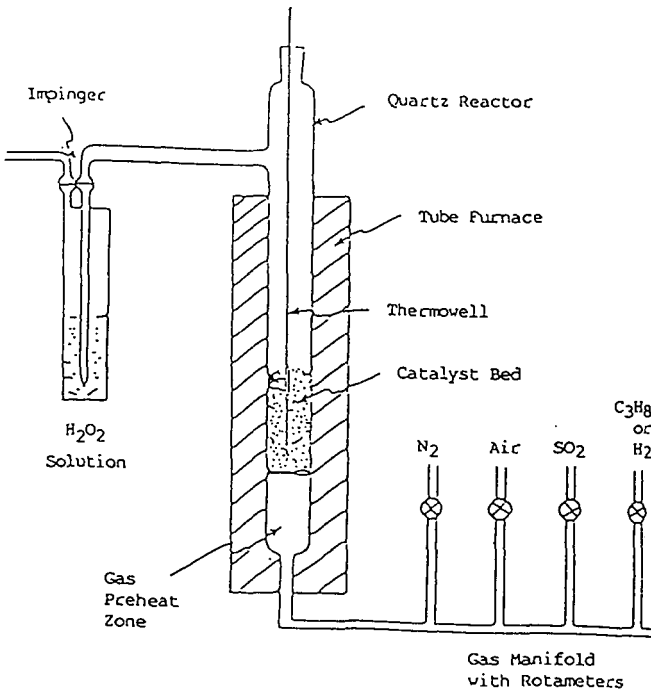


Figure 6

Adsorption And Reduction Half Cycle

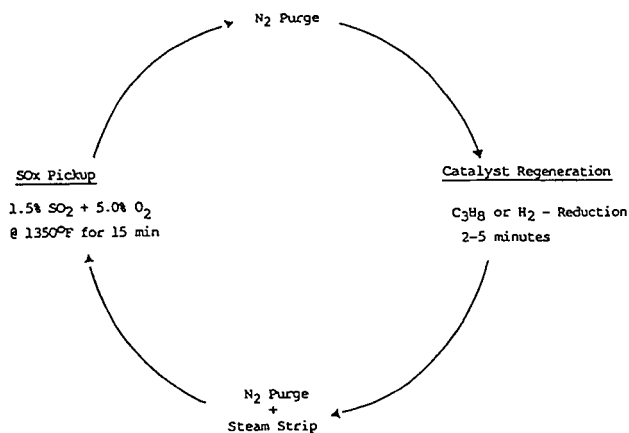
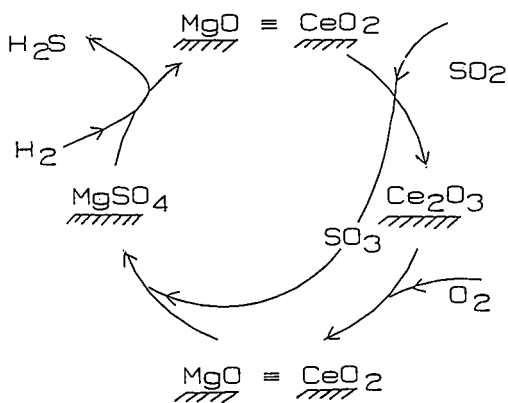


Figure 7

DeSOx Mechanistic Cycle



Agglomeration of Athabasca Petroleum Cokes in the Presence of Various Additives as a means of Reducing Sulfur Emissions during Combustion.

Abdul Majid, V.P. Clancy and Bryan D. Sparks

Division of Chemistry,  
National Research Council of Canada  
Ottawa, Ontario K1A 0R9

The relatively high sulfur content of coke produced during the upgrading of Athabasca bitumen, makes it environmentally unsuitable as a fuel. We have attempted to coagglomerate these cokes with sulphur dioxide capture agents such as: lime, hydrated lime and limestone in an attempt to reduce emissions during combustion. By providing an environment where there is intimate contact between fuel and sorbent it was hoped that greater utilisation of the sorbent could be achieved, compared to fluid bed combustion, where the sorbent is added separately to the bed. Cokes from both Suncor and Syncrude operations were used in this investigation. The effect of conditioning agents such as sodium hydroxide, sodium oleate, and a petroleum sulfonate on the formation of coke oil agglomerates as well as on the efficiency of sulfur dioxide capture was also investigated. Sulfur dioxide capture was found to depend mainly on the calcium to sulfur mole ratio in the agglomerates, the combustion temperature, partial pressure of oxygen, and the type of coke and sorbent. The efficiency of the three capture agents in the reduction of sulfur dioxide emissions, has been compared.

Upgrading of Athabasca oil sands bitumen to form a synthetic crude oil produces a solid carbonaceous material, known as "Coke". The two commercial oil sands plants operating in Alberta produce approximately 4,000 tons of coke per day [1]. This coke contains 6-8% sulfur almost entirely in the form of organic sulfur compounds such as thiophenes, sulfides, disulfides and thiols [2]. Due to serious environmental and corrosion problems associated with the combustion of this coke, its use as a boiler fuel is limited and a significant portion of the coke is being stockpiled as a waste product. However, oil sands coke with a calorific value of about 33 MJ/Kg [3] would be an attractive boiler fuel if it could be desulfurized economically.

Although considerable work has been done on various methods of desulfurizing coal and coal chars, comparatively few studies appear in the literature on the desulfurization of petroleum coke, particularly coke derived from Athabasca oil sand bitumen. There have been some attempts at desulfurization of these cokes employing such methods as hydrodesulfurization, combustion with limestone addition, impregnation with high base loadings followed by calcination in an inert atmosphere and subsequent leaching, chemical oxidation, and solvent extraction [2-5]. However, most of these methods are said to be uneconomical [1]. Fluidized-bed combustion of coal in the presence of limestone is emerging as a promising technology that can achieve high combustion efficiency with significantly reduced sulfur dioxide emissions [6]. The disadvantage of the process is the high calcium to sulfur mole ratios required for acceptable reductions in sulfur dioxide emissions. For example, using limestone as a sulfur sorbent in a fluidized bed for Suncor delayed coking coke, a Ca/S ratio of 3:1 was required to achieve 80% reduction in SO<sub>2</sub> emissions [5].

The objective of this investigation was to develop an economically attractive method by which the oil sands coke may be utilized directly as a boiler fuel without serious environmental damage. To the best of our knowledge there are no reports regarding the coagglomeration of coal, coke or char with sulfur sorbents. The present program was designed to study the feasibility of co-agglomerating sulfur capture agents such as limestone, lime and slaked lime with oil sands bitumen coke as a means of increasing the utilisation of these agents during sulfur dioxide removal on combustion.

### Experimental Methods

**Materials.** Suncor delayed coking coke and Syncrude fluid coke samples were obtained from the Alberta Research Council sample bank. The coke was ground to 150  $\mu\text{m}$  size using a Brinkman ZM-1 Centrifugal Grinding Mill. The composition and Calorific value of these samples are listed in Table I.

TABLE I  
Composition and Physical Data for Cokes

	Suncor Delayed Coke	Syncrude Fluid Coke
Proximate Analysis* (Dry Basis)		
Ash	6.0	8.7
Volatile Matter	11.6	7.3
Fixed Carbon	82.4	84.0
Ultimate Analysis (Dry Basis)		
Carbon	83.0	76.8
Hydrogen	3.4	1.6
Nitrogen	1.5	1.5
Sulfur	5.9	6.9
Oxygen	2.9	4.4
Ash	3.4	8.0
Calorific Value* MJ/Kg	33.4	32.6

\* Alberta Research Council (Fuel Sciences Division)

Bridging liquid used for agglomeration of coke particles was a sample of bitumen obtained from the Alberta Research Council sample bank. This was a sample of coker feed bitumen from Suncor, prepared for use in a round robin study of bitumen analyses [7].

A number of sulfur dioxide capture agents were tried including: limestone, lime and slaked lime. The sample of limestone used was pulverized agricultural limestone (Domtar). It contained approximately 97%  $\text{CaCO}_3$ . A partial size distribution of this sample is given in Table II. Lime was a laboratory grade  $\text{CaO}$  sample. Various samples of slaked lime were prepared as shown in Table III.

Petroleum sulfonate (TRS-10-80), used as a conditioning agent, was obtained from Witco Chemicals Corporation.

TABLE II  
Size Distribution of Limestone

Sieve Size ( $\mu\text{m}$ )	Cumulative Weight Percent Passing
44	67.0
53	74.7
74	91.8

**Procedure.** 20 g of coke was mixed with known amounts of sorbent and the mixture dispersed in 100 ml of tap water contained in a Waring Blendor. An appropriate amount of a conditioning agent was then added and the contents agitated at 250 rps for 15 seconds. At this stage the blending speed was lowered to 120 rps. Bitumen was added slowly while continuing blending until discrete agglomerates or a unitary phase was obtained (5-15 minutes). Coke oil agglomerates/oil phase were then separated from the aqueous phase by screening. A portion of the agglomerates were used for analysis of bitumen, coke and ash content using a procedure described elsewhere [8]. The second portion of the agglomerates was dried at 100°C to a constant weight.

TABLE III  
Experimental Conditions for Various Hydrated Lime Sample Preparation

Sample #	Experimental Conditions
1.	Laboratory grade CaO was mixed with distilled water in the ratio of 1:4 and then air dried at 90°C.
2.	20 g of CaO was mixed with 80 g of distilled water and 740 ml of isopropyl alcohol. The slurry was then dried at 90°C on a rotary evaporator under vacuum.
3.	Same as above, except the excess liquid was removed under atmospheric pressure at 90°C.
4.	10 g of CaO was mixed with 40 g of 0.5% aqueous solution of sodium sulfonate (Witco TRS-10-80) and 370 ml of isopropyl alcohol. Contents were mixed into a slurry and then dried on a rotary evaporator at 90°C under vacuum.
5.	Same as above, except the excess liquid was removed under atmospheric pressure at 90°C.
6.	Same as sample 1 except that the sample was freeze dried.
7.	Same as sample 1 except that the sample was dried in a vacuum oven at 90°C.

Combustion of Oil Agglomerates/Oil Phase. Before combustion wet agglomerates were first dried in an oven at 100°C to a constant weight to facilitate analytical calculations. However, because of the economic advantage in burning wet agglomerates, a separate investigation involving the combustion of wet agglomerates is in progress. The results of this study will be reported elsewhere. Two procedures were used for the ashing of dried coke-oil agglomerates/oil phase. The first procedure involved weighing an agglomerate sample into a porcelain crucible, and placing it directly into a muffle furnace preset at the desired temperature. This technique has been referred to as combustion with limited air. The second procedure involved burning the sample over a bunsen burner in the open air followed by completion of the ashing process in the muffle furnace at an appropriate temperature. This has been referred to as combustion with excess air.

Sulfur Analysis. Attempts were made to measure the sulfur dioxide emissions from coke-oil agglomerates by burning ~ 1.0 g of the sample in a porcelain boat placed inside a quartz tube contained in a tube furnace (ASTM method D4239-83). This method is specifically designed for the determination of sulfur in coke and coal. Sulfur dioxide in the combustion gases was absorbed by 1% hydrogen peroxide solution and the resulting sulfuric acid titrated against 0.05N-NaOH solution to pH 5.0, see equation [1].



The sulfur content of the coke, coke-oil agglomerates and coke-sorbent-oil agglomerates was also determined independently using a Leco sulfur analyzer and by x-ray fluorescence spectrometry. Excellent agreement between the results for sulfur content for coke and coke-oil agglomerates was obtained by the three methods. However, each method gave a different result for the sulfur content of coke-sorbent-oil agglomerates. Reproducibility was extremely poor for these samples when using the ASTM method. Results from the Leco sulfur analyzer were reproducible within ±5% but gave significantly lower sulfur contents than x-ray fluorescence spectrometry. Results from x-ray fluorescence spectrometry were much closer to the expected values than the results from the other two methods. Total sulfur in the ash obtained from the combustion of coke-oil and coke-sorbent-oil agglomerates was also determined using x-ray

fluorescence spectrometry.

The sulfur fixed in the ash during combustion is expressed as a percentage of the total sulfur in the original coke. It was calculated from the equation:

$$\text{Percentage sulfur fixed} = \frac{\text{wt. of sulfur in ash from } y \text{ g of agglomerates}}{\text{wt. of sulfur in } y \text{ g of agglomerates}} \times 100 \quad (2)$$

$$\text{wt. of sulfur in ash} = \frac{\text{wt. ash} \times \% \text{ sulfur in ash}}{100}$$

$$\text{wt. of sulfur in agglomerates} = \frac{\text{wt. agglomerates} \times \% \text{ sulfur in agglomerates}}{100}$$

### Results and Discussion

Sulfur Determination. Sulfur contents of coke and coke agglomerates as determined by: ASTM method D4239-83, Leco sulfur analyzer and x-ray fluorescence spectrometry are listed in Table IV. The three methods gave similar results for coke and coke oil agglomerates, but each method gave a different result for coke-limestone-oil agglomerates with the most scatter being obtained with the ASTM method. The reproducibility of the other two methods was similar. However, the Leco sulfur analyzer gave lower sulfur values compared with the x-ray fluorescence method. Sulfur content, determined using x-ray fluorescence spectrometry, was much closer to the expected values. Hence, all the results discussed in this report are based on the x-ray fluorescence spectrometry method.

TABLE IV  
Comparison of Sulfur Results Obtained Using Different Methods.

Sample	Total oxidisable sulfur (SO <sub>2</sub> emitted) by ASTM Method				Total sulfur (as w/w% of agglomerates)		Total oxidisable sulfur from ash* analysis	
	460°C	750°C	840°C	1000°C	x-ray method	Leco method	460°C	1000°C
Suncor Coke	5.5±0.1 (4)	5.3±0.2 (3)	-	-	5.9±0.2 (4)	5.8±0.1 (4)	-	-
Suncor Coke-Bitumen Agglomerates	5.8±0.1 (2)	5.9±0.2 (2)	-	5.6±0.2 (2)	5.7	5.9±0.1 (3)	5.8	5.7
Suncor Coke-Limestone-Bitumen Agglomerates Ca:S Mole ratio 0.6	3.2±0.7 (3)	2.8±0.7 (3)	3.3±0.1 (2)	4.1±0 (2)	4.75±0.3	3.7±0.2 (3)	3.2	1.3
" Ca:S Mole ratio 0.8	1.8	2.9	-	3.1	4.2±0.3	3.5±0.4 (3)	3.2	1.3
" Ca:S Mole ratio 2.6	1.40±0.1 (2)	3.0±0.5 (3)	1.3	2.1±1.0 (2)	3.5±0.3	2.6±0.1 (10)	2.2	0.9

\* by x-ray fluorescence spectrometry.

Values in parenthesis are number of determinations.

### Sulfur Retention by the Ash from Suncor Coke-Oil Agglomerates.

Tests on several lignites at various laboratories have shown that with no limestone injection, highly variable sulfur retention by the ash is achieved during combustion in a fluidized bed. In some cases the retention of sulfur by the ash alone have been quite significant [9]. Mineral composition of the ash is said to be important in determining the extent of sulfur retention. Iron in particular has been

reported to catalyze the sulfation reaction between  $\text{CaO(s)}$  and  $\text{SO}_2(\text{g})$  [10]. Ash analyses of the Suncor delayed coking coke and Syncrude fluid coke are presented in Table V below:

TABLE V  
Ash analyses of the Cokes (w/w% of Ash)

Component	Suncor delayed Coking Coke	Syncrude Fluid Coke
Total Ash	3.4	8.0
$\text{SiO}_2$	42	41
$\text{Al}_2\text{O}_3$	19	22
$\text{Fe}_2\text{O}_3$	23	12
$\text{NiO}$	2	1
$\text{V}_2\text{O}_5$	5	3
$\text{TiO}_2$	2	3
$\text{CaO}$	3	5
$\text{MgO}$	2	2
$\text{Na}_2\text{O}$	1	2
$\text{K}_2\text{O}$	2	2

As  $\text{Fe}_2\text{O}_3$  is one of the major components of the ash from both cokes, significant amounts of sulfur retention by the ash from these cokes might be expected. However, no significant sulfur retention by the ash from either coke was observed. Sulfur retention by the ash from Suncor coke ranges from 1-3% and for Syncrude coke it is in the 3-5% range. Although the  $\text{Fe}_2\text{O}_3$  content of the ash from Suncor coke is about double that of the Syncrude coke, its sulfur retention is only half that of the Syncrude coke ash. This appears to be more consistent with the  $\text{CaO}$  content of the two ashes and suggests that  $\text{CaO}$  is the only reactive ingredient for sulfur retention in the coke ash.

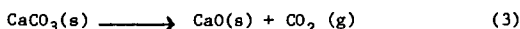
Conditioning agents used did not affect the retention of sulfur by ash. However, conditioning agents were found to facilitate agglomeration, probably by increasing the wettability of the coke particles with respect to the bridging oil. The effect was more pronounced for Syncrude coke than for Suncor coke. This was evident from the lower amount of bridging liquid required to agglomerate Syncrude coke in the presence of conditioning agents, in particular oleic acid and sodium oleate. This is consistent with the fact that Suncor delayed coke is more hydrophobic than Syncrude fluid coke because of the presence of a small amount (0.4% by weight) of a benzene extractable material [11].

#### Coagglomeration of Limestone with Suncor Coke in the absence of a conditioning Agent.

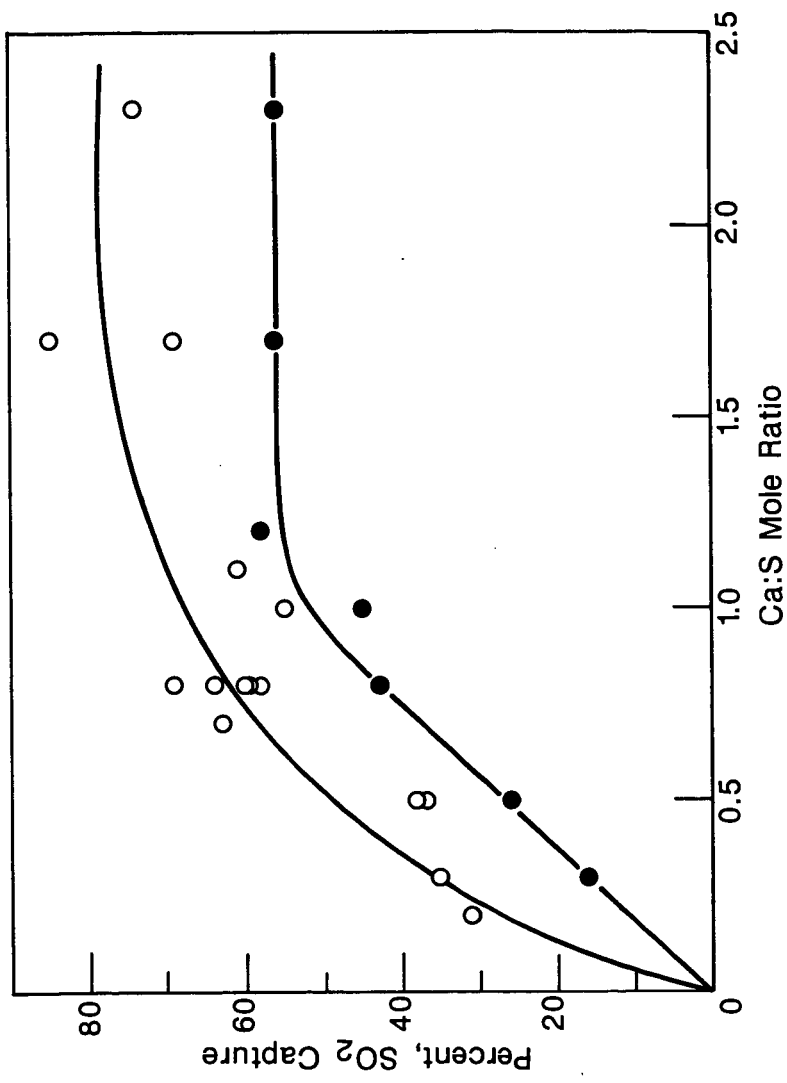
Suncor coke can be easily coagglomerated with limestone. However, individual agglomerates were only obtained when the  $\text{Ca}$  to sulfur ratio was  $< 1.2$ ; beyond this ratio a unitary phase resulted.

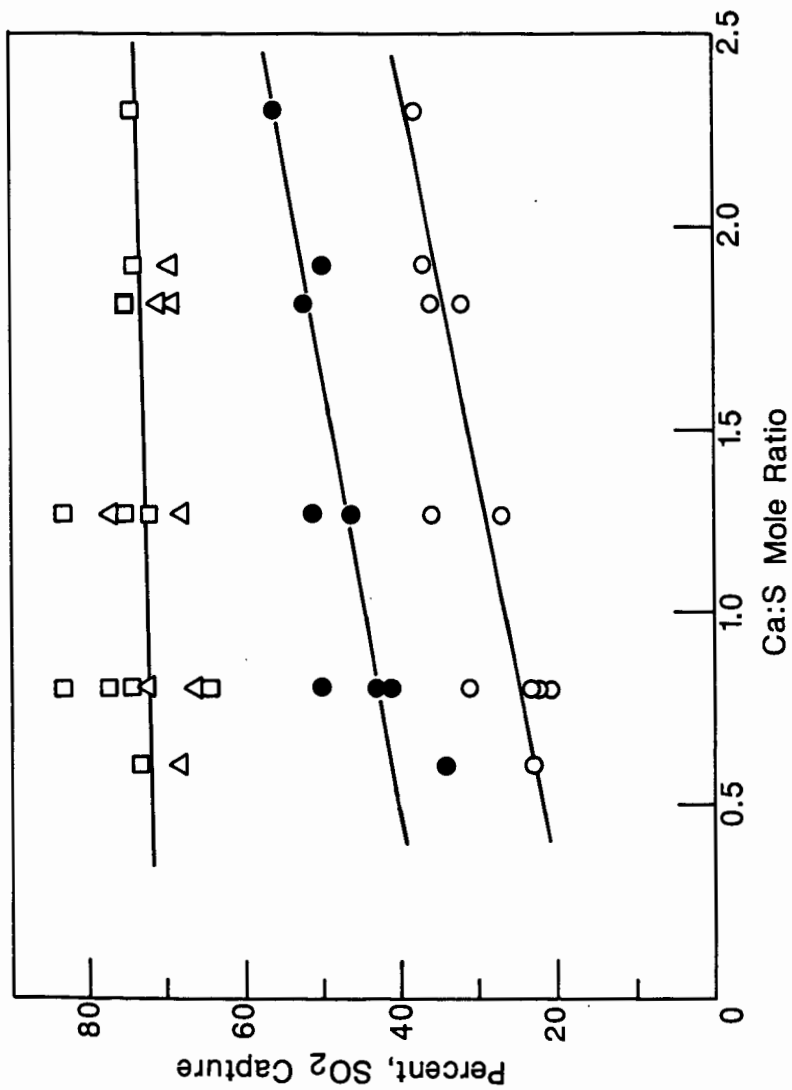
Figure 1, is a plot of the percentage of the sulfur retention versus calcium to sulfur molar ratio. It is obvious from these plots that the efficiency of sulfur dioxide capture mainly depends on the calcium to sulfur mole ratio in the agglomerates, and the combustion temperature. Considerably more sulfur dioxide retention was obtained at  $1000^\circ\text{C}$  than at  $460^\circ\text{C}$ . This is consistent with various published reports [9,12-15]. This greater reactivity of limestone at higher temperatures has been explained on the basis of several mechanisms [9].

The detailed kinetic mechanism of the reaction between carbonate rock and sulfur dioxide is not well understood [16-17]. However it is generally accepted that the reaction involves two steps. The first step is the decomposition of calcium carbonate (calcination) to carbon dioxide and calcium oxide:



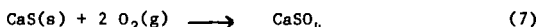
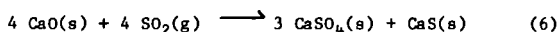
The second step is the reaction of sulfur dioxide and calcium oxide. In the presence of excess air this reaction produces  $\text{CaSO}_4(\text{s})$ :







However, with limited amounts or no air present the preferred product was temperature dependent [12]. At lower temperatures  $\text{CaSO}_3$  was formed whereas the more thermodynamically stable  $\text{CaSO}_4 \cdot \text{CaS}$  was formed at higher temperatures as shown in reactions 5-7 below.



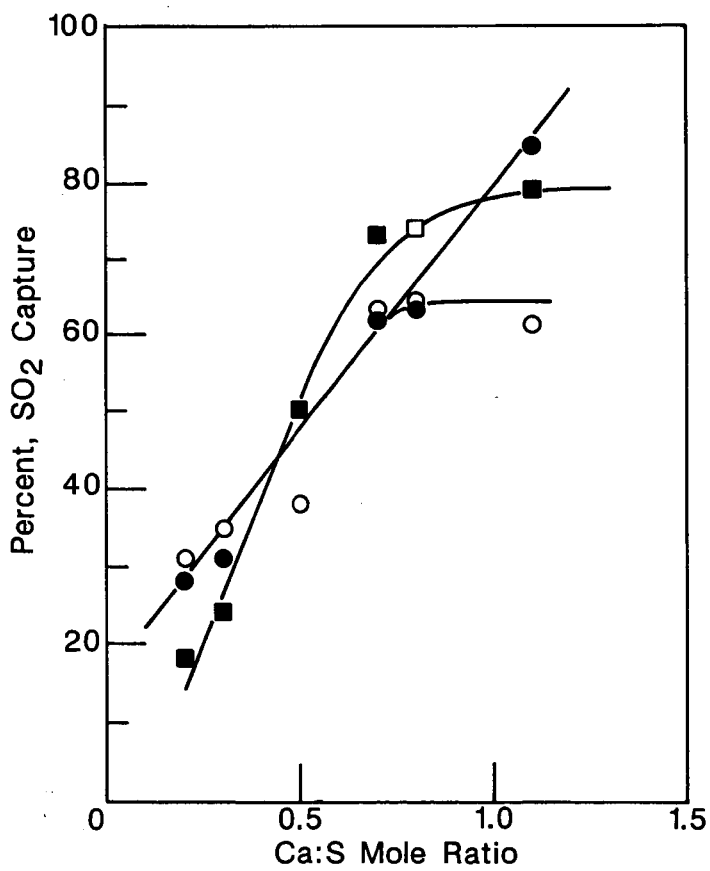
The capacity of limestone to react with  $\text{SO}_2$  in a fixed bed reactor has been studied by various workers [9,12-15]. It has been found that the calcination reaction is the controlling step at low temperatures, and the sulfation reaction is the controlling step at high temperatures. At low temperatures calcination is slow and hence overall conversion of limestone to  $\text{CaSO}_4$  will be low. As the temperature is raised the calcination rate will increase [18]. At the optimum temperature the rate of calcination is so fast that the rate of sulfation dominates the overall reaction resulting in higher utilisation of sorbent.

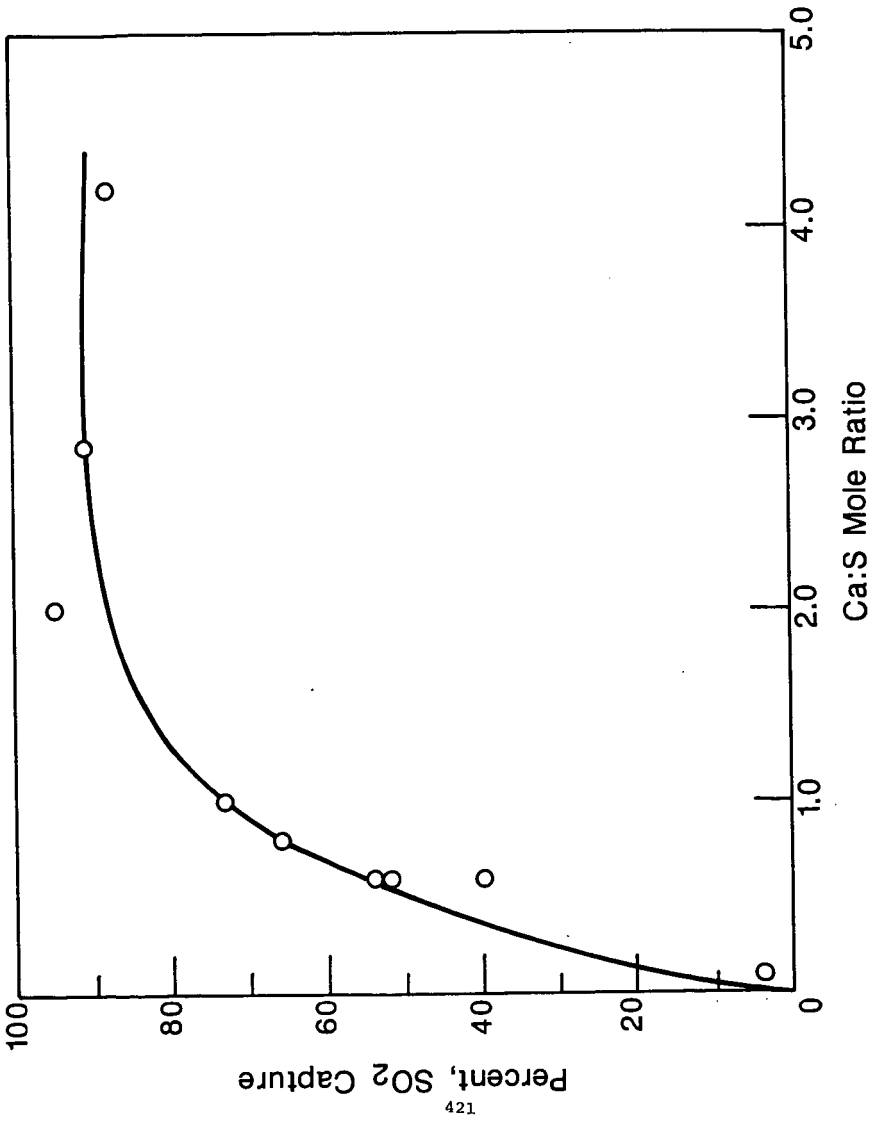
Results summarized in Figure 1 demonstrate that as the limestone content of the agglomerates is increased a corresponding decrease in sulfur dioxide emissions during combustion of Suncor coke is achieved. For small values of the calcium to sulfur ratio there appears to be a linear correlation between sulfur dioxide capture and the calcium to sulfur mole ratio. This is consistent with the fluidized bed combustion studies of coals in presence of limestone. In this range, sulfur retention has been found to be related to the capacity of the stone and not its reactivity [6].

It has been suggested that the rate of reaction between sulfur dioxide and limestone is strongly affected by the diffusion of the gaseous reactants [16,17]. Because calcium sulfate has a molar volume about 3 times larger than that of calcium oxide, the accumulation of reaction product causes the sorbent porosity to decrease and the diffusional resistance to increase. When the pore mouths are filled with the reaction product, a considerable percentage of the interior of the pores become inaccessible to the gaseous reactants and the reaction stops. In addition it has been shown that the pore size distribution is affected by the temperature and  $\text{CO}_2$  partial pressure during calcination [14]. At higher temperatures and under higher partial pressures of  $\text{CO}_2$ , higher rates of reactions between  $\text{SO}_2$  and  $\text{CaO}$  have been reported [19]. This is consistent with the observed lower degree of sulfur fixation at  $460^\circ\text{C}$  than at  $1000^\circ\text{C}$ .

The sulfur retention by limestone was also found to be affected by the oxygen partial pressure during combustion at a particular temperature. Much higher sulfur retention values were obtained under excess air than under limited air at the same combustion temperature ( $460^\circ\text{C}$ ). This is because at lower temperatures, in the presence of excess air  $\text{CaSO}_4$  is formed which is thermodynamically more stable than the  $\text{CaSO}_3$  preferentially formed in the presence of limited air. However, it is noteworthy that the results under discussion were obtained from two stage combustion as described in the experimental section. The initial combustion was carried out on a bunsen burner where the effective combustion temperature could have been considerably higher than  $460^\circ\text{C}$ , the temperature of the furnace for second stage of combustion. Hence, the effect noted above could be due to a combination of excess air and higher initial combustion temperature.

With increasing amounts of limestone, greater quantities of bitumen were required for agglomeration. However, the ratio of coke to bitumen does not affect the extent of sulfur retention by limestone. This suggests that limestone is a good sorbent for sulfur emissions from both bitumen and coke.



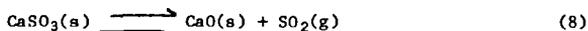


### The Effect of Combustion Temperature on the Retention of SO<sub>2</sub> by Ash from Suncor Coke-Limestone Agglomerates.

As discussed above, the capture of sulfur dioxide by the sorbent is affected by the combustion temperature. The samples of coke agglomerates containing limestone were ashed at 460°C, 750°C and 1000°C in order to find the optimum combustion temperature for maximum sulfur retention. Results are summarized in Figure 2. These results are different from the results shown in Figure 1 in that these were obtained using sodium hydroxide as a conditioning agent. It is obvious from these results that maximum retention is achieved around 750°C to 1000°C. However, an ashing temperature of 1000°C was selected for subsequent work because this is closer to the temperatures used in actual combustion equipment.

At higher temperature sulfur retention is almost independent of the calcium to sulfur mole ratio in the range investigated. Almost 70% sulfur retention can be achieved with a Ca to sulfur mole ratio of 0.6. This can be explained on the basis of much faster rates of reactions for both calcination and sulfation as well as pore plugging at higher temperatures as discussed above [14,16-17,19]. For lower temperatures, sulfur retention is proportional to the Ca to S mole ratio. This could have been due to the greater thermal stability of CaSO<sub>4</sub> at lower temperatures.

At 460°C, for a particular Ca to S mole ratio the extent of sulfur retention was much higher in excess air than in limited air. The effect of oxygen partial pressure at higher temperatures was insignificant. This can be explained on the basis of the formation of thermodynamically more stable CaSO<sub>4</sub> in excess air at low temperature and under any conditions at higher temperatures as against thermodynamically less stable CaSO<sub>3</sub> obtained at low temperatures in limited air. Calcium sulfite will decompose above 400°C according to the equation:



### The Effect of Conditioning Agents on Sulfur Dioxide Capture by Limestone.

In a recent publication it has been reported that when sodium was deposited on CaO, there was a significant increase in SO<sub>2</sub> adsorption, and adsorption increased with increasing sodium deposition [20]. The presence of sodium was suggested to have activated the CaO surface for SO<sub>2</sub> adsorption due to the formation of Na-O-Ca species. In order to investigate the effect of sodium on SO<sub>2</sub> capture by limestone, Suncor coke was coagglomerated with limestone in the presence of various concentrations of sodium hydroxide, sodium oleate and a sodium salt of a petroleum sulfonate (Witco TRS 10/30). The effect of these additives on the retention of sulfur dioxide by limestone has been illustrated in Figure 3.

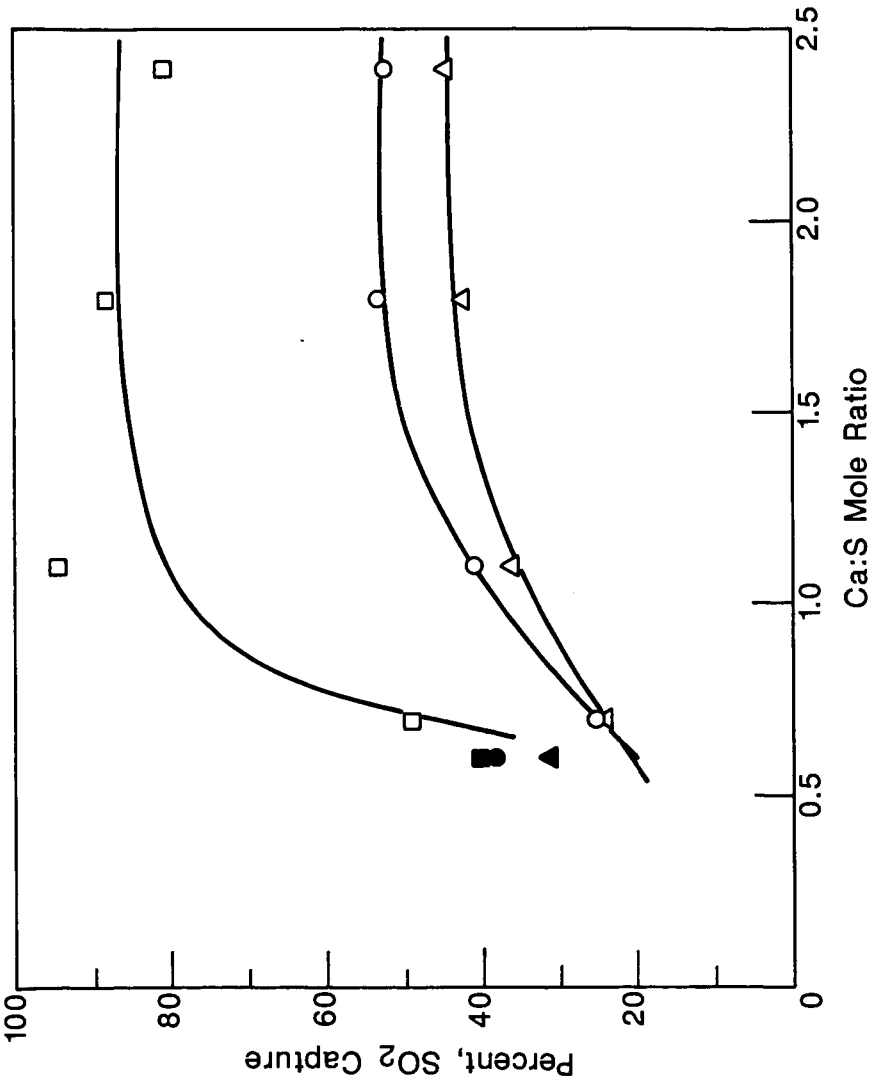
The addition of all three conditioning agents improved the coagglomeration of the components, resulting in the use of smaller quantities of bitumen, especially at higher Ca to sulfur mole ratios. This could have been due to the improved wettability of the components towards the bridging oil as a result of the use of surfactants or by in situ formation of surfactants by reaction between the alkali and certain bitumen components.

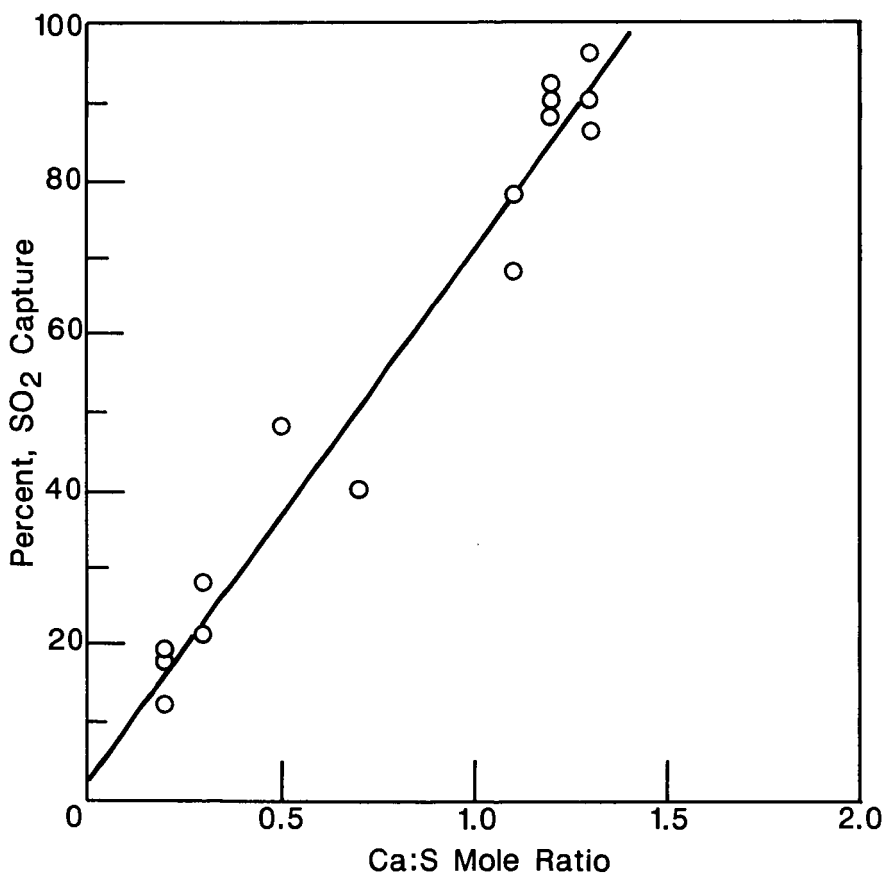
As can be seen from the plots in Figure 3, better sulfur capture was achieved when the agglomerates were prepared in the presence of these additives. This effect was more pronounced for the higher Ca to sulfur ratios. The relative effectiveness of the three additives was essentially identical. As all three additives were sodium salts it is possible that the observed improvement was owing to sodium activation of calcined limestone [20].

It is also apparent that there is a reduced scatter in the data points for experiments carried out in the presence of additives, compared with the blank experiments. It appears that the three additives all have the ability to distribute limestone uniformly within the agglomerates. Overall sulfur capture by limestone was independent of the concentration of the various additives. This is consistent with the presumed catalytic nature of these additives.

### Coagglomeration of Suncor Coke with Lime.

Coagglomeration of Suncor coke with lime was also attempted. This procedure was considerably more difficult than with limestone, resulting in a unitary phase in most cases. Certain bitumen components (carboxylic acids) are known to interact





strongly with calcium ions. For limestone, chemisorption of these components to calcium atoms at the solid surface appears to occur readily. This results in a hydrophobic surface easily wettable by the oil, allowing co-agglomeration with the naturally hydrophobic coke. Lime, however, reacts strongly with water and this reaction probably occurs in preference to interaction with the acidic bitumen components. Thus, the lime surface does not become properly conditioned by the bitumen and co-agglomeration does not readily occur.

The effect of calcium to sulfur mole ratio on the retention of sulfur dioxide by lime is illustrated in Figure 4. As is evident the degree of sulfur dioxide retention increases with increasing amounts of lime in the agglomerates up to about 90% at a calcium to sulfur mole ratio of about 2. Relatively low data scatter in Figure 4 suggests a uniform distribution of lime within the agglomerates.

Figure 5 demonstrates the effect of combustion temperature and amount of excess air on the retention of sulfur by lime. Again, considerably higher sulfur retentions were achieved at 1000°C than at 460°C. This effect is identical to the one noted for limestone. It is also consistent with the published results for the fluidized bed combustion studies with similar systems [9,12-15]. However, contrary to the limestone case, where sulfur capture was found to be independent of the calcium to sulfur mole ratio in the higher ratio range, sulfur capture by lime is dependent on the calcium to sulfur mole ratio at a combustion temperature of 1000°C. This could be partly due to the difference in the reactivities of uncalcined and precalcined limestone at higher temperatures [13]. It has been found that the capacity of uncalcined limestone to react with  $\text{SO}_2(\text{g})$  reached an optimum near 900°C while the capacity of precalcined limestone decreased with increasing temperature above 700°C. Higher reactivity of uncalcined limestone at higher temperatures is said to be due to the higher partial pressure of  $\text{CO}_2(\text{g})$  produced from the calcination reaction [21].

The temperature effect for sulfur dioxide retention by lime is more pronounced for the Syncrude fluid coke-lime system than for the Suncor delayed coking coke-lime system. This reflects the differences in the conditions during formation of the cokes. During fluid coking (FC), more volatile matter is removed from the bitumen feed than during delayed coking (DC) [22]. As a result DC coke may require lower combustion temperatures than the FC coke.

Another important observation relating to the temperature effect is that maximum sulfur dioxide retention was obtained near 750°C for lime in contrast to a value of 1000°C for limestone. This is consistent with the published data of various authors who found that the optimum sulfation temperature for uncalcined particles is generally higher than that for calcined particles of the same material [9,13].

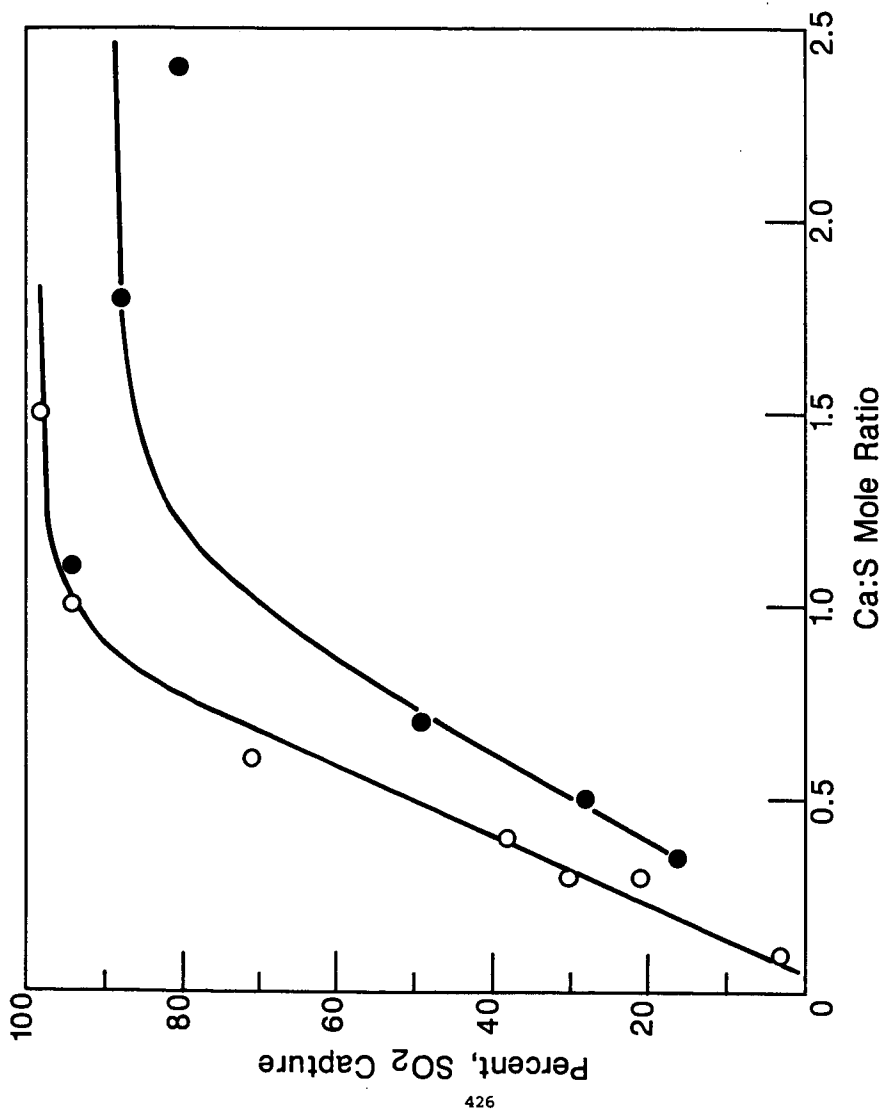
Excess air had a negative effect on the retention of sulfur dioxide by lime at a combustion temperature of 460°C. This is contrary to the effect noted for limestone. The presence of excess air will lead to the formation of thermodynamically stable  $\text{CaSO}_4$  in both cases. However, the rate of sulfation reaction will decrease with the extent of reaction due to pore plugging [16-17]. It is probable that this pore plugging is slower in the presence of  $\text{CO}_2$  produced from the calcination of limestone.

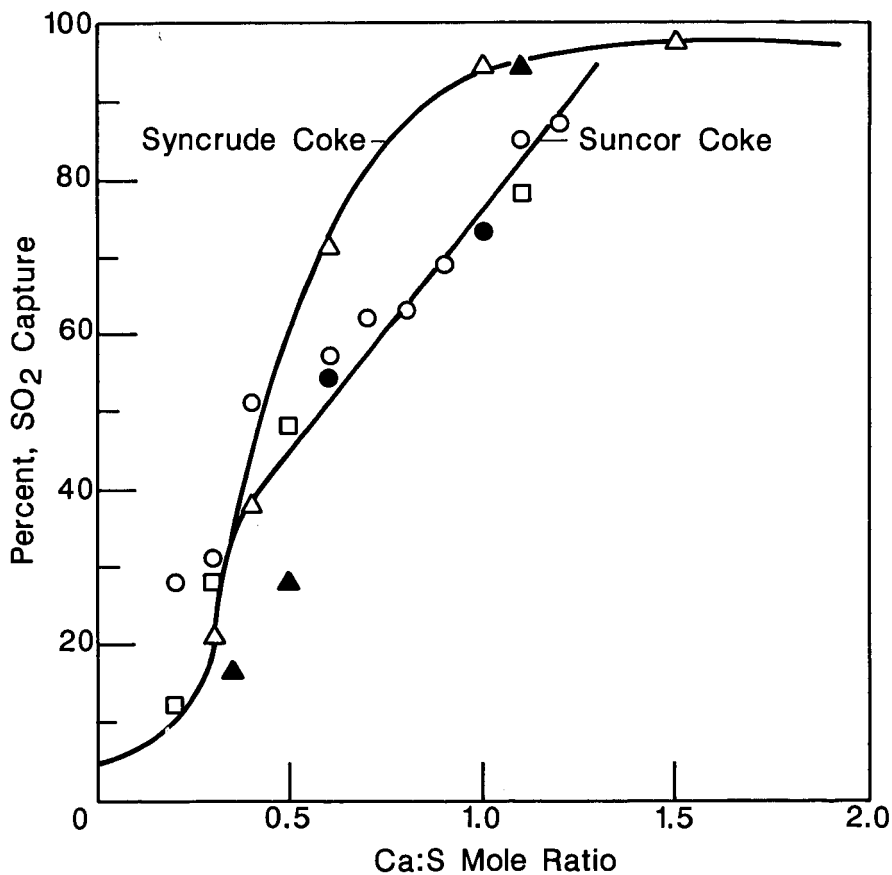
#### Coagglomeration of Suncor Coke with Hydrated Lime.

It was relatively easy to coagglomerate the samples of hydrated lime prepared in the laboratory under different conditions as listed in Table III, compared with the reagent grade  $\text{Ca}(\text{OH})_2$ . The results for the retention of sulfur dioxide from Suncor coke by hydrated lime lead to various observations.

As with lime maximum sulfur dioxide retention was achieved near 750°C for reagent grade  $\text{Ca}(\text{OH})_2$  in contrast to the maximum near 1000°C for the laboratory prepared samples of hydrated lime. The reason for this difference in behavior of the same sorbent obtained from different sources is not well understood. However, this behavior is consistent with the fluidized bed combustion studies of sulfur retention by limestone and dolomite. It has been reported that the maximum in sulfur retention in fluidized bed combustion depends on the specific limestone or dolomite employed [23].

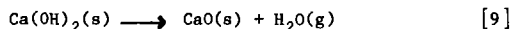
Whereas sodium oleate was found to be beneficial in the agglomeration of laboratory prepared samples of hydrated lime, none of the additives affected either the retention of  $\text{SO}_2$  or agglomeration of the reagent grade  $\text{Ca}(\text{OH})_2$ . This suggests





that reagent grade  $\text{Ca(OH)}_2$  is the least hydrophobic among the sorbents investigated in this work.

Also, decomposition of  $\text{Ca(OH)}_2$  possibly produced reactive  $\text{CaO}$



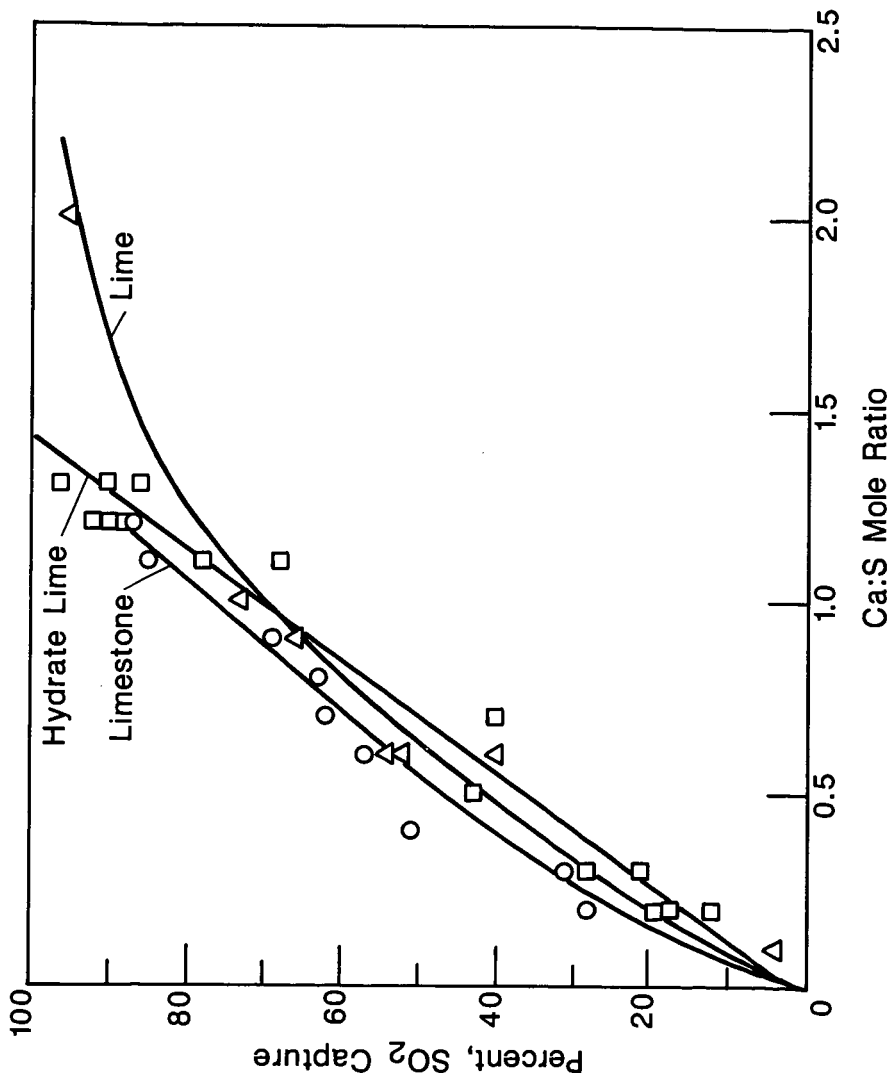
Water vapour and oxygen have been found to show a similar effect on the oxidation rate of  $\text{CaSO}_3$  to  $\text{CaSO}_4$  [24]. Figure 6 is a graphic representation of these results. There is a linear correlation between the amount of sulfur retention and the mole ratio of calcium to sulfur in the agglomerates. About 90% sulfur retention can be achieved with a calcium to sulfur mole ratio of 1.2. Coke to bitumen ratio does not appear to affect the reactivity or capacity of hydrated lime for  $\text{SO}_2$  capture. This suggests that hydrated lime is an effective sorbent for sulfur dioxide from bitumen as well as from coke.

The presence of excess air does not have any significant effect on the overall retention of sulfur dioxide by hydrated lime. This is contrary to the effect noted for  $\text{CaO}$  and limestone. Since water vapor and oxygen have a similar effect on the oxidation rate of  $\text{CaSO}_3$  to  $\text{CaSO}_4$  [24], the need for additional air will be eliminated. Also, it could be possible that water vapor prevents the pore plugging that produced a negative effect for  $\text{CaO}$  in the presence of excess air, leading to almost stoichiometric utilisation of the sorbent. This will also explain the linear relationship between the extent of sulfur dioxide retention and the amount of hydrated lime in the agglomerates.

#### Coagglomeration of Syncrude Fluid Coke with Lime/Limestone.

In order to assess the efficiency of this process for controlling sulfur dioxide emissions from the combustion of various types of cokes, coagglomeration of Syncrude fluid coke with lime or limestone was also attempted. The results were essentially identical to those observed for Suncor coke. The efficiencies of sulfur dioxide retention from the combustion of Syncrude coke by limestone and lime can be compared with the results presented in Figure 7. Although, both curves follow essentially the same trend, it is obvious from the results that limestone is a more efficient sorbent, compared with lime, over the entire range of calcium to sulfur ratios. This could be attributed to the higher porosity and reactivity produced by the in situ calcination reaction [16,17]. The effect of pore size is known to be significant in determining the rate as well as the extent of reaction between  $\text{SO}_2$  and  $\text{CaO}$ . It has been found that small pores in the calcines resulted in high rates of reactions and low overall conversions due to pore plugging, while large pores caused lower rates of reaction with higher conversions [17,21,25]. It is probable that the freshly calcined limestone particles have bigger pores than the  $\text{CaO}$  used. This is a very important result as the ability to use a cheap and readily available material in its natural form has a considerable economic significance. The cost ratio of lime to limestone on a molar basis may vary from 2 to 4 depending on the transportation distance [26]. Even the costs for transportation and handling of limestone tends to be lower than for lime since it can be transported in open trucks.

Results discussed so far have demonstrated that coagglomerating cokes with such sulfur capture agents as limestone, lime and hydrated lime could be an effective way for controlling sulfur dioxide emissions from the combustion of these cokes. In Figure 8 a comparison of the efficiency of this process in terms of sulfur retention by the ash has been made for the two cokes investigated. It is obvious from the plots that although this process is effective for both cokes it is slightly more efficient for Syncrude coke compared with Suncor coke specially at higher calcium to sulfur ratios. Thus, at a calcium to sulfur mole ratio of about 1:1 over 90% sulfur retention can be achieved for Syncrude coke compared with over 80% sulfur retention for Suncor coke. This difference may be due to the reportedly higher bulk gasification reactivity of Syncrude fluid coking coke compared with that of Suncor delayed coking coke [22]. Higher reactivity of fluid coke, compared with delayed coke, is surprising as the former was subjected to more severe treatment in the coking process. However, no reason for this reactivity difference has been suggested.



Comparative efficiencies of the three sorbents investigated; lime, hydrated lime and limestone have been illustrated in the plots shown in Figure 9. These results were obtained in the presence of conditioning agents that activate the sorbent as discussed above. It is obvious from these plots that activated limestone is the most efficient in its capacity to retain  $\text{SO}_2$ . Lime and hydrated lime both have comparable efficiencies for low calcium to sulfur ratios (up to " 1.0). However, in the range of Ca to S ratios beyond 1, hydrated lime appears to be more efficient than lime, approaching in efficiency to that observed for activated limestone. The observed higher efficiency of activated limestone for  $\text{SO}_2$  retention is of considerable significance because of its already mentioned economic advantage over the other sorbents.

According to the findings of Schneider and George [27] calcium has a beneficial effect on the leaching of nickel and vanadium from coke ash using hydrochloric acid. Hence, coagglomeration of coke with calcium compounds will have the added advantage that the ash from these agglomerates would be more suitable for mild acid leaching than the ash from coke alone.

In a fluidized bed combustion of coal the amount of sorbent required to achieve a given reduction in sulfur dioxide emissions mainly depends on the gas retention time in the bed and consequently the flow rate of air. However, in the present case, where there is intimate contact between fuel and sorbent within an agglomerate matrix, sulfur dioxide has to diffuse out through the agglomerate pores, contacting sorbent during its passage, before coming in contact with the fluidizing air. Hence, one might expect greater utilization of the sorbent in this latter case compared to fluidized bed combustion where sorbent is added separately to the bed. A comparison of the results from this investigation with the data from some preliminary experiments on the simulated fluidized bed combustion of Suncor coke does suggest a greater efficiency for coagglomerated sorbents compared to a simple mixture of components. Details of these findings will be presented elsewhere.

#### Conclusions

- (1) There is no significant sulfur retention by the original ash from the Athabasca bitumen cokes.
- (2) Cokes produced during the upgrading of Athabasca bitumen can be successfully coagglomerated with sulfur dioxide capture agents such as: lime, hydrated lime and limestone as a means of reducing sulfur emissions. On combustion, most of the sulfur remains in the recovered ash from these agglomerates instead of escaping to the atmosphere as  $\text{SO}_2$ .
- (3) ASTM method D 4239-83 is not satisfactory for measuring the sulfur dioxide emissions from the combustion of coke-limestone agglomerates.
- (4) Decrease in the sulfur dioxide emitted on combustion of the coke-sorbent agglomerates depends on such variables as the calcium to sulfur mole ratio, combustion temperature, partial pressure of oxygen, conditioning agents and the type of coke and sorbent.
- (5) The quantity of the sulfur dioxide capture agents required for coagglomeration with coke depends on the degree of sulfur removal desired. The decrease in the sulfur dioxide formed on combustion increases with increasing quantities of additive, until further additive confers no additional benefit. Thus over 80-90% reductions in sulfur dioxide emissions can be achieved with a calcium to sulfur mole ratio of approximately 1:1.
- (6) Combustion temperature had a profound effect on the retention of sulfur dioxide by sorbents. In general, at higher temperatures more sulfur dioxide retention was achieved than at lower temperatures. However, the optimum temperature at which maximum sulfur retention could be obtained varies with the type of sorbent.
- (7) At lower combustion temperatures, the presence of excess air had a beneficial effect on the retention of sulfur in the coke-limestone system, and a negative effect in the coke-lime system. For the coke-hydrated lime, presence of excess air does not affect the overall conversion.
- (8) Conditioning agents such as sodium hydroxide, sodium oleate and a petroleum sulfonate had a beneficial effect both on agglomeration and on the extent of sulfur dioxide capture.

- (9) Coagglomeration of Athabasca bitumen cokes with lime, hydrated lime or limestone is an effective desulfurization method. However, Syncrude fluid coke gave slightly better results than Suncor delayed coke.
- (10) Activated limestone is a slightly more efficient sorbent than lime. This has an economic advantage as limestone is 2-4 times cheaper than lime.

#### Acknowledgments

The authors wish to thank P. Maxwell, Martin Lepage, Mrs. M.R. Miedema and F.W. Meadus for some technical assistance; R.D. Coleman and Roger Lafleur of EMR for kindly providing access to a Leco sulfur analyzer.

#### Literature Cited

1. George, Z.M.; Keesick, M.A. Prep. 32nd Can. Chem. Engin. Conf. 1982, 712.
2. Parmar, B.S. and Tollefson, E.L. Can. J. Chem. Engin. 1977, 55, 185.
3. Hall, E.S.; Tollefson, E.L.; George, Z.M. and Schneider, L., Can. J. Chem. Engin. 1982, 60, 418.
4. Phillips, R.C.;; Chao, K.S. Fuel, 1977, 56, 70.
5. Anthony, E.J.; Desai, D.L.; Friedrich, F.D. Canmet Report No. ERP/ERL 81-27, 1981.
6. Lee, D.C.; Georgakis, C. AIChem. Engin. J., 1981, 472.
7. Alberta Committee on Oil Sands Analysis. Bitumen Round Robin No. 2. Dean Wallace, Chairman, Alberta Research Council, February, 1983.
8. Majid, A.; Ripmester, J.A. and Sparks, B.D. Proc. 4th International Symposium on Agglomeration, 1985, 927.
9. Christman, P.G. Ph.D. Thesis, The University of Texas at Austin, 1981.
10. Yang, R.T.; Shen, M.; Sheinberg, M. Environ. Sci. Technol., 1978, 12 (8), 915.
11. Jack, T.R.; Sullivan, E.A. and Zajic, J.E. CIM Bulletin, 1980, 151.
12. Hatfield, J.D.; Kim, Y.K.; Mullins, R.C. and McClellan, G.H. NTIS Publication, no PB202407, 1970.
13. Potter, A.E., Ceramic Bulletin, 1969, 48(9), 855.
14. O'Neill, E.P.; Keairns, D.L. and Kittle, W.F. Thermochimica Acta, 1976, 14, 209.
15. Roberts, A.G.; Stanton, J.E.; Wilkins, J.M.; Beacham, B. and Hoy, H.R. Proc. Fluidized Combustion Conference, 1975.
16. Borgwardt, R.H. Environ. Sci. and Techn., 1970, 4(1), 59.
17. Borgwardt, R.H. and Harvey, R.D. Environ. Sci. and Techn., 1972, 6(4), 350.
18. Hills, A.W.D. Chem. Engin. Sci., 1968, 23, 297.
19. Hoke, R.C.; Nutkis, M.S. and Kinzler, D.D. Proc. Fluidized Bed Technology Exchange Workshop, 1977, 157.
20. R.V. Siriwardane and J.M. Cook, J. Coll. Interface Sci., 1986, 114, 525.
21. Ulerich, N.H.; O'Neill, E.P. and Keairns, D.L., Thermochimica Acta, 1978, 26, 269.
22. Furimsky, E. Fuel Processing Technology, 1985, 11, 167.
23. Berenak, J., Proc. of Control of gaseous sulfur compound emissions, Intr. Conf., 1973, 2.
24. Karlsson, H.T.; Bengtsson, S.; Bjerle, I.; Klingsper, J.; Nilsson, L.I. and Stronberg, A.M. Proc. International Conference on Processing and Utilization of High Sulfur Coals, 1985, 389.
25. O'Neill, E.P.; Ulerich, J.H.; Keairns, D.L.; Newby, R.A. and Archer, D.H. Proc. Fluidized Bed Technology Exchange Workshop, 1977, 371.
26. Miller, J.F.; Oxley, J.H.; Rosenberg, H.S. and Nusum, H.K. Proc. I. International Conference on Processing and Utilization of High Sulfur Coals, 1985, 575.
27. Schneider, L.G. and George, Z.M. Ext. Metal. Conf. 81, Instite Min. Metall. London, 1981.

#### Figure Captions.

- Figure 1. Calcium to sulfur ratio effect on SO<sub>2</sub> capture by limestone ● Ashing temperature 460°C in excess air; ○ Ashing temperature 1000°C in limited air.
- Figure 2. The effect of ashing temperature on SO<sub>2</sub> capture by limestone. ○ 460°C, limited air, ● 460°C, excess air, △ 750°C, excess air and □ 1000°C limited air.

- Figure 3. The effect of various conditioning agents on the retention of sulfur dioxide by limestone.  
 ○, blank; ●, NaOH; □, sodium oleate and ■, TRS 10/80.
- Figure 4. Calcium to sulfur ratio effects on the retention of sulfur dioxide by lime.
- Figure 5. The effect of ashing temperature on SO<sub>2</sub> capture by lime. ○, ●, 460°C limited air; △, ▲, 460°C, excess air and □, ■, 1000°C limited air. Open symbols for Syncrude coke; close symbols, Suncor coke.
- Figure 6. Calcium to sulfur ratio effect on SO<sub>2</sub> capture by hydrated lime.
- Figure 7. The SO<sub>2</sub> capture efficiencies of limestone vs lime ○, limestone; ● Lime; from Syncrude coke.
- Figure 8. Efficiency of SO<sub>2</sub> capture; Suncor coke vs Syncrude coke. ○, △, limestone; ●, ▲, lime; □, hydrated lime; △, ▲, Syncrude coke; ○, ●, □, Suncor coke.
- Figure 9. Comparative SO<sub>2</sub> capture efficiencies of various sorbents for Suncor coke. ○, limestone; △, lime; □, hydrated lime.

## KINETICS AND MECHANISM OF THERMAL DeNOx: A REVIEW

Richard K. Lyon

Energy and Environmental Research Corp.  
1090 King Georges Post Road  
Edison, NJ 08837

In 1972 the author, then with Exxon Research and Eng. Co. (ERE), discovered a new chemical reaction, the gas phase homogeneous reduction of NO to N<sub>2</sub> and H<sub>2</sub>O by NH<sub>3</sub>, in the presence of O<sub>2</sub> (1,2,3). This reaction was both rapid and highly selective, i.e. with reaction times of 0.1 sec or less NO could be nearly quantitatively reduced by equimolar amounts of NH<sub>3</sub> in the presence of O<sub>2</sub> concentrations orders of magnitude greater than the NO. The discovery of this reaction made possible a new and remarkably simple method of controlling the emissions of NO<sub>x</sub> from stationary sources such as utility boilers and industrial process furnaces, the Thermal DeNO<sub>x</sub> process. One simply found the location in the unit at which the temperature was appropriate to the reaction and installed there a grid to inject NH<sub>3</sub> into the hot flue gas. To date this process has had upwards of 60 commercial applications and in recent instances NO reductions in excess of 90% have been achieved.

One factor which helped make this success possible was the development of a predictive kinetic model, i.e. a model which described the kinetics of the reaction in terms of elementary reaction rate constants and which could be used to accurately predict the performance of the process in any given practical application. The model is routinely used in the engineering design of new Thermal DeNO<sub>x</sub> installation. To the author's knowledge this is the first instance in which a model based on elementary reaction rate constants has been so used. This success was the culmination of the efforts of workers both within and outside of ERE but this success has received less attention than it might have otherwise. Several papers and meeting presentations have outlined the general nature of the model (4,5,6,7,8), but the actual model itself has been disclosed only in one somewhat obscure patent (9). In this review the DDHL model will be discussed and compared with models published by others.

The other models of interest were developed by Hanson and Salimian with subsequent refinement by Hanson and Kimball-Linne (10,11), by Miller, Branch and Kee (12), and by Silver, Gozewski and Kolb (13), hereinafter the H&K, MBK, and SGK models, respectively. Silver and Kolb (14) also measured the rate constant of the NH<sub>2</sub> + NO reaction at elevated temperatures. Miller et al. are to be credited with proposing on purely theoretical grounds that the second channel of the NH<sub>2</sub> + NO reaction does not directly yield N<sub>2</sub> + H + OH but rather N<sub>2</sub>H + OH, a suggestion later supported experimentally by Andresen et al. (15). It is to be noted that both of these contributions were incorporated into the DDHL model.

A principal difference among these modeling efforts was the extent to which experimental data on the kinetics of the NO - NH<sub>3</sub> - O<sub>2</sub> reaction were available to the modelers. The MBK and SGK models are a priori models, i.e. in the development of these models if the rate constant of a reaction was unknown, it was estimated on purely theoretical grounds without any effort to choose a value that would make the model fit the data. Both these models were successful in qualitative terms in that they showed the appropriate trends when compared to the limited data of Muzio et al. (16). In the H&K model, however, the model seeks to provide a truly quantitative description of the reaction kinetics. Hanson and Kimball-Linne set up a laboratory scale combustor and generated a block of data showing the kinetics of the Thermal DeNO<sub>x</sub> process for initial temperatures ranging from 1258 K to 1548 K and initial [NO] and [NH<sub>3</sub>] ranging from 141 to 387 ppm and 78 to 556 ppm, respectively. Since the combustor was operated at a constant air/fuel equivalence ratio of 0.9, neither [O<sub>2</sub>] nor [H<sub>2</sub>O] were varied. Sensitivity analysis was done on the model and the rate constants of reactions which were uncertain and sensitive were adjusted to fit the data. Figure 1 shows an example of the model's fit to the data.

The DDHL model was developed in a similar manner, i.e. flow tube experiments were done with synthetic gas mixtures to develop two data bases, one relating to the oxidation of NH<sub>3</sub> in the initial absence of NO (T = 1279 to 1323 K, [NH<sub>3</sub>] = 900 ppm, [O<sub>2</sub>] = 2 to 8% and [H<sub>2</sub>O] = 0 or 1%) and the second larger data base relating to the reduction of NO by NH<sub>3</sub> (T = 1120 to 1390 K, [O<sub>2</sub>] = 2 to 8%, [H<sub>2</sub>O] = 0 to 15%, [NO] = 100 to 460 ppm, [NH<sub>3</sub>] = 270 to 530 ppm, a total of 742 data points). A kinetic model was developed which gave excellent fit to the former data base and with minor modifications which didn't damage the fit to the NH<sub>3</sub> oxidation data base it proved possible to fit the NO reduction data base within 7%, which is within the experimental uncertainty. Figure 2 shows examples of this model's fit to laboratory data (5) while Figure 3 shows a comparison between the model's predicted performance for the Thermal DeNO<sub>x</sub> process in commercial application and what was obtained. (9)

Since then the DDHL and HSK models were derived in general similar manners, the comparison between them is particularly interesting. While the DDHL model uses 31 elementary reactions of H/N/O species, the H&K model uses 52. Of these 30 reactions are common to the two models, DDHL includes one radical radical reaction which is probably unimportant under Thermal DeNO<sub>x</sub> conditions and which the H&K model omits. The H&K model includes ten such radical radical reactions. The other reactions which are used in H&K and omitted in DDHL includes three reactions which form nitrogen atoms and four reactions of N<sub>2</sub>O. The former have high activation energies and will be important only at temperatures well above the Thermal DeNO<sub>x</sub> range. Since Thermal DeNO<sub>x</sub> does not make significant amounts of N<sub>2</sub>O, the latter will be unimportant in the initial absence of N<sub>2</sub>O. While the DDHL model shows the interaction of NH<sub>2</sub> and NO as a two channel reaction, capable of yielding N<sub>2</sub>H + OH and N<sub>2</sub> + H<sub>2</sub>O, the H&K model shows it as having a third far less probable channel yielding HNO + NH. DDHL shows the reactions of NH<sub>2</sub> + O, NH + O<sub>2</sub>, and

NO + HO<sub>2</sub> as single channel processes, each making only one pair of products. While the H&K model agrees that these are the dominant reaction pathways, it does include a second less important channel for each. The H&K model also includes the reaction  $N_2H+O_2=N_2+HO_2$  with a rate constant that is 1000 times less at 1200 K than the rate constant which H&K assumes for the competing  $N_2H+NO=N_2+HNO$  reaction. Thus the omission of this reaction by DDHL does not appear to be a serious disagreement.

Indeed there does not seem to be any disagreement between the two models as to which reactions are central to the Thermal DeNO<sub>x</sub> chemistry. There is also much agreement as to the roles which these reactions play in deciding the overall kinetics of the Thermal DeNO<sub>x</sub> reaction. In both models the overall reaction mechanism may be divided into two submechanisms, a chain reaction in which NH<sub>3</sub> reduces NO and a chain reaction in which NH<sub>3</sub> is oxidized to form NO. In both submechanisms the first step is the attack on NH<sub>3</sub> by O and OH to form NH<sub>2</sub>. In the reduction submechanism the NH<sub>2</sub> reacts with NO yielding either N<sub>2</sub> and H<sub>2</sub>O (a chain terminating step) or yielding NNH and OH. If the latter step is followed by the reactions  $NNH+M=N_2+H+M$  and  $H+O_2=OH+O$  it is strongly chain branching. If, however, the subsequent reaction is  $NNH+NH_2=N_2+NH_3$  or  $NNH+OH=N_2+H_2O$  the result is chain termination. Consequently the NO reduction submechanism is a self controlling explosion. Initially the chain branching sequence is dominant and the concentration of chain carriers grows exponentially, i.e. at a rate that is proportional to the concentration of chain carriers. Since chain termination processes have rates that are proportional to the square of the chain carrier concentration, they soon limit the increase in chain carrier concentration. Thus in the NO reduction submechanism the rate of the overall reaction rapidly grows to a finite limit and proceeds smoothly thereafter.

In the NO formation submechanism NH<sub>2</sub> reacts with O, OH and O<sub>2</sub>. The latter reaction directly produces HNO while the former two reactions produce NH which reacts with O<sub>2</sub> to yield HNO. The function of HNO in the oxidation submechanism is similar to NNH, i.e. dissociation of HNO to yield H atoms causes chain branching while reaction with NH<sub>2</sub> or OH causes chain termination. Thus the oxidation submechanism, left to its own devices, would regulate the chain carrier concentration and overall reaction rate to finite values, though not necessarily the same values as those dictated by the reduction submechanism. This conflict helps make the kinetics of the Thermal DeNO<sub>x</sub> reaction more complex than one might expect from the number of reactions involved.

While there is agreement between the DDHL and H&K models as to which reactions are important, there is significant disagreement as to the roles those reactions play. In table 1 the rate constants of the thirty reactions the two models have in common are listed along with the ratios of those rate constants at 1200 K. Numerically the largest disagreement relates to the  $NH+O_2=HNO+O$  reaction but this is actually trivial since neither model assumes any reaction of NH which could compete effectively with  $NH+O_2=HNO+O$ . The disagreement as to the rate constant for the  $NNH+NO=N_2+HNO$  reaction is more important.

In the DDHL model control of the overall rate is shared between the submechanisms while the high rate constant assumed by H&K for this reaction tends to transfer control of the overall rate from the reduction submechanism to the oxidation submechanism.

Another important disagreement between the models relates to the balance between chain branching and chain termination. In the DDHL model the rate of the chain terminating reaction  $\text{NH}_2 + \text{HNO} = \text{NH}_3 + \text{NO}$  is faster by a factor of 15.8 than in the H&K model. This disagreement is compounded by the fact that in the H&K model the  $\text{N}_2 + \text{H}_2\text{O}$  and  $\text{NNH} + \text{OH}$  channels in the  $\text{NH}_2 + \text{NO}$  reaction are assumed to have equal rate constants while in the DDHL model the former is 1.5 times as fast as the latter. This rate constant ratio is very critical to the kinetics since it controls the chain branching factor.

Finally it is to be noted that in the DDHL model the rate constant for the  $\text{NH}_3 + \text{O} = \text{NH}_2 + \text{OH}$  reaction is a factor of five slower than that used in the H&K model. A recent review of the literature by Cohen (17) recommends a rate constant for  $\text{NH}_3 + \text{O} = \text{NH}_2 + \text{OH}$  that is midway between the H&K and DDHL values with an uncertainty large enough to include both. The result of this and to a lesser extent the other disagreements between the models is that the concentration of O atoms during the deNOx reaction is much lower in the H&K model than it is in the DDHL model. Within DDHL  $\text{NH}_2$  is oxidized to NO chiefly by reaction with O atom but in H&K the  $\text{NH}_2 + \text{OH} = \text{NH} + \text{H}_2\text{O}$  is more important. This leads the two models to rather different predictions of the effect of water vapor on the kinetics of the Thermal DeNOx reaction. Figures 4 and 5 show calculations of the extent of NO reductions as a function of reaction temperature done with the DDHL and H&K models. In the DDHL model adding water vapor shifts the optimum reaction to higher values, i.e. in the DDHL model added water removes O atom via the reaction  $\text{O} + \text{H}_2\text{O} = 2\text{OH}$  and since O is the critical chain carrier removing it with added water retards the reaction. In the H&K model, however, adding water shifts the optimum reaction temperature to lower values because the added water increases the concentration of OH, the critical chain carrier for H&K.

Since the retarding effect of water has been demonstrated experimentally (compare figures 3c and 3d, also see reference 6), this would seem to be a limitation on the H&K model. Such limitations are to be expected when an empirical model is pushed beyond the range of its data base. The DDHL model has the advantage resting on a much broader data base, one that covers all the parameters of practical importance in applications of the Thermal DeNOx process. This makes the model a useful tool in commercial application of the process, but it is to be recognized that when the model "predicts" the extent of NO reduction to be expected in a given boiler or furnace, it is merely interpolating within the base of laboratory data. When one develops a kinetic model by using the rate constants of unknown reactions as adjustable parameters, two kinds of failure are possible. The model can fail to predict kinetics for conditions outside the range of its data base because for these conditions reactions which were unimportant within the conditions of the data base become important. Such failure is less serious since it does not imply that the model is

essentially wrong, merely that it needs extension. It is also possible, however, for the adjustable parameters to produce a compensating set of errors. It is interesting to ask what experiments could be done to test the DDHL model for the latter problem.

A number of fair tests of the model are possible, i.e. in several instances the information in the model is sufficient to make unambiguous predictions about what should happen for conditions significantly different from the data base. Thus, for example, all the observations in the data base were at one atmosphere pressure and it would be interesting to see whether or not the model could correctly predict the effect of varying the pressure while holding  $[NH_3]$ ,  $[NO]$ ,  $[H_2O]$ , and  $[O_2]$  constant. Similarly the model contains the reactions known to be important during the oxidation of  $H_2$  and those which occur during  $CO$  oxidation could readily be added. Thus the model's ability to predict the extent to which adding  $H_2$  or  $CO$  shifts the optimum reaction temperature to lower values is another interesting test.

Another test of the model, one which has been carried out, involves the oxidation of  $NH_3$  at trace concentrations (19). The model's data base includes experiments in which  $NH_3$  at an initial concentration of 900 ppm was oxidized with  $NO$  initially absent. The observed decay of  $NH_3$  was zero order in  $NH_3$ . This somewhat surprising behavior is a result of the balance between chain carrier production and removal. If the production of free radicals by the reaction sequence  $HNO+M=H+NO+M$ ,  $H+O_2=OH+O$  is balanced by their consumption by  $HNO+NH_2=NO+NH_3$ , it follows that  $[NH_2]$  is independent of  $NH_3$  and the rate of  $NH_3$  disappearance is zero order. Obviously, however, if one starts with a sufficiently small initial concentration of  $NH_3$  this mechanism for maintaining  $[NH_2]$  constant has to become ineffective and the rate of  $NH_3$  oxidation must become dependent on  $[NH_3]$ . Specifically using the DDHL model one can calculate that for the conditions shown in figure 6 the decay of  $NH_3$  should be first order in  $NH_3$  and the decay constant should be 5.61/sec in contrast to the observed value of 5.65/sec. Thus in this instance, at least, the extrapolation of the DDHL model to conditions quite different from its data base is valid.

#### REFERENCES

- 1 R. K. Lyon, U.S. Patent 3,900,554, 1975
- 2 R. K. Lyon, Int. J. Chem. Kinet., 8, 315, 1976
- 3 R. K. Lyon and D. Benn, Symp. (Int.) Combust., [Proc], 17th, 1978, 1979, 601
- 4 R. K. Lyon and J. E. Hardy, I&EC Fundamentals, 1986, 25, 19
- 5 A. M. Dean, A.J. DeGregoria, J. E. Hardy, and R. K. Lyon, 7th International Symposium on Gas Kinetics, Gottingen, Germany, August 1982

- 6 A. M. Dean, J. E. Hardy, and R. K. Lyon, *Symp. (Int.) Combust., [Proc]*, 19th, 1982, 1983, 97
- 7 R. K. Lyon, *Envr 44 Paper Presented at the 187th National Meeting of the American Chemical Society, St. Louis, April 1984*
- 8 B. E. Hurst, *Glass Techno.* 24, 97 (1983)
- 9 A. M. Dean, A. DeGregoria, J. E. Hardy, B. E. Hurst, and R. K. Lyon, *U. S. Patent*, 4,507,269, 1985
- 10 S. Salimain and R. K. Hanson, *Comb. Sci. and Technol.* 23, 225, (1980)
- 11 M. A. Kimball-Linne and R. K. Hanson, *Comb. and Flame*, 64, 337, (1986) also see M. A. Kimball-Linne, *Report T244 High Temperature Gas Dynamics Laboratory, Stanford University*
- 12 J. A. Miller, M. C. Branch, and R. J. Kee, *Comb. and Flame*, 44, 181 (1981)
- 13 J. A. Silver, C. M. Gozewski and C. E. Kolb, *Aerodyne Report NO ARI-RR-66*; also see J. A. Silver, *Comb. and Flame* 53, 17 (1983)
- 14 J. A. Silver and C. E. Kolb, *Chem. Phys. Lett.* 75, 191, (1980)
- 15 P. Andresen, A. Jacobs, C. Kleinermanns, and J. Wolfrum, *Symp. (Int.) Combust., [Proc]*, 19th, 1982, 1983, 11
- 16 L. J. Muzio, J. K. Arand and D. P. Tierxeria, *Symp. (Int.) Combust., [Proc]*, 16th, 1976, 1977, 199
- 17 N. Cohen, *Int. J. Chem. Kinet.* 19, 319, 1987
- 18 A. C. Lloyd, *Int. J. Chem. Kinet.* 6, 169, 1974
- 19 R. K. Lyon and J. E. Hardy, *Poster Session at 20th Symposium, (Int.) on Combustion, Ann Arbor, 1984*

TABLE 1

COMPARISON OF THE RATE CONSTANTS USED IN THE DDHL AND H&K MODELS

(In this table R denotes the ratio of the DDHL rate constant to the H&K rate constant at 1200 K. \* indicates reactions which were found to be kinetically sensitive.)

		A	n	E, kcal	R**
1)	DDHL H+O2=O+OH	2.2E+14	-0.	16.80	0.97
	H&K H+O2=O+OH	3.7E+17	-1.00	17.5	
2)	DDHL O+H2=H+OH	1.8E+10	1.0	8.90	1.0
	H&K O+H2=H+OH	1.8E+10	1.00	8.90	
3)	DDHL H2+OH=H2O+H	2.2E+13	0.0	5.15	0.97
	H&K H2+OH=H2O+H	1.17E+09	1.30	3.626	
4)	DDHL OH+OH=O+H2O	6.3E+12	0.0	1.09	0.95
	H&K O+H2O=OH+OH	4.60E+09	1.3	17.10	
5)	DDHL H+O2+M=HO2+M	1.5E+E15	0.0	-0.995	1.45
	(For M=H2O the quoted rate constant is increased by x21)				
	H&K H+O2+M=HO2+M	7.3E+18	-1.0	0.0	
	(For M = N2 or O2 the quoted A factor is changed to 6.7E+19 and n changed to -1.42)				
6)	DDHL H+HO2=OH+OH	2.5E+14	0.0	1.90	1.0
	H&K H+HO2=OH+OH	2.5E+14	0.0	1.90	
7)	DDHL HO2+OH=H2O+O2	5.0E+13	0.0	1.00	1.0
	H&K HO2+OH=H2O+O2	5.0E+13	0.0	1.00	
8)	DDHL HO2+O=O2+OH	5.0E+13	0.0	1.00	1.0
	H&K HO2+O=O2+OH	5.0E+13	0.0	1.00	
9)	DDHL NH3+M = NH2+H+M	4.8E+16	0.00	93.90	1.83
	H&K NH3+M = NH2+H+M	2.5E+16	0.0	93.79	
10)	DDHL NH3+H=NH2+H2	2.5E+13	0.0	17.10	1.22
	H&K NH3+H=NH2+H2	1.3E+14	0.0	21.50	
11)	DDHL NH3+O=NH2+OH	1.5E+12	0.0	6.04	0.23
	H&K NH3+O=NH2+OH	2.19E+13	0.0	8.94	
12)	DDHL NH3+OH=NH2+H2O	3.3E+12	0.0	2.12	0.71
	H&K NH3+OH=NH2+H2O	5.75+13	0.0	8.11	
13)	DDHL NH2+O=NH+OH*	1.7E+13	0.	1.00	0.71
	H&K NH2+O=NH+OH	6.75E+12	0.0	0.0	

Table 1 (continued)

14)	DDHL	$\text{NH}_2 + \text{OH} = \text{NH} + \text{H}_2\text{O}^*$	5.5E+10	0.68	1.29	0.66
	H&K	$\text{NH}_2 + \text{OH} = \text{NH} + \text{H}_2\text{O}$	6.0E+12	0.0	0.0	
15)	DDHL	$\text{NH}_2 + \text{H} = \text{NH} + \text{H}_2$	5.0E+10	0.5	2.00	0.39
	H&K	$\text{NH}_2 + \text{H} = \text{NH} + \text{H}_2$	1.9E+13	0.0	0.0	
16)	DDHL	$\text{NH}_2 + \text{HNO} = \text{NH}_3 + \text{NO}^*$	1.8E+14	0	1.00	15.8
	H&K	$\text{NH}_2 + \text{HNO} = \text{NH}_3 + \text{NO}$	5.0E+11	0.5	2.00	
17)	DDHL	$\text{NH} + \text{O}_2 = \text{HNO} + \text{O}$	3.0E+13	0.0	3.40	110.6
	H&K	$\text{NH} + \text{O}_2 = \text{HNO} + \text{O}$	1.0E+13	0.0	12.00	
18)	DDHL	$\text{HNO} + \text{OH} = \text{NO} + \text{H}_2\text{O}$	3.6E+13	0.0	0.0	0.5
	H&K	$\text{HNO} + \text{OH} = \text{NO} + \text{H}_2\text{O}$	1.26E+12	0.5	2.0	
19)	DDHL	$\text{HNO} + \text{M} = \text{H} + \text{NO} + \text{M}^*$	1.9E+16	0.0	48.68	0.4
	H&K	$\text{H} + \text{NO} + \text{M} = \text{HNO} + \text{M}$	7.56E+15	0.0	-0.6	
20)	DDHL	$\text{NO} + \text{HO}_2 = \text{NO}_2 + \text{OH}$	3.4E+12	0.0	-0.26	1.8
	H&K	$\text{NO} + \text{HO}_2 = \text{NO}_2 + \text{OH}$	2.09E+12	0.0	-0.48	
21)	DDHL	$\text{NH}_2 + \text{NO} = \text{NNH} + \text{OH}^*$	6.1E+19	-2.46	1.87	0.4
	H&K	$\text{NH}_2 + \text{NO} = \text{NNH} + \text{OH}$	1.26E+16	-1.25	0.0	
22)	DDHL	$\text{NH}_2 + \text{NO} = \text{N}_2 + \text{H}_2\text{O}^*$	9.1E+19	-2.46	1.87	0.6
	H&K	$\text{NH}_2 + \text{NO} = \text{N}_2 + \text{H}_2\text{O}$	1.26E+16	1.25	0.0	
23)	DDHL	$\text{O} + \text{NO}_2 = \text{NO} + \text{O}_2$	1.0E+13	0.0	0.6	1.0
	H&K	$\text{O} + \text{NO}_2 = \text{NO} + \text{O}_2$	1.0E+13	0.0	0.6	
24)	DDHL	$\text{NO}_2 + \text{H} = \text{NO} + \text{OH}$	3.5E+14	0.0	1.50	0.99
	H&K	$\text{NO}_2 + \text{H} = \text{NO} + \text{OH}$	3.5E+14	0.0	1.48	
25)	DDHL	$\text{NO}_2 + \text{M} = \text{NO} + \text{O} + \text{M}$	1.1E16	0.0	66.00	1.6
	H&K	$\text{NO} + \text{O} + \text{M} = \text{NO}_2 + \text{M}$	2.00E+15	0.0	1.88	
26)	DDHL	$\text{NNH} + \text{NH}_2 = \text{N}_2 + \text{NH}_3^*$	1.0E+13	0.0	0.	1.0
	H&K	$\text{NNH} + \text{NH}_2 = \text{N}_2 + \text{NH}_3$	1.0E+13	0.0	0.0	
27)	DDHL	$\text{NNH} + \text{M} = \text{N}_2 + \text{H} + \text{M}^*$	2.0E+14	0.0	30.00	0.4
	H&K	$\text{NNH} + \text{M} = \text{N}_2 + \text{H} + \text{M}$	2.0E+14	0.0	28.00	
28)	DDHL	$\text{NNH} + \text{OH} = \text{N}_2 + \text{H}_2\text{O}$	3.0E+13	0.0	0.0	1.0
	H&K	$\text{NNH} + \text{OH} = \text{N}_2 + \text{H}_2\text{O}$	3.0E+13	0.0	0.0	
29)	DDHL	$\text{NNH} + \text{NO} = \text{N}_2 + \text{HNO}^*$	9.1E+11	0.0	0.0	0.02
	H&K	$\text{NNH} + \text{NO} = \text{N}_2 + \text{HNO}$	5.0E+13	0.0	0.0	
30)	DDHL	$\text{NH}_2 + \text{O}_2 = \text{HNO} + \text{OH}^*$	5.1E+13	0.0	30.00	1.4
	H&K	$\text{NH}_2 + \text{O}_2 = \text{HNO} + \text{OH}$	4.5E+12	0.0	25.00	

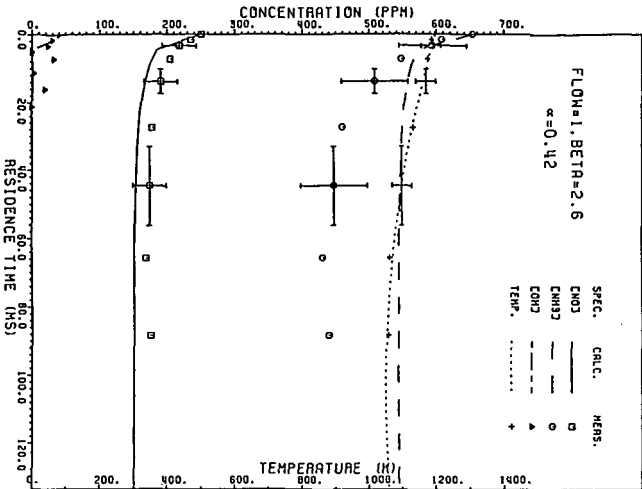


Figure 1. Comparison of H&K Model Predictions With Experiment.  $\text{NH}_3/\text{NO}=2.6$

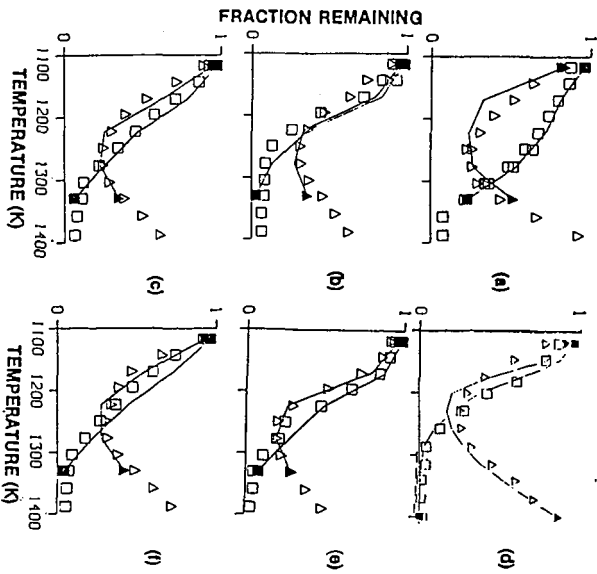


Figure 2. Comparison of DDHL Model Predictions (Lines Terminated by  $\blacksquare$  for  $\text{NO}$  and by  $\blacktriangle$  for  $\text{NH}_3$ ) with Experiment.  $\square = \text{NO}$ ,  $\triangle = \text{NH}_3$ ,  $t=0.1$  sec,  $P=1.2$  atm,  $\text{O}_2=4\%$  (a,b,c,d),  $2\%$  (e),  $8\%$  f,  $\text{NH}_3=385$  ppm  $\text{NO}=100$  ppm (a),  $325$  ppm (b),  $225$  ppm (c,d, e,f),  $\text{H}_2\text{O}=10\%$  (a,b,c,e,f) or  $0\%$  (c).

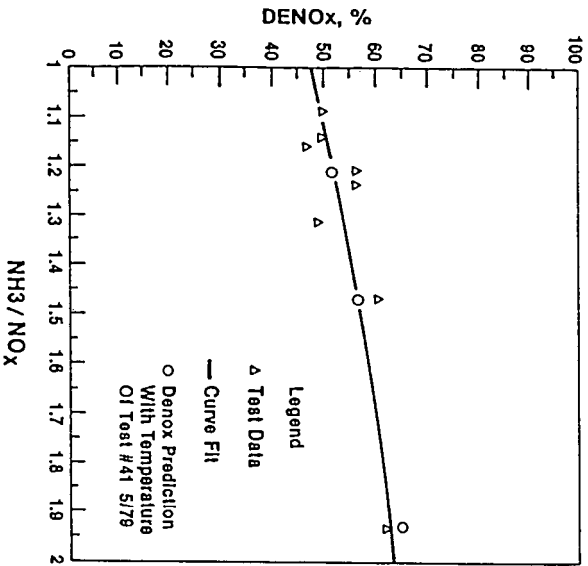


Figure 3. Comparison of DDHL Model Prediction with Observed NO Reduction in a Utility Boiler, LADWP Haynes #4. Curve Fit is to Test Data.

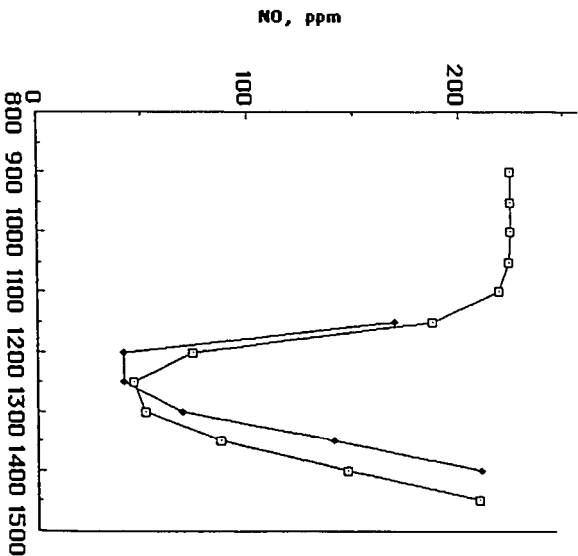


Figure 4. Effect of H<sub>2</sub>O on DENOX as Predicted by DDHL Model, 4% O<sub>2</sub>, 225 ppm NO, 385 ppm NH<sub>3</sub>, 0.1 sec reaction time  
 □ = 10% H<sub>2</sub>O, ◆ = 0% H<sub>2</sub>O.

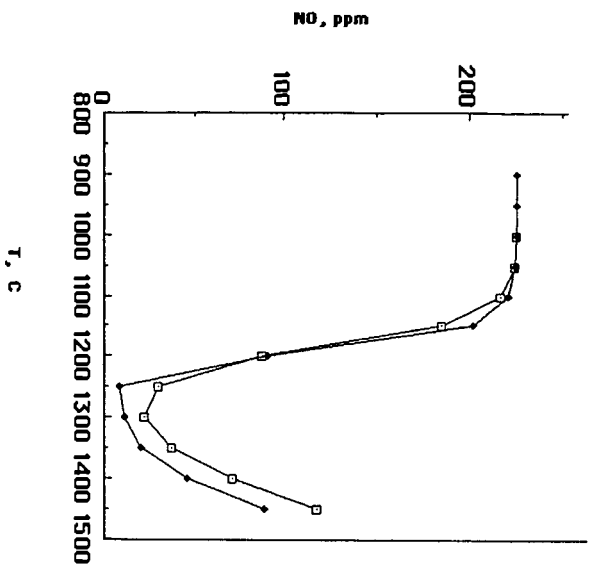


Figure 5. Effect of H<sub>2</sub>O on DenOx as Predicted by H&K Model, 4% O<sub>2</sub>, 225 ppm NO, 385 ppm NH<sub>3</sub>, 0.1 sec Reaction Time

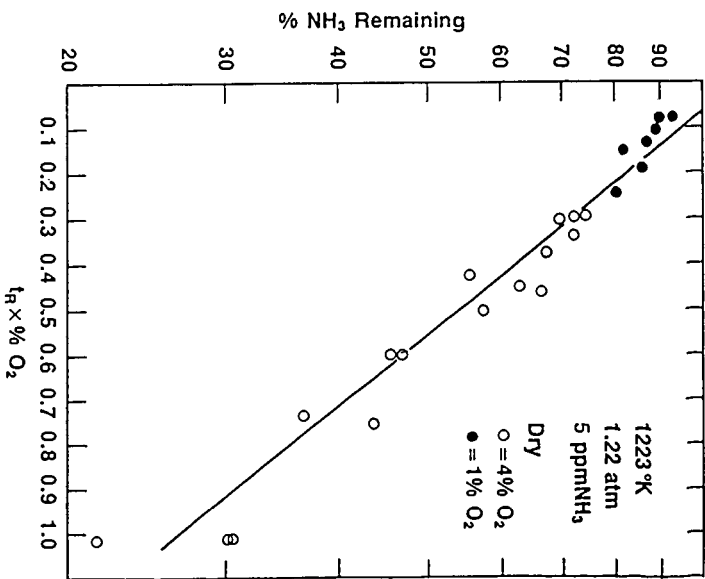


Figure 6. First Order Decay of NH<sub>3</sub> During the Oxidation of NH<sub>3</sub> at Trace Concentrations

**Combined NO<sub>x</sub>/SO<sub>2</sub> Removal from Flue Gas  
Using Ferrous Chelates of SH-Containing Amino Acids and Alkali**

David K. Liu and S. G. Chang

*Applied Science Division  
Lawrence Berkeley Laboratory  
University of California  
Berkeley, CA 94720*

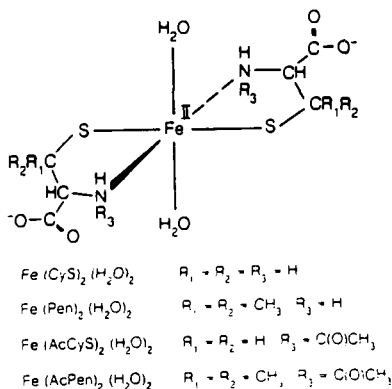
**ABSTRACT**

We report herein the use of ferrous chelates of SH-containing amino acids including cysteine, penicillamine, N-acetylcysteine, and N-acetylpencillamine in neutral or alkaline solutions for the combined removal of NO and SO<sub>2</sub> in wet flue gas clean-up systems. These SH-containing amino acids not only can stabilize ferrous ions in alkaline solutions to promote the absorption of NO, but are also capable of rapidly reducing ferric ions formed during the scrubbing process back to ferrous ions. The disulfide from of the above amino acids can be reduced by SO<sub>2</sub> and H<sub>2</sub>S to regenerate the starting monomeric species. The chemistry relevant to the absorption of NO by the above ferrous chelates and the ligand regeneration process will be discussed.

## INTRODUCTION

A large number of wet flue gas clean-up processes using iron chelates to simultaneously remove  $\text{NO}_x$  and  $\text{SO}_2$  from combustion flue gas have been developed over the past fifteen years. The mechanism for NO absorption using these  $\text{Fe}^{2+}$ (EDTA) type chelates involves the formation and subsequent reaction of a ferrous nitrosyl complex with dissolved  $\text{SO}_2$  and  $\text{O}_2$  to produce  $\text{N}_2$ ,  $\text{N}_2\text{O}$ , dithionate, sulfate, nitrogen-sulfur compounds, and ferric chelates which are unreactive towards NO (1). The regeneration of scrubbing liquors and ferrous chelates associated with such processes is very costly (2). Therefore, these wet absorption processes, even though very efficient in  $\text{SO}_2$  and  $\text{NO}_x$  removal, have not yet reached the commercial stage.

We wish to report the use of ferrous chelates of SH-containing amino acids (or thioamino acids) in neutral or alkaline solutions for the simultaneous removal of  $\text{NO}_x$  and  $\text{SO}_2$  from flue gas. The ferrous chelates investigated in this study include those of L-cysteine (CySH), DL-penicillamine (Pen), N-acetyl-L-cysteine (AcCySH), and N-acetyl-DL-penicillamine (AcPen).



The stereoisomers or racemates of the thioamino acids employed represent the most common and therefore least expensive forms; other stereoisomers or racemates can also be used since they should have identical chemical reactivities. Recent reports from our laboratory have addressed some the chemistry involved in the absorption of NO by ferrous cysteine (3,4). We have also recently communicated preliminary results concerning the use of ferrous chelates of certain cysteine derivatives in the removal of NO from the gas (5). This paper presents a full account of the scrubber chemistry of NO and  $\text{SO}_2$  removal by alkaline solutions containing ferrous chelates of the aforementioned SH-containing amino acids, as well as subsequent regeneration of the thioamino acids for recycling in the scrubber system.

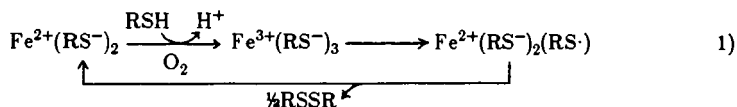
## EXPERIMENTAL

The absorption of NO by neutral or alkaline solutions of ferrous thioamino acid complexes was studied using a bench-scale gas scrubber and a Thermoelectron Model 14A chemiluminescent  $\text{NO}_x$  analyzer (3). For the reduction of the disulfide form of the

thioamino acids, a method similar to that developed for the regeneration of cysteine from cystine was used (4). The identification of all thioamino acids and their derivatives was performed on an amino acid analyzer built in-house (6). The determination of iron-, nitrogen-, and thioamino acid-containing products was based on analytical techniques described previously (3,4).

## RESULTS AND DISCUSSION

The removal of NO from oxygen-containing flue gas can be effected by aqueous solutions containing ferrous chelates of SH-containing amino acids, as shown in Figure 1. It is clear that all the ferrous thioamino acid complexes we tested are much more effective in absorbing NO than  $\text{Fe}^{2+}(\text{EDTA})$  under the same conditions. The greater NO absorption capacity in the cases of ferrous thioamino acid complexes may be accounted for by the ability of the thiol groups to reduce any ferric ion formed upon oxidation of the ferrous chelate by residual  $\text{O}_2$  in flue gas (Equation 1):



This mechanism is well established for  $\text{Fe}^{2+}(\text{Cys})_2$  (7) and is likely also applicable to  $\text{Fe}^{2+}(\text{AcCys})_2$ . In the case of Pen, it has been suggested that the two  $\beta$ -methyl groups serve to inhibit the oxidation-reduction reactions (8). It is therefore likely that the enhanced NO absorption capacity using  $\text{Fe}^{2+}(\text{Pen})_2$  and  $\text{Fe}^{2+}(\text{AcPen})_2$  is the result of the stability of ferrous chelates towards  $\text{O}_2$ . In any case, the concentration of ferrous thioamino acid complex in the absorber is maintained, and NO removal can therefore be sustained. On the contrary, the  $\text{Fe}^{3+}(\text{EDTA})$  complex formed upon oxidation is inactive towards NO. A further advantage of the ferrous thioamino acid systems is that the rapid intramolecular reduction of  $\text{Fe}^{3+}$  to  $\text{Fe}^{2+}$  can prevent the formation of dithionate ion resulting from the reaction between  $\text{Fe}^{3+}$  and  $\text{HSO}_3^-$ .

The effect of pH on the NO absorption capacity of ferrous thioamino acid complexes, as represented by the number of moles of NO absorbed per mole of  $\text{Fe}^{2+}$  used ( $n\text{NO}/n\text{Fe}^{2+}$ ), is shown in Figure 2. While the NO absorption capacity of  $\text{Fe}^{2+}(\text{Cys})_2$  is fairly insensitive to pH,  $\text{Fe}^{2+}(\text{Pen})_2$ ,  $\text{Fe}^{2+}(\text{AcCys})_2$ , and  $\text{Fe}^{2+}(\text{AcPen})_2$  are more efficient as the solutions become less basic, up to  $\text{pH} \sim 6$ . The influence of pH on NO absorption can be attributed to the presence of various ionic forms of thioamino acid, the stability constants of ferrous thioamino acid complexes and ferrous hydroxide, and the rate of  $\text{Fe}^{2+}$ -catalyzed oxidation of the thioamino acids by  $\text{O}_2$ .

The effects of several additives on the NO removal efficiency of  $\text{Fe}(\text{Cys})_2$  were examined, and the results are summarized in Table I (below). Power plant flue gas typically contains several thousand ppm  $\text{SO}_2$ , which dissolves in scrubbing liquors to form primarily  $\text{SO}_3^{2-}$  at  $\text{pH} > 9$ . The effect of  $\text{SO}_2$  on the NO absorption capacity can therefore be studied by the addition of  $\text{SO}_3^{2-}$  to the ferrous cysteine solution. Our results show that  $\text{SO}_3^{2-}$  can improve the NO removal efficiency of  $\text{Fe}^{2+}(\text{Cys})_2$ . Such enhancement could be a result of the reaction of  $\text{SO}_3^{2-}$  with  $\text{O}_2$  to form  $\text{SO}_4^{2-}$ , and/or the reaction of  $\text{SO}_3^{2-}$  with the oxidized product cystine ( $\text{CySSCy}$ ) to form  $\text{CySH}$  and cysteine sulfonate ( $\text{CySSO}_3^-$ ), *vide infra*. High concentrations of  $\text{S}_2\text{O}_3^{2-}$  can also enhance the NO removal efficiency of  $\text{Fe}^{2+}(\text{Cys})_2$ , probably because  $\text{S}_2\text{O}_3^{2-}$  can serve as an oxidation inhibitor. It is expected

Additive	Concentration, M	nNO/nFe <sup>2+</sup>
none	—	0.023
Na <sub>2</sub> SO <sub>3</sub>	0.05	0.040
	0.10	0.050
	0.50	0.068
Na <sub>2</sub> S <sub>2</sub> O <sub>3</sub>	0.05	0.030
	1.00	0.080

<sup>a</sup> The concentrations of Fe<sup>2+</sup> and CySH were 0.01 M and 0.04 M, respectively. The reaction was carried out at pH 9.5 (borate buffer) and 55 °C using a gas mixture of 500 ppm NO, 4% O<sub>2</sub> and the balance N<sub>2</sub>.

that SO<sub>3</sub><sup>2-</sup> and S<sub>2</sub>O<sub>3</sub><sup>2-</sup> will also improve the NO removal efficiency for other ferrous thioamino acid complexes. However, the extent of the improvement may not be as much as that in the Fe<sup>2+</sup>(Cys)<sub>2</sub>, since the adverse effect of O<sub>2</sub> is not as pronounced in those systems (5).

The reaction products collected from the NO absorption reactions by Fe<sup>2+</sup>(Cys)<sub>2</sub> and Fe<sup>2+</sup>(Pen)<sub>2</sub> were analyzed. It has been shown (3) that an iron dinitrosyl complex with an empirical formula [Fe(CySSCy)(NO)<sub>2</sub>] can be isolated when the reaction of NO and Fe<sup>2+</sup>(Cys)<sub>2</sub> was carried out in the absence of O<sub>2</sub>. The same dinitrosyl complex was not found in the presence of 4% O<sub>2</sub>, nor could an analogous iron nitrosyl complex be detected in the case of Fe<sup>2+</sup>(Pen)<sub>2</sub>, whether or not O<sub>2</sub> was present. In both the Fe<sup>2+</sup>(Cys)<sub>2</sub> and Fe<sup>2+</sup>(Pen)<sub>2</sub> systems, most of the absorbed NO was reduced to N<sub>2</sub> and N<sub>2</sub>O, and a small amount (<10% of the NO absorbed) of NO<sub>2</sub><sup>-</sup> was also detected in solution. As a result, minimal formation of nitrogen-sulfur compounds is expected from the reaction between NO<sub>2</sub><sup>-</sup> and HSO<sub>3</sub><sup>-</sup> in the ferrous thioamino acid systems. On the other hand, > 90% of the iron was recovered as insoluble hydroxides in the solid residue, of which ~ 80% was Fe (II) and ~ 20% was Fe (III). The mass balance for the thioamino acid in the NO absorption reaction by Fe<sup>2+</sup>(Cys)<sub>2</sub> was also studied. In the absence of SO<sub>3</sub><sup>2-</sup>, all of the CySH were recovered as CySSCy, as shown in Figure 3. However, if SO<sub>3</sub><sup>2-</sup> as added to the Fe<sup>2+</sup>(Cys)<sub>2</sub> solution, CySSO<sub>3</sub><sup>-</sup> was also formed. It appears that the decrease in [CySSCy] and the increase in [CySSO<sub>3</sub><sup>-</sup>] are linear with respect to increasing [SO<sub>3</sub><sup>2-</sup>]. In each case, 96 ± 2% of the CySH can be recovered as a combination of CySSCy and CySSO<sub>3</sub><sup>-</sup>. It is clear from Figure 3 that unless high concentrations (> 0.5 M) of SO<sub>3</sub><sup>2-</sup> are present, most of the CySH would end up as CySSCy. It is therefore necessary to convert CySSCy back to CySH in order to make this process recyclable and cost-effective.

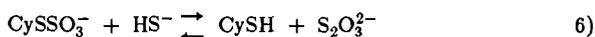
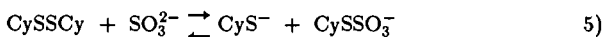
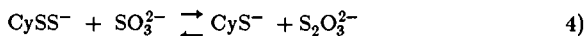
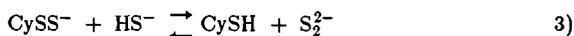
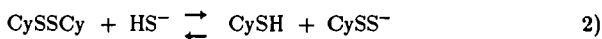
Existing methods for converting CySSCy to CySH require the use of electric energy or expensive reagents, which are not suitable for large-scale applications in flue gas clean up systems. We have discovered a simple and potentially cost-effective method for the regeneration of CySH from CySSCy using H<sub>2</sub>S (or sulfide/hydrogen sulfide ion) and SO<sub>2</sub> (or sulfite/bisulfite) (4). The results for the regeneration of CySH from CySSCy are presented in Table II (below). Methods I (sequential) and II (simultaneous) involve the treatment of a 40 mM CySSCy solution with two equivalents of Na<sub>2</sub>S·9H<sub>2</sub>O and three equivalents of Na<sub>2</sub>SO<sub>3</sub>. Similarly, H<sub>2</sub>S and SO<sub>2</sub> were used to treat the same CySSCy solution, sequentially in Method III and simultaneously in Method IV. The best result was obtained from the reaction of CySSCy with H<sub>2</sub>S and then SO<sub>2</sub> at pH 10 and 60 °C (Method III). The concentrations of HS<sup>-</sup> and SO<sub>3</sub><sup>2-</sup> in solution were estimated to be 0.04

**Table II. Regeneration of CySH from CySSCy under Various Conditions**

Method <sup>a</sup>	pH	T°, °C	CySH, %	CySSO <sub>3</sub> <sup>-</sup> , %	CySSCy, %
I	10	60	59	17	15
II	10	60	36	3	58
III	10	60	90	5	4
IVa	10	60	85	8	6
IVb	10	80	84	10	6
IVc	12	60	84	6	5

<sup>a</sup>See text for description of experimental methods.

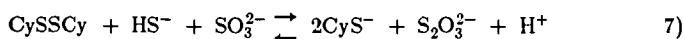
M and 0.22 M, respectively. In this case, a 90% yield of CySH was attained, which increased to 95% upon neutralization of the reaction mixture to pH ~ 7. The concentration-time profile of this reaction is shown in Figure 4. The mechanism for the conversion of CySSCy to CySH can be summarized by the following equations:



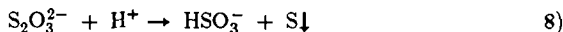
where  $\text{CySS}^-$  represents S-thiocysteine.

In the present study, we have determined that the disulfides of AcCySH and Pen were formed upon the reaction of respective thioamino acid and  $\text{Fe}^{3+}$ . The same  $\text{H}_2\text{S}/\text{SO}_2/\text{OH}^-$  treatment for the regeneration of CySH from CySSCy can be successfully applied to the regeneration of AcCySH from its disulfide. However, the reduction of Pen disulfide did not occur under the same conditions even after 48 hours. As mentioned above, this could be due to the steric effects of the two  $\beta$ -methyl groups in Pen. Therefore, development of a new method to regenerate Pen, and possibly AcPen, from the scrubbing liquor is needed.

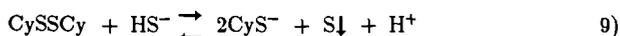
The overall reaction for the regeneration of CySH from CySSCy using  $\text{HS}^-$  and  $\text{SO}_3^{2-}$  can be expressed as



In an acidic medium,  $\text{S}_2\text{O}_3^{2-}$  decomposes to form  $\text{HSO}_3^-$  (and/or  $\text{SO}_2$ ) and colloidal sulfur, as shown in Equation 8.



By adding equations 7 and 8 and taking into account the equilibrium between  $\text{SO}_3^{2-}$  and  $\text{HSO}_3^-$ , we obtain the net equation



Thus, the only reagent consumed in the conversion of CySSCy to CySH is  $\text{HS}^-$ , and elemental sulfur is formed as a product. The latter can be converted back to  $\text{H}_2\text{S}$  by reaction with  $\text{H}_2$ , which can be derived from CO and  $\text{H}_2\text{O}$  (9). Therefore, in essence, the reducing agent consumed in this CySH and the corresponding AcCySH regeneration scheme is CO, which can be easily obtained from the incomplete combustion of coal. It can be inferred from Equation 9 that one mole of CO is required for the regeneration of two moles of CySH or AcCySH.

## CONCLUSIONS

Wet flue gas clean-up systems based on ferrous chelates of thioamino acids possess several major advantages over the conventional  $\text{Fe}^{2+}$  (EDTA) type chelates. These include higher NO absorption capacities, the suppression of dithionate and N-S compound formations, and the ability of the thioamino acids to reduce  $\text{Fe}^{3+}$  to  $\text{Fe}^{2+}$  ion, thus eliminating the need to regenerate ferric chelates from the scrubbing liquor. Reduction of the oxidation products cystine and N-acetylcystine can be accomplished by treatment with  $\text{H}_2\text{S}$  and  $\text{SO}_2$  in basic solutions. However, the same process is not applicable to penicillamine, and possibly N-acetylpenicillamine, due to steric effects. Unfortunately, the application of these ferrous thioamino acid chelates in spray drying systems is limited by the larger stoichiometric ratio of the ferrous chelates to NO (Figure 2) required for obtaining a high ( $\geq 50\%$ ) NO removal efficiency.

## ACKNOWLEDGEMENT

This work was supported by the Assistant Secretary for Fossil Energy, U.S. Department of Energy under Contract No. DE-AC03-76SF00098 through the Pittsburgh Energy Technology Center, Pittsburgh, PA.

## REFERENCES

1. Chang, S.G., *ACS Symp. Ser. No. 919*, 159 (1986), and references therein.
2. Faucett, H.L., Maxwell, J.D., and Burnett, T.A., *EPRI Report AF-568*, (1978).
3. Tu, M.D. and Chang, S.G., *AIChE Environ. Progr.*, 6, 51 (1987).
4. Liu, D.K., Frick, L.P. and Chang, S.G., submitted to *Environ. Sci. & Tech.* (1987).
5. Chang, S.G., Liu, D.K. and Littlejohn, D., Paper No. 76b presented at the AIChE National Meeting in Houston, TX, March 29-April 2, 1987.
6. Liu, D.K. and Chang, S.G., *Can. J. Chem.* 65, 770 (1987).
7. Gilmour, A.D. and McAuley, A., *J. Chem. Soc., (A)*, 1006 (1970).
8. Stadther, L.G. and Martin, R.B., *Inorg. Chem.*, 11, 92 (1972).
9. Kent, J.A., Ed., *Riegels Handbook of Industrial Chemistry*, 7th ed., Van Nostrand Reinhold, New York, NY, 1972, p. 87.

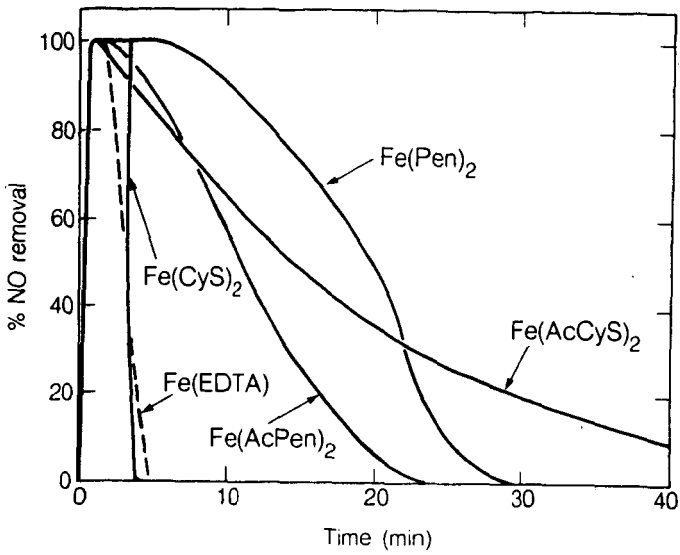


Figure 1. The NO removal efficiency of ferrous thioamino acid and  $\text{Fe}^{2+}$  (EDTA) chelates. Reaction conditions were:  $[\text{Fe}^{2+}] = 0.01 \text{ M}$ ; [thioamino acid] = [EDTA] =  $0.04 \text{ M}$ ;  $[\text{B}_4\text{O}_7^{2-}] = 1.18 \text{ M}$ ;  $P_{\text{NO}} = 500 \text{ ppm}$ ;  $P_{\text{O}_2} = 4\%$ ;  $\text{pH} = 7.0$ ;  $T = 55^\circ \text{C}$ .

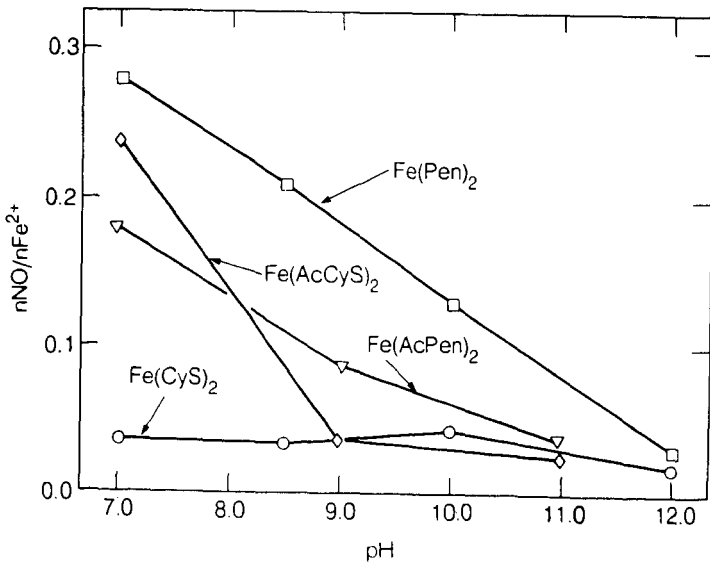


Figure 2. The NO absorption capacity of ferrous thioamino acid chelates as a function of pH. Reaction conditions were:  $[\text{Fe}^{2+}] = 0.01 \text{ M}$ ;  $[\text{CySH}] = 0.04 \text{ M}$ ;  $[\text{B}_4\text{O}_7^{2-}] = 0.09 \text{ M}$ ;  $P_{\text{NO}} = 500 \text{ ppm}$ ;  $T = 55^\circ \text{C}$ .

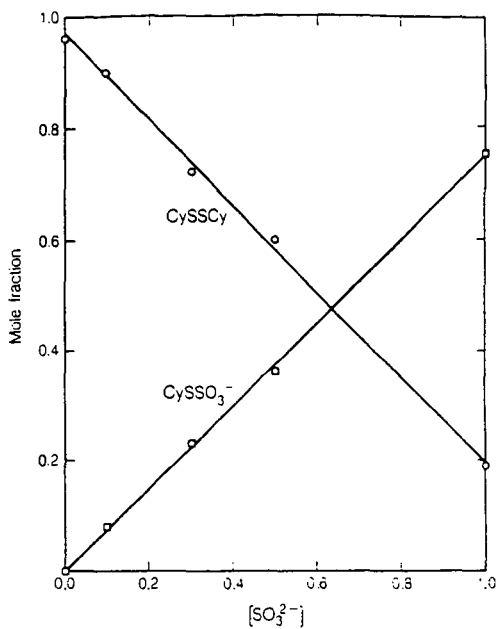


Figure 3. Recovery of CySH as CySSCy and  $\text{CySSO}_3^-$  at various  $[\text{SO}_3^{2-}]$ . Reaction conditions were:  $[\text{Fe}^{2+}] = 0.1 \text{ M}$ ,  $[\text{CySH}] = 1.0 \text{ M}$ ;  $[\text{B}_4\text{O}_7^{2-}] = 0.2 \text{ M}$ ;  $\text{P}_{\text{NO}} = 500 \text{ ppm}$ ;  $\text{P}_{\text{O}_2} = 4\%$ ;  $\text{pH} = 9.0$ ;  $T = 55^\circ \text{C}$ .

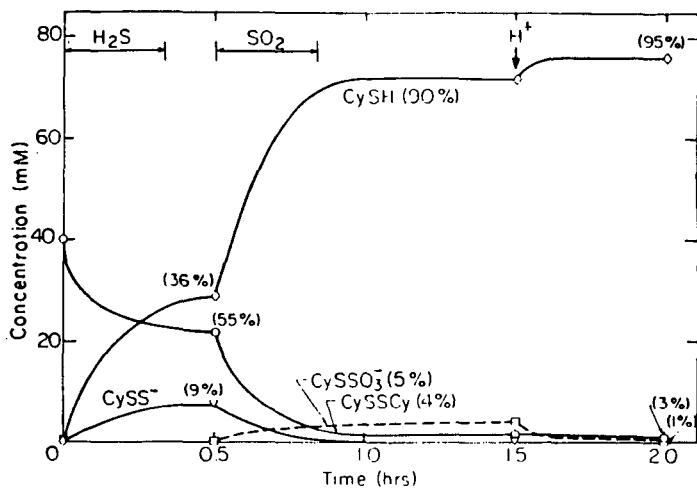


Figure 4. The concentration-time profile of the regeneration of CySH from CySSCy at pH 10 and  $60^\circ \text{C}$  by the reaction of CySSCy first with  $\text{H}_2\text{S}$  and then  $\text{SO}_2$ , followed by neutralization to  $\text{pH} \sim 7$ .

## NO<sub>x</sub> and SO<sub>2</sub> Removal From Flue Gas by Ferrous Ion-Peptide Solutions

D. Littlejohn and S. G. Chang

*Applied Science Division  
Lawrence Berkeley Laboratory  
University of California  
Berkeley, CA 94720*

SO<sub>2</sub> and NO<sub>x</sub> generated by combustion are believed to oxidize in the atmosphere to form H<sub>2</sub>SO<sub>4</sub> and HNO<sub>2</sub>/HNO<sub>3</sub>. The main removal mechanism of these acids from the atmosphere is precipitation, popularly referred to as acid rain. Considerable research is being done to develop efficient, cost-effective procedures to remove SO<sub>2</sub> and NO<sub>x</sub> from power plant flue gases (1). SO<sub>2</sub> can be removed more readily than NO<sub>x</sub> since it is highly soluble in aqueous solutions and can be oxidized to form SO<sub>4</sub><sup>2-</sup>. The sulfate ion can then be precipitated with calcium ions, if desired. Most of the NO<sub>x</sub> is in the form of NO, which has limited solubility in water. Many control strategies for NO<sub>x</sub> have focussed on compounds which enhance the solubility of NO. These systems are usually based on ferrous ion-chelate compounds which readily form nitrosyl complexes (2). Early systems used aminocarboxylic acid chelates such as EDTA, because of their large equilibrium constants for the formation of nitrosyl complexes. However, these systems were very sensitive to the presence of oxygen. In oxygen-free systems, solutions of these compounds can remove significant amounts of NO (3). With oxygen present, the ferrous ion is rapidly oxidized to ferric ion, which does not absorb NO. The oxidized metal ion must then be chemically or electrically reduced to the +2 state. This adds to the cost and complexity of processes using these compounds. The recovery or removal of the absorbed NO is not straightforward in these systems, and it would be desirable to develop a chemical system in which this could be done more easily.

In a search for more suitable iron-chelate combinations, the ferrous ion-cysteine combination was studied (4). It was found that cysteine would readily reduce ferric ion to ferrous ion, and in so doing, keep most of the iron in the ferrous state when exposed to oxygen. The ferrous ion-cysteine system was found to be capable of absorbing significant amounts of NO, with or without the presence of oxygen. Cystine, the oxidized form of cysteine, can be reduced back to cysteine by the appropriate application of HS<sup>-</sup> and SO<sub>3</sub><sup>2-</sup> (5). These compounds can be obtained from the SO<sub>2</sub> removed from the flue gas.

Various cysteine derivatives have been studied to determine if they would be superior to cysteine in removing NO from flue gas. These include glutathione (a tripeptide) and glycylcysteine (a dipeptide) which are the subject of this study. Glutathione (glutamylcysteinylglycine, abbreviated GSH) is a thiol compound that is abundant in living cells. It is composed of the amino acids glutamic acid, cysteine and glycine linked by peptide bonds. Cysteine is the central amino acid. In a manner similar to cysteine, GSH can be oxidized to the disulfide (noted as GSSG).

Glycylcysteine is readily produced by the acid hydrolysis of GSH (6). It also forms a disulfide when oxidized.

## EXPERIMENTAL

Glutathione (Sigma Chemical, 99%) was used without further purification. Glycylcysteine was prepared by hydrolyzing glutathione in 1.2N HCl at 95 °C for 60-90 min. under a nitrogen atmosphere. Yield was in excess of 95%. Pyrrolidone carboxylic acid (pyroglutamic acid) is a co-product of the hydrolysis. It was prepared independently by heating glutamic acid with an equal amount of water in a sealed tube to 140 °C for 3 hours (7). The compounds used for preparing the acetate and borate, as well as the ferrous ammonium sulfate, were of reagent grade quality.

Two types of experiments were done with the ferrous ion - peptide systems in aqueous solutions to study their effectiveness in removing NO from the gas phase. In the first set of experiments, buffered ferrous ion - peptide solutions were prepared on a vacuum line. A bulb of known volume was filled with NO and expanded into the evacuated bulb with the ferrous ion - peptide solution. The pressure was noted and vigorous stirring of the solution was initiated. Once the pressure stabilized, the pressure drop was used to calculate the amount of NO absorbed by the solution. Corrections were made for water vapor pressure and the solubility of NO in water. Runs were done with the pH of the solution ranging from acidic to alkaline. All runs were done with the peptide concentration four times that of the ferrous ion concentration.

The second type of experiment is designed to determine the ability of ferrous ion - peptide to remove NO from the gas phase under realistic conditions. Simulated flue gas was prepared by mixing nitrogen, oxygen, nitric oxide and, in some cases, sulfur dioxide. The gas mixture was passed through the buffered ferrous ion - peptide solution, which had been heated to 55 °C. NO removal was determined by measuring the fraction of NO not absorbed by the solution using a chemiluminescent NO<sub>x</sub> analyzer. The plot of NO absorbed vs. time, was graphically integrated to obtain the total quantity of NO removed by the solution. When SO<sub>2</sub> was used, the amount of SO<sub>2</sub> removed was obtained in a similar manner using a pulsed fluorescent SO<sub>2</sub> analyzer.

The solutions were saved for analysis after the experiments were complete. Ferrous ion was analyzed by the 1,10 phenanthroline method. Nitrate and nitrite ions were analyzed by ion chromatography. An amino acid analyzer was used to measure the amounts of the reduced and oxidized forms of the peptides that were present.

## RESULTS AND DISCUSSION

The NO absorption experiments with glutathione were done over a pH range from 3.0 to 8.5. The ferrous ion concentrations were .02M. The NO:Fe stoichiometry was 2:1 or higher over the pH range studied. The stoichiometric ratio increased as the pH increased. In solutions with pH <7, the nitrosyl complex formed a rust-colored precipitate. This is similar to what is observed in ferrous cysteine solutions when treated with NO. In alkaline solutions, no precipitate was observed.

NO absorption by ferrous ion - glycylcysteine solution was studied over a pH range from 4 to 9. Again, a NO:Fe stoichiometry in excess of 2:1 was found. With glycylcysteine, a solid nitrosyl complex formed at all pH conditions. The appearance of the precipitates was similar to the solids obtained with GSH.

To confirm that glycylcysteine, not pyroglutamic acid, was responsible for the NO absorption observed, separate experiments were run with glutamic acid and pyroglutamic acid. Solutions of these compounds mixed with ferrous ions absorbed NO only marginally better than solutions of ferrous ions alone. This suggests that the peptide forming the complex with the ferrous ion needs to contain cysteine to efficiently bind NO.

The NO absorption experiments discussed above were done with approximately one atmosphere of NO. The second set of experiments, in which the NO-containing gas was bubbled through the heated solution, were done at much lower concentrations. The gas mixture was typically 96% N<sub>2</sub>, 4% O<sub>2</sub> and 500 ppm NO. SO<sub>2</sub>, when included, was typically at 2500 ppm. The ferrous ion concentration used in these experiments was 0.01M, and the peptide concentration was four times higher. The ferrous ion - GSH solutions were studied over a pH range of 4.3 to 10.9, and the ferrous ion - glycylcysteine solutions were studied at pH 4.3 to 9.2.

Essentially no NO was absorbed by the Fe(II)-GSH solution at pH 4.3, suggesting the equilibrium constant for the formation of the nitrosyl complex is small under these conditions. At slightly less acidic conditions (pH 5.4), the best NO removal was found. An NO:Fe stoichiometry of 0.54:1.0 was obtained. This stoichiometry decreased as the pH rose, ending with NO:Fe = 0.17:1.0 at pH 10.9. The decrease with increasing pH is presumably due to the increasing role of oxidation of GSH and Fe(II) with the increase in pH. The rate of NO absorption was found to be highest in neutral and slightly alkaline solutions, and the rate was slowest in the acid solutions. SO<sub>2</sub> was less difficult than NO to remove. It was removed most efficiently by alkaline solutions.

In the alkaline solutions, almost all the NO absorbed was converted to nitrite and nitrate ions. Almost all of the iron in the solution precipitated out in Fe(III) form. Much of the GSH was oxidized to GSSG. Under very alkaline conditions, there was some decomposition of the GSH.

The ferrous ion - glycylcysteine solutions absorbed NO at all conditions studied. The NO:Fe stoichiometry was about 0.3:1.0 in acidic conditions and rose to 0.87:1.0 at pH 7.3. It then dropped off rapidly as the pH increased, falling to 0.05:1.0 at pH 9.2. The rate of NO absorption was slowest under acidic conditions. In neutral or alkaline conditions, the rate of NO absorption was considerably higher than with the corresponding GSH solutions. It appears that oxidation of the Fe(III) and glycylcysteine is significant in alkaline conditions, and this limits how much NO can be absorbed. In acidic conditions the oxidation is slower, but the NO absorption is also slow.

A rust-colored precipitate formed in all of the solution, apparently containing most of the iron as Fe(III). Most of the glycylcysteine was oxidized to the disulfide form.

Both GSH and glycylcysteine are capable of reducing Fe(III) to Fe(II) in solution. Thus, they enhance the NO removal capabilities of an Fe(II) solution not only by forming an effective ferrous nitrosyl complex, but also by maintaining the iron in the ferrous state. Of course, the peptides will be oxidized as a result. The oxidized peptides can be reduced to their original form by several methods. These include the technique developed for cysteine in which the oxidized material is sequentially treated with H<sub>2</sub>S and SO<sub>2</sub> (5).

These compounds have been found to be considerably more effective than cysteine in ferrous ion - based NO removal systems operating at pH 5 to 7. Other cysteine-based peptides might be equally effective. To be commercially useful, however, the compounds must not be excessively expensive and capable of being regenerated without large losses.

## REFERENCES

1. A.E. Martin, ed. *Emission Control Technology for Industrial Boilers* (1981), Noyes Data Corp., Park Ridge, NJ.
2. S.G. Chang, D. Littlejohn and S. Lynn *Environ. Sci. Tech.* (1983) 17, 649.

3. N. Lin, D. Littlejohn and S.G. Chang *ISEC Proc. Des. Dev.* (1982) 21, 725.
4. M.D. Tu and S.G. Chang *Environ. Prog.* (1987) 6, 51.
5. P.C. Jocelyn *Biochemistry of the SH Group* (1972) Academic Press, New York City, NY.
- 5b. D.K. Liu and S.G. Chang *Can J. Chem.* (1987) 65, 770.
6. C.K. Olson and F. Binkley *J. Biol. Chem.* (1950) 186, 731.
7. M. Windholz, ed. *Merck Index* (1976) Merck & Co., Inc., Rahway, NJ.

REDUCTION OF NO WITH NH<sub>3</sub> ON TiO<sub>2</sub>-, Al<sub>2</sub>O<sub>3</sub>- AND Fe<sub>2</sub>O<sub>3</sub>-SUPPORTED METAL OXIDE CATALYSTS

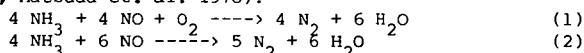
T.I. Maunula and M.A. Hiltunen  
R&D Center, A.Ahlström Co., P.O. Box 18, SF-48601 Karhula, Finland

J.B-son Bredenberg  
Department of Chemical Engineering, Helsinki University of Technology, SF-02150 Espoo, Finland

INTRODUCTION

The pollution of the atmosphere by nitrogen oxides (NO = NO + NO<sub>2</sub>) has been a subject of growing concern during the past decade. During combustion, NO<sub>x</sub> is formed either by reaction of oxygen and atmospheric nitrogen (thermal NO<sub>x</sub>) or conversion of chemically bound nitrogen in the fuel (fuel-NO<sub>x</sub>). The major fraction of these emissions results from the fuel-NO<sub>x</sub> during combustion in industrial and utility boilers. The formation of NO<sub>x</sub> in the boilers can be reduced to a considerable extent by modification in the combustion technique, for example by applying fluidized bed combustion boilers. There still will remain some NO<sub>x</sub> in the flue gases. Hence, other additional methods have been introduced for NO<sub>x</sub>-removal.

The most widely applied method for decreasing NO<sub>x</sub> emissions from existing stationary sources is selective catalytic reduction (SCR) by NH<sub>3</sub>. The most commonly proposed overall reactions between NO and NH<sub>3</sub> are (Odénbrand et al. 1985, Matsuda et al. 1978):



The catalyst used in a commercial plant must possess high activity and selectivity, since the volume of flue gas to be treated is large. In addition, the catalyst must be resistant to SO<sub>2</sub> poisoning (Matsuda et al. 1982, Nam et al. 1986). The purpose of the present study was to examine the kinetics of NO-NH<sub>3</sub>-O<sub>2</sub> reactions on several catalysts promoting the SCR of NO<sub>x</sub>.

EXPERIMENTAL

Catalysts.

The catalysts and their main characteristics are shown in Table 1. The catalysts were supported base metal oxides. Some other materials were also tested for their catalytic activity.

Table 1. Catalysts in experiments.

Catalyst	Pellet size(mm)	Specific surface area(m <sup>2</sup> /g)	Bulk density(g/ml)
1. V(4%)/TiO <sub>2</sub>	>2.0	7	1.1
2. Cu(5%)/TiO <sub>2</sub>	>2.0	7	1.0
3. Fe(6%)/TiO <sub>2</sub>	>2.0	14	1.1
4. Ni(5%)/TiO <sub>2</sub>	>2.0	6	0.8
5. Cu(7%)/Al <sub>2</sub> O <sub>3</sub>	3.2	140	1.0
6. Cr(14%)/Al <sub>2</sub> O <sub>3</sub>	4.0	60	1.1
7. Ni(11%)/Al <sub>2</sub> O <sub>3</sub> (Ni P)	3.2	80	1.1
8. Ni(16%)/Al <sub>2</sub> O <sub>3</sub> (Ni T)	2.0-4.0	210	0.8
9. Slag A (13% Fe)	>1.0	1.4	1.6
10. Slag B (0.4% Fe)	>1.0	0.2	1.1
11. Hematite (66% Fe)	0.2-1.0	<0.1	3.1
12. Ilmenite (36% Fe)	>2.0	0.6	1.1
13. Ilmenite+TiO <sub>2</sub> (5% Fe)	>2.0	-	1.0

The TiO<sub>2</sub>-based catalysts were prepared according to methods developed by Matsuda<sup>2</sup> et al. (1982), Saleh et al. (1986) and Skvortsov et al. (1977). TiO<sub>2</sub> (anatase) was wet-impregnated in a solution of a salt of the active material (V, Cu, Fe, Ni). After drying for 24 hours at 110 °C the catalyst was calcined in air at 400 °C. The Al<sub>2</sub>O<sub>3</sub>-supported catalysts were commercially available materials. The other materials in the experiments were inexpensive iron-containing slags and ores.

The total specific surface areas of the fresh materials were obtained with a Perkin-Elmer 212 C Sorptometer.

#### Apparatus and reactant gases

The schematic diagram of the experimental apparatus is presented in Figure 1. The fixed bed reactor and a pre-heater were made of quartz. The reactor was heated in a Heraeus ROK 4/60 oven and the temperature in the catalyst bed was measured with a Ni-NiCr-thermocouple. The gases were supplied from pressure bottles via high precision Hi-Tech massflowmeters. Gas lines before the pre-heater were made of stainless steel. The mixing of NH<sub>3</sub> with the simulated flue gas took place after the pre-heater, just in front of the reactor, in order to avoid any homogeneous reactions between the components.

Two teflon sampling lines were connected to the reactor. The gas mixture was transported through a EPM 797 diluting unit to a Monitor Labs 8840 chemiluminescent NO<sub>x</sub>-analyser. The analyser was equipped with a thermodynamic converter (Monitor Labs 8750) and it measured NO<sub>x</sub> and NO<sub>x</sub>+NH<sub>3</sub>. NH<sub>3</sub> was calculated by difference. The equipment was calibrated with a gas having 200 ppm NO.

#### Procedures

The NO-NH<sub>3</sub>-O<sub>2</sub> reaction was studied in both an empty tubular reactor and a packed bed reactor with different catalysts. After the temperatures of flue gas in the catalyst bed reached the set value, the concentration of NO<sub>x</sub> was measured until a steady-state reading was obtained. The experimental operating conditions are summarized in Table 2.

Table 2. Experimental operating conditions.

Inlet concentration	NO	0-2000 ppm
	NH <sub>3</sub>	0-2000 ppm
	O <sub>2</sub>	0-5 %
	CO <sub>2</sub>	0 or 10 %
	SO <sub>2</sub>	0 or 500 ppm
	N <sub>2</sub>	carrier gas
Volumetric flow rate		0.57-0.64 m <sup>3</sup> (NTP)/h
Catalyst bed volume		50 cm <sup>3</sup>
Space velocity (SV)		3.2-3.6 m <sup>3</sup> flue gas (NTP)/m <sup>3</sup> (cat)s
Temperature		200-900 °C
Duration of the test		0.25 - 6 h

The SO<sub>x</sub> poisoning experiments were performed with a test gas containing 500 ppm SO<sub>2</sub> using the Cu/Al<sub>2</sub>O<sub>3</sub>, Cr/Al<sub>2</sub>O<sub>3</sub>, Cu/TiO<sub>2</sub> and V/TiO<sub>2</sub> catalysts.

## **RESULTS AND DISCUSSION**

#### Empty reactor

Figure 2 shows the plot of NO<sub>x</sub> conversion versus temperature from 300 to 900 °C. The empty reactor had negligible effects on the NO decomposition. The small effect of the quartz tube on the reaction between NO and NH<sub>3</sub> was also small. The thermal reduction of NO by NH<sub>3</sub> increased once the temperature reached 900 °C. At this temperature the NO conversion was 26 %.

### TiO<sub>2</sub>-supported catalysts

The concentrations of NO<sub>x</sub> after a one hour operation with the Cu, V, Ni and Fe catalysts are shown in Figure 6 as a function of the catalyst temperature. The conversion of NO increased rapidly until about 300 °C which seemed to be the optimal temperature for all these catalysts. Above this temperature the NO<sub>x</sub> concentrations increased. This was due either to the incomplete reduction of NO with NH<sub>3</sub> or direct oxidation of NH<sub>3</sub> with the excess oxygen present or a combination of both factors.

The V/TiO<sub>2</sub> catalyst showed high activity and resistance to SO<sub>2</sub> poisoning (Figure 7). The Cu catalyst lost its activity under 350 °C in the presence of SO<sub>2</sub> (Figure 8). Sulfur was not found to accumulate in great degree on this catalyst at 350 °C (Fresh: 0.23 % S; After SO<sub>2</sub>-test: 0.40 % S). The Fe and Ni catalysts were less active than the V and Cu catalysts. Wong et al. (1986) have shown that the activity of TiO<sub>2</sub>-based iron oxide catalysts is strongly affected by the preparation procedure.

### Al<sub>2</sub>O<sub>3</sub>-supported catalysts

Four commercial Al<sub>2</sub>O<sub>3</sub>-supported catalysts were investigated. These catalysts had large specific surface areas (between 60 and 140 m<sup>2</sup>/g). The results with these catalysts are shown in Figure 3. The optimal operation temperatures were between 300 and 350 °C in the absence of SO<sub>2</sub>. The highest measured conversions were 80 (Cu), 74 (Ni P), 56 (Cr) and 40 % (Ni T) after a one hour operation.

The activity of the Cu catalyst improved in the presence of SO<sub>2</sub> at temperatures above 350 °C (Figure 4). Nam et al. 1986 have found with a V/Al<sub>2</sub>O<sub>3</sub> catalyst similar results. They proposed that the sulfur contamination as Al<sub>2</sub>(SO<sub>4</sub>)<sub>3</sub> increased the NO conversion at temperatures above 400 °C, presumably due to the moderation of the competing reaction of the NH<sub>3</sub> oxidation to NO. Another reason for the behavior can be the formation of CuSO<sub>4</sub>, which is also known to catalyze the reaction concerned (Schrod 1986). Sulfur was accumulated on our Cu/Al<sub>2</sub>O<sub>3</sub> catalyst at 350 °C (Fresh: 0.02 % S; After SO<sub>2</sub>-test: 3.32 % S). Compared with the results with TiO<sub>2</sub>-supported catalysts, it can be concluded that the formation of Al<sub>2</sub>(SO<sub>4</sub>)<sub>3</sub> is probable on Al<sub>2</sub>O<sub>3</sub>-supported catalysts.

The activity of the Cr catalyst decreased at temperatures under 350 °C when SO<sub>2</sub> was present (Figure 5). The life of this catalyst seemed to be short under these circumstances. According to Ando (1983) a portion of SO<sub>2</sub> oxidizes to SO<sub>3</sub> on the catalyst surface to form NH<sub>4</sub>HSO<sub>4</sub>. The SO<sub>2</sub> poisoning test time was too short to make any accurate conclusions about the effects of SO<sub>2</sub>.

It could be concluded that NO reacts with NH<sub>3</sub> at a 1:1 mole ratio at the optimal operation temperature as proposed by Kato et al. (1981). The NH<sub>3</sub> concentration decreased in a similar way than the NO<sub>x</sub> concentration until about 350 °C. Above that temperature the concentration stayed under 100 ppm. The degree of NH<sub>3</sub> oxidation by O<sub>2</sub> increased when the temperature rose over 350 °C.

### Other materials tested.

Iron oxide containing materials vary widely in catalytic activity depending on the composition (Moriguchi et al. 1978). The results of our tests are shown in Figure 9.

At low temperatures (200 - 350 °C) reaction kinetics has a decisive role. In the case that the catalytic material is poorly distributed or the available surface is low, no discernible reaction is observed. When the temperature is increased all reactions, e.g. also the NH<sub>3</sub> oxidation reaction, are speeded up and the final result in a NH<sub>3</sub>-NO-O<sub>2</sub>-system may be either a balance between the competing reactions or, in the worst case, an increase of NO<sub>x</sub> from NH<sub>3</sub> oxidation. The above explanations apply to some of the slag catalysts. The specific surface areas of the investigated materials were probably not sufficient for a measurable selective catalytic reduction.

For the  $\text{NO-NH}_3\text{-O}_2$  reaction the investigated materials can be divided in four groups:

- A. Good catalysts ( $\text{V/TiO}_2$ ,  $\text{Cu/TiO}_2$ ,  $\text{Cu/Al}_2\text{O}_3$  and  $\text{Cr/Al}_2\text{O}_3$ )
- B. Inferior catalysts ( $\text{Ni T/Al}_2\text{O}_3$ )
- C.  $\text{NH}_3$  oxidation catalysts ( $\text{Fe/TiO}_2$ ,  $\text{Ni/TiO}_2$ , slag A and iron containing ores)
- D. Noncatalytic materials (Slag B)

Good catalysts are predicted to be promoting both competitive reactions: NO reduction and straight  $\text{NH}_3$  oxidation.

#### Influence of oxygen.

The role of oxygen in SCR becomes greater when the  $\text{O}_2$  concentration falls below 1 % (Figure 10, 11 and 12). The oxygen affects the reaction rate of NO with  $\text{NH}_3$  as found also by Matsuda and Kato (1983). An  $\text{O}_2$  concentration of 0.1 % was near to the critical value for the NO conversion with the  $\text{Cu/Al}_2\text{O}_3$  catalyst (Figure 10). Kotter et al. (1986) have also shown that an  $\text{O}_2$  concentration below 0.2 % changes the reaction rate markedly.

The NO reduction using the  $\text{Cu/Al}_2\text{O}_3$  catalyst has an optimal operation temperature at about 300 to 350 °C in the presence of 1 to 5 %  $\text{O}_2$ . In the absence of oxygen the NO reduction proceeds according to the reaction (2) at higher temperatures (>350 °C). There exists no oxidation of  $\text{NH}_3$  to NO and the higher temperatures favour this reaction kinetically.

The absence of  $\text{O}_2$  inhibits the NO reduction on  $\text{TiO}_2$ -supported catalysts at 300 to 350 °C. Oxygen concentrations between 1 to 5 % were shown to have some influence only at temperatures below 300 °C especially with  $\text{V/TiO}_2$  catalyst. The possibilities of the formation of  $\text{N}_2\text{O}$  become greater when oxygen is absent (Otto and Shelef 1972).

#### The influence of inlet NO concentration.

The conversions with  $\text{Cu/Al}_2\text{O}_3$  catalyst at different inlet NO concentrations are shown in Figure 12. The degree of NO reduction increases with NO inlet concentration. It is easier to reach the low outlet concentration if the inlet concentration is as low as possible. When the reactant concentration (NO and  $\text{NH}_3$ ) falls below 100 ppm the reaction rate of SCR, however, decreases sharply.

### CONCLUSIONS

Thirteen different SCR catalysts were investigated at temperatures between 200 to 900 °C. Oxygen affects the reaction rate of NO with  $\text{NH}_3$ . In the presence of  $\text{O}_2$  the NO reduction has an optimum temperature between about 300 to 400 °C. In the absence of  $\text{O}_2$  the NO reduction is shifted to higher temperatures. The  $\text{V/TiO}_2$  catalyst is resistant to  $\text{SO}_2$ . The activities of the other catalysts investigated are affected by  $\text{SO}_2$ . There is a clear difference between the  $\text{Al}_2\text{O}_3$ - and  $\text{TiO}_2$ -supported catalysts in regard to the influence of  $\text{SO}_2$ .

### ACKNOWLEDGMENTS

This work was done at the Laboratory of Industrial Chemistry in Helsinki University of Technology in co-operation with Ahlstrom Co. Research and Development Center. The work was partly funded by Ministry of Trade and Industry in Finland.

### REFERENCES

1. Ando, J., Technical report, EPA-600/7-83-027, May 1983.
2. Bosch, H., Janssen, F.J.J.G., Kerkhof van den, F.M.G., Oldenziel, J., Ommen van, J.G. and Ross, J.R.H., Appl. Cat., 25(1986) pp 239-248.
3. Kato, A., Matsuda, S., Nakajima, F., Imanari, M. and Watanabe, Y., J. Phys. Chem., 85(1981) No 12 pp 1710-1713.

4. Kotter, M., Lintz, H-G and Weyland, F., Chem.-Ing.-Tech., 58(1986) No 8 pp 617-623.
5. Matsuda, S., Kato, A., Uno, S., Sakuta, Y., Nakajima, F., US Pat. 4,351,811 Sept 28, 1982.
6. Matsuda, S., Kamo, T., Kato, A., Nakajima, F., Kumura, T. and Kuroda, H., Ind. Eng. Chem. Prod. Res. Dev., 1982 21 pp 48-52.
7. Matsuda, S. and Kato, A., Appl. Cat., 8(1983) No 2 pp 149-165.
8. Moriguchi, S., Abe, H., Takenaka, J., Yoshikoshi, H. and Komatsu, U., US Pat. 4,070,440 Jan. 24, 1978.
9. Nam, I-S, Eldridge, J.W. and Kittrell, J.R., Ind. Eng. Chem. Prod. Res. Dev., 25(1986) No 2 pp 186-192.
10. Odenbrand, C.U.I., Lundin, S.T. and Andersson, L.A.H., Appl. Cat. 18(1985) pp 335-352.
11. Otto, K. and Shelef, M., J. Phys. Chem., 76(1972) No 1 pp 37-43.
12. Saleh, R.Y., Wachs, I.E., Chaw, S.S and Chersich, C.C., J. Cat., 98(1986) No 1 pp 102-114.
13. Skvortsov, G.A., Nizeeva, N.N., Podzharsky, A.I. and Dobrovol'skaya, I.V., US Pat. 4,056,600 Nov. 1, 1977.
14. Wong, W.C. and Nobe, K., Ind. Eng. Chem. Prod. Res. Dev., 25(1986) No 2 pp 179-186.

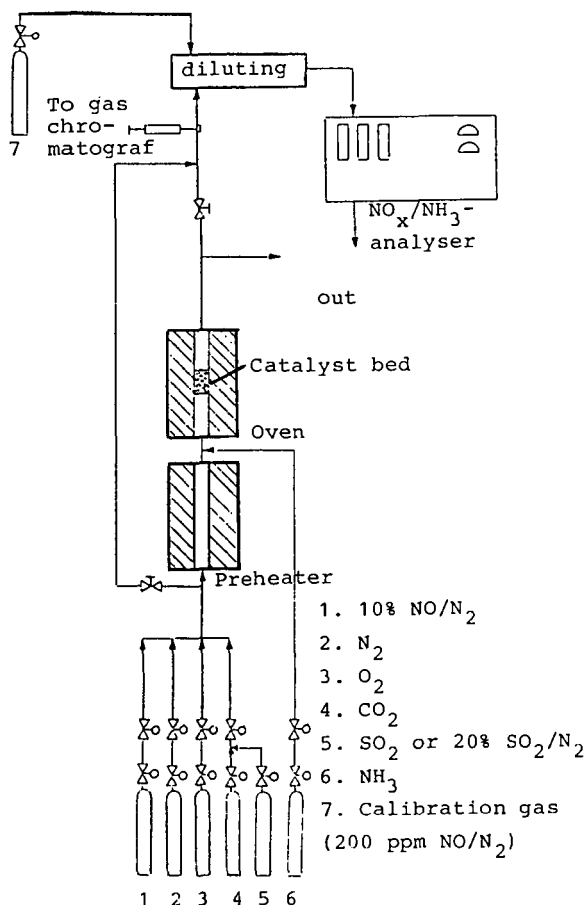


Figure 1. A schematic diagram of the experimental apparatus.

Figure 2. Thermal NO conversion in the quartz tube ( $\text{NO} = 500 \text{ ppm}$ ,  $\text{O}_2 = 5 \%$ ,  $\text{SV} = 3.6 \text{ s}^{-1}$ ,  $\text{SO}_2 = 0$ ).

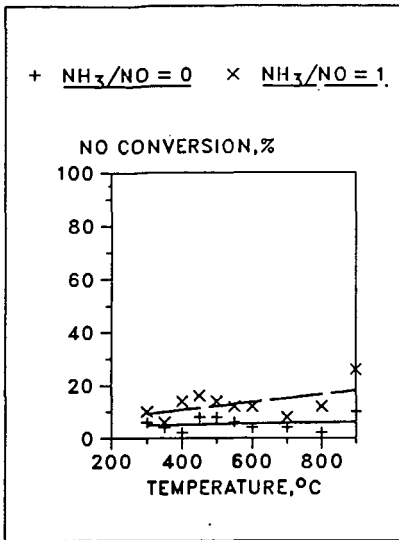


Figure 3. NO conversion with the  $\text{TiO}_2$ -supported catalysts ( $\text{NO} = 500 \text{ ppm}$ ,  $\text{NH}_3/\text{NO} = 1$ ,  $\text{SV} = 3.6 \text{ s}^{-1}$ ,  $\text{SO}_2 = 0$ ).

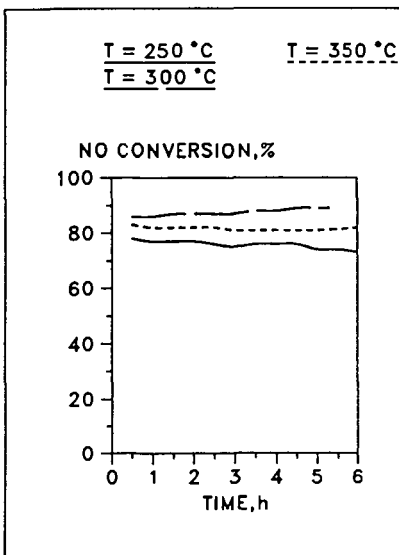
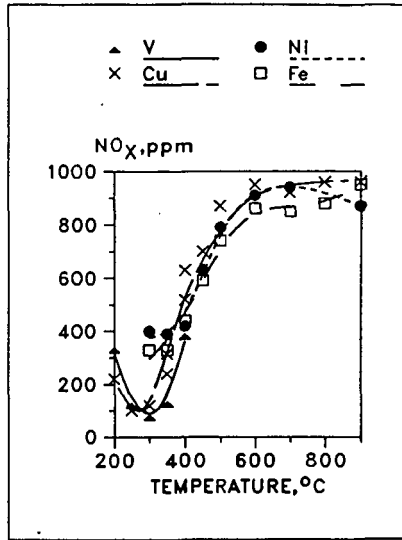


Figure 4. The influence of  $\text{SO}_2$  on the NO conversion with the  $\text{V}/\text{TiO}_2$  catalyst ( $\text{NO} = 500 \text{ ppm}$ ,  $\text{NH}_3/\text{NO} = 1$ ,  $\text{SV} = 3.2 \text{ s}^{-1}$ ,  $\text{SO}_2 = 500 \text{ ppm}$ ).

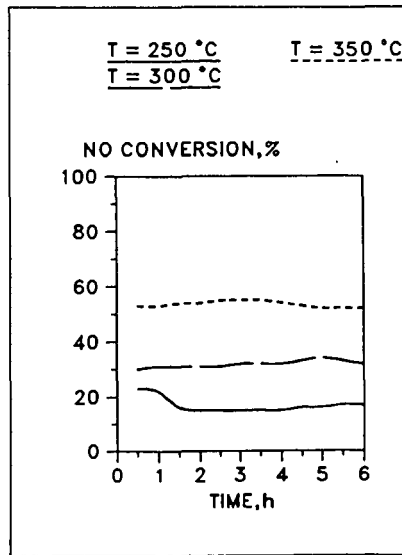


Figure 5. The influence of  $\text{SO}_2$  on the NO conversion with the  $\text{Cu}/\text{TiO}_2$  catalyst ( $\text{NO} = 500 \text{ ppm}$ ,  $\text{NH}_3/\text{NO} = 1$ ,  $\text{SV} = 3.2 \text{ s}^{-1}$ ,  $\text{SO}_2 = 500 \text{ ppm}$ ).

Figure 6. NO conversion with the  $\text{Al}_2\text{O}_3$ -supported catalysts ( $\text{NO}=500$  ppm,  $\text{NH}_3/\text{NO}=1$ ,  $\text{SV}=3.6 \text{ s}^{-1}$ ,  $\text{SO}_2=0$ ).

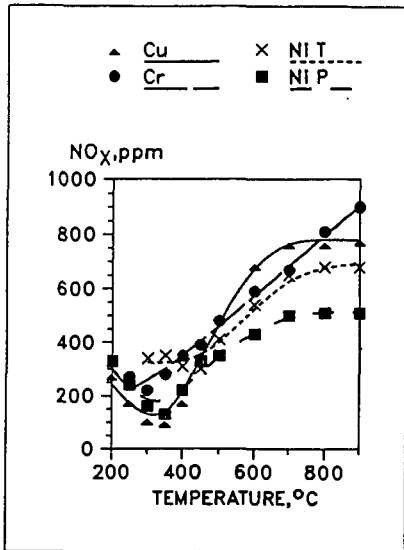


Figure 7. The influence of  $\text{SO}_2$  on the NO conversion with the  $\text{Cu}/\text{Al}_2\text{O}_3$  catalyst ( $\text{NO}=500$  ppm,  $\text{NH}_3/\text{NO}=1$ ,  $\text{SV}=3.2 \text{ s}^{-1}$ ,  $\text{SO}_2=500$  ppm).

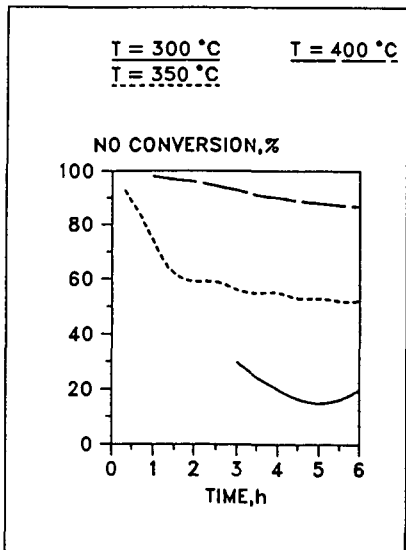
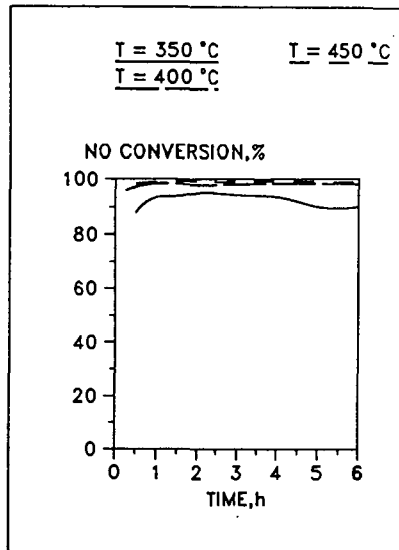


Figure 8. The influence of  $\text{SO}_2$  on the NO conversion with the  $\text{Cr}/\text{Al}_2\text{O}_3$  catalyst ( $\text{NO}=500$  ppm,  $\text{NH}_3/\text{NO}=1$ ,  $\text{SV}=3.2 \text{ s}^{-1}$ ,  $\text{SO}_2=500$  ppm).

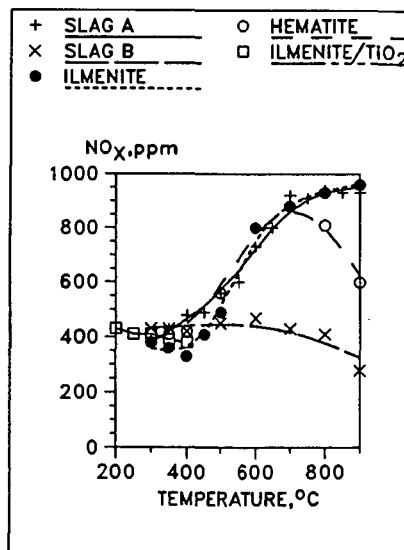


Figure 9. NO conversion with the other catalysts ( $\text{NO}=500$  ppm,  $\text{NH}_3/\text{NO}=1$ ,  $\text{SV}=3.6 \text{ s}^{-1}$ ,  $\text{SO}_2=0$ ).

Figure 10. The influence of the  $O_2$  concentration on the NO conversion with the  $V/TiO_2$  catalyst ( $NO=500$  ppm,  $NH_3/NO=1$ ,  $SV=3.4-3.6$  s $^{-1}$ ,  $SO_2=0$  ).

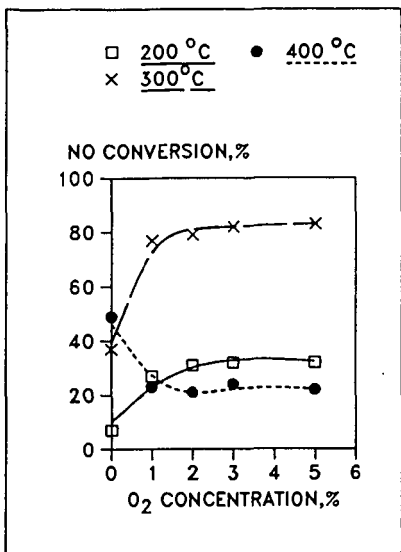


Figure 11. The influence of the  $O_2$  concentration on the NO conversion with the  $Cu/TiO_2$  catalyst ( $NO=500$  ppm,  $NH_3/NO=1$ ,  $SV=3.4-3.6$  s $^{-1}$ ,  $SO_2=0$  ).

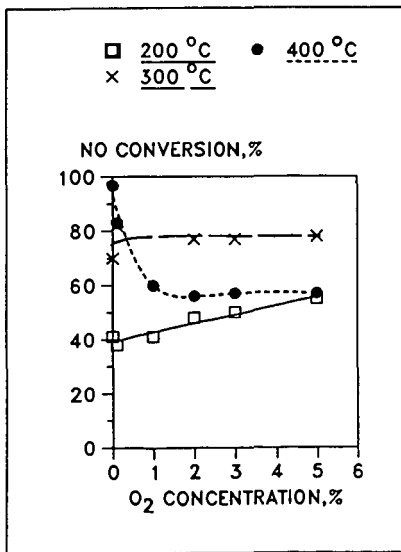
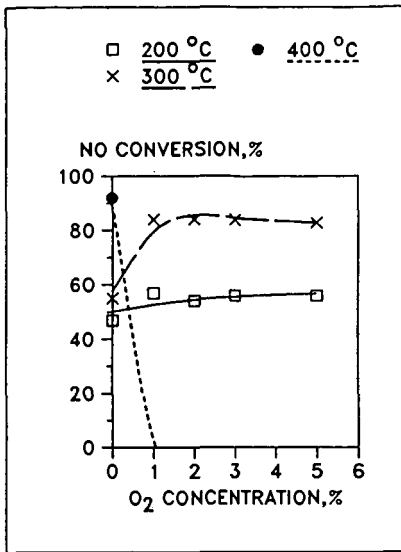


Figure 12. The influence of the  $O_2$  concentration on the NO conversion with the  $Cu/Al_2O_3$  catalyst ( $NO=500$  ppm,  $NH_3/NO=1$ ,  $SV=3.4-3.6$  s $^{-1}$ ,  $SO_2=0$  ).

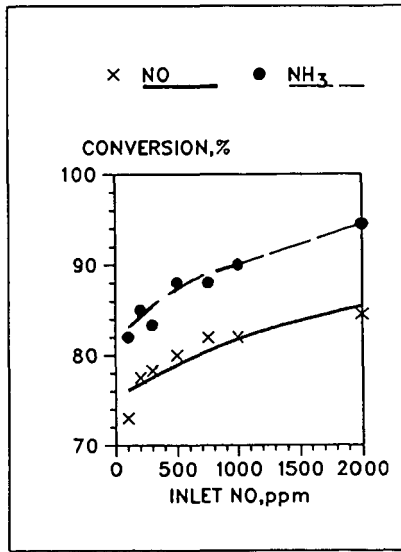


Figure 13. The influence of the NO inlet concentration on the NO conversion with the  $Cu/Al_2O_3$  catalyst ( $NH_3/NO=1$ ,  $O_2=5$  %,  $SV=3.6$  s $^{-1}$ ,  $SO_2=0$  ).

Activation of Flue Gas Nitrogen Oxides  
by Transition Metal Complexes

Michael E. Miller\*, Dennis H. Finseth, and Henry W. Pennline

Pittsburgh Energy Technology Center  
U.S. Department of Energy  
P.O. Box 10940  
Pittsburgh, PA 15236

Introduction

Sulfur and nitrogen oxides are major flue gas pollutants released by coal-fired electric power plants. In the atmosphere these oxides are converted to sulfuric and nitric acids, which contribute to the acid rain problem [1]. Most of the nitrogen oxides (90%-95%) present in coal-derived flue gas exist as the relatively inert and water-insoluble nitric oxide (NO), thus presenting a difficult removal problem.

Nitric oxide reacts with oxygen to form the more reactive nitrogen dioxide:



The equilibrium constant is about 400 at a typical flue gas temperature of 200°C (e.g., after the air preheater). However, the rate law

$$-\frac{d[\text{NO}]}{dt} = k[\text{NO}]^2[\text{O}_2]; \quad k(197^\circ\text{C}) = 3,340 \text{ M}^{-2}\text{sec}^{-1}$$

predicts very slow conversion to NO<sub>2</sub> under normal flue gas conditions (500 ppm NO and 4% O<sub>2</sub>). About 2.5 hours would be required for 50% conversion of the NO to NO<sub>2</sub> [2]. Catalysis would be necessary to increase the rate of this oxidation reaction. Gaseous nitric oxide attacks a wide variety of transition metal complexes to produce nitrosyl compounds [3-5]. Thus transition metal complexes are candidate systems for control of nitrogen oxides via sorption, as well as candidate systems for catalysis of NO transformations.

A practical strategy for nitrogen oxides removal might utilize a solid support that has been impregnated with an active transition metal complex. Some supported transition metals are expected to remove NO<sub>x</sub> by sorption, with regeneration of the sorbent being a necessary property. Others catalyze NO oxidation to the more soluble NO<sub>2</sub> and N<sub>2</sub>O<sub>5</sub>, which has been demonstrated for certain transition metal species [6]. These activated nitrogen oxides can be more efficiently removed along with SO<sub>2</sub> in conventional scrubbing or spray-drying processes, in which an aqueous slurry of sorbent, such as hydrated lime, is injected into the hot flue gas [7,8].

\*Oak Ridge Associated Universities Appointee, Postgraduate Research Training Program.

We present here preliminary studies intended to establish basic homogeneous chemistry of transition metal complexes with nitrogen oxides. The transition metals considered in this work are volatile carbonyl complexes. This work is the first step in the development of supported metal species for enhanced nitrogen oxides removal.

#### Experimental Methods

Reaction mixtures are prepared on a standard glass vacuum manifold. A mercury manometer measures the pressure of each gaseous component of the sample ( $\pm 1$  torr). The reactions take place inside Pyrex reaction cells with KBr or  $\text{CaF}_2$  windows. The cells are mountable inside a Digilab FTS-20C FTIR instrument that records the IR spectra of reacting mixtures. In photochemical experiments, a Hanovia 901B0011 200-watt mercury arc lamp irradiates the sample for periods of 15 or 30 seconds.

Metal carbonyls are obtained from Strem Chemicals and transferred to Pyrex vacuum cells inside a dry nitrogen-purged glove bag. Gases ( $\text{NO}$ ,  $\text{NO}_2$ , and  $\text{O}_2$ ) are used as received from Scott Specialty Gases. Small amounts ( $< 5$  torr) of certain gases are taken from previously made dilution mixtures of each gas in nitrogen.

#### Results and Discussion

Irradiation of a mixture of 0.3 torr  $\text{Fe}(\text{CO})_5$  and 20 torr  $\text{NO}$  produces new infrared bands in the carbonyl-stretching region (2092 and 2049  $\text{cm}^{-1}$ ) and in the nitrosyl-stretching region (1822 and 1787  $\text{cm}^{-1}$ ). The new IR spectrum (see Table 1) agrees with published  $\text{Fe}(\text{CO})_2(\text{NO})_2$  spectra after taking solvent shifts into account [9-11].

Addition of nitrogen dioxide to  $\text{Fe}(\text{CO})_5$  results in the loss of all iron carbonyl spectral features and the appearance of free CO (see Table 2). The reaction produces an orange film on the bottom of the cell, whose IR spectrum was recorded after depositing this coating on a KBr plate. This solid exhibits a weak band in the terminal CO-stretch region (1910  $\text{cm}^{-1}$ ) and a strong band at 1805  $\text{cm}^{-1}$ , which is probably due to a bridging carbonyl. Infrared bands are also observed at 1485, 1355, 1315, and 1220  $\text{cm}^{-1}$ . The highest frequency absorbance may be a bridging nitrosyl, while the others are probably coordinated  $\text{NO}_2$  or nitrite ( $\text{NO}_2^-$ ) groups [5]. The formation of a solid containing bridging ligands indicates that iron clustering results from reaction with  $\text{NO}_2$ . Free CO is generated as this ligand is eliminated between clustering metal centers.

A sequence of chemical changes, which are followed by FTIR, occurs upon addition of 16 torr of oxygen to a mixture of 0.3 torr  $\text{Fe}(\text{CO})_5$  and 25 torr  $\text{NO}$ . Five minutes after mixing, the  $\text{Fe}(\text{CO})_5$  concentration is reduced by 72%, free carbon monoxide appears, and a small amount of  $\text{Fe}(\text{CO})_2(\text{NO})_2$  is observed. Eight minutes following mixing, iron pentacarbonyl is gone, while the  $\text{Fe}(\text{CO})_2(\text{NO})_2$  concentration is halved. Nitrogen dioxide is not observed until eleven minutes after mixing, when all of the iron carbonyls have left the gas phase (see Figure 1). (We observe that binary samples of  $\text{NO} + \text{O}_2$  begin producing  $\text{NO}_2$  immediately upon mixing; see Figure 2.) An orange film results, such as in the reaction of  $\text{Fe}(\text{CO})_5 + \text{NO}_2$ . Our interpretation is that the initial  $\text{NO}_2$  formed by  $\text{NO}$  oxidation reacts with the iron carbonyls

to produce iron clusters, and only after this reaction is complete does free  $\text{NO}_2$  appear.

The next set of experiments involves dicobalt octacarbonyl. Upon addition of  $\text{NO}$ ,  $\text{Co}_2(\text{CO})_8$  is quickly converted to  $\text{Co}(\text{CO})_3\text{NO}$ , as determined by FTIR (see Table 1) [9-12]. No irradiation is necessary to initiate this reaction. Pure  $\text{Co}(\text{CO})_3\text{NO}$ , produced by the introduction of  $\text{NO}$  into a cell containing a crystal of  $\text{Co}_2(\text{CO})_8$ , exhibits no reactivity toward oxygen. Upon addition of  $\text{NO}_2$ , both  $\text{Co}_2(\text{CO})_8$  and  $\text{Co}(\text{CO})_3\text{NO}$  leave the gas phase, and free carbon monoxide is produced. We believe that cobalt clustering results from the interaction with  $\text{NO}_2$ , much as with  $\text{Fe}(\text{CO})_5$  (see above).

### Summary and Conclusions

The metal carbonyls studied take up nitric oxide homogeneously in the gas phase. Iron requires UV light for reaction with  $\text{NO}$ , but the same result is expected with the application of heat. The metal carbonyls also react with nitrogen dioxide but in this case produce polynuclear metal species. Oxygen does not attack the carbonyl or nitrosyl complexes.

The results indicate high potential for  $\text{NO}_x$  removal from stack gases by sorption onto supported metal carbonyl complexes. The solid form allows ease in separation from the flue gas. Regeneration of the sorbent might be achieved by treating with  $\text{CO}$  to liberate  $\text{NO}_x$  by displacement or by heating to decompose and drive off  $\text{NO}_x$ .

Experiments conducted between the time of this writing and the 194th ACS National Meeting will focus on efforts to produce supported transition metal complexes and to conduct fundamental studies involving their testing as  $\text{NO}_x$  sorbents and as catalysts for nitrogen oxide transformations. Support materials will include alumina and titania. Transition metal sources will be metal carbonyls and metal salts, such as the nitrates.

### Acknowledgment

This research was supported in part by an appointment to the U.S. Department of Energy Postgraduate Research Training Program administered by Oak Ridge Associated Universities. Michael Miller wishes to thank Charles Drummond and Richard Walker for helpful discussions.

### Disclaimer

Reference in this report to any specific commercial product, process, or service is to facilitate understanding and does not necessarily imply its endorsement or favoring by the United States Department of Energy.

## References

1. National Research Council, Acid Deposition: Atmospheric Processes in Eastern North America, National Academy Press: Washington, D.C., 1983.
2. W.L. Jolly, The Inorganic Chemistry of Nitrogen, W.A. Benjamin, Inc.: New York, 1964.
3. K.G. Caulton, Coord. Chem. Rev. 1975, 14, 317-355.
4. J.P. Collman and L.S. Hegedus, Principles and Applications of Organotransition Metal Chemistry, University Science Books: Mill Valley, Calif., 1980.
5. F.A. Cotton and G. Wilkinson, Advanced Inorganic Chemistry, 3rd Edition, Interscience Publishers: New York, 1972.
6. H.T. Karisson and H.S. Rosenberg, Ind. Eng. Chem., Process Des. Dev. 1984, 23, 808-814.
7. J. Ratafia-Brown, Assessment of Advanced NO<sub>x</sub> Control Technologies, PETC Report, Burns and Roe Services Corp. Contract Number DE-AC22-84PC72571, June 1986.
8. H.S. Rosenberg, L.M. Curran, A.V. Slack, J. Ando, and J.H. Oxley, Control of NO<sub>x</sub> Emission by Stack Gas Treatment, EPRI Final Report-925, Project 783-1, Battelle Columbus Laboratories, October 1978.
9. P.S. Braterman, Metal Carbonyl Spectra, Academic Press: New York, 1975.
10. W. Beck and K. Lottes, Chem. Ber. 1965, 98, 2657-2673.
11. H. Behrens, E. Lindner, and H. Schindler, Chem. Ber. 1966, 99, 2399-2406.
12. W.D. Horrocks, Jr., and R.C. Taylor, Inorg. Chem. 1963, 2, 723-727.

Table 1. Gas Phase FTIR Spectra of Some Metal Complexes as Measured in this Work.

<u>Compound</u>	<u>Absorbance maxima, cm<sup>-1</sup> (relative intensity)</u>
Fe(CO) <sub>5</sub>	2034(.58), 2014(1.0), 1976(.02)
Fe(CO) <sub>2</sub> (NO) <sub>2</sub>	2092(.34), 2049(.76), 1822(.54), 1787(1.0)
Co <sub>2</sub> (CO) <sub>8</sub>	2075(.64), 2052(1.0), 2037(.69), 2002(.07), 1867(.21), 1825(weak)
Co(CO) <sub>3</sub> NO	2108(.12), 2045(1.0), 2010(.02), 1821(.52)

Table 2. Gas Phase FTIR Spectra of Simple Nitrogen and Carbon Oxides as Measured in this Work.

<u>Compound</u>	<u>Absorbance maxima, cm<sup>-1</sup> (relative intensity)</u>
NO <sub>2</sub>	2920(.07), 2890(.05), 1625(1.0), 1605(.74)
NO	1910(1.0), 1855(.88)
N <sub>2</sub> O	2238(1.0), 2212(.72), 1302(.17), 1275(.14)
CO	2170, 2115
CO <sub>2</sub>	2365(1.0), 2335(.76)

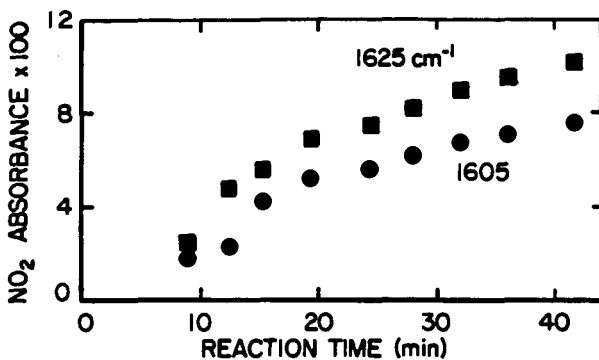


Figure 1. Evolution of  $\text{NO}_2$  in the presence of  $\text{Fe}(\text{CO})_5$  as monitored by FTIR. Initial pressures: 0.18 torr  $\text{Fe}(\text{CO})_5$ , 1.1 torr NO, and 18 torr oxygen. Note: these initial pressures are different from the experiment described in the text, but the overall chemical behavior is the same.

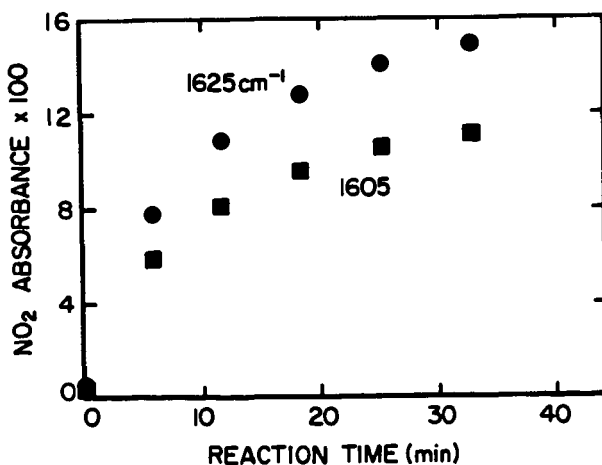


Figure 2. Oxidation of nitric oxide as followed by FTIR. Initial pressures: 1.1 torr NO and 20 torr oxygen.

NOJ13,999

NEW STRATEGY TO DECOMPOSE NITROGEN OXIDES FROM  
REGENERABLE FLUE GAS CLEANUP PROCESSES

James T. Yeh, James M. Ekmann, Henry W. Pennline,  
and Charles J. Drummond

U.S. Department of Energy  
Pittsburgh Energy Technology Center  
Pittsburgh, Pennsylvania 15236

INTRODUCTION

Nitrogen oxides ( $\text{NO}_x$ ) emitted from stationary combustion sources have been identified as important precursors of acid rain formation. Nitric oxide is a precursor to the formation of nitrogen dioxide and is an active compound in photochemical smog formation as well. It initiates reactions in which the products are air pollutants. Consequently, the control of  $\text{NO}$  emissions is an important factor in reducing air pollution. Well over 90 percent of all the man-made nitrogen oxides that enter the atmosphere are produced by the combustion of various fuels. On a nationwide basis, about one-half of the  $\text{NO}_x$  is from stationary sources.

Two sources of nitrogen contribute to the formation of oxides of nitrogen in the combustion reaction: molecular nitrogen from the combustion air and bound nitrogen from the fuel. Two ways exist to reduce the quantity of  $\text{NO}_x$  dispersed into the atmosphere. One method is control over the combustion reaction that produces the pollutant (combustion modification). Recent experience with combustion modification techniques for coal combustion indicate that  $\text{NO}_x$  emissions for combustion when low- $\text{NO}_x$  burners are used can be 50%-60% lower than when employing conventional burners under otherwise identical conditions [1]. Similarly,  $\text{NO}_x$  reductions approaching 70% have been reported in pilot-scale reburning studies [2]. The second method is to remove the pollutant downstream after it is formed (postcombustion cleanup). Postcombustion techniques, which tend to be more complex and expensive, may be necessary when high levels (>70%) of  $\text{NO}_x$  reduction are required or when installing new facilities for which both  $\text{NO}_x$  and  $\text{SO}_x$  controls are mandated.

In certain regenerable, postcombustion cleanup processes, such as the NOXSO process [3], a sorbent is used to remove the  $\text{NO}_x$  from the flue gas. In the regeneration step, a concentrated stream of  $\text{NO}_x$  is produced. This stream would be "recycled" as part of the combustion air back to the coal combustor, where a portion of the  $\text{NO}_x$  would be destroyed. Theoretically, the  $\text{NO}_x$  returned to the coal combustor would cause little change in the concentration of  $\text{NO}_x$  in the exiting flue gas. Thermodynamic equilibrium calculations for  $\text{NO}_x$  formation from combustion indicate that  $\text{NO}_x$  injected into the flame zone of a combustor would be destroyed to a large extent. The formation of  $\text{NO}_x$  and its destruction in practical systems are kinetically controlled, and final concentrations of  $\text{NO}_x$  in flue gas substantially exceed equilibrium values. To assess the extent of the reduction of recycled  $\text{NO}_x$ , experimental tests in practical systems are required.

Simulated  $\text{NO}_x$  recycle tests were recently conducted at the Pittsburgh Energy Technology Center (PETC), U.S. Department of Energy, with excellent results [3]. However, the  $\text{NO}_x$ -recycle technique needs improvement if steady-state removal of 90% of the  $\text{NO}_x$  produced from the combustor is required. This paper reports experimental results for two new techniques to improve the destruction of externally injected  $\text{NO}_x$  into a combustor. The first technique involves doping the  $\text{NO}_x$  gas stream to the combustor with methane (other reductants might also be effective). The second technique is injecting the recycled  $\text{NO}_x$  stream at the optimum location (with and without methane doping) for maximum reduction. Test data showed 100% reduction of injected  $\text{NO}_x$  is possible with this technique. A third approach is proposed using a low- $\text{NO}_x$  burner in combination with the  $\text{NO}_x$  recycle technique to achieve a steady-state 90%  $\text{NO}_x$  removal in the flue gas. The projected results of the third process scheme are based on material balance computations and reasonable expectations of the performance of each component of the process.

#### THEORETICAL BACKGROUND

The  $\text{NO}_x$  control techniques described above are based on concepts utilized in other in-furnace  $\text{NO}_x$  reduction processes. The techniques involve kinetically controlled reduction of  $\text{NO}_x$  based in part on increased residence time at high temperatures and in part on the presence of chemical species that reduce the  $\text{NO}_x$  to  $\text{N}_2$ , particularly doping the externally added  $\text{NO}_x$  with methane ( $\text{CH}_4$ ). Doping recycled  $\text{NO}_x$  with a fuel may appear similar to the reburning technique, a term coined by Wendt et al. [4] to describe the process of  $\text{NO}_x$  reduction by injection of a secondary fuel stream to create a large fuel-rich zone in the combustor. The approach described in this paper, tentatively called "hydrocarbon doping," differs from reburning in that small amounts of secondary fuel are used (approximately 20% of that used in reburning for effective control), and no downstream injection ports are required.

#### Thermodynamic Equilibrium

The thermodynamic feasibility of in-furnace  $\text{NO}_x$  reduction was studied using the PETC Multi-Phase Thermodynamic Equilibrium computer code and Sandia National Laboratory's CHEMKIN computer code. Results of the thermodynamic study show the equilibrium concentration of NO at various flame temperatures (see Figure 1). The thermodynamic model simulates pulverized-coal combustion at 20% excess air. Injection of additional NO (referred to as recycle ratio, expressed as the ratio of moles of NO injected to moles of NO formed in the combustion process) was studied at levels of 0%, 90%, and 100%. The calculated data show that at NO recycle ratios as high as 1, virtually no net increase of NO occurs. However, although thermodynamics indicates nearly total destruction of injected NO is feasible (up to a recycle ratio equal to 1), chemical kinetics reaction rates will dictate the final product mix. At a NO recycle ratio equal to 4, the CHEMKIN equilibrium code predicts a 1.8% increase in NO concentration compared to the case with no recycle.

### Hydrocarbon Doping

The global reactions involved in doping the injected  $\text{NO}_x$  with  $\text{CH}_4$  for  $\text{NO}_x$  reduction are believed to be as follows:



and



However, these reactions compete with the methane combustion reaction:



Figure 2 (taken from Chen et al. [5]) describes the chemical mechanism for  $\text{NO}_x$  destruction by hydrocarbons. The key steps include initial  $\text{NO}$  destruction by reaction with the methylidyne radical ( $\text{CH}$ ) to form  $\text{HCN}$ . Subsequent reactions lead to ammonia (or  $\text{NH}_1$  radicals) and eventually to the formation of  $\text{N}_2$ .

### EXPERIMENTAL APPROACH

#### Test Facilities

The experimental work was conducted at PETC using a tunnel furnace and a 227-kg/hr pulverized-coal combustor. The tunnel furnace is a hot-walled, refractory-lined box with dimensions of 0.97 x 0.97 x 2.80 m and has a single burner in the front wall (interchangeable). It was designed to burn gas, coal-water slurry, or pulverized fuels. Combustion air can be pre-heated to 400°C (750°F). The burner is supplied with separate flows of combustion air, atomizing air, center-fire air, and natural gas (separate ring). The typical firing rate for the coal-water-mixture is approximately  $0.5 \times 10^6 \text{ W}$  (1.7 MMBtu/hr).

The 227-kg/h (500-lb/h) pulverized-coal combustion test facility is shown schematically in Figure 3. The furnace walls are refractory-lined and water-cooled. The unit is 2.13-m (7-ft)-wide, 1.52-m (5-ft)-deep, and 3.66-m (12-ft)-high, and has a volumetric heat liberation rate of about 165,662  $\text{W/m}^3$  (16,000  $\text{Btu/hr-ft}^3$ ) at a thermal input of  $1.9 \times 10^6 \text{ W}$  (6.5 MMBtu/h). The flue gas flow rate is approximately 0.613 cubic meters per second at standard conditions (1300 scfm) (standard condition is 1 atm and 0°C). Coal is charged to the hopper, pulverized to a size consist of 70% minus-200 mesh, and then conveyed by the primary air into a recycle coal loop, where intimate mixing of coal and air occurs. Four adjustable exit tubes are connected to the recycle loop; these convey the primary air-coal mixtures to each of the four burners. It should be noted that the primary air swirl inducer is no longer being used. Secondary air at 315°C (600°F) is fed through swirl vanes surrounding each burner. The flue gas exits the furnace at about 1090°C (2000°F) and passes through a convective heat transfer section and an air preheater.

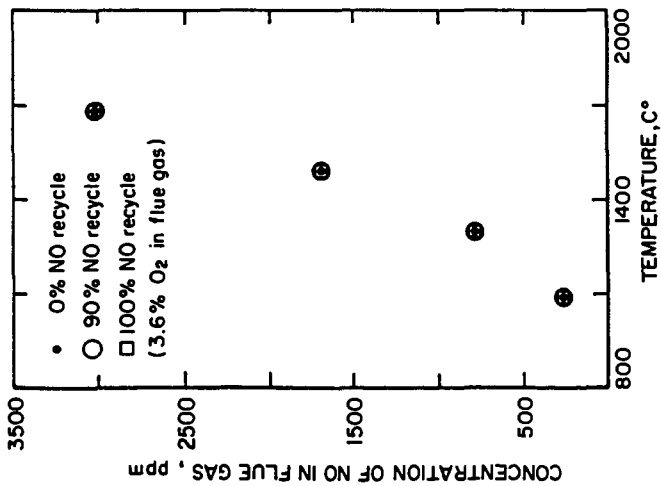


FIGURE 1. THERMODYNAMIC EQUILIBRIUM OF NO IN FLUE GAS.

NO/8116

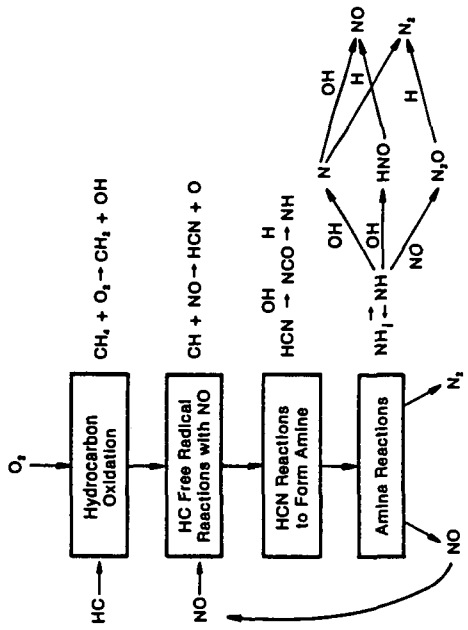


FIGURE 2. REACTION MECHANISM FOR NO<sub>x</sub> DESTRUCTION BY HYDROCARBONS.

NO/14,188

### Test Procedure

To simulate the recycle of  $\text{NO}_x$  from a regenerable  $\text{NO}_x$  control process, nitric oxide (NO) from a compressed-gas cylinder was injected into the combustor through the burner(s). Initial  $\text{NO}_x$  concentration at the exit of the combustor was recorded. Nitric oxide gas was then injected into the burner. The  $\text{NO}_x$  concentration in the exiting flue gas reached a steady-state level. In the case of the 227-kg/h pulverized-coal combustor, the point of  $\text{NO}_x$  injection into the burner could be varied. Also, natural gas could be added to the  $\text{NO}_x$  stream. The burner used in the 227-kg/h combustor is shown in Figure 4.

### RESULTS AND DISCUSSION

The test results of in-furnace reduction of recycle  $\text{NO}_x$  with and without assistance from hydrocarbon doping are given in Tables 1 and 2. Table 1 results were obtained from the tunnel furnace tests while burning natural gas and while burning coal-water mixtures. Table 2 contains test results obtained from the 227-kg/h pulverized-coal combustor. The initial  $\text{NO}_x$  concentration is defined as the  $\text{NO}_x$  concentration in the furnace exit without any NO injection into the furnace (base line). The final  $\text{NO}_x$  concentration is that in the exiting furnace flue gas during injection of NO at steady-state conditions. The net  $\text{NO}_x$  increase is the difference between the concentrations during NO injection and the base-line condition. The reduction of recycled  $\text{NO}_x$  is the difference between the calculated final  $\text{NO}_x$  (assuming no in-furnace reduction) and the final  $\text{NO}_x$  concentration, divided by the difference between the calculated final  $\text{NO}_x$  and the initial  $\text{NO}_x$  concentration. A discussion of the results from the two test series follows.

#### Tunnel Furnace

Simulated  $\text{NO}_x$  recycle tests were conducted by injecting nitric oxide (NO) into the combustion air stream. The pure NO was delivered from a compressed-gas cylinder. The NO was diluted by the air stream before entering the furnace.

The recycled  $\text{NO}_x$  reductions were in the range of 59% to 79%. The data show a nearly linear relationship between  $\text{NO}_x$  recycle ratio and  $\text{NO}_x$  reduction in moles per minute. This indicates that the higher the  $\text{NO}_x$  concentration in the furnace, the more  $\text{NO}_x$  that is being decomposed. The linear relationship perhaps indicates the decomposition of  $\text{NO}_x$  is a first-order kinetics reaction. Since the reduction of  $\text{NO}_x$  returned to the furnace is not complete, thermodynamic equilibrium among all the reactions species is not being reached within the furnace.

#### Pulverized-Coal Combustor

Several parameters were studied during this series of tests. The objective was to maximize the reduction of  $\text{NO}_x$  injected into the combustor.

Table 1. In-Furnace Reduction of Recycled NO<sub>x</sub>, Tunnel Furnace Tests

Fuel Type	Test No.						
	1	2	3	4	5	6	7
		natural gas			coal-water slurry		
Initial NO <sub>x</sub> , ppm	31	31	31	510	510	510	510
Final NO <sub>x</sub> , ppm	80	134	51	580	546	720	840
NO <sub>x</sub> recycle ratio	6.3	12.0	3.0	0.6	0.3	1.0	2.0
Calculated final NO <sub>x</sub> , ppm, if in-furnace reduction efficiency = 0	227	403	124	816	663	1020	1530
Net NO <sub>x</sub> increase, ppm	49	103	20	70	36	210	330
Reduction of recycled NO <sub>x</sub> , %	75	72.3	78.5	77.0	76.0	59.0	68.0
NO <sub>x</sub> reduction, 10 <sup>-3</sup> mol/min	0.061	0.13	0.03	0.2	0.1	0.26	0.6

Table 2. In-Furnace Reduction of Recycled NO<sub>x</sub>,  
227 kg/h Coal Combustor Tests

	Test No.					
	8	9	10	11	12	13
Initial NO <sub>x</sub> , ppm	700	700	700	550	550	550
Final NO <sub>x</sub> , ppm	770	910	980	980	740	750
NO <sub>x</sub> recycle ratio	1.48	1.47	1.47	1.90	1.87	1.77
Calculated final NO <sub>x</sub> , ppm, if in-furnace reduction = 0	1739	1731	1731	1596	1579	1523
Net NO <sub>x</sub> increase, ppm	70	210	280	430	190	200
Reduction of recycled NO <sub>x</sub> , %	93.3	79.6	72.8	58.9	81.5	79.4
No. of burners used for NO <sub>x</sub> injection	2	2	2	4	4	4
Location of NO <sub>x</sub> entering into burners	auxiliary gas line		primary air	secondary air		primary air
NO <sub>x</sub> reduction, 10 <sup>-3</sup> mol/min	2.85	2.44	2.23	1.90	2.58	2.38
mol CH <sub>4</sub> /mol NO <sub>x</sub> reduced	10.1	0	0	0	14.9	0
CH <sub>4</sub> to coal calorie ratio	0.107				0.135	

Table 2 (continued). In-Furnace Reduction of Recycled NO<sub>x</sub>,  
227 kg/h Coal Combustor Tests

	Test No.					
	14	15	16	17	18	19
Initial NO <sub>x</sub> , ppm	550	480	510	510	490	490
Final NO <sub>x</sub> , ppm	650	685	590	570	490	490
NO <sub>x</sub> recycle ratio	1.77	2.04	1.92	1.92	2.05	2.05
Calculated final NO <sub>x</sub> , ppm, if in-furnace reduction = 0	1523	1460	1490	1490	1492	1492
Reduction of recycled NO <sub>x</sub> , %	89.7	79.1	91.8	93.9	100	100
No. of burners used for NO <sub>x</sub> injection	4	4	4	2	2	2
Location of NO <sub>x</sub> entering into burners	primary air			auxiliary gas line		primary air
NO <sub>x</sub> reduction, 10 <sup>-3</sup> mol/min	2.68	2.37	2.75	2.81	3.1	3.1
mol CH <sub>4</sub> /mol NO <sub>x</sub> reduced	12.5	0	4.4	0	3.9	3.9
CH <sub>4</sub> to coal calorie ratio	0.118		0.043	0.043		0.043

The approaches evaluated included variation of the  $\text{NO}_x$  injection location in the burner and the use of hydrocarbon doping of the  $\text{NO}_x$  stream.

The  $\text{NO}_x$  can be injected into the burner and then subsequently into the combustor by three possible routes: (1) with the secondary air (this represents about 80% of total combustion air), (2) with the primary air and coal stream, or (3) through the auxiliary gas lines (see Figure 4). Four wall-mounted burners are at two different vertical elevations. The  $\text{NO}_x$  may be injected through all four burners or just through the two lower burners.

The location of the injection of  $\text{NO}_x$  within the burner is important. The data indicate that the extent of  $\text{NO}_x$  reduction varies in a manner consistent with other kinetically based  $\text{NO}_x$  reduction schemes, such as air staging or reburning. It is reasonable to assume that the concentration of  $\text{NO}_x$  would be lower at the exit of the furnace if the  $\text{NO}_x$  is injected into the combustor in a more concentrated form. A comparison of  $\text{NO}_x$  reduction efficiency can be made when the  $\text{NO}_x$  is injected with the secondary air (test 11) and with the primary air (tests 13 and 15). Tests 13 and 15 show a greater  $\text{NO}_x$  reduction efficiency because the primary air carried the  $\text{NO}_x$  into the combustor at a higher concentration than did the secondary air. The flow rate of secondary air is about four times that of the primary air. The  $\text{NO}_x$  reduction efficiency would be expected to be higher if the  $\text{NO}_x$  is injected into the combustor through the auxiliary gas line (tests 9 and 17) rather than through the primary air line (test 10). By use of the auxiliary gas line to inject the  $\text{NO}_x$ , no other gas is there to dilute the pure  $\text{NO}$  delivered from the gas cylinder. The highest  $\text{NO}_x$  reduction efficiency obtained was when the  $\text{NO}_x$  was injected into the furnace through the auxiliary gas line. Test 17 showed a 93.9% reduction of the externally injected  $\text{NO}_x$ . This is a very substantial improvement over the previously reported results obtained in the same furnace [3].

Methane doping of the  $\text{NO}_x$  stream, especially when the  $\text{NO}_x$  is concentrated, is believed to cause reburning reactions leading to  $\text{NO}_x$  reduction, as shown in Equations (1) and (2) and in Figure 2. The data indicate that the addition of a small amount of methane to the  $\text{NO}_x$  stream greatly improves the in-furnace  $\text{NO}_x$  reduction efficiency. Tests 18 and 19 show 100% reduction of recycled  $\text{NO}_x$ . At this condition, the methane to  $\text{NO}_x$  mole ratio was only 3.9. Other hydrocarbons or reducing gases could also be good candidates as doping reagents for in-furnace  $\text{NO}_x$  reduction.

#### System Material Balance for In-Furnace Decomposition of Recycled Nitrogen Oxides

Figure 5 shows a schematic diagram of a regenerable  $\text{NO}_x$  control process in which the  $\text{NO}_x$  is reinjected into the coal combustor for in-furnace disposal. A number of regenerable  $\text{NO}_x$  control processes now under development employ this approach. In the combustor, "a" mol/h of  $\text{NO}_x$  is being produced and is partially removed downstream by the sorbent within the reactor (absorber). The remaining  $\text{NO}_x$ ,  $(100 - E_1)a/100$  mol/h, is emitted into the atmosphere. The  $\text{NO}_x$  absorbed in the absorber reactor is separated from the sorbent through a regeneration process and is then recycled back to the combustor for in-furnace disposal.

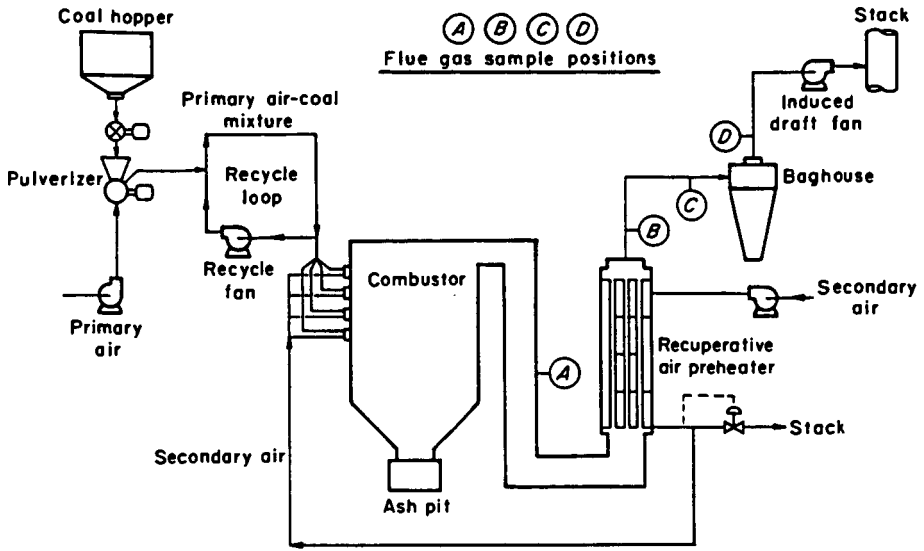


FIGURE 3. SIMPLIFIED FLOWSHEET OF 227 kg/h PULVERIZED-COAL-FIRED FURNACE.

L-81017

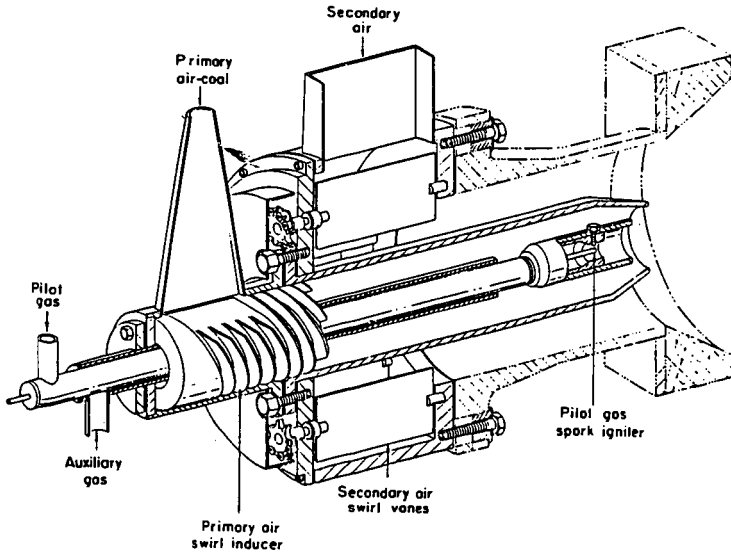


FIGURE 4. MULTI-FUEL BURNER ASSEMBLY.

If the in-furnace  $\text{NO}_x$  decomposition efficiency is not 100%, it would be desirable to determine if the  $\text{NO}_x$  concentration at the outlet of the combustor would reach steady state when the in-furnace  $\text{NO}_x$  disposal concept is applied to the overall operation.

At steady state, a material balance around the absorber may be defined as follows:

$$a + \left[ \frac{(100 - c)x}{100} \right] = \left[ \frac{(100 - E_1)a}{100} \right] + x \quad (4)$$

Therefore,

$$x = aE_1/c \quad (5)$$

Here,  $E_2$  is defined as the absorber  $\text{NO}_x$  removal efficiency relative to the net mass flow of  $\text{NO}_x$  entering the absorber.

$$E_2 = 100x / \left( a + \left[ \frac{(100 - c)x}{100} \right] \right) \quad (6)$$

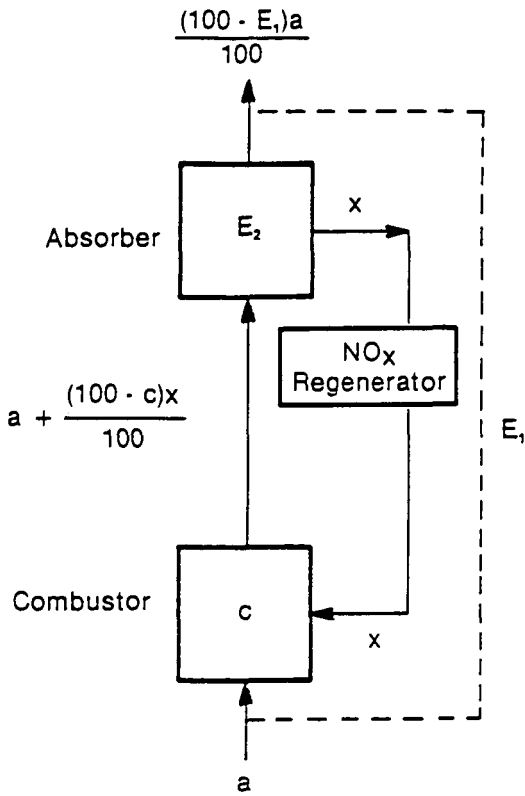
Equations (4) and (6) indicate that the  $\text{NO}_x$  recycle system will reach a steady state of  $\text{NO}_x$  concentration at each stage of the system. For example, given  $a = 100$  mol/h,  $c = 70\%$ , and  $E_1 = 90\%$ , the steady-state recycle rate  $x$  can be found. From Equation (5),  $x = 128.6$  mol/h of  $\text{NO}_x$ . This implies that if the absorber is designed for steady-state 90%  $\text{NO}_x$  removal from the flue gas produced from the combustor in a recycle mode, the  $\text{NO}_x$  removal capacity of this reactor (absorber) must be 128.6 mol/h of  $\text{NO}_x$ .

#### Low- $\text{NO}_x$ Burner and $\text{NO}_x$ Recycle Combination Process Scheme

Other possibilities also exist to reduce recycled  $\text{NO}_x$ . One technique couples a low- $\text{NO}_x$  burner and in-furnace  $\text{NO}_x$  reduction without the use of hydrocarbon doping (see Figure 5). The low- $\text{NO}_x$  burner first reduces the  $\text{NO}_x$  produced from the combustor, thus reducing the burden on the absorber; this is then followed by the recycle of the regenerated  $\text{NO}_x$  for in-furnace reduction.

An example of this technique is demonstrated as follows (refer to Figure 5 and the previous sample calculations): Given  $a = 73$  mol/h  $\text{NO}_x$  (assuming a low- $\text{NO}_x$  burner with 27%  $\text{NO}_x$  reducing efficiency is in place),  $c = 70\%$  (percent of in-furnace reduction of recycled  $\text{NO}_x$ ), and the  $\text{NO}_x$  emission control is 90% removal of the  $\text{NO}_x$  produced in the combustor before the use of a low- $\text{NO}_x$  burner, determine if the combined  $\text{NO}_x$  reduction through the coupling of low- $\text{NO}_x$  burner and in-furnace reduction of recycled  $\text{NO}_x$  can meet the 90%  $\text{NO}_x$  reduction requirement.

The answer may best be illustrated in a tabulated form (see Table 3) by comparing overall  $\text{NO}_x$  removal efficiencies at various  $\text{NO}_x$  recycle rates.



- a = NO<sub>x</sub> produced in the combustor, mol/h
- E<sub>1</sub> = system NO<sub>x</sub> removal efficiency, in relation to "a", %
- E<sub>2</sub> = absorber NO<sub>x</sub> removal (with NO<sub>x</sub> recycle) efficiency, in relation to "a + (100 - c)x/100", %
- c = destruction efficiency of recycled NO<sub>x</sub> in the combustor, %
- x = flow of NO<sub>x</sub> recycled to combustor, mol/hr

**FIGURE 5. SCHEMATIC DIAGRAM OF NITROGEN OXIDE RECYCLE.**

Table 3. Combined NO<sub>x</sub> Reduction Scheme

x	$a + (100-c)x/100$	$(100-E_1)a/100$	E <sub>1</sub>
NO <sub>x</sub> absorbed and then recycled, mol/h	NO <sub>x</sub> entering absorber, mol/h	NO <sub>x</sub> exiting absorber to stack, mol/h	Overall efficiency, %
60	91	31	69
70	94	24	76
80	97	17	83
90	100	10	90

The calculated results show that given a low-NO<sub>x</sub> burner with 27% NO<sub>x</sub> reduction efficiency combined with in-furnace reduction of recycled NO<sub>x</sub> at 70% efficiency, 90% overall NO<sub>x</sub> reduction could be maintained.

#### CONCLUSIONS

The location of injection of recycled NO<sub>x</sub> into the combustor is important. A high degree of mixing between the recycled NO<sub>x</sub> and the entire body of oxidizer and/or combustion gas should be avoided. Doping the recycled NO<sub>x</sub> stream with methane is very effective in destroying the injected NO<sub>x</sub>. It is kinetically advantageous to keep the NO<sub>x</sub> in a concentrated form when it comes in contact with the reducing gas. It appears that this approach generates a locally fuel-rich zone, minimizes the oxidation of methane, and probably creates a pool of hydrocarbon radicals that contribute to the destruction of NO<sub>x</sub>.

Recirculation of NO<sub>x</sub> to the combustor after the regeneration step, plus the use of either hydrocarbon doping or a low-NO<sub>x</sub> burner, can destruct most or all the recycled NO<sub>x</sub>. These techniques should contribute to the development of cost-effective systems in which greater than 90% NO<sub>x</sub> removal efficiencies can be obtained.

#### DISCLAIMER

Reference in this paper to any specific commercial product, process, or service is to facilitate understanding and does not necessarily imply its endorsement or favoring by the United States Department of Energy.

#### REFERENCES

1. Mulholland, J.A.; Lanier, W.S. Application of Reburning for NO<sub>x</sub> Control to a Firetube Package Boiler, Journal of Engineering for Gas Turbines and Power, Vol. 107, p. 739, July 1985.

2. McCarthy, J.M.; Chen, S.L.; Seeker, W.R.; Pershing, D.W. Pilot Scale Studies on the Application of Reburning for  $\text{NO}_x$  Control, presented at the Joint Symposium on Stationary Combustion  $\text{NO}_x$  Control, New Orleans, La., March 1987.
3. Yeh, J.T.; Drummond, C.J.; Haslbeck, J.L.; Neal, L.G. The NOXSO Process: Simultaneous Removal of  $\text{SO}_2$  and  $\text{NO}_x$  from Flue Gas, presented at the AIChE 1987 Spring National Meeting, Houston, Texas, March 29 - April 2, 1987.
4. Wendt, J.O.L.; Sterling, C.V.; Matovich, M.A. Reduction of Sulfur Trioxide and Nitrogen Oxides by Secondary Fuel Injection, 14th Symposium (International) on Combustion, The Combustion Institute, 1973, p. 897.
5. Chen, S.L.; Clark, W.C.; Heap, M.P.; Pershing, D.W.; Seeker, W.R.  $\text{NO}_x$  Reduction by Reburning With Gas and Coal: Bench Scale Studies, Proceedings of the 1982 Joint Symposium on Stationary Combustion  $\text{NO}_x$  Control, Vol. 1, Utility Boiler Applications. EPRI Report No. CS-3182, July 1983.

## COOLSIDE DESULFURIZATION REACTIONS AND MECHANISMS

H. Yoon, M. R. Stouffer and F. P. Burke

Research & Development Department  
Consolidation Coal Company  
4000 Brownsville Road  
Library, PA 15129

### ABSTRACT

Coolside desulfurization is an emerging SO<sub>2</sub> control technology, involving injection of a dry sorbent such as hydrated lime and flue gas humidification by water spraying, downstream of the air preheater in a coal-fired boiler unit. The sorbent entrained in the flue gas removes SO<sub>2</sub> in the humidification zone. It also removes SO<sub>2</sub> in the particulate layer collected by the ESP or baghouse. Based on pilot-scale data, the desulfurization mechanism in the humidifier is highly complex. Hydrated lime entrained in the flue gas rapidly reacts with SO<sub>2</sub> at high relative humidity conditions but, in the absence of liquid water, the reaction utilizes only a small fraction of the sorbent. The presence of water droplets in the humidifier significantly increases the sorbent efficiency and the SO<sub>2</sub> removal level by making the sorbent-SO<sub>2</sub> reaction more effective. Increasing the water droplet size also increases the SO<sub>2</sub> removal in the humidifier.

This paper discusses the results of pilot tests which studied the mechanisms of SO<sub>2</sub> capture by hydrated lime in the presence and absence of water droplets in the flue gas.

### INTRODUCTION

Coolside desulfurization involves injection of a dry sorbent (typically hydrated lime) followed by flue gas humidification with liquid water sprays in the ductwork downstream of the air preheater in a coal-fired boiler. SO<sub>2</sub> is removed by the entrained sorbent particles in the humidification zone and by the sorbent bed in the particulate collector. Since sorbent residence time in the humidifier is very short (typically 1-3 seconds), a highly active sorbent is needed for a significant humidifier SO<sub>2</sub> removal. Water-soluble additives can be injected with the humidification water to enhance the sorbent activity.

The concept of Coolside technology was successfully demonstrated by Consolidation Coal Company (Consol) in 1 MW field tests at Martinsville, Virginia, in 1984 (1,2). In the field tests, SO<sub>2</sub> removals up to 75-80% were achieved across a pilot humidifier and ESP at sorbent utilizations ranging up to 35-40%, using commercial hydrated lime with NaOH as the additive. The field results indicate that the presence of liquid water droplets plays a key role for high humidifier SO<sub>2</sub> removal. The sorbent activities in the field tests were significantly higher than those observed in laboratory differential reactor tests under humid flue gas conditions without evaporating water droplets (1).

To improve the process performance through process optimization and improved sorbent development, Consol constructed a 0.15 MW pilot test unit (3). A first series of process variable tests made in the pilot unit (3) confirmed the consistency of the pilot SO<sub>2</sub> removal data with the removals observed in the 1 MW field tests.

This paper describes the results of a subsequent pilot research program, which studied the SO<sub>2</sub> removal mechanisms in the humidifier. Two types of tests were conducted:

- Tests with steam humidification, to study sorbent-SO<sub>2</sub> reactions at close approach to adiabatic saturation and short contact times, but in the absence of water droplets.
- Tests with water spray humidification downstream of the lime injection (Coolside humidification), with varying nozzle atomizing conditions to produce different droplet sizes and drying times.

### TEST METHODS

The tests of humidifier SO<sub>2</sub> removal mechanisms were made using the 0.15 MW Coolside pilot unit. Both the steam humidification tests and the water spray humidification tests were conducted in this unit.

#### Pilot Unit

Figure 1 shows a schematic of the pilot unit. The unit consists of a flue gas generation system, Coolside process system (including lime injector and humidifier), a baghouse, and continuous flue gas sampling and analysis systems. The flue gas leaving the baghouse is recycled after removal of excess moisture by a condenser/separator, providing about 80% of the flue gas requirement. The recycle gas is mixed with the flue gas introduced from a natural gas burner. By injecting CO<sub>2</sub>, H<sub>2</sub>O, SO<sub>2</sub> and fly ash into this combined gas, the inlet flue gas conditions can be matched to the flue gas conditions downstream of the air preheater in a coal-fired boiler. The fly ash content was about 4 grains/scf flue gas and the SO<sub>2</sub> content was 1500 ppm in the tests reported here. The pilot humidifier is a vertical, 8.3-inch ID, cylindrical duct and provides a 20-foot down-flow humidification zone. The flue gas velocity is variable from 8 to 25 ft/sec, giving 0.8-2.5 sec residence times. The humidifier has thermocouples and observation ports every two feet along its length. Hydrated lime (Table 1) is injected into the flue gas at the top of the humidifier. A series of distribution plates is placed between the lime injector and the spray nozzle locations to provide solids mixing and uniform gas flow. In all the tests with water spraying, commercial two-fluid (air/H<sub>2</sub>O) nozzles were used. The nozzle water flow controls the humidifier exit gas temperature for the desired approach to saturation. A water soluble additive such as NaOH can be fed as an aqueous solution into the humidification water stream.

The pilot baghouse has a total cloth area of 115 ft<sup>2</sup>, giving a maximum air/cloth ratio of 4.1 acfm/ft<sup>2</sup> at 150°F.

The pilot unit is installed with two continuous SO<sub>2</sub>/O<sub>2</sub> flue gas analysis systems to measure the process SO<sub>2</sub> removal. The O<sub>2</sub> analyses are used to correct for air in-leakage. The SO<sub>2</sub> removal can be measured across the humidifier only or across the humidifier and baghouse. The humidifier exit gas sampling system was specially designed to prevent further SO<sub>2</sub> reaction with reactive solids in the sample system.

#### Steam Humidification Tests

In the steam humidification tests, a low-temperature (<180°F) gas stream was produced by running the combustor at very low load and operating with a high recycle. The gas was then humidified with steam upstream of the hydrated lime injection point. The humidifier inlet flue gas in the steam humidification tests was equivalent to the flue gas after complete droplet evaporation with water spray humidification. Since the flue gas was free of water droplets, the tests measured SO<sub>2</sub> removal in a dry but humidified environment. Experimental variables were approach to saturation (10-60°F), and Ca/S molar ratio (1-2).

### Water Spray Humidification Tests

In the water spray humidification tests, a high-temperature (ca. 300°F) simulated flue gas was humidified to a close approach to adiabatic saturation (20-25°F) by spraying liquid water in the humidifier downstream of the lime injection point. Therefore, liquid water droplets were present with the entrained sorbent until they evaporated completely. In these tests, three different atomizing nozzles were tested, each under widely varying atomizing air pressures/flows. The varying degrees of atomization yielded sprays with widely varying droplet size distributions and drying times (0.7-2.1 sec at 30°F approach). Other experimental variables were approach (20-60°F), Ca/S (1 to 2 by mol) and NaOH/Ca(OH)<sub>2</sub> additive ratio (0 to 0.1 by mass).

## RESULTS AND DISCUSSION

### Reactivity of Entrained Lime Particles in Humidified Flue Gas

Tests with steam humidification (Figure 2) revealed that entrained hydrated lime particles have a substantial activity for SO<sub>2</sub> capture under humidified flue gas conditions (at low approach to saturation without the presence of liquid water droplets). At 25°F approach to saturation, 2 Ca/S molar ratio and 2 second contact time, the SO<sub>2</sub> removal was 23%. This level of SO<sub>2</sub> removal in the short contact time shows that hydrated lime particles have a high intrinsic activity under the humidified conditions, even in the absence of water droplets. This result indicates that a significant SO<sub>2</sub> reduction is possible in the humidifier by lime which is not directly wetted by water droplets. It also indicates that the lime can continue to capture a significant amount of SO<sub>2</sub> even after complete evaporation of water sprays.

The activity of entrained lime particles under humidified conditions increased significantly with increasing relative humidity (Figure 2). The SO<sub>2</sub> removal at 2 Ca/S mole ratio increased from 12% to 40% as the approach to adiabatic saturation (ca. 125°F) decreased from 60°F (about 20% relative humidity) to 10°F (about 75% relative humidity). At 1 Ca/S ratio, the SO<sub>2</sub> removal increased from 7% to 20% with the same change in the approach.

At higher approaches, the SO<sub>2</sub> removal was not as sensitive to the level of approach. As shown in the figure, there was little drop in removal from 45°F to 60°F approach. At very high approach (130°F), the removal was still 5 to 6% at 2 Ca/S ratio.

The observed effect of the approach to adiabatic saturation (or flue gas humidity) on the SO<sub>2</sub> removal may be due to the positive role of physically adsorbed water on the internal and external surfaces of porous lime particles. The amount of water adsorbed at equilibrium on the lime surfaces increases strongly with increasing humidity (4). Figure 3 shows that the observed SO<sub>2</sub> removals at varying humidities (data from Figure 2) can be correlated nearly linearly with the calculated number of monolayers of adsorbed water (Table 2), based on data from a published study of water vapor equilibrium adsorption on six different hydrated limes as a function of humidity. The study showed that the adsorption per unit lime surface area (or equivalently the number of H<sub>2</sub>O layers) was independent of the lime source. For example, the equilibrium amounts of H<sub>2</sub>O adsorption on lime are roughly 1.3 and 1.9 monolayers at 50°F and 25°F approaches, respectively. In the steam humidification tests, it is not clear whether the lime rapidly adsorbed water to near the equilibrium level after injection into the flue gas or if the close approach allowed retention of the original surface moisture on the lime. Pilot tests with varying initial lime surface moisture contents can address this question.

The  $\text{SO}_2$  removal by lime particles in steam humidified flue gas increased with increasing lime feed rate in almost direct proportion with the Ca/S mol ratio. Thus, the observed sorbent utilization efficiency remained nearly constant with increasing Ca/S. Figure 2 shows that the  $\text{SO}_2$  removal at each approach roughly doubled as the Ca/S mol ratio doubled from 1 to 2. These results are consistent with the fact that the increased sorbent loading did not change significantly the environment for sulfur capture for individual sorbent particles. Except for the 10°F approach tests, the differences in the flue gas  $\text{SO}_2$  partial pressure were not significant at the two different Ca/S mol ratios because of the relatively low levels of  $\text{SO}_2$  removal. In the 10°F approach tests, the  $\text{SO}_2$  partial pressure was appreciably lower at the higher Ca/S mol ratio, but this did not affect the performance of individual sorbent particles.

#### Effect of Water Droplets

Tests with water spray (Coolside) humidification clearly indicate that the presence of liquid water droplets substantially enhances desulfurization performance. Figure 4 shows that at the same final approach to saturation, humidifier  $\text{SO}_2$  removals with water spray humidification significantly exceeds that with steam humidification. At 25°F approach and 1 Ca/S ratio, the humidifier removal was 30% with Coolside humidification, as compared with 12% with steam humidification. At 45°F approach, the respective removals were 13% and 6%. The flue gas residence time in the humidifier in Coolside tests was 1.7-2.0 seconds, similar to that in the steam humidification tests. Water was atomized using the Spraying Systems J-12 nozzle with 100 psig atomizing air pressure.

The significant enhancement of the sorbent performance in the presence of evaporating water droplets must result from the wetting of lime particles by water droplets through droplet-particle collisions. This wetting by water droplets would be very efficient in supplying moisture to the lime surfaces and would increase the water content in the lime particles well above that possible by physical adsorption alone.

The humidifier  $\text{SO}_2$  removal under conditions of water spraying increased significantly with closer approaches to saturation (Figures 4 and 5). The removal at 1 Ca/S increased from 13% to 31% as the approach decreased from 45°F to 25°F. Above 45°F approach, the removal was less sensitive to the approach.

A lower approach to saturation can enhance  $\text{SO}_2$  removal under Coolside humidifying conditions in two ways. First, a higher liquid water feed rate is required at a lower humidifier exit temperature. The theoretical water requirements for cooling to 45°F, 30°F and 25°F approaches in the above runs were 0.288, 0.329, and 0.354 gal/1000 scf flue gas, respectively. The increased water spraying capacity increases the probability of sorbent/droplet interactions. Secondly, the lower approach increases water evaporation time. This allows the wetted lime particles to retain moisture longer on the particle surfaces.

The effect of Ca/S mol ratio observed in the Coolside tests with water droplets present was somewhat different from that observed in steam humidification tests. In the Coolside tests, increasing the lime feed increased humidifier  $\text{SO}_2$  removals, but not in direct proportion to the increasing Ca/S ratio (Figure 5). The incremental effect of additional sorbent diminished with increasing Ca/S ratio, particularly at the very close (25°F) approach. Therefore, sorbent utilization efficiency decreased with increasing Ca/S ratio. As shown in Figure 5, humidifier  $\text{SO}_2$  removal at 25°F approach was rather insensitive to Ca/S ratio from 1 to 2, increasing from 30 to only 34%. Additional study is required to identify the causes or mechanisms for the

reduced sorbent utilization efficiency with increasing sorbent loading. One possible explanation is that the fraction of the total sorbent particles impacted by the water droplets may be smaller at a higher sorbent particle loading.

#### Effect of Droplet Size and Evaporation Time

Tests with Coolside humidification with widely varying degrees of water atomization showed that  $\text{SO}_2$  removal in the humidifier was higher with larger water droplets and longer droplet drying times at the same final approach to saturation. This result indicates that larger droplets may provide more sorbent-droplet interaction because of either their longer drying times or higher collection efficiencies. The effect of droplet size further confirms the important role of water droplets in the Coolside desulfurization mechanism.

In the Coolside atomization tests, three different nozzles (Spraying Systems J-12, Caldyne 2 mm, and Heat Systems Sonimist 700-3) were tested under widely varying atomizing air pressures and flows. The variation in nozzle type and atomizing pressure produced a wide variation in the drying time in the humidifier (Table 3). The drying time variation resulted primarily from differences in water droplet size distributions produced at different atomizing air pressures, although droplet sizes were not experimentally measured in this study. Humidifier center-line gas temperature profiles were used to estimate drying times in the tests. Figure 6 shows such profiles for the Spraying Systems J-12 nozzle humidifying a 300°F flue gas to 30°F approach at different atomizing air pressures. When enough unevaporated water droplets were present in the flue gas to wet the center-line thermocouples, they read at or close to the adiabatic saturation (wet bulb) temperature. As complete evaporation was approached the thermocouple readings approached the humidifier exit bulk gas (dry bulb) temperature. Thus drying time was estimated from the point at which the profile leveled out at the humidifier exit temperature to within thermocouple error ( $\pm 3^\circ\text{F}$ ). The residence time is based on the plug flow gas velocity at the average humidifier temperature. Based on the temperature profiles, the drying time with the Spraying Systems J-12 nozzle at 30°F approach increased from roughly 0.8 to 2.0 seconds as atomizing air pressure decreased from 115 psig to 45 psig. This reduction in the atomizing air pressure reduced the atomizing air flow through the nozzle. Drying time with the Caldyne nozzle was variable from 0.8-1.2 sec at 30°F by changing the air pressure from 90 to 70 psig (Table 3). The Heat Systems nozzle showed little or no variation in the drying time with air pressure (Figure 7).

Figure 8 shows that the humidifier  $\text{SO}_2$  removal with the Spraying Systems J-12 nozzle increased significantly with decreasing atomizing air pressure and increasing drying time. The removal at 30°F approach and 1.5 Ca/S ratio increased from 20% to 28% as atomizing pressure dropped from 115 psig to 55 psig. A similar effect was observed at 45°F approach, the removal increasing from 15% to 19% over 115 to 45 psig air pressures (Table 3). With 0.1 NaOH/Ca(OH)<sub>2</sub> additive injection, the increase was from 34% to 41% from 115 to 55 psig air pressure, at 30°F approach and 1.5 Ca/S ratio.

Using the Caldyne nozzle, the humidifier  $\text{SO}_2$  removal at 45°F approach increased from 15% to 25% with decreasing atomizing air pressure from 90 psig to 50 psig. At 30°F approach, there was not as much variation in drying time (Table 3) with air pressure (90-70 psig) and thus less variation in the  $\text{SO}_2$  removal (23 to 26%).

The observed  $\text{SO}_2$  removal using the Heat Systems nozzle was lower than with the other two nozzles tested, because it produced very small rapidly evaporating droplets, independent of the atomizing air pressure (Figure 7). At 30°F approach

and 1.5 Ca/S, the removals were 19-21%, independent of the atomizing air pressure, as compared with the 20-28% range observed with the other nozzles. At 45°F approach, removals ranged 10-12%, compared with 15-25% observed with the other nozzles.

#### SO<sub>2</sub> Removal in Baghouse

The baghouse provided significant SO<sub>2</sub> capture in both the steam humidification and Coolside humidification tests. The relative baghouse SO<sub>2</sub> removals, based on the SO<sub>2</sub> content at the baghouse inlet, depended heavily on approach to saturation. In the steam humidification tests, the relative removal at 1 Ca/S increased from 9% to 48% with decreasing approach from 60°F to 10°F. The relative removal also depended on Ca/S ratio, roughly doubling as Ca/S increased from 1 to 2, at lower approaches in the steam humidification tests. The relative baghouse SO<sub>2</sub> removals observed during Coolside testing were about the same or a little less than during steam humidification tests. The total SO<sub>2</sub> removals (across the humidifier and baghouse) were 38% and 21% with Coolside humidification and steam humidification, respectively, at 25°F approach and 1 Ca/S without NaOH (additive) injection. The residence time of solids in the baghouse during the pilot tests ranged 1-2 hours. Because the average solid residence time in the baghouse varied and because some solids dropped out in the baghouse hopper before reaching the bags, observed baghouse removals provide only qualitative desulfurization data.

#### CONCLUSIONS

Pilot test results with steam and water humidification indicate that the SO<sub>2</sub> capture mechanisms by entrained hydrated lime are highly complex and strongly dependent on the humidification level (approach to adiabatic saturation). Hydrated lime particles have a significant activity and thus provide considerable SO<sub>2</sub> removal in only a few seconds of entrainment in the flue gas under highly humidified flue gas conditions with no water droplets. The adsorbed lime surface moisture may play a key role for the desulfurization reaction based on the strong positive effect of the approach to saturation on SO<sub>2</sub> removal. The presence of evaporating water droplets enhanced the SO<sub>2</sub> removal by the entrained hydrated lime particles significantly. The wetting of lime particles by water droplets may play a key role in the enhanced performance. The beneficial effect of the water was greater at a lower approach to saturation and with larger droplets. The above results indicate that lime injection prior to water spraying, as in the Coolside process, is important for maximum sorbent utilization efficiency and SO<sub>2</sub> removal. Additionally, the sorbent efficiency of the Coolside process may be increased by modifying the lime properties for improved activity under humidified flue gas conditions and by increasing the lime particle-water droplet interactions for enhanced wetting of the particles.

#### REFERENCES

1. Yoon, H., Stouffer, M. R., Rosenhoover, W. A., and Statnick, R. M., "Laboratory and Field Development of Coolside SO<sub>2</sub> Abatement Technology", Second Annual Pittsburgh Coal Conference, Pittsburgh, PA, September 16-20, 1985.
2. Yoon, H., Ring, P. A. and Burke, F. P., "Coolside SO<sub>2</sub> Abatement Technology: 1 MW Field Tests", Coal Technology '85 Conference, Pittsburgh, PA, November 12-14, 1985.
3. Yoon, H., Stouffer, M. R., Rosenhoover, W. A., Withum, J. A., and Burke, F. P., "Pilot Process Variable Study of Coolside Desulfurization", AIChE 1987 Spring National Meeting, Houston, Texas, March 1987.

REFERENCES (Continued)

4. Klingspor, J., "Kinetic and Engineering Aspects on the Wet-Dry FGD Process", Department of Chemical Engineering II, Lund Institute of Technology, Lund, Sweden, 1983.

TABLE 1  
CHEMICAL AND PHYSICAL ANALYSES  
OF DRAVO LONGVIEW HYDRATED LIME (a)

<u>Chemical Analyses, wt %</u>		<u>Particle Size Analyses, wt %</u>	
Moisture	0.21	+325 mesh	21.6
Ash	75.59	-325 mesh	78.4
Carbonate	1.75		
<u>Ash Elemental, wt %</u>		<u>BET Analyses</u>	
Na <sub>2</sub> O	0.01	Surface Area, m <sup>2</sup> /g 17.3-20.3	
K <sub>2</sub> O	0.02		
CaO	97.42		
MgO	2.25		
Fe <sub>2</sub> O <sub>3</sub>	0.10		
TiO <sub>2</sub>	0.02		
P <sub>2</sub> O <sub>5</sub>	0.01		
SiO <sub>2</sub>	0.54		
Al <sub>2</sub> O <sub>3</sub>	0.57		
SO <sub>3</sub>	0.07		
Total	101.01		

(a) Typical analysis of batch used in pilot testing.

TABLE 2  
APPROXIMATE EQUILIBRIUM WATER ADSORPTION FOR HYDRATED LIME  
BASED ON PUBLISHED DATA (4)

<u>Approach to Saturation</u>	<u>Water Adsorbed at Equilibrium</u>	
	<u>g H<sub>2</sub>O/m<sup>2</sup> Lime</u>	<u>No. Monolayers</u>
60	0.00053	1.3
45	0.00059	1.5
30	0.00069	1.7
25	0.00075	1.9
15	0.00087	2.2
10	0.00100	2.5

Based on data at 158°F for six different hydrated limes.

TABLE 3  
ATOMIZATION TEST RESULTS

Nozzle	Approach °F	NaOH/ Ca(OH) <sub>2</sub> , mass	Atomizing Air		Estimated Drying Time, sec	Humidifier SO <sub>2</sub> Removal %	
			psig	scf/ gal H <sub>2</sub> O			
Spraying Systems J-12	45	0	115	78	0.5-0.7	15 (15)	
	45	0	100	69	0.9-1.1	15 (14)	
	45	0	85	57	-	17 (16)	
	45	0	70	51	1.1-1.5	17 (18)	
	45	0	55	44	1.5-1.9	19	
	45	0	45	38	1.7-1.9	19	
	30	0	115	74	0.7-0.8	20 (20)	
	30	0	100	63	0.8	23	
	30	0	85	56	1.0	24 (24)	
	30	0	70	46	1.9-2.1	27	
	30	0	55	40	1.9-2.1	28	
	30	0.1	115	62	0.7-0.8	34 (36)	
	30	0.1	100	54	0.8	39	
	30	0.1	85	47	1.0	41	
	30	0.1	70	39	1.9-2.1	40 (41)	
	30	0.1	55	34	1.9-2.1	41	
	Caldyne	30	0	90	131	0.8	23 (23)
		30	0	80	119	0.9-1.1	24 (26)
		30	0	70	101	1.0-1.4	26
		45	0	90	159	0.5-0.8	15 (14)
		45	0	80	139	0.7-0.7	18
45		0	60	108	1.0-1.2	21 (20)	
45		0	50	92	1.5-1.8	25	
45		0	50	92	1.5-1.8	25	
Heat Systems	45	0	70	---	0.6-0.8	10	
	45	0	60	295	0.6-0.8	10	
	45	0	55	273	0.6-0.8	11 (12)	
	45	0	45	213	0.6-0.8	---	
	30	0	70	---	0.7-0.8	19	
	30	0	60	271	0.7-0.8	19	
	30	0	55	260	0.7-0.8	21	
	30	0	45	212	0.7-0.8	23	
	30	0	45	212	0.7-0.8	23	
	30	0	45	212	0.7-0.8	23	

Numbers in parentheses are repeat tests.

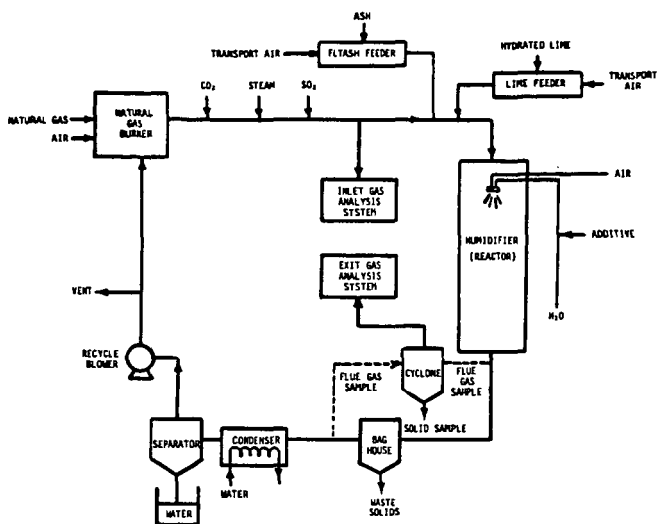


Figure 1. Schematic of Pilot Unit.

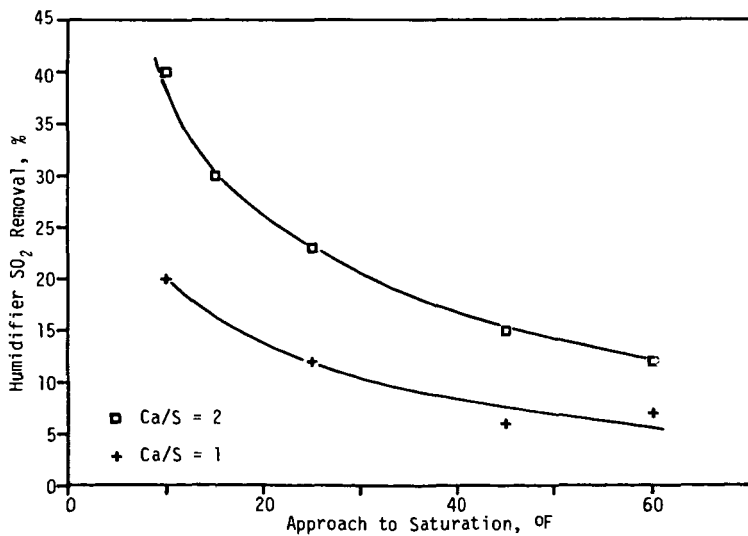


Figure 2. Steam Humidification Tests. Humidifier Removal: 2 sec residence time, 1500 ppm SO<sub>2</sub>.

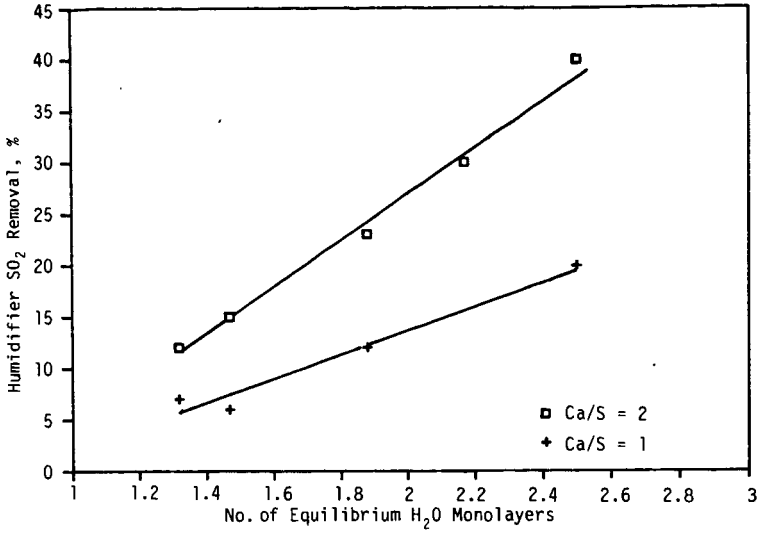


Figure 3. Steam Humidification Tests. Humidifier Removal: 2 sec, 1500 ppm SO<sub>2</sub>.

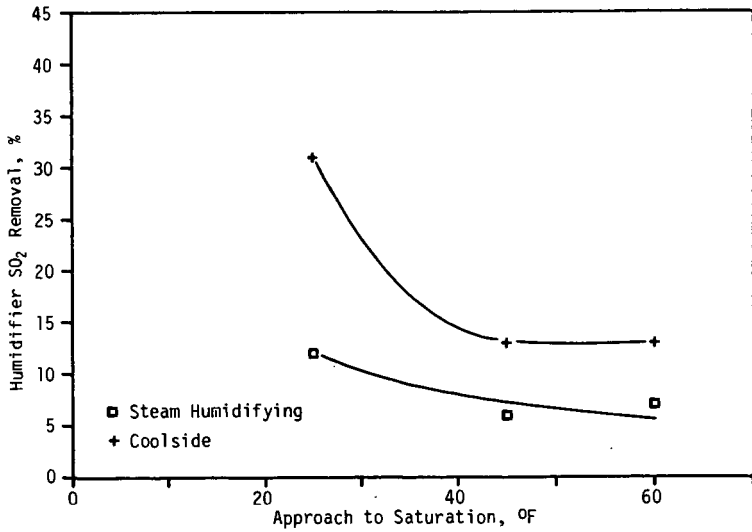


Figure 4. Comparison of Coolside Process and Steam Humidification Test Results. 1 Ca/S, 0 NaOH, 1500 ppm SO<sub>2</sub>.

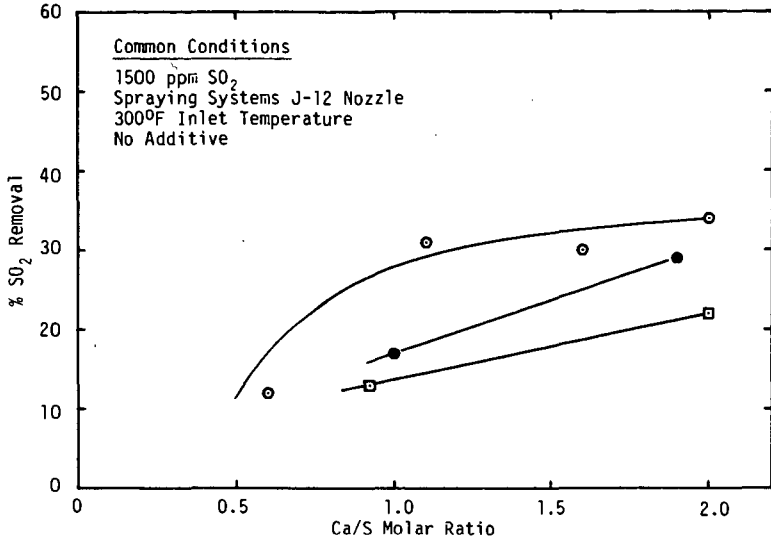


Figure 5. Effect of Ca/S Ratio and Approach on Humidifier SO<sub>2</sub> Removal in Coolside Humidification Tests. ○ 25°F ● 30°F □ 48°F Approach.

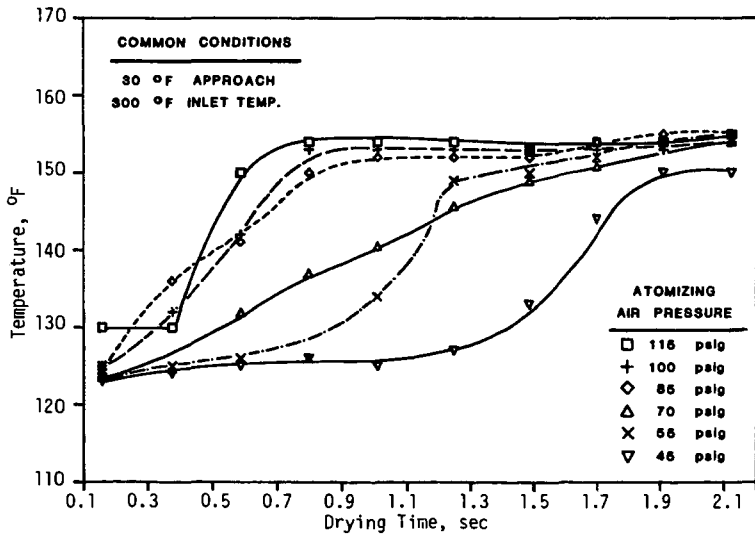


Figure 6. Humidifier Temperature Profile. Spraying Systems J-12 Nozzle.

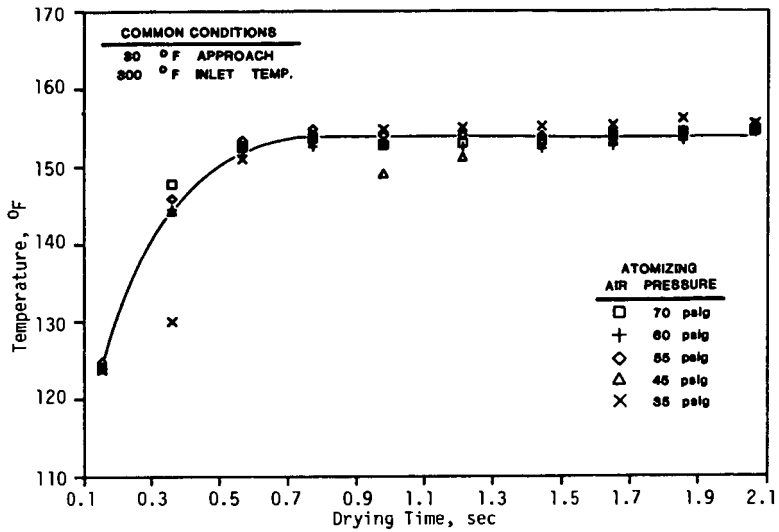


Figure 7. Humidifier Temperature Profile. Heat Systems 700-3 Nozzle.

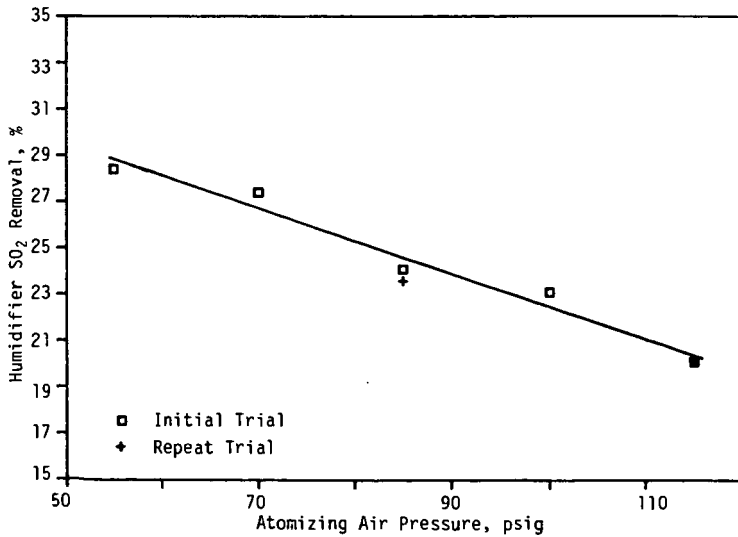


Figure 8. Effect of Atomization on SO<sub>2</sub> Removal. Spraying Systems J-12 Nozzle.

## THE MECHANISM OF CaO SULFATION IN BOILER LIMESTONE INJECTION

M. R. Stouffer, H. Yoon and F. P. Burke

CONSOLIDATION COAL COMPANY  
Research & Development Department  
4000 Brownsville Road  
Library, PA 15129

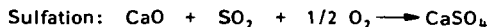
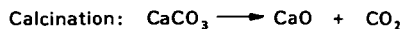
### ABSTRACT

Pilot and industrial-scale tests of boiler limestone injection (BLI) have demonstrated flue gas SO<sub>2</sub> reductions of around 50% at sorbent utilization efficiencies of 15-20%. The objective of the laboratory research program described in this paper was to improve BLI sorbent utilization through an understanding of the limestone calcination and CaO sulfation reaction mechanisms. This paper describes the laboratory sulfation studies. The laboratory work used a differential reactor operated at 700-1000°C and lab-produced calcines from limestones, dolomites, and hydrated limes, having particle sizes in a range applicable to BLI. The lab work determined the intrinsic sulfation reaction rate and rate-controlling steps over this temperature range. The intrinsic rate increased with the square of calcine surface area and was rate controlling only at temperatures below 800°C. At the higher temperatures more applicable to BLI, the sulfation rate was limited by pore diffusion of SO<sub>2</sub> and pore plugging by the sulfate product. Therefore, the reaction rate and the saturated sorbent efficiency depended strongly on particle size and calcine pore structure. The lab data indicate that an optimum calcine pore structure can be obtained by appropriately evaluating sorbents, controlling calcination conditions and incorporating alkali additives in the sorbent.

### INTRODUCTION

Boiler limestone injection is a low capital cost SO<sub>2</sub> control technology, involving injection of pulverized limestone into the high-temperature (1000-1300°C) regions of a coal-fired furnace. Alternate calcium sorbents, such as hydrated lime and dolomite, can also be used. In 1984, Consolidation Coal Company (Consol) successfully demonstrated the technology using a 15 MW industrial boiler at Du Pont's Martinsville nylon plant (1). The target 50% SO<sub>2</sub> removal was achieved by injecting limestone at 2.5-2.75 Ca/S molar ratios, corresponding to 18-20% sorbent utilization efficiencies. Since then, Consol has conducted an extensive laboratory program studying the fundamental mechanisms involved in BLI. The objective has been to significantly improve the sorbent utilization by applying the fundamental information for process improvement.

SO<sub>2</sub> removal by BLI involves sequential calcination and sulfation reactions:



These reactions have been widely studied; however, much of the published work has been limited to low surface area (<5 m<sup>2</sup>/g), large particle size (ca. 1 mm) calcines (CaO), applicable to fluidized bed combustion. The reactivities observed with these calcines are too low to provide significant SO<sub>2</sub> reduction in BLI (2). More recent studies at EPA (3-6) using very fine (ca. 1 micron) limestone particles have shown that very high surface area calcines (up to 80 m<sup>2</sup>/g) could be produced by differential calcination in a dispersed-phase system. In these studies, the intrinsic sulfation activity of the very fine calcine particles was proportional to the square of the calcine BET surface area. This result suggests that production of a high

surface area calcine may be critical for BLI processes. However, the 1 micron limestone particle size used in the EPA studies is much smaller than practical sizes for BLI.

This paper reports a laboratory study of calcination and sulfation for sorbent samples having a range of particle sizes applicable to BLI. Detailed results of the calcination study were previously reported (7). In this work, calcines having up to 70 m<sup>2</sup>/g surface area were produced under differential and dispersed conditions from pulverized limestone samples applicable to BLI. Calcine surface area depended on exposure time, temperature, CO<sub>2</sub> partial pressure, and stone properties. A kinetic model derived for the calcination reaction indicated that calcination occurs very rapidly (<0.1 sec) at BLI temperatures.

In the sulfation study, the intrinsic sulfation kinetics and rate-controlling steps were determined with lab-produced calcines from limestones, dolomites, and hydrated sorbents. In addition, the effect of alkali additive incorporation on limestone was studied as a means of enhancing sulfation performance of calcines. The temperature range of 700-1000°C, limited by the experimental apparatus, was lower than the BLI temperature range of 1000-1300°C. However, the lab data provided valuable insight into BLI sulfur capture mechanisms and comparison of different sorbent performance.

## EXPERIMENTAL

### Test Sorbents

Twelve test sorbents were evaluated including eight different limestones, two dolomitic stones, a hydrated lime and a pressure-hydrated dolomite (Table 2). These sorbents varied widely in particle size as indicated by their specific surface mean diameters, and yielded calcines with widely varying BET surface areas (35-70 m<sup>2</sup>/g). Most of the kinetic data were obtained for calcines produced from one stone, the Dravo Maysville -100 (#1). The other stones in Table 1 were tested for comparison.

### Differential Reactor

A differential reactor (Figure 1) was used to calcine sorbent samples and to measure the sulfation performance of the calcines. This unit allowed control of reaction temperature to within ±3°C and sorbent/SO<sub>2</sub> contact time to within ±1 sec. To maintain differential sulfation conditions with respect to SO<sub>2</sub> partial pressure and temperature and to eliminate bulk mass transfer resistance, very small sorbent samples (down to 8 mg) well-dispersed in quartz wool and large flows (up to 70 scfh) of SO<sub>2</sub>-containing sweep gas were used. Differential sulfation conditions were confirmed up to 900-950°C. Differential conditions were not possible above 950°C because of the extremely high sulfation rate. A few tests at 1000°C provided saturated sorbent utilization data, but no accurate rate data.

### Test Procedures

Before sulfation, the sorbent was calcined in the differential reactor, under a purge flow of air at the same temperature as the subsequent sulfation. The calcination contact time was set to control the calcine surface area. For runs with low surface area calcines, the sorbent was calcined externally in a muffle furnace. After calcination was complete, the purge gas was switched immediately to an SO<sub>2</sub>-containing gas containing 80% N<sub>2</sub>, 15% CO<sub>2</sub>, 5% O<sub>2</sub> and 750-3000 ppm SO<sub>2</sub>. Immediately after a set reaction time between 5 and 600 sec, the SO<sub>2</sub>-containing gas was shut off and the sorbent sample removed from the reactor. The conversion of CaO to CaSO<sub>4</sub> was determined by the Ca and S contents in the recovered sample

measured by atomic adsorption spectroscopy and combustion infrared detection, respectively.

Surface area and pore volume distributions of the calcine intermediates were measured separately by producing calcine samples under conditions duplicating those used prior to sulfation. Calcine surface areas were determined by  $N_2$  adsorption at 77K (liquid  $N_2$ ) and the one-point BET method. Pore distributions were determined from  $N_2$  desorption isotherms (at 77K) following the methods detailed in References 8 and 9.

## DISCUSSION OF RESULTS

### Intrinsic Sulfation Kinetics

Intrinsic sulfation rate data measured for calcines from Dravo -100 mesh limestone were correlated by a kinetic model, originally proposed by Borgwardt (6). Based on the classical unreacted core model or grain model, this model relates fractional calcium conversion ( $x$ ) to the  $SO_2$  contact time ( $t$ , sec), absolute temperature ( $T$ , K),  $SO_2$  partial pressure ( $P_{SO_2}$ , mmHg), and calcine specific surface area ( $A$ ,  $m^2/g$ ) as follows:

$$1 - 3(1-x)^{2/3} + 2(1-x) = k_d \cdot t \quad (1)$$

$$k_d = K (A)^m (P_{SO_2})^n \exp(-E/RT) \quad (2)$$

where the constants are

$E = 37$  kcal/mol, the activation energy  
 $m = 2.0$   
 $n = 0.62$   
 $K = 50$

The model equation is applicable to any calcine (CaO), since it includes a calcine property, the specific surface area,  $A$ . The intrinsic rate increased with the square of the surface area.

In the original development of this kinetic model, Borgwardt (6) used extremely small (95 wt % <2 micron, 30 wt % <1 micron) calcine particles, in order to eliminate pore diffusion limitation. Because of the much larger particle sizes used in the current study (13.4 micron specific surface mean diameter and 28.3 mass median diameter for the Dravo stone, #1), intrinsic rate data without pore diffusion limitation were measured only at low temperatures ( $\leq 800^\circ C$ ) and with low surface area calcines (<15  $m^2/g$ ). Figure 2 shows the good agreement of laboratory data at  $800^\circ C$  with the kinetic model predictions.

### Pore Diffusion Limitation

With calcines produced from sorbent samples having particle sizes applicable to BLI (Table 1), pore diffusion was rate limiting at higher temperatures ( $>800^\circ C$ ) and with higher surface area calcines ( $>15 m^2/g$ ). As a result, observed sulfation rates were significantly lower than the intrinsic rate predicted by the above model. As discussed below, pore diffusion limitation was evidenced by the observed reaction rate dependence on temperature,  $SO_2$  partial pressure, particle size, and calcine surface area and pore structure.

Figure 3 shows that for higher surface area calcines, the apparent activation energy dropped from 37 kcal/mol to 15-20 kcal/mol at higher temperatures, indicative of transition to pore diffusion control. This agrees with the theoretical prediction that

$$E_{\text{apparent}} = \frac{E + E_{\text{diffusion}}}{2} \approx E/2 \text{ under strong pore diffusion control.}$$

The onset of pore diffusion limitation for higher surface area calcines was around 800°C, based on the changes in slope in the Arrhenius plots. For a low surface area calcine (4 m<sup>2</sup>/g), pore diffusion limitation was not evident up to 950°C, based on the activation energy.

The reaction order (n) in SO<sub>2</sub> partial pressure, measured at 900°C with a 55 m<sup>2</sup>/g calcine, was 0.80 over 750-3000 ppm SO<sub>2</sub> concentrations, as compared with 0.62 according to the intrinsic kinetics. This change in the reaction order was also indicative of the pore diffusion control.

Because of the pore diffusion limitation, the initial sulfation rate observed at 900°C varied inversely with particle size (Figure 4). The different stone samples (#1-10) in Table 1 provided the variations in the particle size in the figure.

Under pore diffusion control, the effect of calcine surface area was diminished and high surface area calcines did not necessarily give high reactivity. This is because a calcine with very high surface area contains predominantly very fine pores which are more subject to pore diffusional resistance as well as pore mouth plugging, as discussed below.

#### Calcine Pore Plugging

Calcine pore mouth plugging by product CaSO<sub>4</sub> limited sulfation of highly porous calcines at higher temperatures. Limitation by pore plugging was evident in the lab tests from the exceptionally low apparent activation energies (<10 kcal/mol) observed with some very high surface area calcines and from the reduction in the saturated calcium utilization with increasing sulfation temperature for most of the calcines.

Porous calcines are subject to pore plugging by product sulfate because the molar volume of CaSO<sub>4</sub> (46.0 cm<sup>3</sup>/mol) is considerably greater than that of CaO (16.5 cm<sup>3</sup>/mol). If the mouth of a pore plugs before the interior undergoes reaction, the sorbent utilization is reduced. Further, pore mouth plugging by CaSO<sub>4</sub> can reduce the rate of sulfation by reducing available surface area and by increasing the pore diffusional resistance. Severe product pore mouth plugging is most likely when the rate of sulfation exceeds the rate of diffusion through the pores. Therefore, the degree of deactivation by pore plugging can be expected to increase with increasing temperature because the intrinsic sulfation rate increases more rapidly with temperature than the diffusion rate. Because of this temperature effect, pore plugging can reduce the apparent activation energy for sulfation. Deactivation by pore plugging can be expected to be most severe for smaller pores because the diffusion rate is slower and less CaSO<sub>4</sub> is required for complete pore blockage.

The degree of limitation of sulfation by pore plugging varied widely among calcines produced from different sorbents (Table 2). The apparent sulfation activation energies (based on initial reaction rates) among the different calcines ranged from negative values up to 22 kcal/mol. The activation energies below 15 kcal/mol indicate a rapid pore plugging at a higher temperature since the activation energies are lower than that under pore diffusion control. The wide variation in the activation energy among calcines indicates varying severity of pore plugging with these calcines. The saturated utilizations also varied widely among different calcines (17-80% at 900°C), as did the degree of temperature dependence of the saturated conversion.

The test data confirmed the more severe limitations by pore plugging for calcines with smaller pores. Figure 5 shows that a calcine from Genstar (#6) limestone had

significantly finer pores (mostly 3-10 nm) and less total pore volume than a calcine from the Dravo limestone (#1). The Dravo calcine had many pores in the 8-30 nm range. The apparent activation energy with the Genstar calcine was only 1.4 kcal/mol, significantly lower than the 15 kcal/mol observed for the Dravo calcine. Further, the Genstar calcine showed a more severe drop in final (saturation) calcium utilization with increasing temperature, from 36% to 27% to 18%, at 800°C, 900°C and 1000°C, respectively. The final utilizations with the Dravo calcine were 37%, 36% and 33% at these temperatures.

#### Performance of Different Stones/Sorbents

**Limestones:** Eight different limestones tested exhibited widely varying sulfation performance (Table 2). Saturation utilizations at 900°C varied from 17% to 50% and apparent activation energies varied from 1.4 to 22 kcal/mol over 800-950°C. These differences resulted from differences in both the stone particle size (Table 1) and the calcine intermediate pore structure. Calcine intermediate pore structure (surface area and pore size distribution) varied widely with limestone source. However, the specific properties of the original limestone which lead to a favorable calcine pore structure were not clearly identified.

**Dolomitic Stones:** Calcines from two dolomitic stones (Tables 1, 2) tested showed poor sulfation performance, presumably due to the presence of very small pores. Both showed negative apparent sulfation activation energies and low saturated calcium utilizations (22% at 900°C), indicative of premature pore plugging. Both calcines had very high surface areas (70 m<sup>2</sup>/g). Pore volume analysis of the calcine from the Hommel dolomite (#9) showed that it had over 85% of its pore volume in small pores, 2-10 nm in diameter.

**Hydrated Sorbents:** Calcines derived from a hydrated lime and a pressure-hydrated dolomitic lime showed better sulfation performance, in terms of both rate and saturation calcium utilization, than those derived from most limestones or dolomites. For the Dravo Longview hydrated lime (#11), saturated utilization was 55% at 800°C and dropped only to 53% at 900°C (Table 2). The apparent activation was 20 kcal/mol. Figure 6 clearly shows the superior sulfation performance of a calcine from a pressure hydrated dolomite (#12) to that from a dolomitic limestone (#9), the two calcines having roughly the same chemical composition. Saturated calcium utilizations were 80% and 22% for the pressure dolomitic hydrate and the dolomitic stone, respectively. Also, the saturated calcium utilization with the pressure hydrate did not drop at higher temperature. The excellent performance of the pressure hydrated dolomite again can be attributed to the formation of a very favorable calcine pore structure. Pore volume analysis showed that the calcine from the pressure hydrate had a broad pore size distribution (4-40 nm diameter) with about 60% of its total pore volume contributed by pores of 10 nm diameter and larger, as compared with the predominance of very small pores found in the calcined dolomite.

#### Sulfation Enhancement by Additive Promotion

Of several salts (Na<sub>2</sub>CO<sub>3</sub>, NaCl, CaCl<sub>2</sub>, FeCl<sub>3</sub>) tested, Na<sub>2</sub>CO<sub>3</sub> was found to be the most effective in enhancing the desulfurization performance of limestone. Additives were incorporated in small amounts (0.25-5 wt %) in the limestone sample prior to calcination. The results indicate that the enhancement was primarily due to physical effects, increasing the pore size of the calcine to a range more favorable for pore diffusion. This agrees with the alkali additive effects on calcine porosity in FBC (10-13). The degree of enhancement increased with the Na<sub>2</sub>CO<sub>3</sub> dosage up to 2 wt %.

For this additive study, additive effects were studied for two different limestones, the Dravo limestone (#1) and the Genstar limestone (#6) (Table 1). To produce an

additive promoted limestone sample, limestone was slurried in an aqueous additive solution. Water was then evaporated from the slurry. After preparation, the dry additive-enhanced limestone was charged in the differential reactor and calcined and sulfated in the usual manner.

Figure 7 shows that sodium carbonate promotion of the Dravo stone significantly increased pore size of the calcine intermediate. With no additive, a calcine produced at 900°C had pores mostly in the 6-20 nm diameter range. With 0.5 wt % and 2 wt %  $\text{Na}_2\text{CO}_3$  in the stone, the 900°C calcines had pores mostly in the 6-40 nm and 10-70 nm ranges, respectively. Because of the increased pore size, calcine surface areas decreased. The BET surface areas for these calcines were 52, 21 and 10  $\text{m}^2/\text{g}$ , with  $\text{Na}_2\text{CO}_3$  concentrations of 0, 0.5 and 2 wt %, respectively.

With the increase in calcine pore size with  $\text{Na}_2\text{CO}_3$ , the sulfation performance of the Dravo calcine was significantly enhanced (Figure 8). At 0.5 and 2 wt % additive dosages, saturated calcium utilizations at 900°C increased from 36% (with no additive) to 47% and 52%, respectively. Observed initial sulfation rates were also increased substantially. Similar enhancement was observed at 800°C and 1000°C. Further increase in the additive dosage above 2 wt % did not give additional sulfation enhancement. With 5 wt %  $\text{Na}_2\text{CO}_3$  sulfation, performance of the Dravo calcine was not as good as with 2 wt %  $\text{Na}_2\text{CO}_3$ . The calcine with 5 wt %  $\text{Na}_2\text{CO}_3$  had a low surface area (7  $\text{m}^2/\text{g}$ ) and thus a lower intrinsic reaction rate. This result indicates that the pore size was increased excessively above an optimum level.

With Genstar limestone (#6),  $\text{Na}_2\text{CO}_3$  showed similar positive effects. The saturated calcium utilization at 900°C was increased to 60% with 2 wt %  $\text{Na}_2\text{CO}_3$ , a substantial improvement over the 27% utilization with no additive. Initial reaction rate was likewise enhanced.

Other additives tested were not as effective as  $\text{Na}_2\text{CO}_3$  in promoting sulfation. Sodium chloride ( $\text{NaCl}$ ) showed some enhancing effect. The saturation conversion with calcined Dravo stone (#1) at 900°C increased from 36% to 42% at 2 wt %  $\text{NaCl}$ . Calcium chloride ( $\text{CaCl}_2$ ) and ferric chloride ( $\text{FeCl}_3$ ) showed no significant enhancement of sulfation performance.

## CONCLUSIONS

Sulfur capture by boiler limestone injection involves complex calcination and sulfation phenomena and is limited by both chemical and physical processes including intrinsic sulfation reaction,  $\text{SO}_2$  pore diffusion in the calcine, and pore plugging by the product  $\text{CaSO}_4$ .

An intrinsic sulfation kinetic model, developed by Borgwardt of EPA, was experimentally confirmed. The intrinsic reaction rate increased with the square of calcine surface area and the 0.6 power of  $\text{SO}_2$  partial pressure, and had an activation energy of 37 kcal/mol. The intrinsic reaction was rate limiting only at lower temperatures ( $\leq 800^\circ\text{C}$ ) and with lower surface area calcines ( $< 15 \text{ m}^2/\text{g}$ ).

Under conditions applicable to BLI, sulfation is limited by pore diffusion and by product pore mouth plugging. Observed sulfation rates at 900°C with high surface area calcines varied inversely with sorbent particle size because of the pore diffusion limitation. Because of the pore plugging effect, the capacity for sulfation was lower for calcines with finer pore structures. These results indicate that an optimum calcine pore structure (in terms of surface area and pore size) may exist for effective sulfation. The lab data indicate that the pore structure of a calcine depends on sorbent source and calcination conditions. Different limestones gave widely varying sulfation performances because they produced calcines having different pore structures. Hydrated sorbents gave significantly better sulfation performance

than limestones, because they yielded a more favorable calcine structure. These results indicate that sorbent selection for BLI may be very important.

Small amounts of sodium carbonate added to limestones prior to calcination yielded calcines with larger pores and thus significantly enhanced desulfurization performance.

#### REFERENCES

1. Fink, C. E., Harding, N. S., Koch, B. J., McCoy, D. C., Statnick, R. M. and Hassell, T. J., "Demonstration of Boiler Limestone Injection in an Industrial Boiler", 1st Joint Symposium on Dry SO<sub>2</sub> and Simultaneous SO<sub>2</sub>/NO<sub>x</sub> Control Technologies, San Diego, California, November 13-16, 1984.
2. Borgwardt, R. H., "Kinetics of the Reaction of SO<sub>2</sub> with Calcined Limestone", *Environmental Science and Technology* 4, 59 (1970).
3. Borgwardt, R. H., Bruce, K. R. and Blake, J., "EPA Experimental Studies of the Mechanisms of Sulfur Capture by Limestone", Proceedings: 1st Joint Symposium on Dry SO<sub>2</sub> and Simultaneous SO<sub>2</sub>/NO<sub>x</sub> Control Technologies, San Diego, California, November 13-16, 1984.
4. Borgwardt, R. H., "Calcination Kinetics and Surface Area of Dispersed Limestone Particles", *AIChE Journal*, 31, 103 (1985).
5. Borgwardt, R. H., Roach, N. F. and Bruce, K. R., "Method for Variation of Grain Size in Studies of Gas-Solid Reactions Involving CaO", *Ind. Eng. Chem. Fund.*, 25 (1), 1986.
6. Borgwardt, R. H. and Bruce, K. R., "Effect of Specific Surface Area on the Reactivity of CaO with SO<sub>2</sub>", *AIChE Journal*, 32, 2 (1986).
7. Stouffer, M. R. and Yoon, H., "Laboratory Calcination and Sulfation Studies for Boiler Limestone Injection", presented at 6th Workshop on Coal Liquid and Alternate Fuels Technology, Halifax, Nova Scotia, September 1986.
8. Barrett, E. P., et al., "Determination of Pore Volume and Area Distributions in Porous Substances, I. Computations from Nitrogen Isotherms", *Journal of American Chemical Society*, 73, 3155, 1951.
9. Pierce, C., "Computation of Pore Sizes from Physical Adsorption Data", *Journal of Physical Chemistry*, 57, 147, 1953.
10. Shearer, J. A., Lenc, J. F., Johnson, I. and Turner, C. B., "The Effect of Sodium Carbonate Additive on the Reaction of SO<sub>2</sub>/O<sub>2</sub> Mixtures with Carbonate Rocks", Argonne National Laboratory, Report ANL/CEN/FE-79-11, July 1979.
11. Shearer, J. A., "The Effect of CaCl<sub>2</sub> Additive on the Reaction of SO<sub>2</sub>/O<sub>2</sub> Mixtures with Carbonate Rocks", Argonne National Laboratory, Report ANL/CEN/FE-79-7, 1979.
12. Gasner, L. L., "The Addition of Salt to Fluidized Bed Combustors", Proc. Fifth Intl. Symposium on Salt - No. Ohio Geological Society, 439-445.
13. Shearer, J. A., Johnson, I. and Turner, C. B., "The Effects of Sodium Chloride on Limestone Calcination and Sulfation in Fluidized-Bed Combustion", *Journal of Environmental Science and Technology*.

TABLE 1  
TEST SORBENTS

No.	Sorbent	Elemental Analysis		Avg Particle Diameter, (a) micron		BET Surface Area of Raw Stone, m <sup>2</sup> /g	Maximum BET Surface Area of Calcine, m <sup>2</sup> /g
		CaO, wt %	MgO, wt %	Mass Median	Specific Surface Mean(b)		
1	Dravo Maysville Limestone, -100 mesh	50.82	2.74	28.3	13.4	1.4	55
2	Dravo Maysville Limestone, -325 mesh	51.86	2.81	7.2	8.5	6.3	35
3	Pfizer Marble White 200 Limestone	54.79	0.36	23.1	14.6	0.7	60
4	Warner Bell Mine Limestone	54.71	0.58	25.9	15.8	1.8	45
5	Mississippi R-1 Limestone	55.20	0.30	300.0	112.0	0.9	70
6	Genstar Apex Limestone	56.53	0.46	28.3	16.1	1.0	60
7	Utah Marblehead Limestone	56.55	0.29	48.0	27.0	0.9	65
8	Baker Reagent CaCO <sub>3</sub>	56.54	0.01	13.2	11.2	0.5	55
9	Hommel #1974 FF Dolomite	32.00	20.11	32.9	22.0	0.8	70
10	Warner Dolomite	28.90	21.96	98.2	55.8	0.3	70
11	Dravo Longview Hydrated Lime	72.01	2.44	12.0	12.0	21.1	40
12	Pressure Hydrated Dolomite	41.70	30.38	39.2	24.9	23.3	45

(a) Particle size determined by wet screening in CH<sub>3</sub>OH and by Coulter Counter.

(b) Specific surface mean,  $D_p = \frac{\sum Y_i}{\sum Y_i D_i}$

where Y<sub>i</sub> = weight fraction of size cut, D<sub>i</sub> = Average diameter of size cut.

TABLE 2  
SULFATION PERFORMANCE OF HIGH SURFACE AREA CALCINES FROM TWELVE TEST SORBENTS

No.	Sorbent	D <sub>p</sub> micron (a)	Calcine Surface Area, m <sup>2</sup> /g	E <sub>apparent</sub> (b)	Saturation Ca Conversion, %		
					800°C	900°C	1000°C (c)
1	Dravo Maysville Limestone, -100 mesh	24.5	55	15	39	36	33
2	Dravo Maysville Limestone, -325 mesh	8.5	35	15	50	50	36
3	Pfizer Marble White 200 Limestone	14.6	60	4.1	23	21	--
4	Warner, Bell Mine Limestone	15.8	45	15	37	33	23
5	Mississippi R-1 Limestone	112.0	70	4.1	20	17	9
6	Genstar Apex Limestone	16.1	60	1.4	36	27	18
7	Utah Marblehead Limestone	27.0	65	15	31	20	11
8	Baker Precipitated CaCO <sub>3</sub>	11.2	55	22	45	36	--
9	Hommel #1974 Dolomite	22.0	70	Negative	32	22	--
10	Warner Dolomite	55.8	70	Negative	30	22	--
11	Dravo Longview Hydrated Lime	12.0	40	20	55	53	--
12	Pressure Hydrated Dolomite	24.9	45	21	80	80	--

(a) Specific surface mean particle diameter, as defined in Table 1.

(b) Apparent sulfation activation energy over 800-950°C.

(c) Runs at 1000°C deviated from differential conditions.

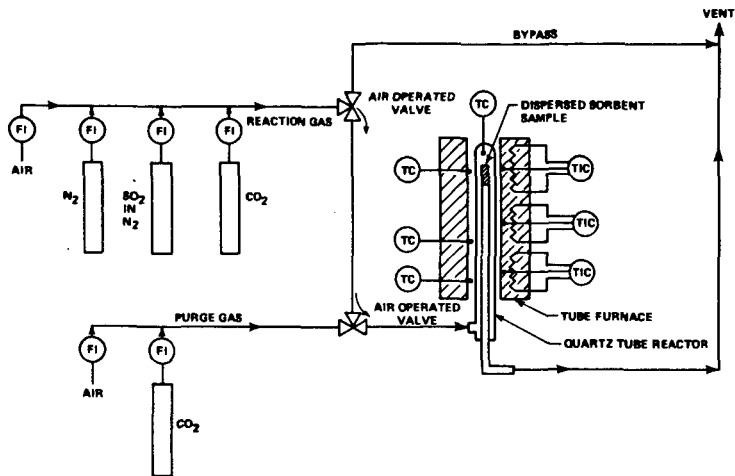


Figure 1. Schematic of Differential Reactor Unit.

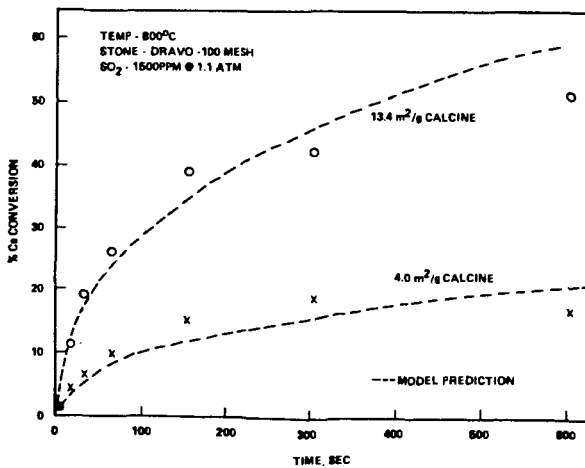


Figure 2. Comparison of Sulfation Rate Data with Intrinsic Sulfation Kinetic Model.

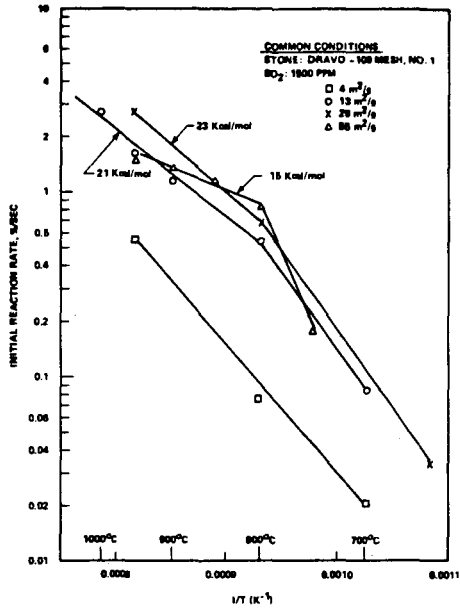


Figure 3. Initial Sulfation Rate vs Temperature.

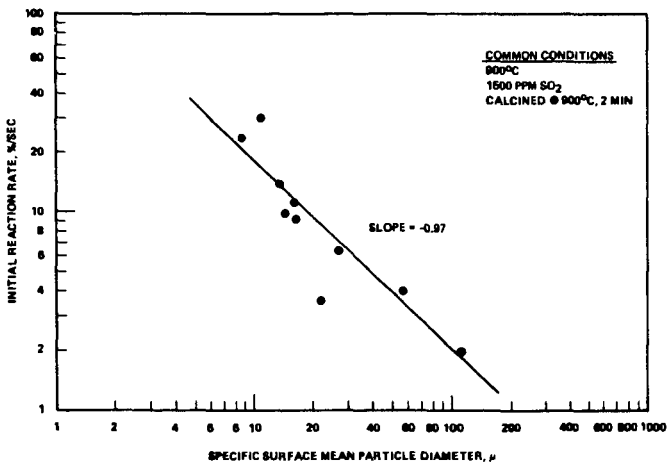


Figure 4. Effect of Stone Particle Size on Sulfation Rate.

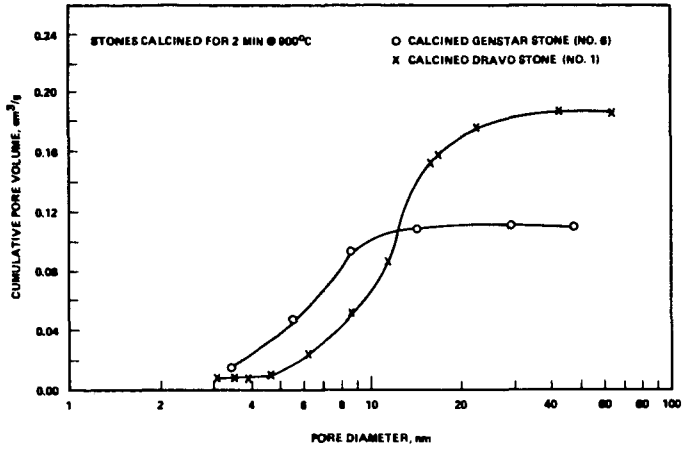


Figure 5. Cumulative Pore Volume Distribution for Two Calcined Limestones.

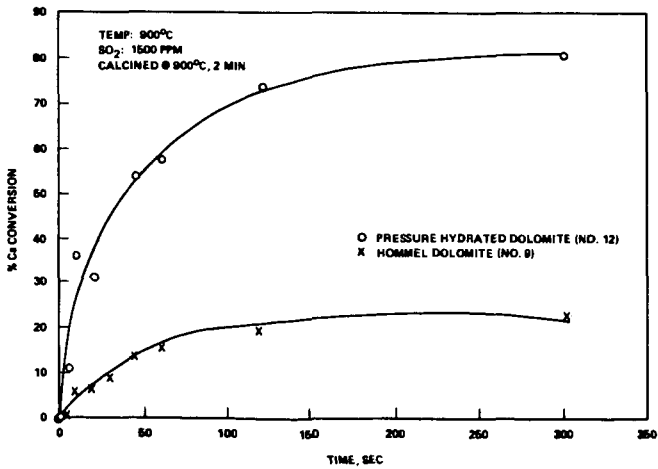


Figure 6. Performance Comparison of Pressure Hydrated Lime and Dolomitic Stone.

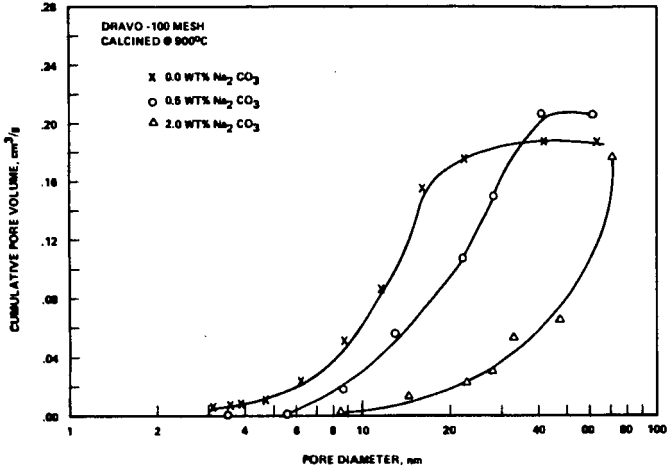


Figure 7. Effect of Na<sub>2</sub>CO<sub>3</sub> Additive on Calcine Pore Distribution.

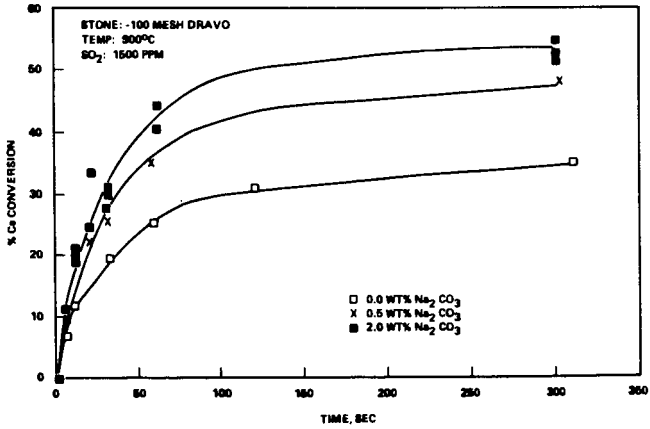


Figure 8. Sulfation Enhancement by Na<sub>2</sub>CO<sub>3</sub> Additive.

## SULFUR DIOXIDE SORPTION REACTIVITY OF HYDRATED LIME: EFFECT OF HYDRATION METHOD

D. L. Moran, M. Rostam-Abadi, R. D. Harvey, and R. R. Frost  
Illinois State Geological Survey, Champaign, Illinois 61820

and

G. C. Sresty  
Illinois Institute of Technology Research Institute

### INTRODUCTION

The Furnace Sorbent Injection (FSI) process is a relatively low capital cost technology for control of SO<sub>2</sub> emissions produced during combustion of high sulfur coal. A major factor in the total cost of the FSI concept is the effective utilization of the sorbent. In pilot plant tests performed by previous investigators, calcium utilization efficiencies (at Ca/S feed ratio of 2:1) ranged from 15 to 20% for limestone, 25 to 30% for dolomitic limestone, 20 to 30% for hydrated lime, and 35 to 40% for pressure-hydrated dolomitic lime (1,2,3,4). The low calcium utilizations observed in these and many other studies have motivated researchers to develop methods of producing more reactive calcium-based sorbents with the goal of reducing SO<sub>2</sub> removal costs.

The hydration method has received considerable attention in recent years because it appears to be the least expensive method of producing fine (<10 micrometer) lime particles with high surface area. Particles of this size range are more reactive than larger particles because they lack significant resistance to pore diffusion. Recent hydration studies have focused on developing sorbents with higher surface areas than those of commercial hydrates. In laboratory-scale hydrators, under controlled processing conditions, hydroxides having surface areas ranging from 42 to 50 m<sup>2</sup>/g (2 to 3 times greater than those of commercial hydrates) have been produced (4,5,6,7). Materials with surface areas up to 45 m<sup>2</sup>/g have been produced by hydration with methanol-water solutions (7,8).

The objective of this investigation was to produce hydrated lime with high surface area. Three hydration methods were studied: 1) lime was hydrated with water or alcohol-water solutions, 2) lime was reacted with water at pressures and temperatures up to and exceeding supercritical conditions and the hydrated lime produced was ejected to atmospheric conditions, 3) lime was hydrated with steam. Sulfur dioxide sorption capacities were obtained by thermogravimetry and surface areas were determined by the BET (N<sub>2</sub>) technique.

### EXPERIMENTAL

#### Materials

Two different limestones were calcined for the experiments (table 1). Both consisted of more than 95% CaCO<sub>3</sub> (calcite). Limestone A is characterized as coarse grained and low specific gravity and limestone B as fine grained and somewhat higher specific gravity.

#### Calcination

The limestones were calcined in a 2.5-cm I.D. batch fluidized bed reactor constructed from a type 316 stainless steel pipe. Twenty to fifty grams of limestone (100-150 micrometer particles) were heated at a rate of 20°C/min to 850°C. The sample was held at this temperature for 30 minutes to assure complete conversion of carbonate to lime. Nitrogen was the fluidizing gas flowing at a rate of 1000 cc/min (STP).

### Hydration

A 500 ml, three-neck flask was used to hydrate the lime at atmospheric pressure with water or alcohol-water mixtures. Two methods were used: 1) dry hydration (twice stoichiometric water or less) and 2) wet hydration (five times stoichiometric water or more). The hydrate was prepared by adding hydrating solution to one gram of lime while stirring the mixture. The temperature of the mixture increased from ambient to between 50 and 90°C due to the exothermic nature of the hydration reaction. Some of the hydrating solution boiled off during dry hydration runs as a result of localized overheating. The reaction was assumed to be complete after the sample had cooled to room temperature. The hydrated lime product was dried under vacuum and gently crushed for one to two minutes to break up loosely agglomerated particles. Some of the products were filtered and washed with 3 to 25 ml of alcohol prior to vacuum drying. The products were stored in vials under nitrogen to avoid recarbonation.

Pressure-hydrated lime was prepared at the Illinois Institute of Technology Research Institute in a batch reactor constructed of 1.3-cm I.D. stainless steel pipe. The reactor consisted of two sections separated by a metal disk that was designed to rupture at a specific pressure. The upper portion of the reactor (6.4 cm) was charged with one gram of lime and three to four grams of water, capped, and quickly heated using a torch. During the heating period (4 to 5 minutes), the pressure and temperature of the reactor simultaneously increased until the disk ruptured. During this rupturing period (on the order of milliseconds) the reactor pressure dropped to one atmosphere. The pressure-hydrated lime slurry was collected in the lower portion of the reactor (30 cm). The product was vacuum-dried prior to testing for sulfation reactivity.

Lime was hydrated with steam at 200°C for 30 to 60 minutes in a thermogravimetric analyzer system. The partial pressure of steam in the reactor was 0.13 atmospheres. The hydration was assumed to be complete when no further increase in weight was observed. The product was then heated in nitrogen at 20°C/min to 850°C and was tested for sulfation reactivity.

### SO<sub>2</sub> reactivity

Reactivity data were obtained by Thermogravimetry (TG) using a Cahn RG balance. The sample holder (1-cm diameter and 0.5-cm height) was constructed of 100 mesh platinum gauze and was suspended from the microbalance by a platinum wire (0.01-cm diameter). The reaction temperature was measured by a Pt/Pt-13% Rh thermocouple located 5 mm below the sample holder. The reactant gas was passed upward through the reactor tube (3.2-cm I.D.). The lower portion of the reactor (10 cm) was filled with 0.64-cm ceramic raschig rings which served as a gas mixing and pre-heating zone and as a gas distributor. The system was interfaced with an IBM-PC to provide automated collection and storage of the microbalance and thermocouple outputs.

In a typical run, sample particles were dispersed in layers of quartz wool located in the sample holder. The sample was heated in nitrogen at a rate of 20°C/min to 850°C. The reaction gas containing 0.5% SO<sub>2</sub>, 5% O<sub>2</sub>, 20% CO<sub>2</sub>, and balance N<sub>2</sub> (which simulated the flue gas from combustion of a high sulfur coal) was introduced to the reactor and the increase in weight due to sulfation and the reaction temperature were recorded at 10 second intervals for 60 minutes. Results of preliminary experiments revealed that sulfation rates were not affected when sample weights of less than 10 mg and gas flow rates between 300 and 900 cc/min (STP) were used. Sample weights of 8 mg and flow rates of 300 cc/min were used in subsequent experiments.

## RESULTS AND DISCUSSION

### Physical characteristics of hydrates

Hydrated lime products were examined under a light microscope. Dry-hydrated (atmospheric) lime and a commercial pressure-hydrated lime prepared from limestone B consisted of particles which were predominantly less than 10 micrometers in diameter. However, some 10 to 50 micrometer particles were present in the atmospheric hydrate. Reduction in particle size (mmd=2 to 4 micrometers) is achieved in commercial pressure hydration processes due to the ejection of the products through an orifice (9). The surface area, BET ( $N_2$ ), of the pressure-hydrated lime was 17.2  $m^2/g$  compared to 34.3  $m^2/g$  for the atmospheric product (table 2).

Wet hydration produced agglomerated particles with clusters as large as 0.5 cm. The agglomerates were easily reduced in size by gently crushing with a spatula. However, several large particles were observed in the samples even after crushing. Examination of lime A hydrated with twenty times stoichiometric water followed by vacuum-drying and mild crushing showed that particles were predominantly less than 20 micrometers in diameter, although some as large as 150 micrometers were also present.

Hydration with methanol-water solutions generally produced hydroxides with particles that were finer and more uniform than those prepared with water alone. Few particles greater than 20 microns were observed in these samples. Depending on the amount of methanol used, surface areas ranging from 43 to 70  $m^2/g$  were obtained (table 3). Comparable surface areas were obtained for products hydrated with ethanol-water solutions. These values show improvement over surface areas of hydrates prepared in water alone and are three to five times greater than those of commercially available hydrates.

### SO<sub>2</sub> reactivity

As described earlier, the hydrated samples were heated in nitrogen to 850°C prior to sulfation. A weight loss of 21-23% was observed between 350 and 500°C due to the dehydration reaction. The theoretical weight loss for the dehydration of pure calcium hydroxide is 24%. The samples lost an additional 1-3% weight between 500 and 700°C. This weight loss was attributed to the calcination of any residual carbonate material in the sample.

The progressive increase in weight during sulfation was attributed to the reaction of the calcined product with oxygen and sulfur dioxide according to:



X-ray diffraction analyses of samples exposed to the reaction gas mixture confirmed that calcium sulfate was the sole product formed. The following relationship was used to calculate the percent conversion (calcium utilization) of the sorbent as a function of reaction time:

$$\text{Percent conversion} = X_t = \frac{W_t - W_0}{Y W_0} \frac{M_{CaO}}{M_{SO_3}} \times 100 \quad 2)$$

where:  $W_t$  = weight of sorbent at time  $t$   
 $W_0$  = initial weight of sorbent at 850°C  
 $Y$  = weight fraction of calcium oxide in sample at 850°C  
 $M_{CaO}$  = molecular weight of calcium oxide  
 $M_{SO_3}$  = molecular weight of sulfur trioxide

Reactivity curves were obtained by plotting  $X_t$  against sulfation time.

### Hydration with water

The sorption capacities of hydrates prepared at atmospheric pressure depended on the method of hydration (dry or wet) and the parent limestone (figure 1). The surface areas of the dry and wet hydrates produced from lime A were 37 and 46 m<sup>2</sup>/g compared to the value of 13 m<sup>2</sup>/g for the starting lime (100x150 micrometers). The calcium utilizations of these samples were 59, 69 and 37%, respectively. No improvement in utilization was achieved for samples hydrated with five times stoichiometric water or more. Dry and wet hydrates produced from lime B had surface areas which were similar to those obtained for hydrates prepared from lime A (table 2). However, hydrates prepared from lime B had calcium utilizations exceeding 90%.

The results of a recent study showed that calcination conditions, i.e. temperature and sintering time, were not important in producing hydroxides with high surface areas (6). The effect of calcination atmosphere was not investigated in that study. A sample was prepared by calcination of limestone A in one atmosphere carbon dioxide followed by hydration with twenty times stoichiometric water. This treatment increased the utilization of wet hydrate to 78% (vs 69% for hydrate produced from limestone calcined in nitrogen). The sorbent surface area was 33 m<sup>2</sup>/g, surprisingly lower than that of the hydrate produced from lime prepared in nitrogen atmosphere (46 m<sup>2</sup>/g).

Sulfation data for the -325 mesh (<45 micrometers) and 100x150 micrometer limes are also shown in figure 1 for comparison. These samples were calcined in the TGA system prior to sulfation. It is interesting to note that although hydrates made from limestone B were more reactive than those made from limestone A, the -325 mesh calcine of the latter (surface area of 20 m<sup>2</sup>/g) was more reactive than that of the former. Little difference in reactivity was observed for the 100x150 micrometer particles.

### Hydration with methanol-water solution

Hydration of lime with alcohol-water solution was tested because a previous study had shown that this method of hydration produced samples with surface areas as high as 50 m<sup>2</sup>/g (10). Alcohol affects the solubility and interfacial tension of hydrates in water and acts as a dispersing agent, thus minimizing particle agglomeration. The reactivity data for lime B hydrated with a 50% methanol-water solution and washed with ten grams of methanol are shown in figure 1. This sample had a sulfation capacity which was greater than that of the commercially prepared pressure-hydrated lime. A sorption capacity of 100% was observed for this sample as compared to 95% for the commercial hydrate. High calcium utilizations were also observed for samples prepared by hydration of lime A with methanol or ethanol-water solutions (see table 3). This indicates that costs associated with pressure hydration can be eliminated by hydration with methanol-water solution at atmospheric pressure.

Limestone A was subjected to a more extensive study on this method of hydration. The objective was to evaluate the effects of the concentration of alcohol in the hydrating solution and the amount of alcohol used in the post-hydration washing step on the reactivity of the products. The hydration conditions, calcium utilizations and surface areas of the hydrates are summarized in table 3. Reactivity data are shown in figure 2. Increasing the concentration of methanol in the hydrating solution and the amount used in the post-hydration wash resulted in increased calcium utilizations. This is clearly shown in figure 3 where the calcium conversions after 60 minutes are plotted as a function of methanol concentration.

The relationship between the surface area and calcium utilization for the hydrates prepared in methanol-water solution is shown in figure 4. BET (N<sub>2</sub>) surface areas of hydrates (prior to dehydration) correlated well with ultimate sorption capacities.

#### Pressure hydration

The sulfation data for the pressure-hydrated products (Lime A) are shown in figure 5. The calcium conversion of the product prepared at 475 atmospheres and 480°C was 76%. The surface area of this sorbent was 15.4 m<sup>2</sup>/g. A conversion of 91% was achieved for the sample prepared at 120 atmospheres and 290°C. The reason for the higher capacity observed for this sample is not known. Although the sulfation capacities of the products prepared under pressure were higher than those of the wet hydrates, their surface areas were lower (see table 2).

#### Steam hydration

The reactivity of the steam-hydrated lime A is also shown in figure 5. A calcium utilization of 68 % was observed for the hydrated sorbent. This is comparable to the utilization observed for the lime hydrated with water (wet method) at atmospheric pressure. Calcination of limestone under a carbon dioxide atmosphere prior to steam hydration did not influence the reactivity of the sorbent.

### CONCLUSIONS

Hydration of lime with alcohol-water solution (ethanol or methanol) at atmospheric pressure produced sorbents with surface areas as high as 75 m<sup>2</sup>/g. The hydrates had sulfur dioxide sorption capacities equal to or greater than those of commercially prepared pressure-hydrated limes. Calcium utilization depended on the parent limestone, the concentration of alcohol in the hydrating solution and the amount of alcohol used during the post-hydration step. A linear relationship was obtained between calcium utilization and BET (N<sub>2</sub>) surface area. Reactivities of the samples tested showed the following trend:

Ethanol-water hydration = methanol-water hydration > pressure hydration > steam hydration = hydration with water > lime

Finally, it should be noted that the calcium utilizations were obtained at 850°C for sulfation times of 60 minutes. For practical application of results, reactivity data should be evaluated under conditions representative of coal-fired boilers, i.e. high temperature, short residence time.

### ACKNOWLEDGEMENTS

We gratefully acknowledge the Illinois Coal Industry Committee and the Center for Research on Sulfur in Coal for their financial support of this project.

### REFERENCES

1. Attig, R. C., and Sedor, P., Additive Injection for Sulfur Dioxide Control: EPA report APTD 1176 (NTIS PB 226-761) March, 1970.
2. Beittel, R., Gooch, J. P., Dismukes, E. B., and Muzio, L. J., Studies of Sorbent Calcination and SO<sub>2</sub>-Sorbent Reactions in a Pilot-Scale Furnace. Proceedings: First Joint Symposium on Dry SO<sub>2</sub> and Simultaneous SO<sub>2</sub>/NO<sub>x</sub> Control Technologies, Volume 1, p. 16-1, July, 1985.
3. Payne, R., and Abele, A. R., Evaluation of Low-NO<sub>x</sub> Burners for SO<sub>2</sub> Control. Proceedings: First Joint Symposium on Dry SO<sub>2</sub> and Simultaneous SO<sub>2</sub>/NO<sub>x</sub> Control Technologies, Volume 1, p. 21-1, July, 1985.

4. McCarthy, J. M., Chen, S. L., Kramlich, J. C., Seeker, W. R., and Pershing, D. W., Reactivity of Atmospheric and Pressure Hydrated Sorbents for SO<sub>2</sub> Control. Proceedings: 1986 Joint Symposium on Dry SO<sub>2</sub> and Simultaneous SO<sub>2</sub>/NO<sub>x</sub> Control Technologies, Volume 1, p. 10-1, December, 1986.
5. Yoon, H., Stouffer, M. R., Rosenhoover, W. A., and Statnick, R. M., Laboratory and Field Development of Coolside SO<sub>2</sub> Abatement Technology. Proceedings of the Second Pittsburg Coal Conference, U. S. DOE, Pittsburgh, PA, p.223, 1985.
6. Borgwardt, R. H., and Bruce, K. R., EPA Study of Hydroxide Reactivity in a Differential Reactor. Proceedings: 1986 Joint Symposium on Dry SO<sub>2</sub> and Simultaneous SO<sub>2</sub>/NO<sub>x</sub> Control Technologies, Volume 1, p. 15-1, December, 1986.
7. Gooch, J. P., Dismukes, E.B., Beittel, R., Thompson, J. L., and Rakes, S. L., Sorbent Development and Production Studies. Proceedings: 1986 Joint Symposium on Dry SO<sub>2</sub> and Simultaneous SO<sub>2</sub>/NO<sub>x</sub> Control Technologies, Volume 1, p. 11-1, December, 1986.
8. Muzio, L. J., Offen, G. R., Boni, A. A., and Beittel, R., The Effectiveness of Additives for Enhancing SO<sub>2</sub> Removal with Calcium Based Sorbents. Proceedings: 1986 Joint Symposium on Dry SO<sub>2</sub> and Simultaneous SO<sub>2</sub>/NO<sub>x</sub> Control Technologies, Volume 1, p. 13-1, December, 1986.
9. Weber, G. F., Schelkoph, G. L., and Ness, H. M., Pilot Scale Studies of Simultaneous Control of SO<sub>x</sub>/NO<sub>x</sub> Emissions Derived from the Combustion of Low-Rank Coal. Proceedings: 1st Annual Pittsburgh Coal Conference, p.241, Sept, 1984.
10. Staley, H., Micrometrics of Lime, Research Report to National Lime Association, 1946.

Table 1. Characterization of limestones \*

Sample ID Location	Geologic unit Grain-size	Spec. grav.	CaO	MgO	CO <sub>2</sub>	Al <sub>2</sub> O <sub>3</sub>	Fe <sub>2</sub> O <sub>3</sub>	SiO <sub>2</sub>	Na <sub>2</sub> O
Limestone A Western Ill.	Burlington Ls. Coarse	2.61	53.8	0.3	42.6	0.1	tr <sup>+</sup>	1.1	0.02
Limestone B Upper Mich.	Fiborn Ls. Fine	2.64	54.3	0.9	43.8	0.2	0.2	0.7	nil

\* Analyses in weight percent.

+ trace

Table 2. Summary of sulfation data of hydrates

Limestone	Particle size <sup>a</sup> (mesh)	Calcination atmosphere	Hydration method	Calcium conversion <sup>b</sup> %	Surface area (m <sup>2</sup> /g)
B <sup>c</sup>	-100	---	---	95	17.2
A	100x150	N <sub>2</sub>	steam	68	---
A	100x150	N <sub>2</sub>	475 atm	76	15.4
A	100x150	N <sub>2</sub>	120 atm	91	21.4
A	-325	N <sub>2</sub>	none	85	20.7
B	-325	N <sub>2</sub>	none	75	---
B	100x150	N <sub>2</sub>	dry	93	34.3
A	100x150	N <sub>2</sub>	dry	59	37.4
A	100x150	N <sub>2</sub>	wet (20xstoich)	67	47.3
B	100x150	N <sub>2</sub>	wet (20xstoich)	94	49.0
A	100x150	N <sub>2</sub>	none	37	12.9
A	100x150	N <sub>2</sub>	wet (5xstoich)	69	46.1
A	100x150	CO <sub>2</sub>	wet (20xstoich)	78	33.3
A	100x150	CO <sub>2</sub>	steam	68	10.5
B	100x150	N <sub>2</sub>	none	33	---

<sup>a</sup>particle size prior to hydration step

<sup>b</sup>after 60 minutes

<sup>c</sup>commercial hydrate

Table 3. Summary of sulfation data of alcohol-water hydrates<sup>a, b</sup>

TG No.	Hydration method	Concentration of alcohol in solution weight %	Amount of alcohol wash gm/gm lime	Calcium conversion <sup>c</sup> %	Surface area (m <sup>2</sup> /g)
91	dry (2xstoich)	0	0	59	37.4
92	dry (2xstoich)	10	0	67	43.5
98	dry (2xstoich)	50	0	79	64.3
106	wet (5xstoich)	0	0	69	46.1
104	wet (5xstoich)	0	7	79	49.1
105	wet (5xstoich)	30	0	79	44.7
96	wet (5xstoich)	30	3	86	66.4
100	wet (5xstoich)	30	7	93	70.1
95	wet (20xstoich)	0	0	67	47.3
93	wet (15xstoich)	14	10	94	59.4
97	wet (10xstoich)	10	3	78	53.9
89	wet (10xstoich)	50	25	96	63.7
90	wet (10xstoich)	50	25	94	75.3
108	wet (10xstoich)	50	10	100	---

<sup>a</sup>hydrates were produced from lime A except TG 108 which was prepared from Lime B

<sup>b</sup>methanol was used for alcohol-water hydration tests except for TG 90 ethanol was used

<sup>c</sup>after 60 minutes

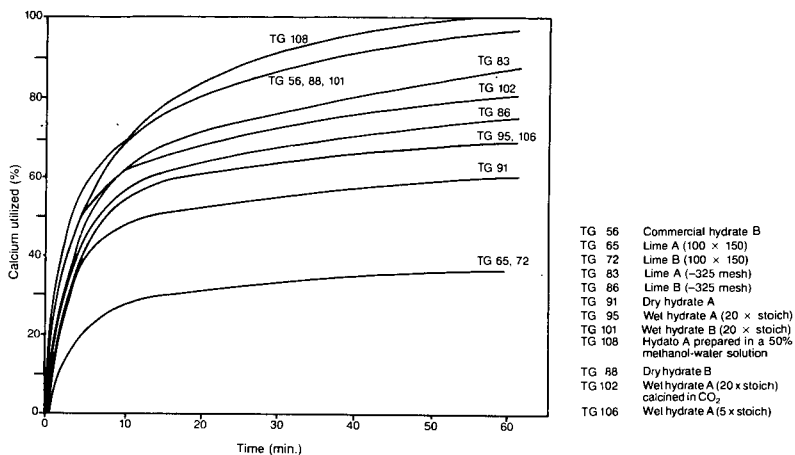


Figure 1. The effects of hydration method, parent limestone, and calcination atmosphere on the reactivity of hydrates.

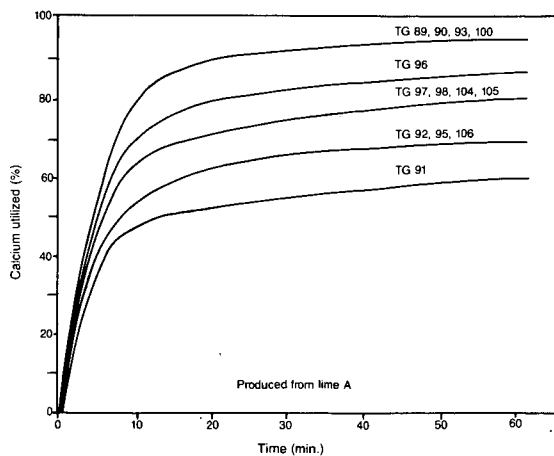


Figure 2. Sulfation reactivities of alcohol-water hydrates.

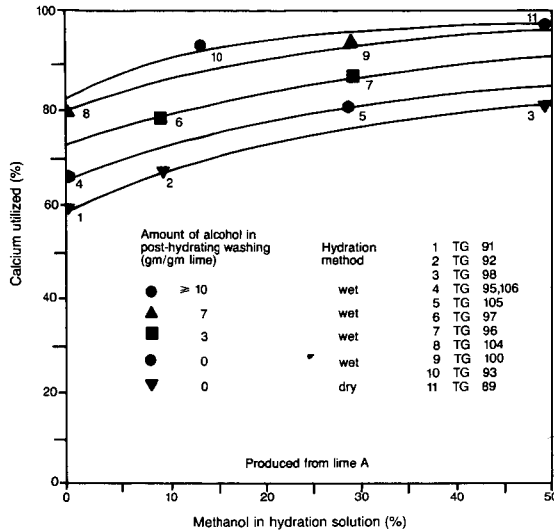


Figure 3. The influence of methanol on hydrated products.

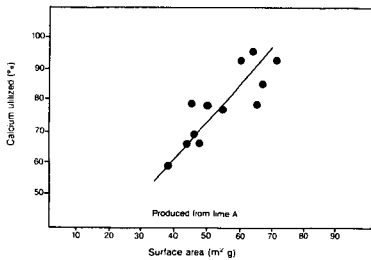


Figure 4. Relationship between calcium utilization and surface area for methanol-water hydrates.

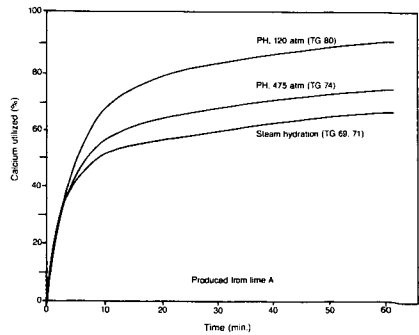


Figure 5. Sulfation reactivities of samples prepared by steam and pressure hydration (PH) methods.

REACTION OF ACID GASES WITH SOLID ALKALI FLOWING IN A DUCT:  
SO<sub>2</sub> REACTION WITH LIME

BRUCE WEINSTEIN

RESEARCH COTTRELL INC.  
ROUTE 22 WEST  
BRANCHBURG, NJ 08876

ABSTRACT

Many new flue gas desulfurization processes are being developed where an acid gas and alkali are reacted cocurrently in a duct. Solutions to the material balance equations for cocurrent flow processes have been solved for the cases when the conversion is limited by gas phase diffusion, reaction kinetics, or diffusion through the product layer. The solutions are presented in a graphical form and can be used to determine the residence time required to achieve a specified conversion of the gaseous component providing the appropriate rate constant is known. The curves can also be used to determine a rate controlling step from conversion versus time data taken in an isothermal flow reactor. This method is applied to the application of the high temperature reaction of lime with SO<sub>2</sub> for conditions that would occur in the duct downstream of a direct coal fired heat engine combustor.

INTRODUCTION

Low capital cost flue gas desulfurization processes are being developed to address the potential market for retrofit systems on existing boilers burning medium to high sulfur coal. Many of these new systems involve the injection of a dry solid of calcium or sodium alkali in the duct to react with the SO<sub>2</sub> in the flue gas. Calcium alkali tend to be the preferred reagents compared to those of sodium because of the availability and lower cost.

The stoichiometry ratio of moles of calcium fed to the moles of SO<sub>2</sub> is often in the range of 2 to 3 for the in-duct processes. Attempts to improve the utilization of reagent have stressed the need for small particles of high BET surface area and porosity. Calcium hydroxide, commercially produced, with those properties has achieved the highest utilizations compared to other calcium alkali.

Injection processes may also be feasible for removing SO<sub>2</sub> from flue gas produced by a direct coal fired heat engine combustor. In this application the gas is expected to be at a high temperature and pressure. This paper presents estimates of the reaction time required for a variety of operating conditions where the reagent is calcium hydroxide.

PREVIOUS WORK

Borgwardt, et al.(2) have shown that the utilization of calcium oxide particles with a BET surface area of 32 m<sup>2</sup>/g reacting with COS at 5000 ppm at 700°C is independent over a particle size range of 1 to 9.4 microns. They concluded that the reaction occurs equally throughout the particle and that pore diffusion resistance must be insignificant.

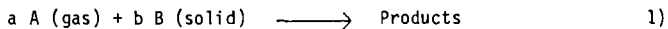
In a later study Borgwardt and Bruce (1) measured the conversion of 1 micron calcium oxide particles by reaction with SO<sub>2</sub> at a concentration of 3000 ppm in a differential reactor over a temperature range of 760 to 1125°C. The primary

resistance to  $SO_2$  absorption was ionic diffusion thru the product layer. A conventional grain model accurately correlated the data when the concentration of the diffusing ion was computed to be proportional to the gas concentration to the 0.62 power.

Bortz, et al.(3) has studied the reaction of small particles of calcium hydroxide at temperatures of 450 to 600°C which are typical of economizers on utility boilers. These tests were done in an isothermal flow reactor. With particles in the range of 1 to 5 microns with BET surface areas greater than 20  $m^2/gm$ , the absorption of  $SO_2$  was dependent on the gas phase mass transfer rates of  $SO_2$  relative to the kinetic rate of  $CO_2$  with the hydroxide. Pore diffusion resistance was negligible.

#### THEORY

A generalized reaction of a single gas A reacting irreversible with solid B is given by Equation 1 where a and b are the stoichiometric coefficients.



When the reaction rate is controlled by diffusion of the gaseous reactant thru the inert layer of product formed over the unreacted core of solid reagent, the radius of the unreacted core, r, at any time is given by (4):

$$-\rho \frac{r^2 dr}{M} \left( \frac{1}{r} - \frac{1}{R} \right) = D_d C_A (b/a) dt \quad 2)$$

Following the approach used by Borgwardt and Bruce (1) the initial grain radius of the solid, R, is related to the BET area by:

$$R = 3/(S_a \rho) = 3/(10^4 S_g \rho) \quad 3)$$

By expressing the moles of solid reactant remaining at any time per mole of gas reactant at the inlet to the fraction of reactant A remaining the partial pressure of reactant A can be expressed as:

$$P_A = P_{Ain} \left[ \frac{F_a}{b} \left( \frac{r}{R} \right)^3 + 1 - \frac{F_a}{b} \right] = P_{Ain} \left[ S \left( \frac{r}{R} \right)^3 + 1 - S \right] \quad 4)$$

where F is the moles of solid reactant B fed/moles of gas reactant A.

The fraction removal efficiency is related to the partial pressure of reactant A by:

$$1-E = P_A/P_{Ain} \quad 5)$$

Combining Equations 4 and 5 gives the grain radius at any time in terms of the fractional removal efficiency:

$$(r/R) = \left[ 1 - (E/S) \right]^{1/3} \quad 6)$$

The concentration term  $C_A$  in Equation 2 is that of the specie that diffuses thru the product layer. Borgwardt and Bruce (1) expressed the concentration in terms of the partial pressure of the gas as:

$$C_A = k_o P_A^m \quad 7)$$

Substitution of Equation 4 into Equation 7, and then substitution of the result into Equation 1 and integrating from the initial condition  $r/R$  equal 1.0 at time zero gives:

$$I_d = \int_1^{xf} \frac{(x^2 - x)dx}{[Sx^3 + 1 - S]^m} = k_g dt \quad 8)$$

where  $x$  is set equal to  $r/R$  and  $k_d$  is the lumped constant:

$$k_d = (k_o D_d M b) / (\rho R^2 a) P_{Ain}^m = 10^8 k_o D_d M S g^2 \rho (b/a) P_{Ain}^m / 9 \quad 9)$$

Assuming  $m$  is fixed the value of the integral is determined for any specified feed ratio and final fractional conversion efficiency. The upper limit on the integral is found from Equation 6. Analytical solutions for the integral for all real value of  $m$  when  $S$  equals 1.0 and for all values of  $S$  when  $m$  equals 1.0 are listed in Table 1.

When the conversion of reactant A is controlled by a first order reaction with respect to A at the surface of the unreacted core, the radius of the unreacted core is given by (4):

$$-\frac{\rho}{M} \frac{dr}{dt} = k_r C_A (b/a) \quad 10)$$

By utilizing Equations 3 to 7 in an analogous manner, with  $m$  set equal to 1.0 the Equation 10 can be expressed as:

$$I_c = - \int_1^{xf} \frac{dx}{Sx^3 + 1 - S} = k_r dt \quad 11)$$

where  $k_c$  is:

$$k_c = 10^4 k_r k_o M S g (b/a) P_{Ain} / 3 \quad 12)$$

The analytical solution of the integral in Equation 11 is given in Table 1.

If the conversion of reactant A is controlled by diffusion from the bulk gas to the outer surface of the grain, the radius of the unreacted core is given by (4):

$$\frac{\rho}{M} \left( \frac{r}{R} \right)^2 \frac{dr}{dt} = k_G C_A (b/a) \quad 13)$$

With  $m$  equal to 1.0, Equation 13 can be expressed as:

$$I_g = - \int_1^{xf} \frac{x^2 dx}{Sx^3 + 1 - S} = k_g dt \quad 14)$$

where  $k_g$  is:

$$k_g = 10^4 k_G k_o P_{Ain} M (b/a) S g / 3 \quad 15)$$

The analytical solution of the integral is given in Table 1.

The values of the integrals given by Equations 8 for  $m=1$  and Equations 11 and 14 are plotted on Figures 1, 2, and 3, respectively. These relationships do not account for expansion or contraction of the outer radius of the grain from the differences in the molar volumes of the reactant and product.

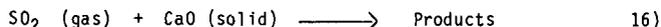
## APPLICATION OF THE GRAPHICAL SOLUTIONS

With conversion versus time data taken in a flow reactor the graphical solutions provide a rapid method of determining if the conversion is controlled by one of the three assumed mechanisms. For the known value of  $S$  and measured value of  $E$ , a value of  $I$  is read from each curve and divided by the residence time to get values for the constants  $k_d$ ,  $k_c$ , and  $k_g$ . This process is repeated for each set of data taken. If the lumped parameter for any one of the mechanisms is constant then that mechanism is applicable to the process. If some test runs used different initial gas concentrations that effect can be isolated from the computed constants.

For a known reaction system where one of the three assumed mechanisms is applicable and if the rate constant is also known then the graphical solution can be used to compute the residence time in a flow reactor. For example, assume a reaction is controlled by diffusion of the gas thru the product layer, so that  $m$  is 1.0, the BET area is known, and the diffusion coefficient had been determined from a data on a differential reactor. The lumped parameter  $k_d$  can be computed from Equation 9. Figure 1 would then be used to read a value of the integral for any values of  $S$  and  $E$  selected. The required residence time can be easily computed for each case by dividing the value of the integral by the lumped constant.

## SO<sub>2</sub> REACTION WITH LIME AT HIGH TEMPERATURE

If calcium hydroxide is injected into a hot flue gas where the temperature exceeds 700°C dehydration of the particle occurs very rapidly. The calcium oxide that forms is a small particle with about 50 % porosity and a high surface area. For this application the grain model should be applicable. The reaction of the SO<sub>2</sub> with the lime at these conditions produces calcium sulfate, and can be expressed as:



For this reaction  $a$  and  $b$  are both 1.0.

One such commercial application may be in the removal of SO<sub>2</sub> from the combustion gas from a direct coal fired turbine operating at temperatures in the range of 950 to 1200°C at pressures of 1013 to 1520 kPa (10 to 15 atm). By removing the SO<sub>2</sub> at the high pressure the volume of the gas being treated is much less than downstream of the turbine. The feasibility of using calcium hydroxide injection upstream of the turbine to remove the SO<sub>2</sub> depends on the reaction time required.

The data of Borgwardt and Bruce (1) can be used in conjunction with Equation 8 to estimate the residence time. They concluded the conversion of lime at these temperatures is controlled by ionic diffusion thru the product layer, where  $m$  is 0.62 and the diffusion coefficient in Equation 9 is expressed as:

$$D_d = D_o * \exp(-E'/RT) \quad (17)$$

where  $E'$  in Equation 17 is the activation energy of 36,600 kcal/mol and  $T$  is the temperature in °K. Substitution of Equation 17 into Equation 9 yields:

$$k_d = (10^8 M k_o D_o \rho / 9) (S_g^2 P_{SO_2 in}^{.62} \exp(-E'/RT)) \quad (18)$$

Borgwardt and Bruce correlated  $k_d$  by:

$$k_d = (10^8 M k_o D_o \rho / 9) (6 S_g^2 P_{SO_2 in}^{.62}) * \exp(-E'/RT) = 2.65 S_g^2 P_{SO_2 in}^{.62} \exp(-E'/RT) \quad (19)$$

Equating the second and third terms in Equation 19 gives:

$$10^8 * M * k_0 * D_0 * / 9 = 2.65/6 = 0.4417 \quad 20)$$

Equation 18 can now be written as:

$$k_d = 0.442 * S_g^2 P_{SO_2 in}^{.62} * \exp(-36,600/RT) \quad 21)$$

Since  $m$  equals 0.62, Equation 8 must be solved numerically except when  $S$  equals 1.0. The values for the integral are given in Figure 4. To compute the conversion time, the temperature, feed ratio, inlet  $SO_2$  concentration and operating pressure must be specified. The inlet partial pressure of  $SO_2$  is then computed and Equation 19 is used to compute  $k_d$ . For the specified fractional removal efficiency a value of  $I_d$  is read from Figure 4 and divided by  $k_d$  to obtain the reaction time. Table 2 summarizes calculations for the reaction time when the operating pressure is set at 1520 kPa (15 atm). At the higher temperature a lower BET area was assumed to account for sintering.

#### CONCLUSIONS

For dry injection FGD processes utilizing small particles of calcium hydroxide or calcium oxide a grain model can be used to represent the reagent utilization.

The reaction time required for the high temperature, high pressure conversion of  $SO_2$  with small lime particles can be predicted with a modified grain model that accounts for the changing  $SO_2$  partial pressure when the rate controlling step is diffusion thru the product layer.

## NOMENCLATURE

A	- gaseous reactant
a	- stoichiometric coefficient for gas A
B	- solid reactant
b	- stoichiometric coefficient for solid reactant B
C	- concentration of diffusing specie, gmol/cm
D <sub>d</sub>	- diffusion coefficient in product layer, cm /sec
D <sub>0</sub>	- Arrhenius pre-exponential factor
E	- fraction conversion efficiency of gaseous reactant
E'	- apparent activation energy taken as 36,600 cal/gmol
F	- moles of reactant solid fed/mole of gas reactant fed
I <sub>C</sub>	- integral defined by Equation 11
I <sub>d</sub>	- integral defined by Equation 8
I <sub>g</sub>	- integral defined by Equation 14
k	- $((1-S)/S)^{1/3}$
k <sub>C</sub>	- constant defined by Equation 12
k <sub>d</sub>	- constant defined by Equation 9
k <sub>g</sub>	- constant defined by Equation 15
k <sub>G</sub>	- gas phase coefficient in Equation 13, cm/sec
k <sub>0</sub>	- constant defined by Equation 7
k <sub>r</sub>	- reaction rate constant in Equation 10, cm/sec
M	- molecular weight of reactant solid
m	- constant defined by Equation 7
P <sub>A</sub>	- partial pressure of gas A, Pa
P <sub>Ain</sub>	- partial pressure of gas A at inlet conditions, Pa
P <sub>SO<sub>2</sub></sub>	- partial pressure of SO <sub>2</sub> , Pa
P <sub>SO<sub>2</sub>in</sub>	- partial pressure of SO <sub>2</sub> at inlet conditions, Pa
R	- initial grain radius defined by Equation 3, cm; the gas constant in Equations 17, 18, 19 and 20, 1.987 cal/gmol- K
S	- $Fa/b$
S <sub>a</sub>	- BET area of solid, cm <sup>2</sup> /g
S <sub>g</sub>	- BET area of solid, m <sup>2</sup> /g
T	- temperature, °K
t	- time, sec
x	- r/R where R is the initial grain radius
x <sub>f</sub>	- r/R at the end of the reaction time
∫	- mass per unit volume of grain, g/cm <sup>3</sup>

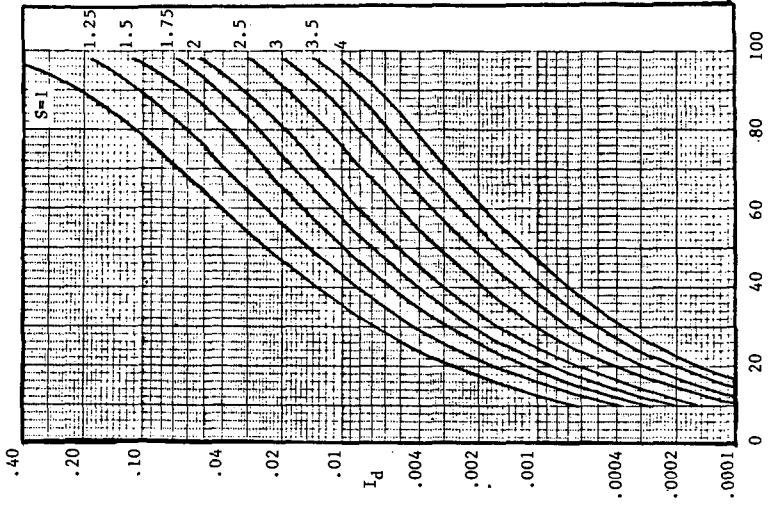
## LITERATURE CITED

1. Borgwardt, R.H., and Bruce, K.R., AIChEJ. 1986 32, 239.
2. Borgwardt, R.H., Roache, N.R., and Bruce, K.R., Environ. Prog. 1984a, 3, 129.
3. Bortz, S., Roman V. P., Yang, R. J., and Offen, G. R., EPA/EPRI Dry SO<sub>2</sub> and Simultaneous SO<sub>2</sub>/NO<sub>x</sub> Control Technology, 1986, Paper 6C, Raleigh, NC.
4. Levenspiel, O. "Chemical Reacting Engineering", Wiley, New York, NY, 1062.

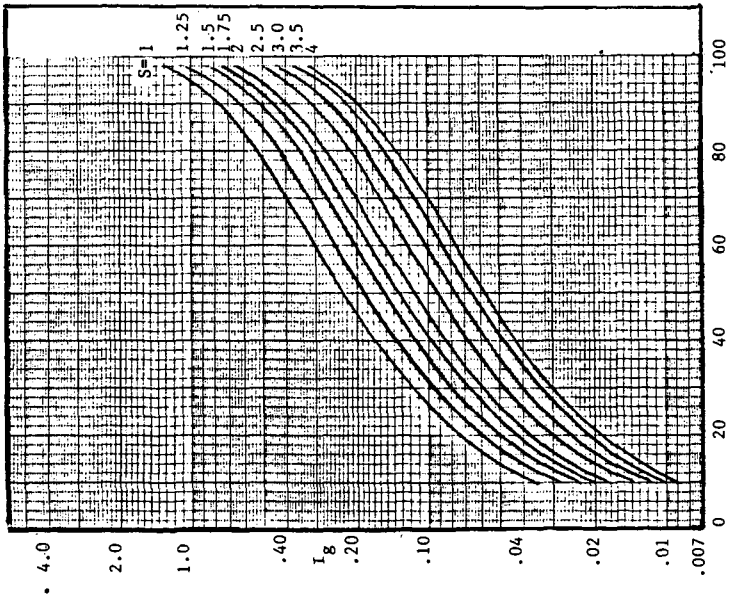
TABLE 1: ANALYTICAL SOLUTIONS TO THE INTEGRALS IN EQUATIONS 8, 11 AND 14	
m = 1, S ≠ 1	
$I_d = \frac{1}{3S} \ln(Sx_f^3 + 1 - S) - \frac{1}{6Sk} \ln \left[ \left( \frac{k + x_f}{k + 1} \right)^3 (Sx_f^3 + 1 - S) \right] - \frac{1}{3 \cdot 5 S k} \left[ \tan^{-1} \left( \frac{2-k}{k-3} \right) - \tan^{-1} \frac{2x_f - k}{k-3} \right]$	
S = 1, m ≠ 1:	$I_d = \frac{1}{S} \left[ \frac{x_f^{3(1-m)} - 1}{3(1-m)} - \frac{x_f^{2-3m} - 1}{2-3m} \right]$
S = 1, m = 1:	$I_d = \ln(x_f) + (1/x_f) - 1$
S ≠ 1:	
$I_r = \frac{k}{6(1-S)} \ln \left[ \left( \frac{k+1}{k+x_f} \right)^3 (Sx_f^3 + 1 - S) \right] - \frac{k}{3 \cdot 5 (1-S)} \left[ \tan^{-1} \left( \frac{2x_f - k}{k3 \cdot 5} \right) - \tan^{-1} \left( \frac{2-k}{k3 \cdot 5} \right) \right]$	
S = 1:	$I_r = \frac{1}{2x_f^2} - \frac{1}{2}$
$I_g = - \frac{1}{3S} \left[ \ln(Sx_f^3 + 1 - S) \right]$	

**TABLE 2**  
**PREDICTION OF REACTION TIME AT**  
**A TOTAL PRESSURE OF 1520 kPa**

Inlet SO2 ppm	Temp. deg C	BET Area sq m/g	Feed Ratio S	% Gas Absorbed	% Utilization	Reaction Time sec
2000	1149	8	2.5	90	36	1.904
1000	1149	8	2.5	80	32	1.880
500	1149	8	2.5	70	28	1.908
2000	1149	15	2.5	90	36	0.541
1000	1149	15	2.5	80	32	0.535
500	1149	15	2.5	70	28	0.543
2000	927	20	2.5	90	36	3.352
1000	927	20	2.5	80	32	3.310
500	927	20	2.5	70	28	3.360
2000	927	30	2.5	90	36	1.490
1000	927	30	2.5	80	32	1.471
500	927	30	2.5	70	28	1.493
2000	927	30	1.0	90	90	17.478
2000	927	30	1.5	90	60	5.033
2000	927	30	2.0	90	45	2.486
2000	927	30	3.0	90	30	0.994



PERCENT OF GAS REACTED  
 FIGURE 4 VALUES OF  $I_d$  FOR  $m = 0.62$



PERCENT OF GAS REACTED  
 FIGURE 3 VALUES OF  $I_g$

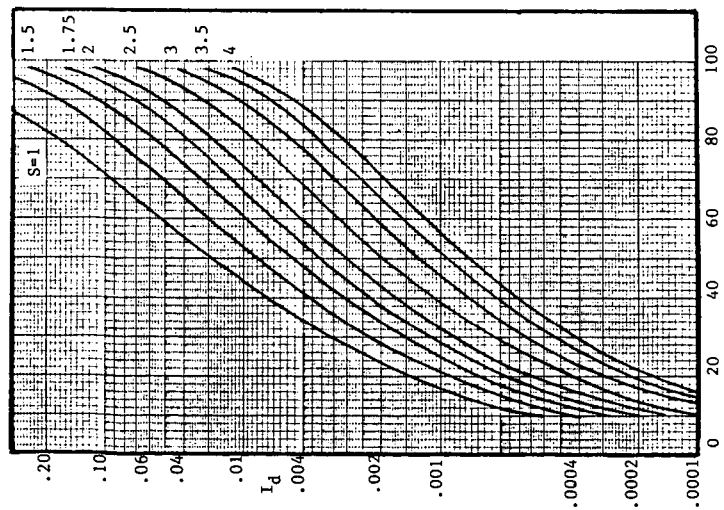


FIGURE 1 VALUES OF  $I_d$  FOR  $m = 1.0$

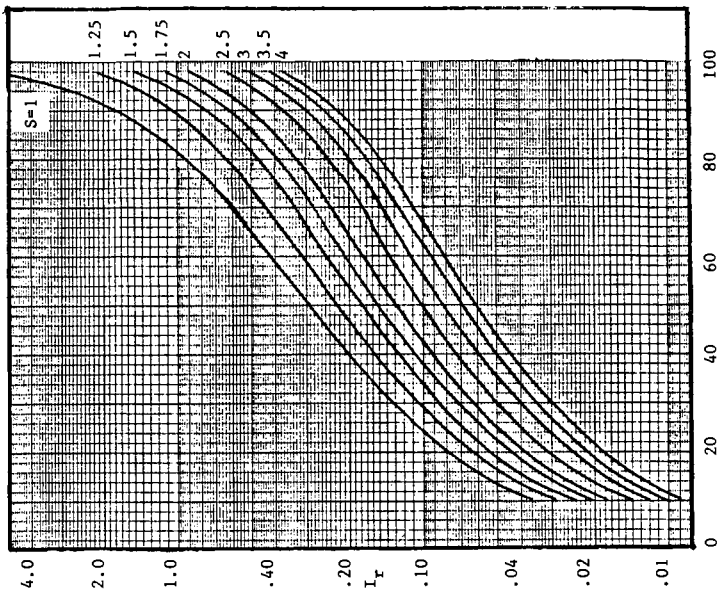


FIGURE 2 VALUES OF  $I_r$

THE USE OF ZINC OXIDE SORBENTS TO REMOVE HYDROGEN SULFIDE  
FROM COAL GASES

Aysel T. ATIMTAY and Susan L. LITTLEFIELD  
Department of Chemical Engineering, Tulane University,  
New Orleans, LA 70118

It is anticipated in the future that synthetic fuels derived from coal will be needed to replace the limited resources of petroleum and natural gas. Coal gasification is a necessary step in the production of these synthetic fuels. During coal gasification hydrogen sulfide is produced in oxygen deficient systems due to the sulfur compounds present in coal. In order to be able to use coal gas in molten carbonate fuel cells (MCFC) for electric power generation, hydrogen sulfide needs to be removed down to 1 ppm level. Therefore, it is very important to develop some sorbents to remove  $H_2S$  from a few percent down to 1 ppm level at high temperatures (600 to 650°C) to obtain greater process efficiency.

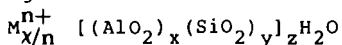
Several metal oxides are capable of high temperature sulfur removal (Westmoreland and Harrison, 1976). Iron oxide is one of the metal oxides that has been used to desulfurize coke oven gases. However, thermodynamic limitations does not allow  $H_2S$  removal with iron oxide to the low partial pressures necessary for MCFC operation. But it can be done with zinc oxide. Therefore, metal oxide-based sorbents for high temperature  $H_2S$  removal has been an active research area in recent years.

There has been much study concerning reactions between zinc oxide (ZnO) and hydrogen sulfide ( $H_2S$ ). Westmoreland and Harrison (1976) has reported the results of thermodynamic screening of the high-temperature desulfurization potential of 28 metal oxides by use of the free energy minimization method. According to the results of this study ZnO is among the most favorable oxides because of the high equilibrium constant for the ZnO- $H_2S$  reaction. In 1977 Westmoreland and Harrison published the results of a comparative study of the kinetics of high-temperature reactions between  $H_2S$  and selected metal oxides. The relative magnitude of the reaction rates determined was  $MnO > ZnO = CaO > V_2O_5$ . The major reasons that ZnO is a desirable sorbent are its high reactivity, high equilibrium constant for the ZnO -  $H_2S$  reaction and ability of ZnS to be regenerated (Rao and Kumar, 1981).

Results regarding structural changes in the pure ZnO sorbent at high temperatures are reported in the literature (Ranade and Harrison, 1980). Sintering actually causes the particles to shrink radially, thus with the same mass of particles there is a smaller amount of surface available for reaction.

The solution to this problem can be proposed by supporting the zinc oxide on a support which can stand to high temperatures. Such a support can be zeolites. Thus, more reaction surface area will be available for the reactant and sorbent efficiency can be increased.

Information about zeolites is given by Maxwell (1982). Zeolites are crystalline aluminosilicates with a chemical composition of this general formula:



$M^{n+}$  is the cation that balances the negative charge of the framework ions,  $Si_4^{+}$  and  $Al_3^{+}$ . The framework ions are tetrahedrally coordinated to four oxygen anions. The three-dimensional network is formed by linking  $(SiO_4)$  and  $(AlO_4)^-$  tetrahedra through shared oxygen ions. The tetrahedra form rings which are entrances to channels or cages in zeolites. The cages define the pore diameter of the zeolite particle. The drawing below shows the structure of the mordenite, Z type zeolite, which has been used for this study. In general, zeolites have good thermal stability, and the framework cations, usually sodium can be exchanged for different types of cations, including zinc. The mordenite type of zeolite is silica rich; therefore its hydrothermal stability is great (stability increases with decreasing aluminum content). This stability made the mordenite the obvious choice for this study. Zeolites seem to be a good way to combat the loss of surface area of the ZnO, due to sintering, because the zeolite support will be thermally stable during the ZnO-H<sub>2</sub>S reaction.

The objective for this paper is to determine if using zeolite supports for the zinc oxide-based sorbents improves conversion, making zinc oxide supported on zeolites a more efficient sorbent. Experimentally, the reactivity of zinc oxide-zeolite particles will be investigated, and kinetic data will be determined for the reaction. The results will then be compared with data found in the literature.

#### EXPERIMENTAL

The reaction of H<sub>2</sub>S with ZnO on zeolite support, whose mean diameter was 0.442 mm, was studied in the temperature range of 500 to 700°C. A plug-flow reactor was used which was 52 cm long and had an inside diameter of 2.2 cm. Figure 2 shows the schematic diagram of the reactor system. The total gas flow rate was held at high rate (1200 cm<sup>3</sup>/min) to eliminate the effect of external mass transfer for the gas solid reaction. The simulated gas mixture consisted of 4% H<sub>2</sub>S, H<sub>2</sub> and the rest N<sub>2</sub>. Gas analyses for each run were checked by taking samples from the sample port indicated in Figure 2 and injecting into the Gas Chromatograph.

Sorbent particles were prepared by soaking zeolite support particles in concentrated zinc sulfate solution, then drying them

about an hour at 100°C and finally roasting them for 24 hours at 500-600°C.

After zeolite particles were prepared, a sample of them was used to test for the determination of zinc loading on the particles. This test is performed by dissolving the zinc on the zeolite support in concentrated hydrochloric acid and determining the zinc content of the solution by atomic absorption spectrophotometer.

The reaction,  $H_2S + ZnO \rightarrow ZnS + H_2O$  was performed in the reactor. The reactor temperature was varied in a range of 500-700°C and gas samples were taken every 2 minutes during the reaction and analyzed by GC. After the reaction is completed, the feed gas was cut off and reactor was cooled down to room temperature with  $N_2$  gas. Finally, the samples were removed and analyzed to determine the extent of conversion of ZnO to ZnS.

The solubilization of ZnO and ZnS were different at different acidity solutions. By making use of this difference ZnO and ZnS were dissolved in solutions having different acidity and the zinc content of these solutions were determined by Atomic Absorption Spectrophotometer. Using the concentration of zinc in each solution, the conversion of ZnO to ZnS was found. A zinc balance was done for the samples to make sure that the amount of zinc (in ZnO and ZnS form) in the particles after the reaction was equal to the total amount of zinc in the particles before the reaction. This balance was met within +2%.

## RESULTS AND DISCUSSIONS

The results obtained from this experimentation are presented in Figures 3 and 4. Figure 3 represents the overall solid conversion of ZnO to ZnS with respect to time for the particle size under study at 500°C, 600°C and 700°C. As can be observed from the figure, the overall solid conversion depends on temperature and reaction time. The overall solid conversion increases as the temperature and reaction time increases. The conversion reaches to 100% at 500°C in about a total reaction time of 40 minutes. The total reaction times for 100% conversion at 600°C and 700°C are about 30 and 10 minutes, respectively. The reaction temperature above 700°C is not tested, because of the formation of metallic zinc vapor above 750°C. The maximum temperature in the ZnO- $H_2S$  system is limited to about 750°C thermodynamically (Westmoreland and Harrison, 1976). Experimental results have also been reported about this temperature at somewhat higher values by Beveridge (1962). During the tests hydrogen has been added to the feed gas mixture in a ratio of 3 mol  $H_2$ /mole of  $H_2S$  to prevent the decomposition of  $H_2S$  at high temperatures. It has been shown by Westmoreland and Harrison (1977) that the  $H_2$  does not measurably alter the  $H_2S$ -ZnO kinetics at low temperatures (<500°C) where  $H_2S$  decomposition should be unimportant.

One of the important reasons to support ZnO on zeolite in this study was to provide better contact between H<sub>2</sub>S and ZnO through increasing the surface area. The other reason was to minimize the structural changes of the ZnO particles during reaction due to sintering effects. Ranade and Harrison (1980) have found in their study of ZnO-H<sub>2</sub>S reaction that surface area of pure ZnO particles decreases from 34 m<sup>2</sup>/g to 16 m<sup>2</sup>/g at 500°C (a 53% decrease in the surface area). This change is more severe at higher temperatures. Since the molar volumes of ZnO and ZnS are not very different, pore plugging could not be a problem during the reaction. Therefore, they have attributed this decrease in surface area to sintering effects which causes the particles to shrink under the effect of high temperatures, thus decreasing the available surface area for the reaction considerably.

The answer to the question "Did structural changes occur in the ZnO-zeolite particles due to reaction?" was important in this study. The BET surface area measurements on the particles before and after reaction were performed using the Accusorb apparatus (Micromeritics Model 2100E).

Table I lists the surface area of reacted and unreacted particles for the longest reaction times for each reaction temperature. The BET surface area of (an average of five batches) unreacted ZnO-zeolite particles is 31.8 m<sup>2</sup>/g. The corresponding surface areas for particles reacted at 500° and 600°C for 50 minutes are 28.2 and 28.1 m<sup>2</sup>/g, respectively. The change is only 11% for these temperatures. At 700°C, the change becomes a little higher, being 15%. These changes in surface area are small as compared to 53% change reported by Ranade and Harrison (1981) at 500°C. Zeolite support is not expected to sinter. It is thermally stable. Therefore, the change in surface area could be attributed to partial sintering of ZnO with zeolite, especially around 700°C. However, some in-depth surface studies are needed to answer this question correctly.

A direct comparison of the conversion versus time curves with the data obtained from literature could not be done, because of the vast difference in the systems. Ranade and Harrison (1980) have investigated the H<sub>2</sub>S absorption with pure ZnO pellets, however our study uses ZnO supported on zeolite. Also, particle size, shape, zinc content will make the difference in comparison. Practically no information is available in the literature on the use of zinc oxide on a carrier or support to absorb hydrogen sulfide from hot coal gases.

Kinetic constants have been calculated for the reaction between H<sub>2</sub>S and ZnO. Zeolite particles using experimental data. The rate constant has been found to obey the Arrhenius relationship.

$$k = A \exp (-E/RT)$$

The Arrhenius plot is shown on Figure 4. A least squares linear fit has been used for the data points to find the slope and the intercept. The correlation coefficient is 0.929. The frequency factor, A, has been found to be  $1.781 \text{ cm}^2/\text{min-mol}$  and the activation energy, E, has been found to be 4355.5 calories/mol. The activation energy is small. Normally, such a low value would indicate mass transfer limitations. This is expected in this system, because of use of zeolites as support for ZnO. Usually zeolites have small pores. The diffusion resistance in zeolites is high. Also, high temperature gas-solid reactions tend to be diffusion controlled. However, this is the first trial on this concept of using support material for metal oxides to increase the surface area available for reaction. Also, authors wanted to test if zeolite had any effect by itself on H<sub>2</sub>S absorption. A base experiment has been conducted using plain zeolites (no ZnO deposits). No decrease in H<sub>2</sub>S concentration has been observed with time.

#### CONCLUSIONS

Using zeolite as support material for zinc oxide does not seem to be suitable. A higher porosity and larger pores are desirable for this kind of application. Nevertheless, the results of this study showed that sintering of sorbent particles can be minimized or prevented by using this new concept of depositing metal oxides on thermally stable supports. Further research on this subject is in progress.

#### REFERENCES

- Beveridge, G.S.G., "Agglomeration International Symposium", Interscience, New York, N.Y., 1962.
- Maxwell, I.E.: Nonacid Catalysis with Zeolites, "Advances in Catalysis," Vol. 31, pp. 2-5 (1982).
- Ranade, P. V. and D. P. Harrison, "The Variable Property Grain Model Applied to the Zinc Oxide-Hydrogen Sulfide Reaction," Chemical Engineering Science, Vol. 36, pp. 1079-1089 (1981).
- Rao, T. R., and R. Kumar, "An Experimental Study of Oxidation of Zinc Sulfide Pellets," Chemical Engineering Science, Vol. 37, pp. 987-996 (1982).
- Westmoreland, P. R., J. B. Gibson, D. P. Harrison, "Comparative Kinetics of High-Temperature Between H<sub>2</sub>S and Selected Metal Oxides", Environmental Science and Technology, pp. 488-491 (1977).
- Westmoreland, P. R. and D. P. Harrison, "Evaluation of Candidate Solids for High-Temperature Desulfurization of Low-Btu Gases", Environmental Science and Technology, Vol. 10, No. 7, pp. 659-661 (1976).

TABLE I. BET SURFACE AREAS FOR MAXIMUM REACTION TIME  
(TIME = 50 MINUTES)

SAMPLE	SURFACE AREA ( $m^2/g$ )
*****	*****
RUN NO. 5 T=500 C	28.2
RUN NO. 10 T=600 C	28.1
RUN NO. 11 T=700 C	26.9
UNREACTED ZnO-ZEOLITE PARTICLES	31.8

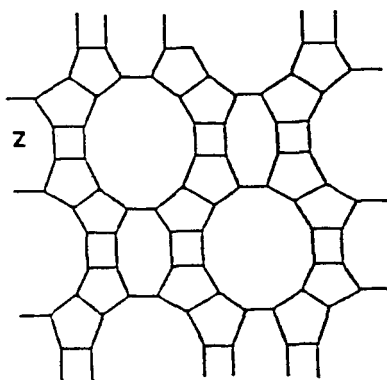


FIGURE 1. SCHEMATIC DIAGRAM OF A Z TYPE ZEOLITE

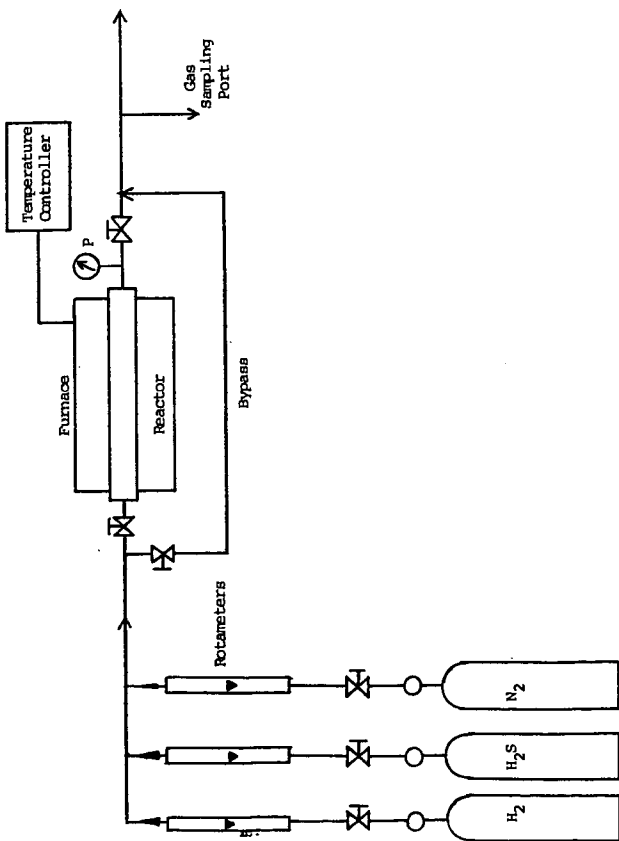


Figure 2. Schematic diagram of laboratory set up for kinetic studies.

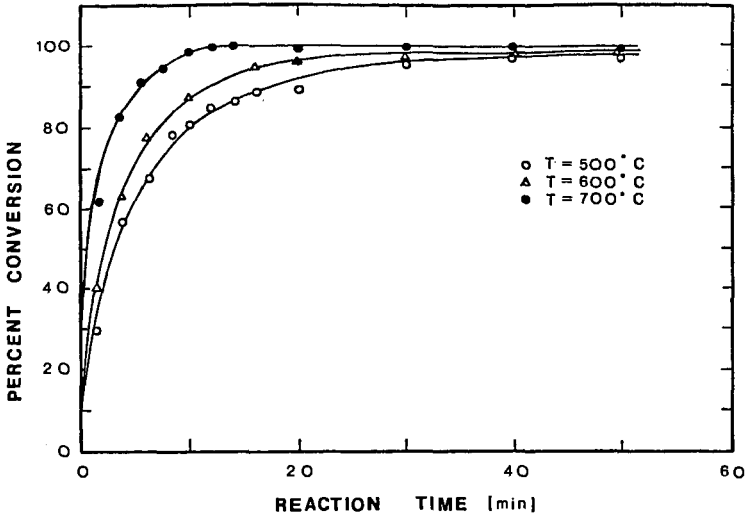


Figure 3. Conversion with reaction time, ZnO - H<sub>2</sub>S reaction.

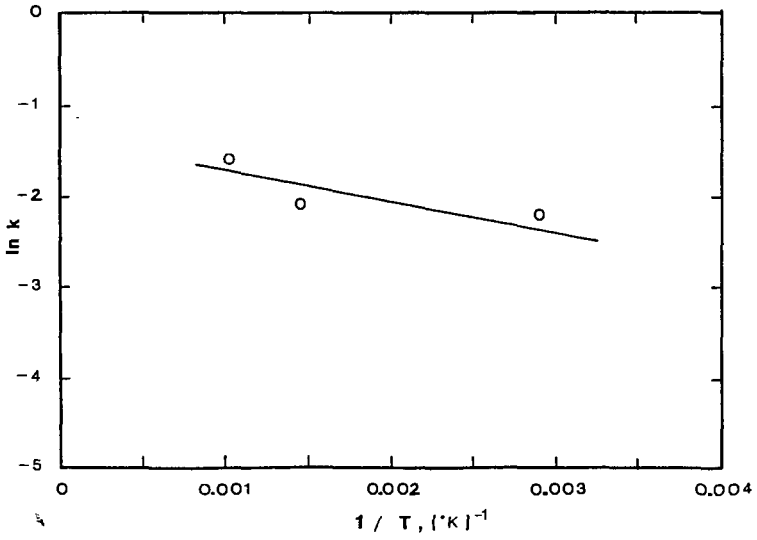


Figure 4. Arrhenius plot ZnO - H<sub>2</sub>O reaction.